27th Benelux Meeting

on

Systems and Control

March 18 – 20, 2008

Heeze, The Netherlands

Book of Abstracts

The 27^{th} Benelux Meeting on Systems and Control is sponsored by

and supported by

Gjerrit Meinsma and Hans Stigter (eds.)
Book of Abstracts 27th Benelux Meeting on Systems and Control

Wageningen University – Systems and Control Group
P.O. Box 9101
6700 HB Wageningen
The Netherlands

A catalog record is available from Wageningen University Library.

ISBN: 978-90-8504-963-0

Part 1

Programmatic Table of Contents

Tuesday, March 18, 2008

P0 **Samenspel**
Welcome and opening
Chair: Gjerrit Meinsma **11.25–11.30**

Plenary: P1 **Samenspel**
Self-Optimizing Control
Sigurd Skogestad (Norway)
Chair: Hans Stigter **11.30–12.30**

TuM01 **Samenspel**
Identification A
Chair: Jan Swevers **14.00–16.05**

TuM02 **Samenkomst**
System Theory A
Chair: Hans Zwart **14.00–16.05**

TuM03 **Samenwerking**
Modeling for Control
Chair: Adrie Huesman **14.00–16.05**

TuM04 **Visie**
Electro-Mechanical Eng. A
Chair: Johannes van Dijk **14.00–16.05**

TuM04-1 **14.00–14.25**
Dynamics of magnetic electron lenses 32
Patrick J. van Bree Eindhoven University of Technology

TuM04-2 **14.25–14.50**
A modular active bearing for noise reduction of rotating machinery 33
W. Symens Flanders' Mechatronics Technology Center
S. Devos Flanders' Mechatronics Technology Center
B. Stallaert Katholieke Universiteit Leuven
G. Pinte, P. Sas, J. Swevers

TuM04-3 **14.50–15.15**
The effect of various disturbance sources on vibration isolation performance 34
G.W. van der Poel University of Twente
J. van Dijk University of Twente
J.B. Jonker University of Twente
H.M.J.R. Soemers

TuM04-4 **15.15–15.40**
6-DOF Electromagnetic Suspension System with Passive Gravity Compensation for Large Load 35
C.Ding Eindhoven University of Technology
A.A.H. Damen Eindhoven University of Technology
P.P.J. van den Bosch Eindhoven University of Technology

TuM04-5 **15.40–16.05**
Validation of the series impedance of a quad cable for DSL applications 36
Wim Foubert VUB
Patrick Boets VUB
Leo Van Biesen VUB
Carine Neus

TuM05 **Uitdaging**
Games and Agent Based Models
Chair: Jacob Engwerda **14.00–16.05**

TuM05-1 **14.00–14.25**
The Open-Loop Linear Quadratic Differential Game for Index One Descriptor Systems 37
Jacob Engwerda Tilburg University
Salmah Gadjah Mada University

TuM05-2 **14.25–14.50**
Robust Minimax Strategies for the Pursuit-Evasion Game 38
E.J.Trottemant TU Delft
C. W. Scherer TU Delft

TuM05-3 **14.50–15.15**
H_2 differential games with incomplete and imperfect information 39
Arie J. T. M. Weeren University of Antwerp

TuM05-4 **15.15–15.40**
Distributed design for linear quadratic control 40
Jean-Charles Delvenne Université catholique de Louvain
Cédric Langbort University of Illinois

TuM05-5 **15.40–16.05**
Consensus seeking using distributed MPC 41
T. Keviczky Delft University of Technology
K.H. Johansson Royal Institute of Technology (KTH)

TuP01 **Samenspel**
Identification B
Chair: Rik Pintelon **16.35–18.40**

TuP01-1 **16.35–17.00**
Frequency Domain Identification of Linear Slowly Time-Varying Systems 42
J. Lataire Vrije Universiteit Brussel
R. Pintelon Vrije Universiteit Brussel

TuP01-2 **17.00–17.25**
Finite data performance of parametric confidence regions in prediction error identification using output error models: a simulation study 43
A. Klomp Delft University of Technology
X.J.A. Bombois Delft Univeristy of Technology
A.J. den Dekker Delft Univeristy of Technology
P.M.J. van den Hof

TuP01-3 **17.25–17.50**
Model selection for short data records using AIC . . . 44
B. Van der Hasselt Vrije Universiteit Brussel
A. de Brauwere Vrije Universiteit Brussel
J. Schoukens Vrije Universiteit Brussel
R. Pintelon

TuP01-4 **17.50–18.15**
Improved FRF measurements in the presence of nonlinear distortions via overlap 45
K. Barbé Vrije Universiteit Brussel
R. Pintelon Vrije Universiteit Brussel
L. Vanbeylen Vrije Universiteit Brussel
J. Schoukens

TuP01-5 **18.15–18.40**
Consistent impulse response estimation and system realization 46
Edwin Reynders K.U.Leuven
Rik Pintelon Vrije Universiteit Brussel
Guido De Roeck K.U.Leuven

TuP02 **Samenkomst**
Medical Applications
Chair: Damien Ernst **16.35–18.40**

TuP02-1 **16.35–17.00**
Dynamic properties of a canine ventricular cell: model vs. myocyte 47
J. Heijman Maastricht University
D.M. Johnson Maastricht University
P.G.A. Volders Maastricht University
R.L.M Peeters, R.L. Westra

TuP02-2 **17.00–17.25**
Dynamical phenomena in pulse-coupled networks of firing integrators 48
Alexandre Mauroy University of Liège
Rodolphe Sepulchre University of Liège

TuP02-3 **17.25–17.50**
Effect of transient response of PID pressure control loop on cascade position control of a pneumatic artificial muscle 49
Tri Vo-Minh Faculty of Bioscience Engineering, KULeuven
Prof. Herman Ramon Faculty of Bioscience Engineering, KULeuven
Prof. Hendrik Van Brussel Faculty of Engineering, KULeuven

TuP02-4 **17.50–18.15**
Variable selection for dynamic treatment regimes . . . 50
Raphaël Fonteneau University of Liège
Louis Wehenkel University of Liège
Damien Ernst University of Liège

TuP02-5 **18.15–18.40**
Relating human lung pathology with non-integer orders model 51
C.M. Ionescu Ghent University, Belgium
R. De Keyser Ghent University, Belgium

TuP03 **Samenwerking**
Biochemical Eng. A
Chair: Gerrit van Straten **16.35–18.40**

TuP03-1 **16.35–17.00**
Detection of filamentous bulking problems: evaluation of different modeling/classification approaches 52
J. Vanlaer Katholieke Universiteit Leuven
G. Gins Katholieke Universiteit Leuven
I.Y. Smets Katholieke Universiteit Leuven
J.F. Van Impe

TuP03-2 **17.00–17.25**
Modelling the temporal evolution of Drosophila gene expression 53
A. Haye Université Libre de Bruxelles
Y. Dehouck Université Libre de Bruxelles
J. M. Kwasigroch Université Libre de Bruxelles
Ph. Bogaerts, M. Rooman

TuP03-3 **17.25–17.50**
Hurdles and challenges in parameter estimation for individual based models 54
A.J. Verhulst Katholieke Universiteit Leuven
K. Bernaerts Katholieke Universiteit Leuven
J.F. Van Impe Katholieke Universiteit Leuven
A.R. Standaert

TuP03-4 **17.50–18.15**
Analysis of Nonlinear Software Sensors Applied to Bioprocesses : Particle Filtering and Unscented Kalman Filtering 55
Johan Mailier Faculté Polytechnique de Mons
Guillaume Goffaux Faculté Polytechnique de Mons
Alain Vande Wouwer Faculté Polytechnique de Mons

TuP03-5 **18.15–18.40**
Two-step identification procedure for biological reaction schemes when stoichiometry and kinetics can not be decoupled 56
V. Vastemans Université Libre de Bruxelles
M. Rooman Université Libre de Bruxelles
Ph. Bogaerts Université Libre de Bruxelles

TuP04 **Visie**
Electro-Mechanical Eng. B
Chair: Maarten Steinbuch **16.35–18.40**

TuP04-1 **16.35–17.00**
Analysis of a Variable Geometry Active Suspension . . 57
Willem-Jan Evers Eindhoven University of Technology
Albert van der Knaap TNO Automotive
Igo Besselink Eindhoven University of Technology
Henk Nijmeijer

TuP04-2 **17.00–17.25**
Automatic control code generation for mechatronic systems 58
O. Aydin Tekin Delft University of Technology
R. Babuska Delft University of Technology
B. De Schutter Delft University of Technology

TuP04-3 **17.25–17.50**
A linear programming reformulation of input shaping . 59
L. Van den Broeck K.U.Leuven
G. Pipeleers K.U.Leuven
J. De Caigny K.U.Leuven
B. Demeulenaere, J. Swevers, J. De Schutter

TuP04-4 **17.50–18.15**
Non-centralized model predictive control of power networks 60
A.C.R.M.Damoiseaux Eindhoven University of Technology
A. Jokic Eindhoven University of Technology
M. Lazar Eindhoven University of Technology
P.P.J. v.d. Bosch

TuP04-5 **18.15–18.40**
A rare-event approach for analyzing power system reliability 61
Florence Belmudes University of Liège
Damien Ernst University of Liège
Louis Wehenkel University of Liège

TuP05 **Uitdaging**
Aerospace Eng.
Chair: Johan Schoukens **16.35–18.40**

TuP05-1 **16.35–17.00**
Global Aerodynamic Modeling with Multivariate Splines 62
C.C. de Visser Delft University of Technology
J.A. Mulder Delft University of Technology
Q.P. Chu Delft University of Technology

TuP05-2 **17.00–17.25**
Nonlinear analysis of flutter 63
M. Van de Walle Vrije Universiteit Brussel
J. Schoukens Vrije Universiteit Brussel
S. Vanlanduit Vrije Universiteit Brussel

Wednesday, March 19, 2008

Plenary: P2 **Samenspel**
Noncooperative Cooperation
Jeff Shamma (USA)
Chair: Hans Stigter **8.30– 9.30**

Mini Course: P3 **Samenspel**
The Port-Hamiltonian Approach (Part 1)
Arjan van der Schaft (The Netherlands)
Chair: Gjerrit Meinsma **10.00–11.00**

Plenary: P4 **Samenspel**
Effective Implementation of Optimal Operation
Sigurd Skogestad (Norway)
Chair: Gjerrit Meinsma **11.30–12.30**

WeM01 **Samenspel**
Identification C
Chair: Paul Van den Hof **14.00–16.05**

WeM01-5 **15.40–16.05**
Velocity and acceleration estimation for optical incremental encoders using time stamping 71
R.J.E. Merry Eindhoven University of Technology
M.J.G. van de Molengraft Eindhoven University of Technology
M. Steinbuch Eindhoven University of Technology

WeM02 **Samenkomst**
System Theory B
Chair: Gerard van Willigenburg **14.00–16.05**

WeM02-1 **14.00–14.25**
Studying the Properties of Unimodular Maps and Interconnected Behaviors by means of Galois Connections . 72
Tzvetan Ivanov Université Catholique de Louvain

WeM02-2 **14.25–14.50**
The positive LQ-problem for linear continuous time systems 73
Charlotte Beauthier University of Namur (FUNDP)
Joseph J. Winkin University of Namur (FUNDP)

WeM02-3 **14.50–15.15**
Bisimulation for switching linear systems with inequality constraints 74
F. J. Kerber University of Groningen
A. J. van der Schaft University of Groningen
M. K. Camlibel University of Groningen

WeM02-4 **15.15–15.40**
Temporal linear system structure 75
L.G. Van Willigenburg Wageningen University
W.L. De Koning former associate professor at TU Delft

WeM02-5 **15.40–16.05**
On the stabilization problem for a certain class of decentralized control systems 76
Ciprian Deliu Technische Universiteit Eindhoven
Anton A. Stoorvogel University of Twente

WeM03 **Samenwerking**
Biochemical Eng. B
Chair: Denis Dochain **14.00–16.05**

WeM03-1 **14.00–14.25**
Dynamic behaviour of the CSTR: a thermodynamic point of view 77
Audrey Favache Université catholique de Louvain
Denis Dochain Université catholique de Louvain
Bernhard Maschke Université Claude Bernard - Lyon 1

WeM03-2 **14.25–14.50**
Robust Nonlinear Receding-Horizon Observer applied to continuous cultures of phytoplankton 78
Guillaume Goffaux Faculté Polytechnique de Mons
Alain Vande Wouwer Faculté Polytechnique de Mons

WeM03-3 **14.50–15.15**
Unravelling E. coli dynamics close to maximum growth temperature through heterogeneous modelling 79
E. Van Derlinden K.U.Leuven
I. Lule K.U.Leuven
J. F. Van Impe K.U.Leuven
K. Bernaerts

WeM03-4 **15.15–15.40**
Global tracking for a plug flow tubular reactor 80
N.Beniich Université Catholique de Louvain
D.Dochain Université Catholique de Louvain
A.El Bouhtouri Université Chouaib Doukkali

WeM03-5 **15.40–16.05**
Dynamical Analysis of a Biochemical Reactor with Time Delay 81
A.K. Drame University of Nevada Las Vegas
D. Dochain Universite Catholique de Louvain (UCL)
J.J. Winkin University of Namur (FUNDP)

WeM04 **Visie**
Electro-Mechanical Eng. C
Chair: Jan Swevers **14.00–16.05**

WeM04-1 **14.00–14.25**
Mechanics and control issues for piezo actuated positioning stages 82
J.R. van Hulzen Delft University of Technology
P.M.J. Van den Hof Delft University of Technology
J. van Eijk Delft University of Technology

WeM04-2 **14.25–14.50**
Iterative Learning Control for wet-plate clutches . . . 83
Gregory Pinte Flanders' Mechatronics Technology Center
Wim Symens Flanders' Mechatronics Technology Center
Jan Swevers Katholieke Universiteit Leuven

WeM04-3 **14.50–15.15**
Filtered-X LMS versus repetitive control for active structural acoustic control 84
Bert Stallaert Katholieke Universiteit Leuven
Gregory Pinte
Steven Devos
Wim Symens, Jan Swevers, Paul Sas

WeM04-4 **15.15–15.40**
A generalized repetitive controller design 85
Goele Pipeleers K.U.Leuven
Bram Demeulenaere K.U.Leuven
Joris De Schutter K.U.Leuven
Jan Swevers

WeM04-5 **15.40–16.05**
Nuclear fusion: principles and challenges 86
Gert Witvoet Technische Universiteit Eindhoven
Maarten Steinbuch Technische Universiteit Eindhoven
Niek Doelman TNO Science and Industry

WeM05 **Uitdaging**
Aerospace and Traffic
Chair: Bart De Schutter **14.00–16.05**

WeP03-2 **17.00–17.25**
Multiple objective optimisation of jacketed tubular reactors with dispersion 105
Filip Logist K.U.Leuven
Peter M.M. Van Erdeghem K.U.Leuven
Jan F. Van Impe K.U.Leuven
Ilse Y. Smets

WeP03-3 **17.25–17.50**
Evaluating the robustness of the estimation of microbial cardinal temperatures from optimized temperature inputs 106
E. Van Derlinden K.U.Leuven
K. Bernaerts K.U.Leuven
J. F. Van Impe K.U.Leuven

WeP03-4 **17.50–18.15**
Predicting the quality of a batch process using an inferential sensor 107
G. Gins Katholieke Universiteit Leuven
I.Y. Smets Katholieke Universiteit Leuven
J.F. Van Impe Katholieke Universiteit Leuven
B. Pluymers, W. Van Brempt

WeP03-5 **18.15–18.40**
Productivity optimization of yeast fed-batch cultures using an extremum-seeking strategy 108
Laurent Dewasme Faculté Polytechnique de Mons
Alain Vande Wouwer Faculté Polytechnique de Mons

WeP03-6 **18.40–19.05**
Convex Analysis Tools Applied to Underdetermined Reaction Networks 109
Francisca Zamorano Faculté Polytechnique de Mons
Alain Vande Wouwer Faculté Polytechnique de Mons
Georges Bastin Université Catholique de Louvain

WeP04 **Visie**
Mechanical Eng.
Chair: Bram de Jager **16.35–19.05**

WeP04-1 **16.35–17.00**
An Adaptive Sub-Optimal Energy Management Strategy for Hybrid Drive Trains 110
Thijs van Keulen Eindhoven University of Technology
Bram de Jager Eindhoven University of Technology
Maarten Steinbuch Eindhoven University of Technology

WeP04-2 **17.00–17.25**
Acceleration constraints of moving-magnet planar actuators with integrated magnetic bearing 111
C.M.M. van Lierop Eindhoven University of Technology
J.W. Jansen Eindhoven University of Technology
A.A.H. Damen Eindhoven University of Technology
P.P.J. van den Bosch

WeP04-3 **17.25–17.50**
Control of induction motors with voltage saturation . . 112
C. Bastin University of Liège
R. Sepulchre University of Liège
F. Jadot Schneider Toshiba Inverter Europe
F. Malrait

WeP04-4 **17.50–18.15**
Energy-based modeling and lontrol of longitudinal tyre forces. 113
J.J. Koopman Delft University of Technology
D. Jeltsema Delft University of Technology
M. Verhaegen Delft University of Technology

WeP04-5 **18.15–18.40**
LQG control of a doubly-fed induction machine for wind turbine applications 114
Manuel Gálvez-Carrillo Université Libre de Bruxelles
Michel Kinnaert Université Libre de Bruxelles

WeP05 **Uitdaging**
Observers
Chair: Karel Keesman **16.35–19.05**

WeP05-1 **16.35–17.00**
State-of-charge observers for lead-acid storage unit in photovoltaic installations 115
A. Skrylnyk Faculte Polytechnique de Mons
R. Lepore Faculte Polytechnique de Mons
C. Renotte Faculte Polytechnique de Mons
M. Remy

WeP05-2 **17.00–17.25**
Observer Design and Output Feedback Stabilization for a Class of Underactuated Mechanical Systems 116
A. Venkatraman University of Groningen
A. J. van der Schaft University of Groningen
R. Ortega Laboratoire de Signaux et Systemes
I. Sarras

WeP05-3 **17.25–17.50**
Hybrid State Observer for a Locally Lipschitz System . 117
Denis V. Efimov University of Liege

WeP05-4 **17.50–18.15**
Non-linear observers (estimators) and symmetries : theory and examples. 118
S. Bonnabel Liege University
P. Rouchon Ecole des Mines

WeP05-5 **18.15–18.40**
Boundary observer synthesis: static and dynamic structure design 119
D. Vries Wageningen University
K.J. Keesman Wageningen University
H. Zwart University of Twente

Thursday, March 20, 2008

Mini Course: P5 **Samenspel**
The Port-Hamiltonian Approach (Part 2)
Arjan van der Schaft (The Netherlands)
Chair: Hans Stigter **8.30– 9.30**

The Port-Hamiltonian Approach to Physical System Modeling and Control (Part 2) 184
Arjan van der Schaft (The Netherlands)

Plenary: P6 **Samenspel**
Learning in Games under Dynamic Reinforcement
Jeff Shamma (USA)
Chair: Gjerrit Meinsma **10.00–11.00**

Learning in Games under Dynamic Reinforcement . . 174
Jeff Shamma (USA)

Mini Course: P7 **Samenspel**
The Port-Hamiltonian Approach (Part 3)
Hans Zwart (The Netherlands)
Chair: Gjerrit Meinsma **11.30–12.30**

The Port-Hamiltonian Approach to Physical System Modeling and Control (Part 3) 208
Hans Zwart (The Netherlands)

ThP01 **Samenspel**
Identification D
Chair: Rik Pintelon **14.00–15.40**

ThP01-1 **14.00–14.25**
Initial Estimates for Wiener-Hammerstein Models using the Best Linear Approximation 120
Lieve Lauwers — Vrije Universiteit Brussel
Johan Schoukens — Vrije Universiteit Brussel
Rik Pintelon — Vrije Universiteit Brussel

ThP01-2 **14.25–14.50**
Parameter-varying decoupling for 3-DOF platform with manipulator on top of it 121
M. Gajdusek — Technical University Eindhoven
A.A.H. Damen — Technical University Eindhoven
P.P.J. van den Bosch — Technical University Eindhoven

ThP01-3 **14.50–15.15**
Identification of a harmonic signal in the presence of additive noise, an unknown time base distortion, and an averaging effect 122
Veerle Beelaerts — Vrije Universiteit Brussel
Fjo De Ridder — Vrije Universiteit Brussel
Maite Bauwens — Vrije Unviversiteit Brussel
Rik Pintelon

ThP02 **Samenkomst**
Optimization
Chair: Jan Bontsema **14.00–15.40**

ThP02-1 **14.00–14.25**
A hybrid steepest descent method for constrained convex optimization 123
Mathieu Gerard — Delft University of Technology
Michel Verhaegen — Delft University of Technology
Bart De Schutter — Delft University of Technology

ThP02-2 **14.25–14.50**
Identification of Wiener-Hammerstein systems by means of Support Vector Machines for Regression 124
A. Marconato — University of Trento, Italy
D. Petri — University of Trento, Italy
J. Schoukens — Vrije Universiteit Brussel, Belgium

ThP02-3 **14.50–15.15**
Neural network global optimization using interval analysis 125
E. de Weerdt — Delft University of Technology
Q.P. Chu — Delft University of Technology
J.A. Mulder — Delft University of Technology

ThP03 **Samenwerking**
Dynamic Optimization
Chair: Adrie Huesman **14.00–15.40**

ThP03-1 **14.00–14.25**
Dynamic optimization for minimizing the fuel consumption of a gasoline engine 126
Bart Saerens — Katholieke Universiteit Leuven
Jeroen Vandersteen — Katholieke Universiteit Leuven
Jan Swevers — Katholieke Universiteit Leuven
Moritz Diehl, Eric Van den Bulck

ThP03-2 **14.25–14.50**
Formulation and Solution of Economic Dynamic Process Optimization 127
Adrie E.M. Huesman — Delft University of Technology
Okko H. Bosgra — Delft University of Technology
Paul M.J. Van den Hof — Delft University of Technology

ThP03-3 **14.50–15.15**
Efficient solution of multiple objective optimal control problems 128
Peter M.M. Van Erdeghem — K.U.Leuven
Filip Logist — K.U.Leuven
Jan F. Van Impe — K.U.Leuven
Ilse Y. Smets

ThP03-4 **15.15–15.40**
Convexity-base homotopy method for the initialization of optimal control problems 129
Julian Bonilla — Katholieke Universiteit Leuven
Moritz Diehl — Katholieke Universiteit Leuven
Jan Van Impe — Katholieke Universiteit Leuven
Bart De Moor

ThP04 **Visie**
Optimal Control
Chair: Siep Weiland **14.00–15.40**

Part 2

Contributed Lectures

Identification and Modelling of a Distillation Column

Bart Huyck, Jos De Brabanter
KaHo Sint Lieven - Department Industrieel Ingenieur
Gebroeders Desmetstraat 1, B-9000 Gent
Email: bart.huyck@kahosl.be jos.debrabanter@kahosl.be

Filip Logist, Jan Van Impe
K.U.Leuven - Department of Chemical Engineering (CIT)
Willem de Croylaan 46, B-3001 Heverlee
Email: filip.logist@cit.kuleuven.be jan.vanimpe@cit.kuleuven.be

Bart De Moor
K.U.Leuven - Department of Electrical Engineering (ESAT - SCD)
Kasteelpark Arenberg 10, B-3001 Heverlee
Email: bart.demoor@esat.kuleuven.be

1 Introduction

Advanced control techniques such as Model Predictive Control (MPC), have been and are still heavily studied in the academic world. However, in industrial practice these techniques are still relatively scarcely exploited (and most often only in high tech or worldwide competing industries). Hence, it would be interesting to spread these techniques also in other industry branches. Therefore, in this research a proliferation of these methods is envisioned by implementing them using industry standard control hardware like Programmable Logic Controllers (PLCs). To test the possibilities of this hardware for MPC, a pilot scale distillation column is selected as a case study.

2 The distillation column

The distillation column under study concerns a pilot scale experimental set-up for the separation of a binary mixture of methanol and isopropanol. For practical reasons, the set-up is a closed system that mixes the two fractions again after separation. The column is a multiple input, multiple output (MIMO) system with four *manipulated variables* or *inputs* (i.e., reboiler duty, feed flow rate, feed temperature and distillate flow rate), and eleven *controlled variables* or *outputs* (i.e., distillate flow rate, feed flow rate and nine temperatures measurements between the bottom and the top of the column). The concentration of the top and bottom fraction is measured by taking samples at chosen intervals.

3 Modelling the column

To exploit MPC, a mathematical model of the column is required. Hereto, *black box* models are derived based on data driven techniques. Although the intension is to use in the future linear models around certain operating points, both linear and nonlinear models are fitted. After some first experiments with pseudo random binary noise (PRBS) input signals, a linear model has been calibrated [1]. However, since the system under study is a test set-up, all kinds of input signals can be used. Therefore, new experiments with random noise inputs will be used to refine the current linear model. Also a nonlinear model will be constructed with the help of Least Square Support Vector Machines (LS-SVM) [2]. LS-SVM is a state-of-the-art method for solving highly nonlinear modelling problems. Afterwards the constructed models will be employed to design the controller and to implement it on the column set-up.

4 Acknowledgements

Work supported in part by Projects OT/03/30 and EF/05/006 (Center-of-Excellence Optimization in Engineering) of the Research Council of the Katholieke Universiteit Leuven, and by the Belgian Program on Interuniversity Poles of Attraction, initiated by the Belgian Federal Science Policy Office. The scientific responsibility is assumed by its authors.

References

[1] Huyck B., De Brabanter J., Van Impe J., De Moor B., Identifcation and Modeling of a Dynamical System, submitted for ecumict 2008, Gent, België

[2] J. A. K. Suykens, T. Van Gestel, J. De Brabanter, B. De Moor, J. Vandewalle, Least Squares Support Vector Machines, World Scientific Pub. Co., Singapore, 2002 (ISBN 981-238-151-1)

Identification and control of a 3DOF metrological AFM

Roel Merry*, Mustafa Uyanik,
René van de Molengraft and Maarten Steinbuch
Department of Mechanical Engineering
Eindhoven University of Technology
P.O. Box 513, 5600 MB Eindhoven
The Netherlands
Email: *r.j.e.merry@tue.nl

Richard Koops and Marijn van Veghel
NMi Van Swinden Laboratorium
Thijsseweg 11
2629 JA Delft
The Netherlands

1 Introduction

The metrological AFMs are used to calibrate transfer standards for commercial AFMs. In contrast to commercial AFMs, the accuracy of the measurements is much more important than the scanning speed. In current AFMs MIMO aspects are commonly disregarded and the positioning of the sample is often done in an open-loop manner [1].

In this research, nonparametric MIMO identification of the AFM in all 3 degrees of freedom (DOFs) is used to investigate the amount of coupling between the various axes. Furthermore, feedback control is applied to all 3 DOFs.

2 Identification

The AFM and the feedback control loops of all 3 DOFs are shown schematically in Fig. 1. Although the different axes are theoretically decoupled, practically some amount of cross coupling will be inevitable in the 3DOF stage, e.g. due to alignment errors.

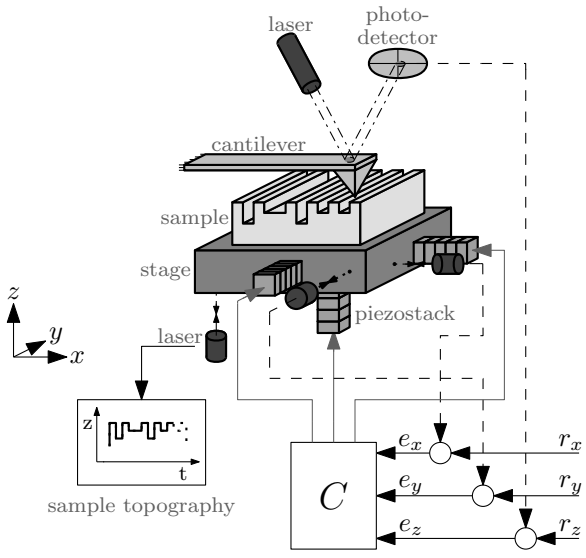

Figure 1: Schematic representation of the AFM and the feedback control.

Using the non-parametric open-loop identification method, a full non-parametric MIMO identification is performed. The frequency-dependent relative gain array shows that the different axes can be assumed decoupled for frequencies $f \leq 100$ Hz.

3 Control

Three SISO feedback controllers are designed resulting in bandwidths $f_{BW} << 100$ Hz. The characteristic loci show that the MIMO system with SISO controllers has a good MIMO phase margin. The feedback control in scanning direction also significantly reduces the effect of hysteresis in the piezo driven stage.

Since the piezo actuators act as position actuators, a position feedforward is added to the scanning axes. Fig. 2 shows that the feedforward reduces the tracing error by a factor 2 for a scan in *x* direction.

Future research includes the design and application of a hysteresis feedforward and MIMO control to remove the small amount of coupling that is present.

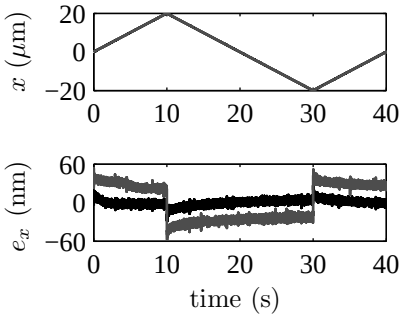

Figure 2: Position and tracing errors; reference (dashed), with (black) and without (dark-grey) feedforward.

References

[1] L. Y. Pao, A. Butterworth, and D. Y. Abramovich. Combined feedforward/feedback control of atomic force microscopes. *American Control Conference*, pages 3509–3515, 2007.

Interpolation-based multiparameter LPV identification

Jan De Caigny, Joris De Schutter, Jan Swevers
Department of Mechanical Engineering
Katholieke Universiteit Leuven
Celestijnenlaan 300B, B-3001 Heverlee, Belgium
Email: jan.decaigny@mech.kuleuven.be

Juan F. Camino
School of Mechanical Engineering
State University of Campinas
CP 6122, 13083-970, Campinas, Brazil

1 Introduction

This work presents an identification technique for SISO linear parameter varying (LPV) systems with multiple varying parameters. The method is based on the interpolation of LTI models estimated for fixed values of the varying parameters. It results in an LPV model with a numerically well-conditioned state-space representation. An illustrative example shows the potential of the methodology.

2 Interpolation Methodology

The LPV model is parameterized by the following polynomial state-space representation[1]:

$$H(\theta) := \begin{cases} \delta[x] = \sum_{\alpha} A_\alpha \theta^\alpha \, x + \sum_{\alpha} B_\alpha \theta^\alpha \, u, \\ y = \sum_{\alpha} C_\alpha \theta^\alpha \, x + \sum_{\alpha} D_\alpha \theta^\alpha \, u \end{cases} \tag{1}$$

where $\theta^\alpha := \theta_1^{\alpha_1}\theta_2^{\alpha_2}\ldots\theta_n^{\alpha_n}$ and $\sum_{i=1}^{n}\alpha_i \leq N$ with $\alpha_i \in \mathbb{N}$, N the polynomial degree and $\theta \in \mathbb{R}^n$ the vector of n varying parameters. The purpose of the LPV model (1) is to interpolate M local LTI models

$$H_\ell := \begin{cases} \delta[x] = \tilde{A}_\ell \, x + \tilde{B}_\ell \, u, \qquad \ell = 1,\ldots,M \\ y = \tilde{C}_\ell \, x + \tilde{D}_\ell \, u, \end{cases} \tag{2}$$

identified for M distinct values of θ. To properly interpolate these local models, they need to be defined with respect to the same state basis.

Similarly to the method in [1], our approach represents the local models (2) as a gain multiplied with the series connection of first and second order submodels. However, compared to [1], our approach has the advantage that it incorporates multiparameter dependency and allows the transition between complex and real pairs of poles (zeros) to be interpolated.

3 Illustrative Example

The test setup presented in Fig. 1 consists of two rotating discs connected by a flexible beam. Each disc has an electromagnetic brake that allows to vary its damping coefficient. Based on the equations of motion

$$I_1\ddot{x}_1 = -(C_1 + c_1(t))\dot{x}_1 + k(x_2 - x_1) + T$$
$$I_2\ddot{x}_2 = -(C_2 + c_2(t))\dot{x}_2 + k(x_1 - x_2)$$

[1] The operator $\delta[\cdot]$ denotes the time derivative for continuous-time models and the shift operator for discrete-time models.

local models were obtained for 15 combinations of the varying parameters $c_1(t)$ and $c_2(t)$. Fig. 2 shows their poles (blue squares) and zeros (green circles). There is a fixed real pole at the origin, a varying real pole and a varying complex pole pair. The two zeros clearly migrate from a real to a complex pair between local model 8 and 9 and back again between local model 14 and 15. For these 15 local models an interpolating LPV model of polynomial degree $N = 2$ was obtained. Fig. 2 shows (in black dots) the poles and zeros of this LPV model evaluated for 150 intermediate combinations of the varying parameter. A smooth interpolating behavior of the local poles and zeros can be observed.

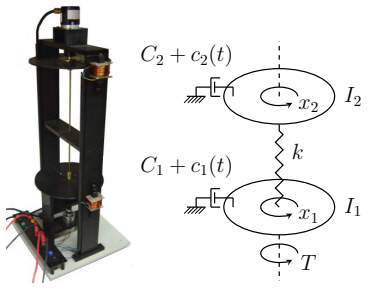

Figure 1: Linear parameter varying system.

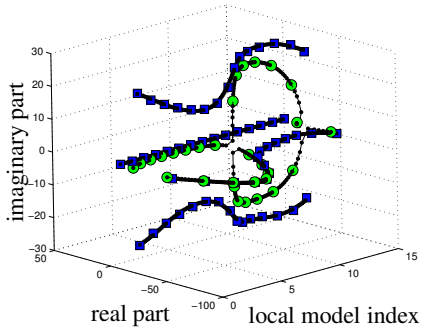

Figure 2: Poles and zeros of the local and LPV models.

4 Acknowledgements

This work has been carried out within the framework of projects G.0446.06 of the Research Foundation - Flanders (FWO - Vlaanderen). This work also benefits from K.U.Leuven-BOF EF/05/006 Center-of-Excellence Optimization in Engineering.

References

[1] B. Paijmans, W. Symens, H. Van Brussel and J. Swevers, "Identification of Interpolating Affine LPV Models for Mechatronic Systems with One Varying Parameter," European Journal of Control, *accepted for publication*.

Channel Capacity Estimation of Digital Subscriber Lines

Carine Neus, Wim Foubert, Patrick Boets, Leo Van Biesen

Vrije Universiteit Brussel, Pleinlaan 2, 1050 Brussels, Belgium
Department of Fundamental Electricity and Instrumentation (ELEC),
Email: cneus@vub.ac.be

1 Introduction

Although fiber is being deployed steadily in the telephone network for broadband services, complete penetration will take several decades. This motivates using the omnipresent copper telephone network as effectively as possible during the transition period. This is already widely done by the telephone operators through the provision of xDSL services (e.g. ADSL, VDSL). The achievable capacity, i.e. bit rate, is different for every customer, because each telephone loop has a different transfer function, detemined by the loop make-up (loop topology, line lengths, cable types,...). When the received noise is known or measured, then the channel capacity C can be estimated using Shannon's formula:

$$C = \int_{f_1}^{f_2} \log_2 \left(1 + \frac{|H(f)|^2 S(f)}{N(f)} \right) df$$

with $H(f)$ the transfer function, $S(f)/N(f)$ the signal-to-noise ratio and $[f_1,f_2]$ the frequency band in which the xDSL service operates.

2 Transfer function estimation

In this research, we focus on the estimation of the transfer function $H(f)$, from measurements solely at the central office side. Therefore $H(f)$ cannot be measured directly, but it can be calculated from the estimated loop make-up, which is obtained through reflectometry. The basic principle is to inject an excitation signal on the loop under test. The signal propagates along the line and when an impedance discontinuity (e.g. end of line, splice with other cable,...) is encountered, a part of the signal is reflected and travels back to the measuring instrument. By performing signal processing on these reflections, the loop makeup can be estimated. Till now measurements have mainly been done in the frequency domain, followed by an inverse Fourier transform to yield the time domain signal, which represents the trace of received reflections one would get when sending in a pulse excitation [1,2]. However, several factors complicate the identification process: limited a priori knowledge, dispersion, high attenuation, power constraints,... Moreover, if the measurement is to be done by the DSL-modem (preferred implementation), the low-frequent voiceband signals are suppressed, which severely distorts the reflections.

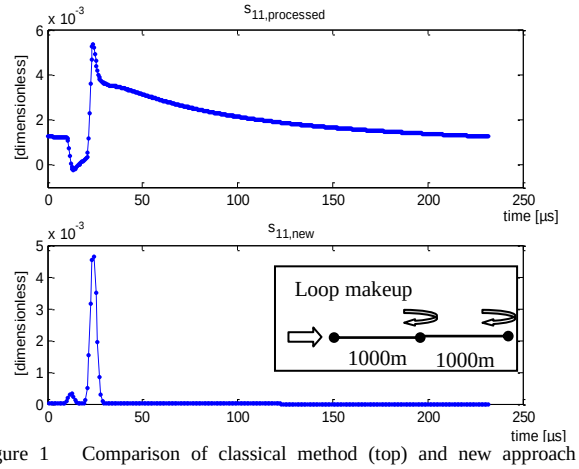

Figure 1 Comparison of classical method (top) and new approach (bottom), for a cascade of 1000 m (0.4 mm cable) and 1000 m (0.5 mm cable). In both cases two reflections are visible, but with the new approach, the dispersion is strongly reduced.

Therefore, we propose a new identification method which is less prone to these influences. The main difference is that we perform most of the signal processing on the measured data (directly in the frequency domain) and only then tranform it to the time domain. As a consequence, the yielded time domain signal loses its physical meaning (it does not correspond anymore to the reflections one would get when sending in a pulse), but the dispersion is strongly reduced. Figure 1 compares both methods. Moreover, missing or distorted frequencies are not problematic, as only the reliable frequencies are used.

3 Conclusions

By working with the frequency domain data instead of the time domain data, as usually done, the new approach is able to deal with suppressed or missing frequencies. By applying well-chosen processing steps, the dispersion is strongly reduced. A measurement campaign confirms that the new algorithm leads to good loop identification. Once the loop makeup is known, the channel capacity can be estimated.

References

[1] P. Boets, T. Bostoen, L. Van Biesen and T. Pollet, "Pre-Processing of Signals for Single-Ended Subscriber Line Testing", *IEEE Trans. Instrum. Meas.*, vol. 55, no. 5, pp.1509-1518, Oct. 2006.

[2] S. Galli and K. Kerpez, "Single-Ended Loop Make-Up Identification - Part I: A Method of Analyzing TDR Measurements", IEEE *Trans. Instrum. Meas.*, vol. 55, no. 2, pp.528-537, Apr. 2006.

Introducing the Power-Scalable Best Mixer Approximation

Koen Vandermot, Wendy Van Moer, Ludwig De Locht and Yves Rolain
Vrije Universiteit Brussel, dep. ELEC, Pleinlaan 2, 1050 Brussels, BELGIUM
e-mail: koen.vandermot@vub.ac.be

I. INTRODUCTION

For the design of telecommunication systems, designers rely on models of the different components of their system. For mixers [1] there exists already a model that is easy to create out of input and output signals: the Best Mixer Approximation [2]. This model describes the mixer as an approximation (in a least squares sense) of an ideal mixer, perturbated by nonlinear noise as well as measurement/ simulation noise. However, this approximation is only valid for the chosen class of signals: the class of the gaussian noise signals with a fixed power spectrum (rms value and coloring are fixed) [3]. A consequence of this approach is that the BMA will be different for an other RMS value of the input signal. Since the input power is one of the tuning parameters in the design of a communication system, the model for the mixer has to predict the behavior also for a variation of the input power. In this abstract a technique is proposed to build up such a power scalable model.

II. FROM A NONPARAMETRIC BMA TO A PARAMETERIZED POWER-SCALABLE BMA

The proposed power scalable model can be created by a four step method. In a first step the BMA is estimated for a given set of input powers $\{P_0, \ldots, P_{n_P}\}$. For each input power P_i, the BMA can be written in an FRF-like way:

$$\frac{Y(\omega_k+\omega_{LO})}{U(\omega_k)LO(\omega_{LO})} = G_0(\omega_k+\omega_{LO}) + G_B(\omega_k+\omega_{LO}) + G_S(\omega_k+\omega_{LO}) + N_G(\omega_k+\omega_{LO}) \quad (1)$$

Where Y represents the output signal, U the input signal and LO the local oscillator signal. ω_{LO} is the angular frequency of the local oscillator signal, which is assumed to be a pure sinewave. G_0 is the "transfer function" of the underlying ideal mixer system, G_B represents the systematic non-ideal nonlinear contributions, G_S is the stochastic nonlinear contribution and N_G represents the simulation or measurement noise. The sum G_0+G_B is defined as the Best Mixer Approximation G_{BMA} and can be estimated based on a measurement or a simulation. A popular way to retrieve G_{BMA}, G_S and N_G is by performing a persistent set of simulations or measurements with multisine excitations [2].

In the next step, a parametric BMA is estimated by parameterizing in the poles p_a, zeros z_b and the gain K:

$$G_{BMA}(\omega_k+\omega_{LO}) = K\frac{\prod_{b=1}^{n_b}(z_k-z_b)}{\prod_{a=1}^{n_a}(z_k-p_a)} \quad (2)$$

Here, $z = \exp(-j2\pi\omega_k f_s/N)$ and f_s and N represent respectively the sample frequency and the number of sample points in one period. As a consequence, a set of poles, zeros and a gain can be found for every power P_i of the input signal:

$$\left\{z_1^i, z_2^i, \ldots, z_{n_b}^i, p_1^i, p_2^i, \ldots, p_{n_a}^i, K^i\right\} \quad (3)$$

In step 3, the corresponding poles and zeros will be selected over the different input powers P_i. As a consequence a set of locations for every pole $p_a(i)$ as well as for every zero $z_b(i)$ is found over different powers P_i of the input signal. In the last step, the location of the different poles/zeros and the value of the gain for any power within the given range $P \in [P_0, P_{n_p}]$ will be estimated by a special interpolation method: cubic smoothing spline. At the end, trajectories $p_a(P), z_b(P)$ are found that describes the move of every pole/zero over any power within a given range $P \in [P_0, P_{n_p}]$. Also a gain function $K(P)$ is found. These trajectories and this gain function allow to define a 2-dimensional high-level power-scalable BMA:

$$G_{PBMA}(\omega_k+\omega_{LO}, P) = K(P)\frac{\prod_{b=1}^{n_b(P)}(z_k-z_b(P))}{\prod_{a=1}^{n_a(P)}(z_k-p_a(P))} \quad (4)$$

III. EXPERIMENTAL VERIFICATION

In a simulation experiment, a power-scalable model for a mixer is created. The mixer under test has a static nonlinearity in the input and the local oscillator path, and it has a bandpass filter followed by a static nonlinearity in the output path. For this simulated mixer, the power scalable model $G_{PBMA}(\omega_k+\omega_{LO}, P_{val})$ and the BMA $G_{BMA}(\omega_k+\omega_{LO})$ for the same validation input power P_{val} are similar if the variation due to the noise sources is neglected. This indicates that the power scalable model allows to predict the behavior of the mixer under test for any power within the given range of input powers.

IV. REFERENCES

[1] S.A. Maas. *Nonlinear Microwave Circuits*, John Wiley & Sons, Boston, USA, 1988.

[2] K. Vandermot, W. Van Moer, Y. Rolain and R. Pintelon Extending the Best Linear Approximation for Frequency Translating Systems: The Best Mixer Approximation, *IEEE Instrumentation and Measurement Technology Conference Proceedings*, Warsaw, Poland, 2007, pp. 1-6.

[3] R. Pintelon, G. Vandersteen, L. De Locht, Y. Rolain and J. Schoukens. Experimental Characterization of Operational Amplifiers: A System Identification Approach - Part I: Theory and Simulations, *IEEE Transactions on Instrumentation and Measurement*, vol. 53, no. 3, pp. 854-876, June 2004.

Port-Hamiltonian mechanical systems with dynamic extension

D.A. Dirksz
University of Groningen
Fac. of Mathematics &
Natural Sciences
Nijenborgh 4
9747 AG Groningen
The Netherlands
d.a.dirksz@rug.nl

J.M.A. Scherpen
University of Groningen
Fac. of Mathematics &
Natural Sciences
The Netherlands
j.m.a.scherpen@rug.nl

R. Ortega
LSS, SUPELEC
Gif-sur-Yvette
France
romeo.ortega@lss.supelec.nl

Abstract

In [1] a dynamic extension for Euler-Lagrange mechanical systems was presented. The advantage in that case was the possibility of asymptotically stabilizing a system without having to measure velocity. Damping was injected through the designed controller (the dynamic extension). The purpose now is to apply the same idea for port-Hamiltonian systems with an interconnection similar to the one applied in the Euler-Lagrange case. In [2] already a port-Hamiltonian system was interconnected with a port-Hamiltonian controller. In [3] damping injection by dynamic extension was proposed for port-Hamiltonian system. However, velocity measurements were needed in order to realize the interconnection between plant and controller.

Here, we extend this interconnection scheme by considering a controller that depends on both plant coordinates (q) and controller coordinates (q_c). We interconnect the plant and controller without velocity measurements resulting in a different closed loop interconnection matrix than the one showed in [3], which is realized by applying Interconnection and Damping Assignment Passivity-Based Control (IDA-PBC). A different closed loop interconnection matrix is realized since the systems are not interconnected through the ports. Applying IDA-PBC results in a new energy function which is the result of solving some partial differential equations, also called matching conditions [4]. In combination with our dynamic extension we achieve a new energy function that is partially the result of solving the partial differential equations, as presented in [3, 5] and partially selected as in the Euler-Lagrange framework case in [1].

We study the special case of *underactuated* mechanical systems having a constant mass matrix and no physical damping (e.g. friction) in more detail. For these systems the new method described above results in a control signal that does not depend on the velocity $\dot{q}$ to achieve the desired equilibrium points. Asymptotic stability is then achieved by injecting damping through the dynamic extension. This approach results in a control signal achieving the desired equilibrium points and asymptotic stability without the need of velocity measurements, which is advantageous for applications. With some examples it is shown how the idea of a dynamic extension works for port-Hamiltonian mechanical systems.

References

[1] R. Ortega, A. Loria, P.J. Nicklasson, H. Sira-Ramírez, *Passivity-based control of Euler-Lagrange systems: mechanical, electrical and electromechanical applications*, Londen, Springer-Verlag, 1998.

[2] A.J. van der Schaft, Theory of port-Hamiltonian systems, chapter 2, *Network Modeling and Control of Physical Systems, DISC course*, 2005.

[3] R. Ortega, E. García-Canseco, Interconnection and damping assignment passivity based control, *European Journal of Control*, Vol. 10, 432-450, 2004

[4] G. Blankenstein, R. Ortega, A.J. van der Schaft, The matching conditions of controlled Lagrangians and IDA-passivity based control, *International Journal of Control*, Vol. 75, 645-665, 2002.

[5] R. Ortega, A.J. van der Schaft, B. Maschke, G. Escobar, Interconnection and damping assignment passivity-based control of port-controlled Hamiltonian systems, *Automatica*, Vol. 38, 585-596, 2002.

Optimizing the Distance between Isometric Projections of Matrices

Thomas Cason* Pierre-Antoine Absil* Paul Van Dooren*

*Université catholique de Louvain, Department of Mathematical Engineering
Bâtiment Euler, avenue Georges Lemaître 4, B-1348 Louvain-la-Neuve, Belgium
http://www.inma.ucl.ac.be/{∼cason, ∼absil, ∼vandooren}

Let A and B be two matrices respectively of dimension $m \times m$ and $n \times n$. We consider the distance between the *isometric projections* U^*AU and V^*BV, namely

$$f : St(k,m) \times St(k,n) \to \mathbb{R} : \\ (U,V) \mapsto \operatorname{tr}\begin{pmatrix} (U^*AU - V^*BV)^* \\ (U^*AU - V^*BV) \end{pmatrix}, \tag{1}$$

where $St(k,m) = \left\{U \in \mathbb{C}^{m\times k} : U^*U = I_k\right\}$ denotes the *compact Stiefel manifold*.

We are interested in finding extremal values of f. This is an optimization problem of a smooth function defined on a compact domain, and hence there always exists an optimal solution where the first order optimality condition,

$$\operatorname{grad} f(U,V) = 0, \tag{2}$$

is satisfied. For our problem, (2) yields

$$\begin{pmatrix} U \operatorname{Sym}\left(U^*AU\ \Delta_{AB}^* + U^*A^*U\ \Delta_{AB}\right) \\ V \operatorname{Sym}\left(V^*BV\ \Delta_{BA}^* + V^*B^*V\ \Delta_{BA}\right) \end{pmatrix} \\ = \begin{pmatrix} AU\ \Delta_{AB}^* + A^*U\ \Delta_{AB} \\ BV\ \Delta_{BA}^* + B^*V\ \Delta_{BA} \end{pmatrix}, \tag{3}$$

where $\Delta_{AB} := U^*AU - V^*BV =: -\Delta_{BA}$ and $\operatorname{Sym} : X \mapsto (X + X^*)/2$, returns the symmetric part of a square matrix.

If A and B are Hermitian or normal, one can prove that the minimal value for the cost function is simply given by

$$\sum_{i=1}^{k} \min_{\substack{a_i \in [\alpha_i, \alpha_{i-k+n}] \\ b_i \in [\beta_i, \beta_{i-k+n}]}} |a_i - b_i|^2 \ ,$$

where $\alpha_1 \le \alpha_2 \le \cdots \le \alpha_m$ and $\beta_1 \le \beta_2 \le \cdots \le \beta_m$ are the eigenvalues of respectively A and B. In particular, if $a_i \neq b_i$, then equation (3) simply reduces to impose the i^{th} columns of U and V to be eigenvectors of respectively A and B.

For the general case, there is no closed-form expression for the optimizers of (1). One must then resort to iterative algorithms.

To this end, it is useful to note that (1) takes a constant value on the sets

$$[U,V] := \{(W,Z) = (UQ, VQ),\ Q \in O(k)\},$$

where $O(k)$ is the orthogonal group of degree k. We may hence rewrite the original problem in terms of the equivalence class $[U,V]$, and the feasible set simply reduces to the quotient of $\mathcal{M}$ by the orthogonal group:

$$St(k,m) \times St(k,n)/O(k).$$

One can prove that this set presents a manifold structure. We hence further choose to develop iterative optimization algorithms using concepts and formalism of manifold theory; see, *e.g.*, [1]. For instance, *line seach algorithms* consist in iterating from an initial point $(U,V)_0$ on the manifold, through the following steps until convergence.

1. Choose a *tangent vector* to the manifold at iterate $(U,V)_k$ that "indicates" a descent direction for f.
2. "Wind up" that *tangent vector* on the manifold in order to find the next iterate $(U,V)_{k+1}$.

Specific choice of *tangent vector* leads, for instance, to the well known steepest descent methods or conjugate gradient methods.

Finally, one may observe that the optimization problem analyzed in [2] is defined on the same feasible set, and may hence be solved using our numerical algorithms. Moreover, this problem turns out to be similar to ours when $k = m = n$.

References

[1] P.-A. Absil, R. Mahony, and R. Sepulchre. *Optimization Algorithms on Matrix Manifolds*, Princeton University Press, 2008

[2] C. Fraikin, Y. Nesterov, and P. Van Dooren. *Optimizing the Coupling Between Two Isometric Projections of Matrices*, accepted for publication in SIAM J. Matrix Anal. Appl., 2007

Relation between the growth of $\exp(At)$ and $\left((A+I)(A-I)^{-1}\right)^n$

Niels Besseling
Department of Applied Mathematics
University of Twente
P.O. Box 217, 7500 AE Enschede
The Netherlands
Email: n.c.besseling@math.utwente.nl

Hans Zwart
Department of Applied Mathematics
University of Twente
P.O. Box 217, 7500 AE Enschede
The Netherlands
Email: h.j.zwart@math.utwente.nl

1 Introduction

Consider the linear differential equation

$$\dot{x}(t) = Ax(t), \qquad x(0) = x_0 \tag{1}$$

with $x \in \mathbb{R}^n$. A standard way of solving this differential equation is the Crank-Nicolson method. In this method the differential equation (1) is replaced by the difference equation

$$x_d(n+1) = \left(I + \frac{\Delta A}{2}\right)\left(I - \frac{\Delta A}{2}\right)^{-1} x_d(n), \quad x_d(0) = x_0, \tag{2}$$

where Δ is the time step. We denote the matrix $(I + \Delta A/2)(I - \Delta A/2)^{-1}$ by A_d.

If we know that the solutions of the differential equation (1) are exponentially stable, so $\|\exp(At)\| \leq M_1 e^{-\omega t}$, with $\omega > 0$, what can be said about the solutions of the difference equation (2) and $\|A_d^n\|$?

In [2] an estimate is presented in case $A \in \mathbb{R}^{s\times s}$: The solutions of (1) are bounded if and only if the solutions of (2) are bounded:

$$\sup_{t\geq 0} \|e^{At}\| =: M_c$$

if and only if

$$\sup_{n\in N} \|A_d^n\| \leq sM_d,$$

where M_d depends on M_c.

However, if matrices keep getting bigger and bigger, an estimate depending on the dimension is not convenient. Especially if one is also interested in infinite dimensional spaces. Therefore we looked at an estimate, which does not depend on the dimension, but on the power n of matrix A_d.

2 The growth of A_d^n

In [3] the following result is shown:

Theorem 1 *Let A be a matrix, such that*

$$\|\exp(At)\| \leq M_1 e^{-\omega t}, \quad \text{with } \omega > 0 \text{ and } t \geq 0,$$

then there exists a constant $M_2 > 0$, depending on M_1 and ω, such that for all $n \in \mathbb{N}$

$$\|A_d^n\| \leq M_2 \ln(n+1).$$

The proof of [3] uses estimates on resolvents and contour integrals. We present a proof which is based on techniques from system theory. More precisely, we use Lyapunov equations to obtain the estimate.

We remark that this result also holds for a general Hilbert space. So if A is not a matrix but an operator. In this case, one can prove boundedness of A_d^n by posing extra conditions on the inverse or the resolvent of A, see [1], [4], and [5].

References

[1] T.Ya. Azizov, A.I. Barsukov, and A. Dijksma, Decompositions of a Krein space in regular subspaces invariant under a uniformly bounded C_0-semigroup of bicontractions, *Journal of Functional Analysis*, **211**, (2004), 324–354.

[2] J.L.M. van Dorsselaer, J.F.B.M. Kraaijevanger, and M.N. Spijker, Linear stability analysis in the numerical solution of initial value problems, *Acta Numerica*, (1993), 199–237.

[3] A.M. Gomilko, The Cayley transform of the generator of a uniformly bounded C_0-semigroup of operators, *Ukrainian Mathematical Journal*, **56**, no. 8, (2004), 1018-1029 (in Russian). English translation in *Ukrainian Math. J.*, **56**, no. 8, (2004), 1212–1226.

[4] A.M. Gomilko and H. Zwart, The Cayley transform of the generator of a bounded C_0-semigroup, *Semigroup Forum*, **74**, (2007), 140–148.

[5] B.Z. Guo and H. Zwart, On the relation between stability of continuous- and discrete-time evolution equations via the Cayley transform, *Integral Equations and Operator Theory*, **54**, (2006), 349–383.

Structure preserving model reduction of port-Hamiltonian systems

R. Polyuga, A. J. van der Schaft
Institute for Mathematics and Computing Science
University of Groningen
P.O. Box 407, 9700 AK Groningen
The Netherlands
r.polyuga@math.rug.nl

1 Introduction

Port-based network modeling of (lumped-parameter) physical systems leads directly to their representation as port-Hamiltonian systems which are an important class of passive state-space systems. At the same time modeling of physical systems often leads to high-dimensional dynamical models. State-space dimensions are enormously high as well if distributed-parameter models are spatially discretized. Therefore an important issue concerns model reduction of these high-dimensional systems, both for analysis and control. The goal of this work is to show that the specific model reduction techniques of linear port-Hamiltonian systems preserve port-Hamiltonian structure, and, as a consequence, passivity.

2 Model reduction of uncontrollable/unobservable linear port-Hamiltonian systems

It is a well known fact that port-Hamiltonian systems are not only passive but also have a specific natural structure which depends on the total energy or so-called Hamiltonian. Other important issues like interconnection between port-Hamiltonian systems and energy dissipation are also reflected by the port-Hamiltonian structure. General theory on port-Hamiltonian systems can be found in [1]. We will show by applying Kalman decomposition that the reduction of the dynamics of an uncontrollable/unobservable linear port-Hamiltonian system to a dynamics on the reachability/observability subspace preserves the port-Hamiltonian structure. This result holds both for energy and co-energy variable representations of linear port-Hamiltonian systems and it is also shown that the reduced models in the co-energy variable representation take a somewhat ”dual” form to the reduced models obtained in the energy variable representation.

3 Model reduction of general linear port-Hamiltonian systems

Within the systems and control literature a popular and elegant tool for model reduction is balancing. One favorable property of model reduction based on balancing, as compared with other techniques such as modal analysis, is that the approximation of the dynamical system is explicitly based on its input-output properties. Balancing for lossless and passive systems is considered in [2]. Since standard open-loop balancing assumes that the system is asymptotically stable it cannot be directly applied to lossless port-Hamiltonian systems. In order to overcome this difficulty it is useful to switch to scattering representation. We will apply ”Effort constraint” and ”Flow constraint” methods of model reduction to linear port-Hamiltonian systems in scattering representation and show that the reduced-order models inherit properties of the port-Hamiltonian structure.

References

[1] A. J. van der Schaft ”L2-Gain and Passivity Techniques in Nonlinear Control”, Springer, 2000.

[2] A. J. van der Schaft ”Balancing of Lossless and Passive Systems”, Submitted for publication.

Power–based Control of Physical Systems

Eloísa García–Canseco
University of Groningen
Faculty of Mathematics and Natural Sciences
ITM, Nijenborgh 4, 9747 AG Groningen
The Netherlands
Email: E.Garcia.Canseco@rug.nl

Jacquelien M.A. Scherpen
University of Groningen
Faculty of Mathematics and Natural Sciences
ITM, Nijenborgh 4, 9747 AG Groningen
The Netherlands
Email: J.M.A.Scherpen@rug.nl

Romeo Ortega
Laboratoire des Signaux et Systèmes,
SUPELEC, Plateau de Moulon,
91192, Gif-sur-Yvette, cedex,
France
Email: Romeo.Ortega@lss.supelec.fr

Dimitri Jeltsema
Delft Institute of Applied Mathematics
Mathematical Systems Theory Group
Delft University of Technology
Mekelweg 4, 2628 CD Delft The Netherlands
Email: d.jeltsema@tudelft.nl

1 Introduction

It is well known that energy balancing control is stymied by the presence of pervasive dissipation. To overcome this problem in electrical circuits, the alternative paradigm of *power shaping* was introduced in [2]—where, as suggested by its name, stabilization is achieved shaping a function akin to power instead of the energy function. In a previous work [1] we have extend this technique to general nonlinear systems. The method relies on the solution of a PDE, which identifies the open–loop storage function. Despite the intrinsic difficulty of solving PDEs, we show through some physical examples, that the power–shaping methodology yields storage functions corresponding to the system power.

2 Power–Shaping Control

Our main result [1], which we state without the proof, is contained in the following proposition.

Proposition 1 *Consider the general nonlinear system*[1] $\dot{x} = f(x) + g(x)u$, $y = h(x)$, *where* $x \in \mathbb{R}^n$, *and* $u, y \in \mathbb{R}^m$ *are the input and output vectors, respectively. Assume*

A.1 There exist a matrix $\mathbf{Q} : \mathbb{R}^n \to \mathbb{R}^{n\times n}$, $|\mathbf{Q}(x)| \neq 0$, *that*

i) solves the partial differential equation

$$\nabla(\mathbf{Q}(x)f(x)) = [\nabla(\mathbf{Q}(x)f(x))]^\top, \qquad (1)$$

ii) and verifies $\mathbf{Q}(x) + \mathbf{Q}(x)^\top \leq 0$.

A.2 There exist a scalar function $P_a : \mathbb{R}^n \to \mathbb{R}$ *verifying*

iii) $g^\perp(x)\mathbf{Q}^{-1}(x)\nabla P_a = 0$, *where* $g^\perp(x)$ *is a full–rank left annihilator of* $g(x)$,[2] *and*

iv) $x^\star = \arg\min P_d(x)$, *where*

$$P_d(x) := \int [\mathbf{Q}(x)f(x)]^\top dx + P_a(x). \qquad (2)$$

Under these conditions, the control law

$$u = \left[g^\top(x)\mathbf{Q}^\top(x)\mathbf{Q}(x)g(x)\right]^{-1} g^\top(x)\mathbf{Q}^\top(x)\nabla P_a \qquad (3)$$

ensures $x^\star$ *is a (locally) stable equilibrium with Lyapunov function* $P_d(x)$. *Assume, in addition,*

A.3 $x^\star$ *is an isolated minimum of* $P_d(x)$ *and the largest invariant set contained in the set*

$$\{x \in \mathbb{R}^n | \nabla^\top P_d \left[\mathbf{Q}^{-1}(x) + \mathbf{Q}^{-\top}(x)\right] \nabla P_d = 0\}$$

equals $\{x^\star\}$.

Then, the equilibrium is asymptotically stable and an estimate of its domain of attraction is given by the largest bounded level set $\{x \in \mathbb{R}^n \mid P_d(x) \leq c\}$.

3 Examples

To motivate the application of this control technique beyond the realm of electrical circuits, we illustrate the procedure with two academic and practical examples, including the magnetic levitation system and a two–tank system.

[1] All vectors defined in the paper are *column* vectors, even the gradient of a scalar function that we denote with the operator $\nabla = \partial/\partial x$. Also, we use $(\cdot)'$ to denote differentiation for functions of scalar arguments.

[2] That is, $g^\perp(x)g(x) = 0$, and $\text{rank}(g^\perp(x)) = n - m$

References

[1] E. García-Canseco, R. Ortega, J. M. A. Scherpen, and D. Jeltsema. Power shaping control of nonlinear systems: A benchmark example. In *3rd Workshop on Lagrangian and Hamiltonian Methods for Nonlinear Control*, Nagoya, Japan., July 19-21 2006.

[2] R. Ortega, D. Jeltsema, and J.M.A. Scherpen. Power shaping: a new paradigm for stabilization of nonlinear RLC circuits. *IEEE. Trans. on Automatic Control*, 48(10):1762– 1767, October 2003.

Model-based control of hydrodynamics in a bubble column

S. Djordjevic[1], P.M.J. Van den Hof[1], D. Jeltsema[1], R.F. Mudde[2]
[1]Delft Center for Systems and Control
[2]Department of Multiscale Physics
Delft University of Technology
2628 CD Delft, The Netherlands
Email: s.djordjevic@tudelft.nl

1 Introduction

Bubble columns are type of reactors that are frequently used in the chemical industry as absorbers or fermenters for processes which require high contact areas between gas and liquid phases. The current processes operate on models that are balanced in time and assume good mixing and a homogeneous regime over the entire space. However, in many engineering applications the mixing of two or more fluids is essential to obtain good performance for the upstream processes. Inefficient stirring leads to large blowing periods and consequently affects the process economy. Extending the models for fluid motion leads to better productivity and energy consumption. Growing interest in this area resulted in flow control theory, following the steps from linear and nonlinear ODE models. The control of fluid motion has been tackled in many different ways (open-loop and closed-loop system representations, feedback stabilization of linearized Navier-Stokes equation, off-line optimization, Lyapounov-based control etc.) [1], [2]. The channel flow became a standard benchmark for single phase flow control. In this talk, we consider a mathematical model that describes the motion of two fluids (gas and water) in a bubble column using an averaging approach.

2 Problem description

The mixing process in a bubble column is accomplished by injecting gas from the bottom of a vessel in order to accelerate the rates of chemical reactions and to achieve homogenization. The gas injection, as a manipulative variable, influences the gas distribution and motion of both phases in the column. Depending on the gas injection, the operating regime varies over a wide range between two different extreme flows: homogeneous regime (plug flow) and heterogeneous regime (turbulent nature), see Figure 1.

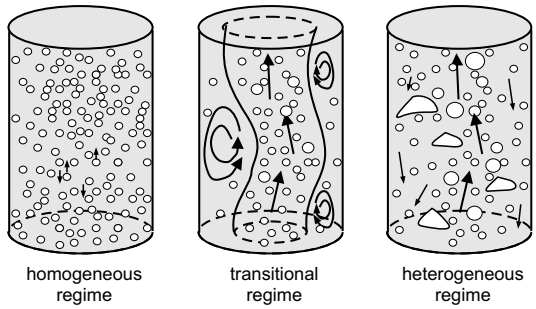

Figure 1: Flow regimes in a bubble column

3 The dynamical model

The mathematical model of the hydrodynamics in a bubble column is derived by averaging the Navier-Stokes equations over an observed space with total volume V using a phase indicator k for the phase distribution α_k, i.e.,

$$V = \sum_{k=1}^{p} V_k, \quad \alpha_k = \frac{V_k}{\sum_{k=1}^{p} V_k}, \quad \sum_{k=1}^{p} \alpha_k = 1,$$

where k is set to 1 for the gas phase and to 2 for the liquid phase [3]. The governing equations can be derived by averaging the fundamental conservation equations for each phase separately and couple them through an interactive term F. This yields the following equations

$$\frac{\partial \alpha_k}{\partial t} + \nabla \cdot (\alpha_k v_k) = 0,$$
$$\frac{\partial \alpha_k v_k}{\partial t} + \nabla \cdot (\alpha_k v_k v_k) = -\frac{\alpha_k}{\rho_k}\nabla p + \frac{1}{\rho_k}\nabla \cdot (\alpha_k \tau_k) + \alpha_k g + (-1)^k \frac{F}{\rho_k},$$

for continuity and momentum, respectively. The system exhibits a highly nonlinear behavior and strong spacial variation. Our goal is to design a boundary controller that stabilizes the homogeneous regime and equalizes the bubble distribution over the observed space ($\nabla \alpha_k = 0$, $\alpha_k \neq 1$).

References

[1] O.M. Aamo and M. Krstic, Flow Control by Feedback, Springer, 2003.

[2] T.R. Bewley, Flow control: New challenges for a new renaissance, *Progress in Aerospace Sciences*, vol. 37, pp. 21-58, 2001.

[3] D.A. Drew, Mathematical modeling of two-phase flow, *Ann. Rev. Fluid Mech.*, vol. 15, pp. 261-291, 1983.

Local and non-steady state actuation in catalytic reactions

Jasper Stolte
TU Eindhoven
J.Stolte@tue.nl

1 Introduction

Most reactions in the process industry are operated under strictly constant temperature assuming ideally mixed conditions. That way the reactor can be assumed to be in thermal equilibrium which simplifies analysis and benefits safety of operation. However, from a control systems perspective relaxing the thermal equilibrium constraint introduces additional degrees of freedom which could be used advantageously. Studies such as [1] and [2] suggest advantageous effects can be found by periodic and local actuation. In this project the transient effects caused by fast local actuation are investigated more closely.

2 Reaction Rate for Fast Local Actuation

When the temperature in a certain volume is constant, the Boltzmann distribution is assumed to apply to the energy of individual molecules. The probability of reaction is largest when two molecules of high energy collide together. By adding energy locally and quickly a spatial variation is introduced in the energy distribution, and it becomes possible to have many high energy molecules together. In this way the chance of reaction can be locally greatly enhanced. In time, the energy will spread throughout the whole volume and thermal equilibrium will be restored in the system. Figure 1 is a simplified representation of the distribution of energy over the molecules. The total energy is the same in both cases, but due to the different distribution the reaction rates will be different.

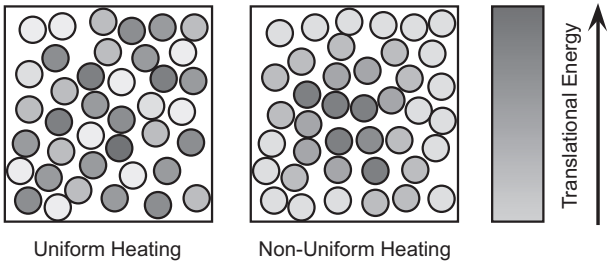

Figure 1: Simplified molecular energy distributions.

3 Control at the Catalyst Site

The focus of this project is on heterogeneous catalytic reations. In this type of reaction there is at least one subreaction for which the surface of the catalyst is the only place where it can take occur. The reaction rate therefore has a naturally occuring spatial dependence. Since the catalyst is typically a solid metallic compound, it allows for actuation by resistive heating or actuation through electromagnetic waves. Energy pulses creating high energy density are applied directly to the catalyst, and not to the bulk material. The reactor could then be modeled as consisting of two volumes, one consisting of all the catalyst particles and their immediate surroundings, and one consisting of the bulk materials. Both volumes are assumed to be ideally mixed. These two volumes are interchanging energy and mass through their shared surface area. Figure 2 shows a graphical representation of the model.

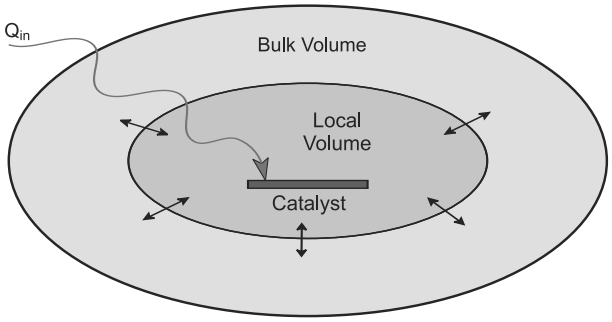

Figure 2: Two compartment model. Energy is applied directly to the catalyst material.

4 Experimental Verification

In process control the models that are available are typically not very accurate or extremely cumbersome. Furthermore some parameter values in the models are unknown, or vary for temperature, gas composition etcetera. Also the traditional models are not designed to model transient phenomena in the time range of interest for this project. Experimental verification of simulation results is therefore very important. Currently a prototype reactor is being designed in cooperation with the surface catalysis group for this purpose. The reactor will allow for heating of the catalyst material with timeconstants in the millisecond range.

References

[1] Bailey, J.E. *Chemical Engineering Communications* **1974**, 1, 111

[2] Wan, J.K.S. *Research on Chemical Intermediates* **1993**, 19, 147

Controlling friction in contact mode atomic force microscopy

Paul Rutten
Delft Center for Systems and Control
Delft University of Technology
Mekelweg 2, 2628 CD Delft
P.E.Rutten@TUDelft.nl

Georg Schitter
Delft Center for Systems and Control
Delft University of Technology
Mekelweg 2, 2628 CD Delft
G.Schitter@TUDelft.nl

1 Introduction

In Atomic Force Microscopy (AFM) a sample's height image with up to atomic resolution is obtained by scanning it with a sharp tip. The force between the tip and the sample is measured using an optical cantilever scheme and is used in a feed back loop to keep the force at a given setpoint, see figure 1 left. The sample topography is obtained by tracking the sample elevation z that is required to maintain the setpoint force.
Despite the fact that there are many operation modes for AFM in general, in ambient environments it can mainly be subdivided in tapping-mode and contact-mode. In tapping-mode the cantilever-tip ensemble is excited at a fixed frequency near or at its free resonance frequency and the oscillation amplitude of the cantilever deflection is used as a feedback parameter for the topographical imaging. In contact mode the tip directly contacts the surface and the cantilever deflection is used for feedback. Due to the direct contact this mode is also capable of measuring friction forces between the sample and the tip by means of the torsional bending of the cantilever as illustrated in figure 1 right [1]. The main differences between the two AFM modes is that the tapping mode is rather slow in imaging speed but handles the sample very gentle, whereas the contact mode can be used for high speed imaging but can destroy delicate samples due to its larger tip-sample friction forces. Here we propose a solution to control and reduce the friction forces in contact mode to enable imaging of fragile samples.

2 proposed solution

A recent experiment showed that friction forces on a sharp tip sliding over an atomically flat surface can be controlled by modulating the normal force acting between the tip and sample [2]. At well defined frequencies corresponding to the resonances of the tip-sample-cantilever system friction is reduced to below the noise level ($\sim 10pN$). We propose to implement this method in a high speed AFM setup to increase the imaging speed for fragile biological samples in the contact mode. In the proposed implementation the cantilever is attached to a dither piezo as illustrated in figure 1 left, that is driven at the tip-sample-cantilever resonance frequency and the fast scanning direction of the sample is set perpendicular to the cantilever to measure the friction force by its torsional bending. The modulation frequency is set higher than the bandwidth of the feedback loop that is tracking the sample topography so that topography measurement is not affected by the modulation signal.
The reduction of friction forces may enable imaging of fragile biological systems and is thus an important step towards observation of dynamic processes on the molecular level.

3 Acknowledgements

This work has been supported by faculty 3mE grant PAL614, the Netherlands Organization for Scientific Research (NWO) Innovational Research Incentives Scheme (VENI DOV.7835), and by the National Institutes of Health under Award RO1 GM 065354-05.

References

[1] R. W. Stark *et al*. Ultramicroscopy **100** 309 (2004)

[2] A. Socoliuc *et al*. Science **313** 207 (2006)

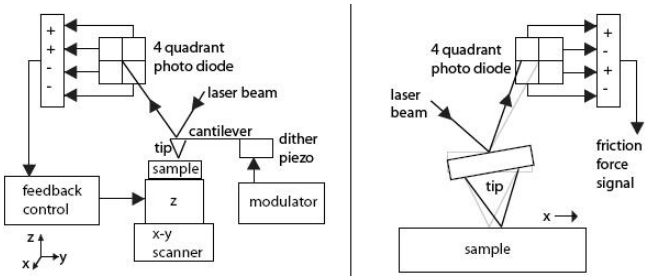

Figure 1: **(left)** Schematic of AFM. The sample is scanned in the x-y plane (fast along the x-axis). The tip contacts the sample and exerts a force on the cantilever bending it over. The cantilever bending alters the path of the laser beam what is detected by the photodiode. The difference between the upper and lower quadrants is the topographic error signal. This signal is fed back through a controller to the sample height actuator 'z' in order to keep the tip-sample force constant. **(right)** Schematic of friction-force microscopy. The sample is moving along the x-axis. Due to the tip-sample friction force the cantilever is twisted. The twisting angle alters the path of the laser beam what is detected by the photodiode. The difference between the left and right quadrants is the friction force signal.

Sensorless damping of a piezoelectric tube scanner

Stefan Kuiper
Delft Center for Systems and Control
Delft University of Technology
stefan.kuiper@tudelft.nl

Georg Schitter
Delft Center for Systems and Control
Delft University of Technology
g.schitter@tudelft.nl

1 Introduction

Scanning probes microscopy (SPM) is an extensively used tool in nanotechnology. Although SPM's are capable of very high precision imaging, one of the major drawbacks is the low imaging speed. As a result, scanning probe microscopy is a very time consuming process taking several minutes per frame[1]. This makes it impossible for a SPM to capture dynamic processes. The goal of this research is to speed up the imaging of SPM's by modern control techniques.

2 Problem description

In SPM, the sample is moved underneath the probe in a raster scan pattern by a piezo driven scanner stage. One of the limiting factors on the speed of the SPM are the mechanical resonances of the scanner stage, which are often weakly damped. One way of increasing the scan speed is to add damping to these resonances. This can be done by use of additional sensors to measure the position of the scanner stage and using this signal for a feedback controller. However, this use of external sensors is expensive and thereby difficult to implement on existing scanner designs. To overcome this use of external sensors, one could make use of the self-sensing capabilities of piezo-electric transducers. Figure 1 shows the basic principle of this method, where the piezo-electric transducer is connected in a bridge circuit along with three capacitors[2]. The voltage measured across the bridge circuit is induced by the strain within the piezo-element. At the mechanical resonances, the deflexion of the scanner stage is drastically increased which results in a measurable voltage across the bridge circuit. By feeding back this signal it is possible to add damping to the mechanical resonances.

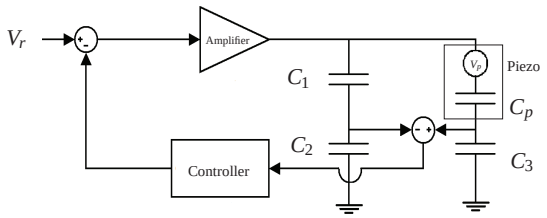

Figure 1: Circuit for sensorless control of piezo actuator. Here, $C_1/C_2 = C_p/C_3$, V_r is the reference voltage and V_p is the voltage induced by the mechanical strain in the piezo.

3 Results

The control scheme of figure 1 is implemented on a commercial piezo-electric tube scanner (E-scanner, Veeco, Santa Barbara, CA, USA). This scanner has its first resonance mode at a frequency of 2800Hz. Figure 2b. shows the open loop tracking performance of this tube scanner on a 260 Hz triangular reference signal, measured with a laser Doppler vibrometer. The oscillation due to the mechanical resonances are clearly visible here. Figure 2c. shows the closed loop tracking performance of the same tube scanner using the proposed control scheme. Here, the oscillations due to the mechanical resonances are significantly reduced. Consequently, it is shown that when using this control method it is possible to make a significant performance increase of existing piezo-electric scanner stages, without the need for additional sensors.

4 Acknowledgement

This work has been supported by faculty 3mE grant PAL614 and by the National Institutes of Health under Award RO1 GM 065354-05. Netherlands Organization for Scientific Research (NWO), Innovational Research Incentives Scheme (VENI DOV.7835).

References

[1] P.K. Hansma, G. Schitter, G.E. Fanters, and C. Prater, *Science 314*, p. 601-602 (2006).

[2] J.J. Dosch, D.J. Inman and E. Garcia, *Journal of Intellegent Material Systems and Structures 1992; 3; 166.*

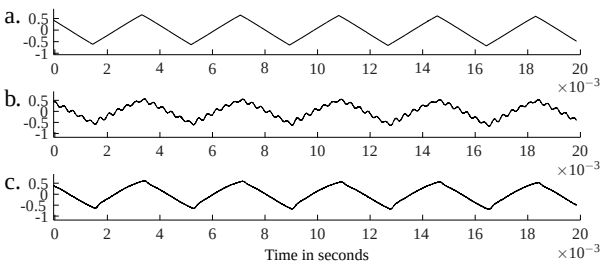

Figure 2: Tracking of a 260 Hz triangular waveform. Reference signal (a.), and tracking position in micrometer of undamped (b.) and controlled (c.) tube scanner.

Real-time Optimal Control of a Seeded Fed-batch Evaporative Crystallizer

Ali Mesbah, Adrie E.M. Huesman and Paul M.J. Van den Hof
Delft Center for Systems and Control, Delft University of Technology
Mekelweg 2, 2628 CD Delft, the Netherlands
E-mail: ali.mesbah@tudelft.nl

1 Introduction

A substantial amount of materials in the pharmaceutical, food and fine chemical processes is produced in crystalline form. Batch crystallization is a key separation and purification unit in such industries, with a significant impact on the efficiency and profitability of the overall process. The control of batch crystallization processes is often a challenging task due to their highly non-linear behavior, plant-model mismatch, irreproducible start-up, unmeasured process disturbances and lack of reliable measurements for the system states. Due to these limitations, the open-loop implementation of the off-line optimized profiles often degrades the effectiveness of the optimal control strategy in real applications. This study aims to reveal that the on-line computation of the optimal operating policy during a batch crystallization process is an effective strategy to cope with such performance deteriorations.

2 Methodology

In this study, the design and real-time implementation of an optimal feedback control strategy on a 75-liter draft tube crystallizer are investigated. The objective is to maximize the crystal growth rate in a fed-batch crystallization of ammonium sulphate to reduce the required batch time and, consequently, increase the total throughput of the crystallizer. The dynamics of the seeded fed-batch crystallization of an ammonium sulphate-water system are modeled by a population balance equation, a solute concentration balance equation and empirical correlations to express the kinetics of the secondary nucleation and the crystal growth rate.

The aforementioned process model is used for the design of a dynamic optimizer based on the simultaneous optimization strategy. The dynamic optimizer is devised to optimize the heat input trajectory in accordance with an objective function corresponding to the maximization of the crystal yield subject to a growth rate constraint. The growth rate constraint is imposed to avoid an irregular growth of crystals that might degrade the product quality. The dynamic optimizer is then embedded in the framework of a feedback system, where an extended Luenberger-type observer [1] is used to estimate the evolution of the supersaturation and, subsequently, soft-sensing the crystal growth rate during the batch crystallization process. The effectiveness of the optimal feedback control strategy is verified by a number of implementations on the 75-liter crystallizer.

3 Results and Perspectives

It is observed that the crystal growth rate effectively follows its maximum admissible value at the optimal heat input profile. Experimental results also demonstrate that the application of the proposed optimal control strategy leads to a substantial increase in the crystal volume fraction at the end of the batch, while the reproducibility of batches with respect to the product crystal size distribution is sustained.

The results are also compared with a preceding study [2] in which the process was represented by a moments model; the optimal profiles are in very good agreement with those obtained in the previous study. Furthermore, it is revealed that lowering the heat input constraint after the initial phase of the batch, when the crystal growth rate is higher than its maximum admissible value, enables the dynamic optimizer to follow the growth rate constraint more closely. This is, however, achieved at the expense of lower overall batch crystal yield.

In future, the process model will be tailored for an 1100-liter draft tube baffle crystallizer such that two fines removal loops are included into the model; the fines removal loops offer an extra degree of freedom to better control the crystal size distribution throughout the batch crystallization process. Subsequently, the process model will be utilized to devise an optimal feedback control strategy similar to that introduced in this work.

References

[1] Kalbasenka, A., J. Landlust, A. Huesman and H. Kramer. Application of observation techniques in a model predictive control framework of fed-batch crystallization of ammonium sulphate. In Proceedings of 5^{th} World Congress on Particle Technology, Vol. 5, 2006.

[2] Mesbah, A., Kalbasenka, A., Huesman, A., Kramer, H., Jansens, P., and Van den Hof, P. Real-time dynamic optimization of crystal yield in fed-batch evaporative crystallization of ammonium sulphate. In Proceedings of 14^{th} International Workshop on Industrial Crystallization, 2007.

Dynamics of Magnetic Electron Lenses

Patrick van Bree
Department of Electrical Engineering
Eindhoven University of Technology
P.O. Box 513, 5600 MB Eindhoven
The Netherlands
Email: p.j.v.bree@tue.nl

1 Magnetic electron lenses

Measurements on an experimental scanning electron microscope (SEM) lens system (immersion-type probe forming lens and vacuum chamber) in combination with first principle models and finite element methods have to provide insight into the dynamic behavior of the lens influenced by phenomena as Eddy currents, a nonlinear B-H curve and hysteresis.

For decades the electron microscope has been used as a manual controlled imaging device. For the next generation of microscopes there is a need for automation and calibration. Static characterization of electron optic elements such as magnetic electron lenses is known in detail. However, to reduce the time involved and to increase reproducibility of lens settings, taking into account dynamics is crucial.

Within a SEM an electron beam is focussed into a fine spot which can be as small as 1nm. The spot size is limited by aberrations of different electron optical components. The area which is scanned is in the order of μm. Magnifications in the order of a few 100,000 times are obtained, [1]. A schematic diagram of a SEM is provided in Figure 1.

The focal distance **f** (1) is related to both the acceleration voltage ($\mathbf{U} \in [0.2, 30]\mathbf{kV}$, [1]) and the magnetic field at the optical axis $\mathbf{B_z}$, [2]. Here e and m represent the charge and mass of an electron.

$$\frac{1}{f} = \frac{e}{8mU} \int B_z^2 dz \qquad (1)$$

Magnetic electron lenses are controlled by the current running through the lens' coil (about 1,000 Ampere turns). The magnetic field ($\mathbf{B} \in [0, 1]\mathbf{T}$) is shaped by the lens-yoke. Stability demands on both current and the magnetic field are in the order of 10 ppm. The yoke-material is selected such that the best steady state results are obtained.

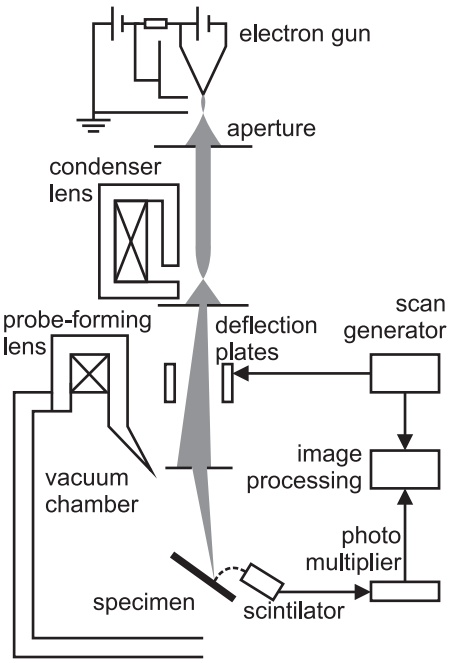

Figure 1: Schematic diagram of a scanning electron microscope.

2 Acknowledgement

This work has been carried out as part of the CONDOR project under the responsibility of the Embedded Systems Institute. This project is partially supported by the Netherlands Ministry of Economic Affairs under the Embedded Systems Institute (BSIK03021) program.

CONDOR is a joint project of a consortium of the Embedded Systems Institute (ESI), industrial (FEI Company, Technolution) and academic partners (Eindhoven University of Technology, Delft University of Technology, Katholieke Universiteit Leuven and University of Antwerp),

References

[1] FEI Company brochure. *"All You Wanted to Know about Electron Microscopy but Didn 't Dare to Ask"*, 2002.

[2] Ludwig Reimer, *"Scanning electron microscopy: physics of image formation and microanalysis"*, Berlin Springer, 1985.

A modular active bearing for noise reduction of rotating machinery

Wim Symens [1], Steven Devos [1], Bert Stallaert [2], Gregory Pinte [1,2], Paul Sas [2], Jan Swevers [2]
[1]Flanders' Mechatronics Technology Center
Celestijnenlaan 300 D, 3001 Heverlee, Belgium
[2]Department of Mechanical Engineering, Division PMA, Katholieke Universiteit Leuven
Celestijnenlaan 300 B, 3001 Heverlee, Belgium
Email: wim.symens@fmtc.be

1 Introduction

Traditionally, active control of structural radiators has approached the problem through integrating sensors and actuators on or into the structure. In such an approach, the goal is to modify the systems response to disturbance, rather than influence the disturbance path to the radiating structure. Many practical issues exist, which ultimately limit the effectiveness of such an approach. A general problem in industry is noise radiation from a structure housing a rotating device, where the rotating device creates the disturbance. We have attacked the problem by seeking to reduce the force transmission in the path rather than the vibration on the radiating surface itself.

2 Implementation and results

A setup on lab scale has been built (Fig. 1), such that in the frequency range of interest, up to 1 kHz, several plate resonances, frame resonances and the shaft resonance show up. Next, a modular active bearing was designed that uses piezo stacks for actuation and both force and acceleration measurements as sensing signals.

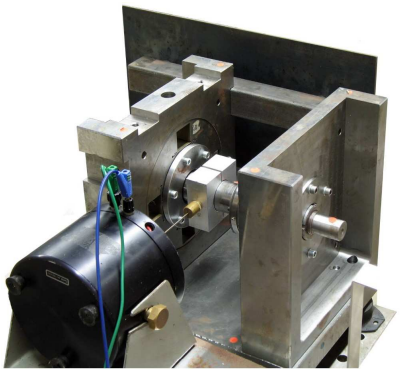

Figure 1: Setup with active bearing

To evaluate different control approaches, a simplified model of the setup was made. Based on simulation results, force feedback control has been implemented, leading to a significant noise reduction above 500 Hz. Because of the periodic nature of the disturbance forces of rotating machinery, a repetitive controller was also implemented and this further reduces the radiated noise. As in the frequency region below 500 Hz, the achievable reduction with the force feedback is limited, a repetitive control using the frame acceleration was implemented. Figure 2 presents the achieved noise reduction using only feedback control and feedback control combined with repetitive control (i.e. hybrid control) in the frequency range of 400-900Hz. This result shows the effectiveness of the selected approach.

In the presentation a general overview of the work conducted will be given. Details on bearing design and controller implementation can be found in [1] and [2] respectively.

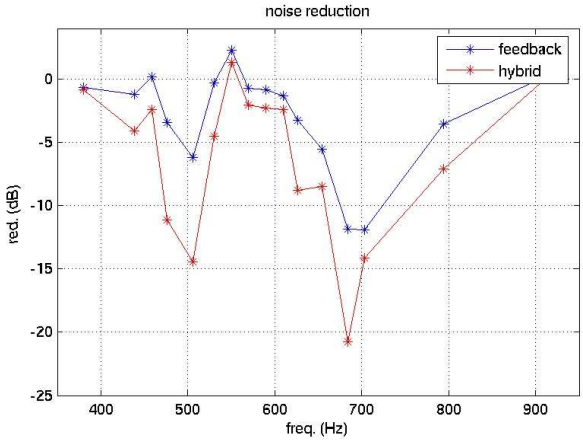

Figure 2: Noise reduction with feedback and hybrid (feedback+repetitive) control

References

[1] B. Stallaert, S.G. Hill, J. Swevers, P. Sas, "Design of active bearings for gearbox noise control," *25th Benelux meeting on systems and control*, Heeze, The Netherlands, 2006.

[2] B. Stallaert, G. Pinte, S. Devos, W. Symens, J. Swevers, P. Sas, "Filtered-X LMS versus repetitive control for active structural acoustic control," *Submitted to 27th Benelux meeting on systems and control*, Heeze, The Netherlands, 2008.

The effect of various disturbance sources on vibration isolation performance [1]

G.W. van der Poel, J. van Dijk, J.B. Jonker and H.M.J.R. Soemers
University of Twente, Laboratory of Mechanical Automation
P.O.Box 217, 7500 AE Enschede, The Netherlands
Email: {g.w.vanderpoel, j.vandijk, j.b.jonker, h.m.j.r.soemers}@utwente.nl

1 Introduction

To achieve the required level of accuracy in high-precision equipment, e.g. photolithography machines or electron microscopes, much effort is put in minimizing the effects of disturbances. Hence, state-of-the-art machines incorporate vibration isolation systems, which aim at rejecting disturbances that emanate from the support structure. For this purpose, the suspension resonance frequencies are designed to be low (typically 1 Hz). However, this may lead to dynamic instability for high center-of-gravity machines. Moreover, the sensitivity to disturbances acting directly on the payload is increased.

Another approach, which is investigated by the authors, is to use a hard mounted payload, i.e. suspension resonance frequencies are in the order of 10 Hz. An active vibration isolation control system must now be used to reject disturbances emanating from the support structure. The controller combines an adaptive feedforward controller with feedback control and requires measurements of the support structure motion and the payload motion.

2 Disturbance sources

Besides the external disturbance sources, e.g. floor vibrations and acoustic noise, additional disturbance sources are introduced by the control system:

- sensor & signal conditioning noise
- ADC noise
- DAC noise
- amplifier & reconstruction filter noise

Due to the nonlinear (adaptive) nature of the feedforward controller, the effects of these disturbance sources should be considered simultaneously. However, for sufficiently large SNR, it is assumed that the disturbance sources only affect the isolation performance, not the adaptation of the feedforward controller. Under this assumption, the isolation performance can be analysed using *dynamic error budgetting*.

Figure 1 shows a block diagram of the complete system and the various disturbance sources. The plant model G incorporates the mechanical system and the sensor and actuator dynamics. The controller consists of a feedback controller C and an adaptive feedforward controller W.

[1] *This research project is sponsored by the Innovation–oriented Research Program (IOP) Precision Technology, which is carried out by SenterNovem by order of the Dutch Ministry of Economic Affairs*

F_e denotes the external disturbances, v_1 denotes the combined DAC, amplifier and reconstruction filter noise, and v_2 denotes the combined sensor, signal conditioning and ADC noise.

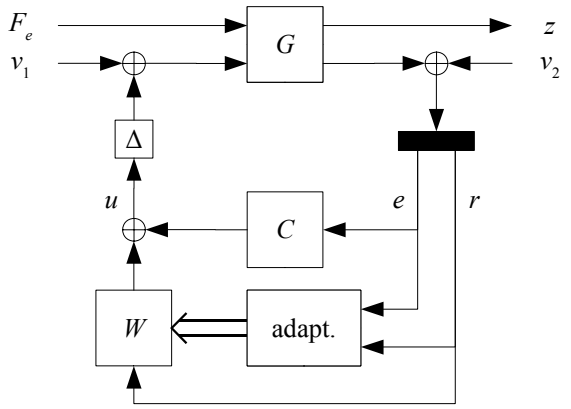

Figure 1: Block diagram of an active vibration isolation system with disturbance sources

The figure also shows the delay Δ due to:

- signal reconstruction
- signal conditioning
- AD- and DA-conversion
- computational delay

This delay can have significant effects on the stability of the feedback loop, as well as on the (high frequency) performance of the feedforward controller.

3 Results & future research

The mentioned disturbance sources and delay are analysed for a laboratory setup of a single directional vibration isolation system. The disturbance sources are characterised from measurements or estimated. The dynamic error analysis is compared to experimental results.

Future research activities will focus on feedback controller (re-)design using robust/optimal control, signal conditioning improvements and reduction of the calculation delay.

6-DOF Electromagnetic Suspension System with Passive Gravity Compensation for Large Load

C. Ding, A.A.H. Damen, P.P.J. van den Bosch
Control Systems, Department of Electrical Engineering
Eindhoven University of Technology
Email: c.ding@tue.nl

Introduction

Vibration isolation is crucial to many areas of accurate positioning applications. For a predefined payload, vibration isolation can be achieved by playing with allocation of the actuators and the system stiffness and damping ratio. Current vibration isolation systems which are designed for large load (in scales of thousand kg), for example, the Air-Mount in the wafer scanner, achieve gravity compensation by means of pumping in high pressure air. However, the working bandwidth of this system is quite narrow. One possible reason is the high frequency dynamics of the high pressure air. Jie Liu and Kefu Liu [1] designed a novel electromagnetic vibration isolation system which is able to isolate vibrations with varying frequencies by means of instantaneous varying the system stiffness. However, it is a 2-DOF system with small payload. A 6-DOF, absolutely contactless vibration isolation system by means of electromagnetic actuators, Gauss-Mount, is proposed to work with large payload and to wider its working frequency band.

Objective

Each of the Gauss-Mount actuators will be able to compensate gravity passively and stable by means of electromagnetic fields. On top of that, there are two integrated Lorentz actuators for the vertical translation and one of the horizontal translations. Three actuators are integrated to suspend a 3000 Kg payload which has 6 DOF controllable and at the meantime reduce the disturbances and resonances with a frequency band of 1 Hz to 50 Hz. The design target is given by the form of transmissibility, plotted in Figure 1.

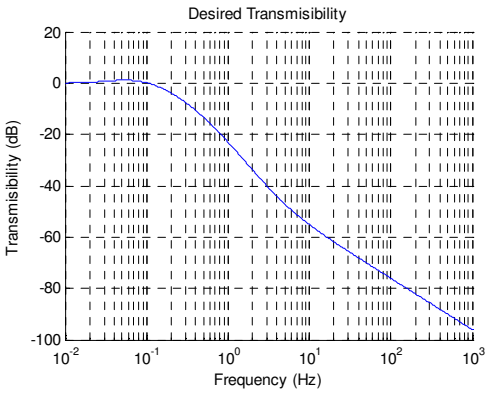

Figure 1

Future Design Work

1. The dependence of system performance and power consumption on placement of the actuators is being investigated by means of modeling.
2. A scaled prototype of Gauss-Mount is planning to be built. A reasonable way of scaling should be found out.
3. The built-in sensor system should be properly designed.
4. The appropriate control structure and the control methods are going to be designed to achieve the desired transmissibility.

Reference

[1] Jie Liu and Kefu Liu. *Journal of Sound and Vibration*, Vol. 295 (2006) 708 – 724

Validation of the series impedance of a quad cable for DSL applications

Wim Foubert, Patrick Boets, Leo Van Biesen, Carine Neus

Vrije Universiteit Brussel, Pleinlaan 2, 1050 Brussels, Belgium
Department of Fundamental Electricity and Instrumentation (ELEC),
Email: wfoubert@vub.ac.be

1 Introduction

DSL technology (‘digital subscriber line’) provides broadband services over the twisted pair copper wires of the existing telephone network. In order to accomplish the ever increasing demand of the user, new techniques are developing. Current DSL systems make only use of differential mode signals (DM), which refers to the electrical voltage difference between two wires. In next generation DSL technologies, the common mode signal (CM) will also be exploited. In this way, the capacity can be three times higher [1]. Figure 1 shows how those signals are defined.

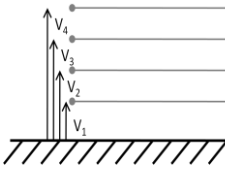

$$DM_1 = V_4 - V_3$$
$$DM_2 = V_2 - V_1$$
$$CM = \frac{(V_1 + V_2) - (V_3 + V_4)}{2}$$

Figure 1: The definition of the DM signals and the CM signal

2 Series Impedance

In order to use also the common mode signal, we need reliable transmission line models which take also this signal into account. The derivation of the new models is based on the multiconductor transmission lines (MTL) theory [2]. Figure 2 shows how a binder with twisted pairs can be modeled.

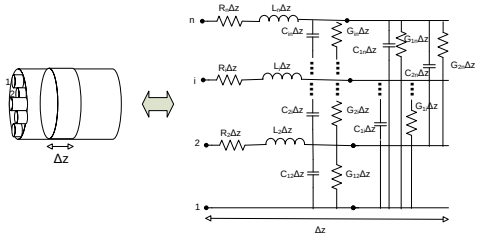

Figure 2: The MTL equivalence for a binder with twisted pairs

For each wire, you need an approximation for the resistance R and the inductance L. These parameters can be found, taking the real and the imaginary part of the series impedance. The exact formula and his derivation can be found in [3]. The impedance is valid for a quad and takes beside the skin effect also the proximity effect into account. However this formula has never been verified in the past. Different setups have been built to validate the series impedance.

3 Measurements

The validation will be done by S_{11}-measurements. Concerning the setup, the length of the multiconductor transmission line is limited because of some practical mechanical problems. This length constraint makes it difficult to measure the one-port quantities because the instrument must operate in a range of just a few decibels due to the limited line attenuation. There are still some other challenges you have to cope with for the validation. Due to the construction constraint there will be calibration errors. Also drift and coupling with the environment makes the validation very difficult.

The setup consists of four small copper wires of 2m surrounded by air. At regular distances, spacers are placed so that the conductors stay parallel over the whole line length. When measuring the S_{11} parameters with an open and a short termination, it’s possible to derive the series impedance. In figure 3, this is compared with the simulated impedance. Because of the above-mentioned problems there is still a difference between the two curves. New measurements will take place to reduce this error.

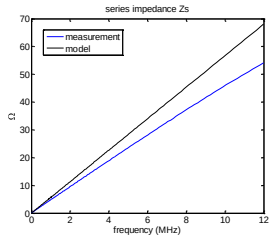

Figure 3: comparison measured and simulated Zc

4 Conclusions

New transmission line models will be set up, using also the common mode signal. This will lead to much faster DSL technology. For the models, we need good approximations for the parameters R and L, which follows from the formula of the series impedance. In this abstract it’s shown how this formula can be validated.

References

[1] T. Magesacher, P. Odling, P. O. Borjesson, T. Nordstrom, "Exploiting the common-mode signal in xDSL", Proceedings EUSIPCO-04, pp. 1217-1220, September 2004, Vienna, Austria.

[2] C.R. Paul, "Analysis of Multiconductor Transmission Lines", John Wiley & Sons, Inc., 1994.

[3] V. Belevitch, Philips Research Reports "Theory of the Proximity effect in multiwire cables", pp. 16-43, 1977

The Open-Loop Linear Quadratic Differential Game for index one Descriptor Systems

Jacob Engwerda
Tilburg University, Dept. of Econometrics and O.R., P.O. Box: 90153, 5000 LE Tilburg
Engwerda@uvt.nl

Salmah
Gadjah Mada University, Dept. of Mathematics, Yogyakarta - 55281, Indonesia
syalmah@yahoo.com

1 Abstract

In this paper (see [3]) we consider the linear quadratic differential game for descriptor systems that have index one. We derive both necessary and sufficient conditions for existence of an open-loop Nash equilibrium.

We consider the problem of two players who like to optimize their performance given by a usual quadratic cost function depending both on the state and control variables. The underlying system is described by a set of differential and algebraic equations of index one. That is, we assume that the dynamics of the game is described by

$$E\dot{x}(t) = Ax(t) + B_1u_1(t) + B_2u_2(t),\ x(0) = x_0,$$

where E, $A \in \mathbb{R}^{(n+r)\times(n+r)}$, $\mathrm{rank}(E) = n$, $B_i \in \mathbb{R}^{(n+r)\times m_i}$ and $u_i \in \mathbb{R}^{m_i}$ are the controls player i can use to manipulate the system. Each player i has a quadratic cost functional J_i given by:

$$\int_0^{t_f} \{x^T(t)\bar{Q}_i x(t) + u_i^T(t)\bar{R}_i u_i(t)\}dt + x^T(t_f)\bar{Q}_{it_f}x(t_f).$$

Here all matrices are constant in time, $\bar{Q}_i = \bar{Q}_i^T$, and $\bar{R}_i$ is positive definite (> 0).

The considered information structure of the game is of the open-loop type. That is, both players only know the initial state and structure of the system, and the set of admissible control actions are functions of time.

Linear quadratic control problems play an important role in applications. Therefore the linear quadratic control problem for descriptor systems has been considered in the literature by various authors too. The theory on the autonomous linear quadratic control problem for descriptor systems is, e.g., well documented in [5]. Here one can find also many references to this literature. Like most approaches for solving the linear quadratic control problem for descriptor systems, in this paper we solve the corresponding game problem by first applying an appropriate transformation to the pencil $\lambda E - A$ (see [4]). Under some additional simplifying assumptions on the system it is possible then to solve the game, for both a finite and infinite planning horizon, using the theory for affine linear quadratic differential games as documented in [1] and [2]. Moreover, conditions are presented that are both necessary and sufficient for the existence of a unique equilibrium.

References

[1] Engwerda J.C., 2005, *Linear Quadratic Dynamic Optimization and Differential Game Theory*, John Wiley & Sons, Chichester.

[2] Engwerda, J.C., 2007, Uniqueness conditions for the affine open-loop linear quadratic differential game. To appear in Automatica.

[3] Engwerda, J.C., and Salmah, The Open-Loop Linear Quadratic Differential Game for index one Descriptor Systems, to appear in Proceedings IFAC WC 2008, Seoul, Korea.

[4] Gantmacher F., 1959, *Theory of Matrices*, vol. I,II. Chelsea: New York.

[5] Mehrmann V.L., *The Autonomous Linear Quadratic Control Problem*. In: Lecture Notes in Control and Information Sciences (Eds. M. Thoma and A. Wyner), Vol.163. Springer-Verlag: Berlin.

Robust Minimax Strategies for the Pursuit-Evasion Game

E. J. Trottemant and C. W. Scherer
Delft Center for Systems and Control
Delft University of Technology
Mekelweg 2, 2628 CD Delft, The Netherlands

1 Abstract

The nature of the interception problem with 2 non-cooperative players namely the interceptor and target, leads to the field of differential games and more specifically to pursuit-evasion games. Traditionally saddle-point strategies are based on a nominal model. However in real-life uncertainties are unavoidable. Introducing a model with uncertainties to the saddle-point strategies will lead to highly reduced performances and/or an overly conservative, computationally intractable problem. Robust programming can be applied to effectively handle the model uncertainties and evader disturbances. The pursuit-evasion problem can be reformulated as a convex optimization problem by using a Lagrange relaxation technique called the S-procedure. The strategy based on the relaxed semi-definite program guarantees a level of performance to the pursuer against all allowable evader disturbances and model uncertainties. The robust minimax strategies are implemented as so-called open-loop feedback policies and guaranteed performances are derived for these strategies.

2 Approach

The objective of this paper is to demonstrate that finite-horizon pursuit-evasion games, with discrete time-variant real-parametric uncertainties, can effectively be solved by using robust programming. The so-called robust minimax strategies will supply an upper bound to the performance of the pursuer and satisfy the imposed constraints. In other words, the robust minimax strategy provides a guaranteed performance to the pursuer against all allowable uncertainties and disturbances. As the main difference with the traditional approaches, we no longer consider saddle-point solutions but rather guaranteed-cost strategies. The problem is furthermore restricted to possible time-variant, set-constrained (box/ellipsoid) control inputs, disturbances and uncertainties.

Since the robust problem with its semi-infinite constraints is hard to solve a Lagrange relaxation technique, namely the S-procedure [3], will be applied. The relaxed problem results in a linear matrix inequality (LMI) and hence a semi-definite program (SDP), which is convex and easy to solve. The price paid for the convexification of the problem is that the relaxation can possibly introduce a relaxation gap and hence lead to a sub-optimal minimax strategy. The derived robust minimax strategies turn out to be rather conservative, even in case of tight relaxations. The conservatism is a consequence of the fact that the robust minimax strategy is designed in open-loop form against all allowable evader disturbances and system uncertainties. The conservatism can be reduced by implementing the robust minimax strategies as open-loop feedback policies (OLFP) [1].

3 Results

This paper will show the influence of these approaches and provide an upperbound to the pursuers performance using a dynamic programming approach. The work presented here is closely related to the PhD work of Lofberg [2]. Adaptations have been made to make this work suitable for the classical pursuit-evasion game formulation. The main differences can be found in the fact that the problem has been reformulated such that a larger range of multipliers, like full-block multipliers [3] can be applied, possible leading to a decrease in the relaxation gap. Furthermore the robust minimax strategies have been implemented as OLFP for the finite-horizon problem. The LMI problem is solved at each time-step, and prediction horizon and problem horizon coincide.

References

[1] Bertsekas, D.P., Dynamic Programming and Optimal Control, Athena Scientific, 2005

[2] Lofberg, J., Minimax approaches to robust model predictive control Linkoping University, 2003

[3] Scherer, C.W., LPV control and full block multipliers, Automatica, 2001, 37, 361-375

H_2 Differential Games with Incomplete and Imperfect Information

Arie Weeren
University of Antwerp
Academic Support - Department ICT
Prinsstraat 13
B-2000 Antwerpen, Belgium
arie.weeren@ua.ac.be

1 Abstract

In this talk we consider differential games with incomplete and imperfect information. Imperfect information relates to the fact that the information we have on the underlying dynamics can not be measured perfectly, i.e. is corrupted by some form of noise. The notion of incomplete information reflects the common fact that we can only observe the dynamic system partially. In the context of linear quadratic differential games we already considered the case of incomplete information (see [1, 2]), where we concluded that it might be more interesting to introduce imperfect information.

The game we consider is a direct generalization of the LQG optimal control problem to a two player differential game. We restrict ourselves in this talk to two-player games, but it should be noted that generalization to the N-player case is straightforward. We avoid the stochastic framework by studying the equivalent H_2 setting. As e.g. explained in [3] the minimization of the H_2 norm of the closed loop transfer matrix can be given the stochastic interpretation of minimizing the expected value of the squared norm of the output in case that the disturbance is a standard white noise process. Although the solution of the LQG optimal control problem was already well-known in the early seventies, the LQG differential game with incomplete and imperfect information is a much harder problem. The LQG optimal control problem has traditionally been solved using the celebrated *separation principle*, which unfortunately does not hold for LQG differential games. We show that it is not very likely that a finite dimensional Nash equilibrium exists under generic conditions, hence we aim for ε-Nash equilibria in a predetermined class of linear dynamic compensators. We formulate an algorithm to calculate these ε-Nash equilibria and discuss the obtained results.

Finally it should be noted that we chose the H_2 norm as a suitable measure to deal with the imperfections, the same approach can be followed for other performance measures like e.g. the H_∞ norm.

References

[1] Engwerda, J.C. and A.J.T.M. Weeren, A result on output feedback linear quadratic control, *Automatica*, volume: 44, no.: 1, 2008

[2] Weeren, A.J.T.M. and J.C. Engwerda, *A Note on Linear Quadratic Optimal Control Problems and Differential Games with Incomplete Information*, working paper University of Antwerp, 2006

[3] Trentelman, H.L., A.A. Stoorvogel and M.L.J. Hautus, *Control Theory for Linear Systems*, Springer Verlag, 2001.

Distributed Design for Linear Quadratic Control

Jean-Charles Delvenne
Université catholique de Louvain
B-1348 Louvain-la-Neuve
Belgium
Email: jean-charles.delvenne@uclouvain.be

Cédric Langbort
University of Illinois
Urbana-Champaign
United States
Email: clangbort@ae.uiuc.edu

1 Abstract

We introduce the notion of distributed design methods, which construct controllers by accessing a plant's description in a constrained manner. We propose performance and information metrics for these design methods, and investigate the connection between closed-loop performance of the best controller they can produce and the amount of exchanged information about the plant. For a class of linear discrete-time, time invariant plants, we show that any communication-less distributed control method results in controllers whose performance is, at least, twice the optimal in the worst-case. We then give a bound on the minimal amount of exchanged information necessary to beat the best communication-less design strategy. We also show that, in the case of continuous-time plants, the worst-case performance of controllers constructed by communication-less design strategies is unbounded.

2 Motivation and results

A lot of literature has been devoted to distributed or decentralised control, where a set of interconnected systems is controlled by a set of controllers interconnected in the same way. Let us consider a (discrete-time or continuous-time) global system described by a square matrix A as a set of interconnected scalar systems. Then a distributed control aims at finding a control matrix K that has the same null entries as A. For instance, if A is tridiagonal, then so should be K. In general, the controller matrix K that minimises some quadratic cost is the solution of a convex optimisation problem (cf. Langbort, Chandra and D'Andrea, 2004.).

Relatively little attention has been paid to controllers *designed in distributed way*, however. Suppose that for every system, the corresponding controller is designed locally, from the knowledge of the local model of the system. We call such a design method *distributed*. If the global system is given by a matrix A then every row of the controller matrix is computed from the corresponding row of the matrix A. If we fix a quadratic cost, we can ask what is the best distributed design method. This requires a notion of "best distributed design method".

Suppose that we have a given discrete-time plant $x_{t+1} = Ax_t + u_t$ with a given initial condition x_0. The optimal static controller, without any constraint on the type of controller, is given by a matrix $u_t = K_{optimal}x_t$, usually computed through a Riccati equation. For a fixed distributed design method, we also find a static controller matrix $K_{distr-design}$. Those two controllers will lead to two costs $J_{optimal}$ and $J_{distr-design}$, functions of the plant and the initial condition. We call the supremum $\frac{J_{optimal}}{J_{distr-design}}$ over the plant A and the initial condition x_0, the *competitive ratio* of the distributed design method. A similar notion was introduced by Manasse, McGeoch and Sleator (1988) in computer science. The competitive ratio is always greater than or equal to one. In this sense, the best distributed design method is the one with the smallest competitive ratio.

Another way to compare two distributed design methods M and N is pointwise comparison of cost functions: M is not worse than N if $J_{distr-designM} \leq J_{distr-designN}$ for all plants and initial conditions. This introduces a partial order on distributed design methods, the minimal elements of which are to be found.

For a given plant A, initial condition x_0 and controller, we consider the quadratic cost $J = \sum_{t\geq 1} \|x_t\|_2^2 + \sum_{t\geq 0} \|u_t\|_2^2$. Our main results are the following.

The deadbeat (i.e., choosing $K = -A$) is a distributed-design with the best possible competitive ratio, equal to 2, and is minimal with respect to pointwise comparison among methods with the same competitive ratio.

We also show that if we allow partial communication between the agents that compute the controller, the communication graph must be weakly connected to do better than the deadbeat. Hence at least $n-1$ messages are required between n agents.

For continuous-plant, we prove that every distributed-design method has an infinite competitive ratio.

Consensus seeking using distributed MPC

Tamás Keviczky
Delft Center for Systems and Control
Delft University of Technology
2628 CD Delft, The Netherlands
Email: t.keviczky@tudelft.nl

Karl Henrik Johansson
Automatic Control Lab
School of Electrical Engineering
Royal Institute of Technology (KTH)
100 44 Stockholm, Sweden
Email: kallej@ee.kth.se

1 Abstract

We study convergence properties of a distributed model predictive control (DMPC) scheme, where agents negotiate to compute an optimal consensus point using an incremental subgradient method based on primal decomposition as described in [1]. The objective of the distributed control strategy is to agree upon and achieve an optimal common output value for a group of agents in the presence of constraints on the agent dynamics using local predictive controllers. Stability analysis using a receding horizon implementation of the distributed optimal consensus scheme is performed. Conditions are given under which convergence can be obtained even if the negotiations do not reach full consensus.

2 Introduction

An important problem that arises among distributed decision-making systems (often called agents), is related to consensus-seeking and rendezvous, which has received a high level of interest in the recent literature [2]. This problem consists of designing distributed control strategies such that the state or output of a group of agents asymptotically converge to a common value, a consensus point, which is agreed upon either a priori or on-the-fly using some negotiation scheme. In this work, we assume that a consensus point is *not fixed in advance*, but is rather determined by an optimal control problem. We focus on the combination of model predictive controllers and subgradient-based negotiation of optimal consensus (along the lines of the work in [1]), and investigate conditions for asymptotic convergence of such distributed control schemes. We propose an algorithm for distributed model predictive consensus, which guarantees convergence under reasonable assumptions given a sufficient number of subgradient iterations can be performed without interruption. We model agents as constrained linear dynamical systems and build on the decentralized negotiation algorithm described in [1] to compute exactly or at least approach the optimal consensus point.

3 Solution approach

The consensus problem is defined as a collection of local finite-time optimization problems, where agents seek to achieve a common terminal output value of their dynamics. The consensus point is an optimization variable as well and agents minimize a quadratic cost penalizing deviations from the state and control equilibrium values corresponding to the chosen consensus point. The solution of this problem is distributed among the agents in [1] using primal decomposition in combination with an incremental subgradient method [3]. Each agent performs individual planning of its trajectory and negotiates with neighbors to find an optimal or near optimal consensus point, before applying a control signal. The optimal control sequence (along with the final consensus point) is constantly updated based on new measurements in a receding horizon fashion.

4 Stability analysis

Stability of such a combination of DMPC and incremental subgradient methods is not a trivial question, especially since the terminal constraint value in the receding horizon scheme is an optimization variable as well. We propose an algorithm that requires the subgradient iterations in subsequent time steps approach the optimal consensus point to an increasingly more accurate level and at the same time the local MPC solutions satisfy an improvement property along the closed-loop evolution of the agents' dynamics. The first requirement ensures that the mismatch between different interrupted terminal point values diminishes as $t \to \infty$. The second requirement is analogous to a standard suboptimal MPC scheme, where feasibility of such an improvement constraint implies stability of the receding horizon control scheme. Based on the convergence analysis of the combined DMPC / optimal consensus approach a sufficient minimum number of subgradient iterations is established.

References

[1] B. Johansson, A. Speranzon, M. Johansson, and K. H. Johansson, "On decentralized negotiation of optimal consensus," *Automatica*, vol. 44, no. 4, Apr. 2008, to appear.

[2] R. Olfati-Saber, J. A. Fax, and R. M. Murray, "Consensus and cooperation in networked multi-agent systems," *Proceedings of the IEEE*, vol. 95, no. 1, pp. 215–233, 2007.

[3] D. P. Bertsekas, A. Nedić, and A. E. Ozdaglar, *Convex Analysis and Optimization*. Athena Scientific, 2003.

Frequency Domain Identification of Linear Slowly Time-Varying Systems

J. Lataire[(1)] R. Pintelon[(1)]

(1) Vrije Universiteit Brussel, Department ELEC, Pleinlaan 2, B-1050 Brussels, Belgium, e-mail: jlataire@vub.ac.be

1. Introduction

The framework of LTI (Linear Time Invariant) systems has been shown to provide good approximating models for a large amount of real-life dynamic systems. However, the assumption of time invariance is not always satisfied for some applications, such as systems with a varying set point (e.g. a moving robot arm) or systems with varying parameters (e.g. pitting corrosion or metal deposition). In this work we model linear, slowly time-varying (LSTV) systems via linear continuous-time models with piece-wise polynomially time-varying coefficients. Contrary to most previous work (e.g. [2] and [3]), the identification is performed in the frequency domain using multisine excitations. The most important advantages are, first, that a lot of non-parametric information and insight is gained from the spectrum of the output signal, next, that a colored non-parametric noise model can easily be used and, finally, that the frequency band of interest is well-defined.

2. Problem statement

In this study the considered systems are assumed to be described by linear ordinary differential equations with coefficients varying piece-wise polynomially as functions of time:

$$\sum_{n=0}^{N_a}\left(\sum_{p=0}^{N_p} a_{n,p}t^p\right)\frac{d^n}{dt^n}y_0(t) = \sum_{n=0}^{N_b}\left(\sum_{p=0}^{N_p} b_{n,p}t^p\right)\frac{d^n}{dt^n}u_0(t) \qquad (1)$$

with u_0 and y_0, respectively, the noiseless in- and output signals. $a_{n,p}$ and $b_{n,p}$ are constants. A motivation for using this class of models is that any linear time-varying (LTV) dynamic system can be approximated by a system with piece-wise polynomial parameters as long as the length of each piece is chosen small w.r.t. the fastest rate of change of the parameters.

When noisy input/output measurements $u(t)$ and $y(t)$ of this system are available, satisfying (subscript 0 refers to the noiseless case)

$$u(t) = u_0(t) + n_u(t) \;,\; y(t) = y_0(t) + n_y(t) \qquad (2)$$

an identification procedure can be set up, involving the minimization of the equation error (the difference of left and right hand side of (1)). Two different approaches are found in the state-of-the-art identification tools for time-varying systems. The first assumes the input to be noiseless and the noise on the output to be white. The second identifies a parametric noise model, simultaneously with the plant model [3]. When working in an errors-in-variables framework, estimates of the (cross-) power spectra of the noise sources $n_u(t)$ and $n_y(t)$ are required. On the other hand, for frequency domain approaches, non-parametric noise models are sufficient, which are easily extracted from the measurements as illustrated in section 3.

Acknowledgement: This work is sponsored by the Fund for Scientific Research (FWO-Vlaanderen), the Flemisch Government (Methusalem: METH1) and the Belgian Federal Government (IUAP VI/4). J. Lataire is on a Ph. D. fellowship from the Research Foundation - Flanders (FWO)

3. Taking advantage of multisine excitations

For linear slowly time-varying systems, the response to a multisine provides information on the speed of variation of the instantaneous frequency response function. This is illustrated in Figure 1 where the output spectrum of an LSTV system excited by a multisine is plotted. The considered system is a second order electronic circuit with a time-varying resonance frequency. In Figure 1 a distinction is made between the excited frequencies (black arrows) - the frequencies where energy is present in the exciting multisine - and the non-excited ones (grey dots). The non-excited frequencies form valleys in-between two excited frequencies. Since they wouldn't be present in the LTI case, they must be due to the time variations. The faster the time variations are, the higher the level of the valleys.

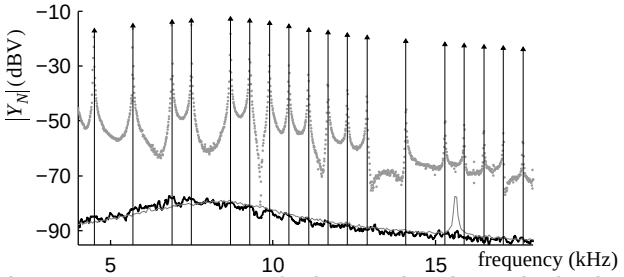

Figure 1. Output spectrum of a time-varying electronic circuit of second order, excited by a multisine. The arrows are the excited frequencies, the grey dots are the non-excited ones. The black and the grey full lines are estimations of the noise power spectra, respectively extracted from one measurement on a time-varying system and from multiple measurements on the same system but with frozen time variations.

When identifying an LSTV system in an errors-in-variables framework an estimation of the noise level is required, which can readily be accomplished by using multisines. As seen in Figure 1, the output signal consists of regions with high Signal-to-Noise Ratio or SNR (in the vicinity of the excited frequencies) and low SNR (in the valleys). In the latter regions, the influence of the deterministic part of the signal can be reduced significantly, leaving only the noise [1]. A non-parametric estimation of the noise power spectrum from one measurement is given by the black full line. It coincides quite well with the noise spectrum estimated using classical tools on the same system but with frozen time variations (given by the full grey line).

4. References

[1] J. Lataire, R. Pintelon - *Frequency Domain Identification of Linear, Deterministically Time-Varying Systems* - internal note.

[2] A.G. Poulimenos, S.D. Fassois - *Parametric time-domain methods for non-stationary random vibration modelling and analysis - A critical survey and comparison* - Mechanical Systems and Signal Processing 20 (2006), pp. 763 - 816.

[3] Fujimori A., Ljung L. (2006) - *Model identification of linear parameter varying aircraft systems* - Proc. IMechE Vol. 220 Part G: JAERO28 - pp. 337 - 346.

Finite Data Performance of Parametric Confidence Regions in Prediction Error Identification using Output Error models: a simulation study

Asbjørn Klomp
Delft Center for Systems and Control
Delft University of Technology
Mekelweg 2, 2628CD Delft
The Netherlands
Email: a.klomp@student.tudelft.nl

A.J. den Dekker, X.J.A. Bombois
P.M.J. van den Hof
Delft Center for Systems and Control
Delft University of Technology
Mekelweg 2, 2628CD Delft
The Netherlands

1 Introduction

A general linear time invariant (LTI) system with a noise corrupted output can be given by the following discrete-time transfer function relation:

$$y(t) = G_0(z)u(t) + e(t)$$

where $u(t)$ and $y(t)$ are the input and output of the system at time t, respectively and where $e(t)$ is a zero mean white noise sequence perturbing the measured output. A system structure as such is known as an Output Error (OE) system. Using the measured dataset of size N

$$Z^N = \{u(1), y(1) \ldots u(N), y(N)\}$$

one usually aims at finding the true system $G_0(z)$. However, as the dataset is noise corrupted the true system can never be found exactly. For estimation of the true system we use prediction error identification methods, being of parametric nature.
As an alternative to an estimate of the true system one can choose to construct a confidence region. This region in the parameter space covers the true system' parameters with a certain predefined probability of $100(1-\alpha)\%$, consequently covering the true system with an equal probability. Controlling the full set of systems described by the parameters inside the confidence region will result in a minimum probability of $100(1-\alpha)\%$ that one can control the true system.

2 Problem Statement

The nowadays used method in system identification and Matlab of parametric confidence region construction is based on several asymptotic expressions. For the **commonly used method**, introduced by Ljung [3], one accepts the use of a Taylor expansion. Convergence of the Taylor expansion is evidently correct for a large dataset, though for lower amounts of data questionable.
The research on ARX models by Den Dekker, Bombois and Van den Hof [1] has been extended by this research to Output Error (OE) models. Monte-Carlo tests on OE systems have yielded that, for low amounts of data, the confidence regions will cover the true system with a significant lower probability then initially specified. Solutions to this problem are yet to be found.

3 Solutions

Multiple alternatives with respect to the commonly used methods of parameter uncertainty bounding have been researched. All presented alternatives have shown to give more reliable confidence regions when using small data sets. From the field of statistics the **Rao test** and the **Likelihood Ratio test** are used to construct confidence regions. Furthermore, the **LSCR method** (Leave-out Sign-dominant Correlation Regions method) by Campi & Weyer [2] has been reviewed for OE model structured systems. The resulting confidence regions have extensively been tested for small amounts of data.
Though the alternatives show more reliable confidence regions, usability problems are present. A dilemma arises for finite sample based OE confidence regions. The uncertainty boundary in the parameter space will either have an exact confidence level or will be well-defined (ellipsoidal) in the parameter space.

This research has been done under supervision of A.J. den Dekker, X.J.A. Bombois and P.M.J. van den Hof.

References

[1] A.J. den Dekker, X.J.A. Bombois, P.M.J. van den Hof, *'Likelihood Based Uncertainty Bounding in prediction error Identification using ARX models: A Simulation Study'*, Proceedings of ECC'07, Kos, Greece, Edited by S. Tzafestas, pp. 2879-2886, 2007

[2] M.C. Campi, E. Weyer, *'Guaranteed Non-asymptotic Confidence Regions in System Identification'*, Automatica, Vol. 41, 10:1751-1764, 2004

[3] L. Ljung, *'System Identification - Theory for the User'*, Second edition, Prentice Hall, Upper Saddle River, NJ, 1999

Model Selection for Short Data Records Using AIC

B. Van der Hasselt, A. de Brauwere, J. Schoukens, R. Pintelon
ELEC - Vrije Universiteit Brussel, Pleinlaan 2, B-1050 Brussels, Belgium
Email: Ben.Van.der.Hasselt@vub.ac.be

1 Introduction

The goal is to select the model that describes 'best' (according to some criterion depending on the intended use of the model) a data record where the number of data is not significantly larger than the number of parameters (=short data record). This is still an open problem for short data records and we will analyse a modification of the AIC (see Table 1) to search for a trustfull prediction.
Any model selection criterion makes a trade off between reducing the systematic errors (complex models) and reducing the noise sensitivity (simple models). The properties of these procedures are well understood if the number of data samples N goes to infinity. The best we can do at this moment for short data records is to give the confidence level of the test.
Assume now that the model parameters $\hat{\theta}$ are obtained by minimizing a nonlinear weighted least squares (WLS) cost function $V_{WLS}(\hat{\theta})$, which decreases with the number of free model parameters n_θ. To avoid overfitting, model selection criteria add a penalty term $p(N,n_\theta)$, which increases with n_θ and where N is the number of observations. The optimal ('best') model is then the one that minimizes $V_{WLS}(\hat{\theta})p(N,n_\theta)$. Formally, the 'best' model should be the best compromise between goodness-of-fit and model variability.

2 Akaike Information Criterion (AIC)

Classically, in the prediction error framework, the AIC rule was presented for cases where the noise model is estimated together with the plant model [2]. It was constructed to perform well for large sample sizes ($n_\theta \ll N$) (see AIC in Table 1).
In [3], one has further modified this model selection criterion in order to improve their performance for short data records ($n_\theta \to N$) (see AIC_S in Table 1). These criteria are designed for the situation that the noise variances are known or priorly estimated.

Name	Expression $V_{WLS}(\hat{\theta})p(N,n_\theta)$	Applicability
AIC	$\frac{V_{WLS}(\hat{\theta})}{N}\left(1+\frac{2n_\theta}{N}\right)$	$n_\theta \ll N$
AIC_S	$\frac{V_{WLS}(\hat{\theta})}{N-n_\theta}\left(1+\frac{2n_\theta}{N-n_\theta}\right)$	$n_\theta \to N$

Table 1

3 Hypothesis Testing Interpretation of AIC_S

Here we combine the improved AIC_S criterion with the hypothesis testing interpretation proposed in [1].
Suppose we want to choose between two models $\mathscr{M}_1$ and $\mathscr{M}_2$ to characterise a certain dataset with N samples. $\mathscr{M}_1$ has n_1 parameters θ_1 and $\mathscr{M}_2$ has n_2 parameters θ_2 with $n_1 < n_2$. We also know that $\mathscr{M}_2$ is the correct model.
Then, for short data records, a modified AIC_S will select model $\mathscr{M}_2$ iff

$$\frac{V_{WLS}(\hat{\theta}_1)}{N-n_1}\left(1+\frac{2n_1}{N-n_1}\right) > \frac{V_{WLS}(\hat{\theta}_2)}{N-n_2}\left(1+\frac{2n_2}{N-n_2}\right). \quad (1)$$

Moreover, $V_{WLS}(\hat{\theta}_2) \approx N-n_2$, because $\mathscr{M}_2$ is the correct model, such that equation (1) can be rewritten as:

$$V_{WLS}(\hat{\theta}_1) > (N-n_1)\left(\frac{1+\frac{2n_2}{N-n_2}}{1+\frac{2n_1}{N-n_1}}\right). \quad (2)$$

$\mathscr{M}_2$ will be selected by a χ^2-test [4] iff the simpler model $\mathscr{M}_1$ is rejected by this χ^2-test:

$$V_{WLS}(\hat{\theta}_1) > \chi^2_{N-n_1,1-\alpha}. \quad (3)$$

Both righthand sides of (2) and (3) can be equated, such that:

$$(N-n_1)\left(\frac{1+\frac{2n_2}{N-n_2}}{1+\frac{2n_1}{N-n_1}}\right) = \chi^2_{N-n_1,1-\alpha}.$$

So, for a given N, n_1 and n_2 we can verify to which significance level an AIC_S model selection corresponds.

References

[1] T. Söderström, P. Stoica (1988) *System Identification*, Prentice Hall, Englewood Cliffs.

[2] L. Ljung (1999) *System Identification: Theory for the User (2nd ed.)*, Prentice Hall, Upper Saddle River.

[3] F. De Ridder, R. Pintelon, J. Schoukens, D.P. Gillikin, Modified AIC and MDL Model Selection Criteria for Short Data Records, *IEEE Trans. on Instrum. and Meas.*, vol. 54, no. 1, pp. 144-150, February 2005.

[4] A. de Brauwere, F. De Ridder, R. Pintelon, M. Elskens, J. Schoukens, W. Baeyens, Model selection through a statistical analysis of the minimum of a weighted least squares cost function, *Elsevier Chemometrics and Intelligent Laboratory Systems*, vol. 76, pp. 163-173, 2005.

Improved FRF measurements in the presence of nonlinear distortions via overlap

Kurt Barbé (kbarbe@vub.ac.be), Rik Pintelon, Laurent Vanbeylen and Johan Schoukens
Vrije Universiteit Brussel, Dept. ELEC, Pleinlaan 2, 1050 Brussel

1 Introduction

All real life systems are to some extent nonlinear. However in many applications a linear system is postulated if the nonlinear distortion is small with respect to the measurement noise, or if the system behaves linearly in the frequency band of interest. In many applications the nonlinear behavior is apparent such that the use of the classical linear identification framework fails. While the behavior of the disturbing noise is well studied for linear systems, [1], [2], [3], the situation becomes more involved for nonlinear systems.
When non-linearities are detected, the user wants to know how large they are with respect to the measurement noise. One way to do this, [4], is by computing the Frequency Response Function (FRF) over different periods of the periodic excitation signal and this for multiple realizations of the input signal. For the excitation signal periodic Gaussian noise or a random phase multisine, [2], is considered, like in the classical case, [4]. The variability of the FRF over the different periods provides the user with an estimate of the level of the measurement noise and the variability of the FRF over the different realizations provides the user with an estimate of the level of the nonlinearities. We propose a method that allows the user

1. to extract the level of nonlinear distortion and the measurement noise
2. a significant reduction in measurement time with respect to the classical method, [4].

2 Main method

For the excitation signal periodic Gaussian noise or a random phase multisine, a sum of harmonically related sines [2], is considered, like in the classical case, [4]. We propose to use two periods and two realizations only to extract the noise characteristics, by computing the FRF over the different periods, [5], [6], and over the different realizations via circular overlap (Figure 1). This method provides the user with a significant reduction in measurement time with respect to the classical method, [4] and a reduction in uncertainty on the estimate of the FRF. The user gets these advantages for free as the main estimation procedure remains unchanged. In Figure 2 a simulation example is shown. The black curve is the estimated FRF, the light gray curves are the level of the nonlinear distortion plus the measurement noise and the dark gray curves are the level of the measurement noise. For the dashed curves circular overlap was used, for the solid curves the classical method, [4], without overlap, was used.

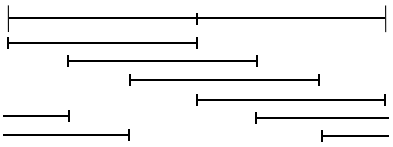

Figure 1: Circular overlap with $2/3$ overlap on two independent periods.

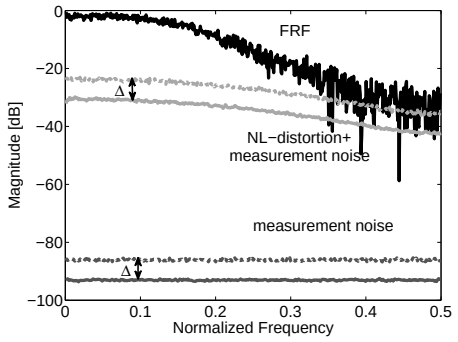

Figure 2: Simulation example on a Wiener nonlinear system, where $\Delta = 6dB$ the gain due to overlap.

3 Conclusion

This allows the user for a specified measurement time to improve the frequency resolution of the FRF or for a specified frequency resolution to reduce the measurement time. The user receives these advantages for free as the estimation procedure remains unchanged.

References

[1] L. Ljung, *Identification of Linear Systems: Theory of the User*. Upper Saddle River (NJ.): Prentice Hall, 1999.

[2] R. Pintelon and J. Schoukens, *System Identification: a Frequency Domain Approach*. Piscataway (NJ.): IEEE Press, 2001.

[3] T. Söderström and P. Stoica, *System Identification*. Prentice Hall, 1989.

[4] R. Pintelon, W. V. Moer, and Y. Rolain, "Identification of linear systems in the presence of nonlinear distortions," *IEEE Transactions on Instrumentation and Measurement*, vol. 50, no. 4, pp. 855–863, 2001.

[5] J. Antoni and J. Schoukens, "A comprehensive study of the bias and variance of frequency-response-function measurements: Optimal window selection and overlapping strategies," *Automatica*, vol. 43, pp. 1723–1736, 2007.

[6] K. Barbé, J. Schoukens, and R. Pintelon, "Frequency domain errors-in-variables estimation of linear dynamic systems using data from overlapping sub-records," *IEEE Transactions on Instrumentation and Measurement*, [Under Review].

This research was funded by a grant of the Flemish Government (GOA-54), Science Policy programming (IUAP VI/4) and the OZR.

Consistent impulse response estimation and system realization

Edwin Reynders and Guido De Roeck
Dept. of Civil Engineering
Katholieke Universiteit Leuven
Kasteelpark Arenberg 40, B-3001 Leuven
Belgium
Email: edwin.reynders@bwk.kuleuven.be

Rik Pintelon
Dept. ELEC
Vrije Universiteit Brussel
Pleinlaan 2, B-1050 Brussels
Belgium
Email: rik.pintelon@vub.ac.be

1 Introduction

An important problem in signal processing and system identification is the nonparametric determination of impulse response matrices. Recent research by Markovsky et al. [1] yielded a new and computationally efficient algorithm for the exact computation of the impulse response directly from noiseless input-output data using arbitrary input signals (the only condition on the input is a persistency of excitation condition). A generalization [2] of this algorithm is presented that it is consistent if the measured output data are prone to noise that is independent from the inputs, which holds for open loop systems. The main application considered is deterministic system realization.

2 Consistent impulse response estimation

Let $\mathscr{H}_{0|2i-1}$ denote the matrix consisting of the impulse response matrices H_k of interest:

$$\mathscr{H}_{0|2i-1} = \begin{bmatrix} H_0{}^T & H_1{}^T & \dots & H_{2i-1}{}^T \end{bmatrix}^T \qquad (1)$$

In [2] it is shown that if (i) the measured inputs can be considered as noise-free, (ii) the considered system is controllable, (iii) the output noise is uncorrelated with the input, and (iv) a persistency of excitation condition on the inputs is satisfied, the following estimate for $\mathscr{H}_{0|2i-1}$ is strongly consistent:

$$\hat{\mathscr{H}}_{0|2i-1} = \mathscr{D}_b \mathscr{D}_a{}^{\dagger} \begin{bmatrix} 0_{m\times m\ell} & I_m & 0_{m\times(2i-1)m+\ell l} \end{bmatrix}^T \qquad (2)$$

where $\mathscr{D}_b$ and $\mathscr{D}_a$ are calculated by projecting Hankel matrices containing measured inputs and outputs on row spaces of Hankel matrices containing measured inputs.

3 Consistent deterministic system realization

Here we deal with the classical realization problem, i.e. to obtain a deterministic state-space model from 'measured' impulse responses. If the algorithm of the previous section is used for the estimation of these responses, the strong consistency of any classical realization algorithm follows since a continuous function and its almost sure limit may be interchanged. The combination of the impulse response estimation algorithm presented above and Kung's realization algorithm will be named IREAR (Impulse Response Estimation And Realization).

4 Numerical experiment

The results of a numerical experiment, described in [2], are briefly and partially presented. The experiment involves the identification of the deterministic part of a system with uncoupled deterministic-stochastic dynamics using four popular subspace identification methods and IREAR. The figure below shows the standard deviation of element $(1,1)$ of the FRF matrix, estimated from 1000 Monte Carlo runs, using 80 block rows in the data block Hankel matrix where all algorithms start from. It can be seen from the figure that IREAR yields statistically the most efficient results. Also computationally IREAR was the most efficient algorithm, needing only half of the CPU time of the other algorithms.

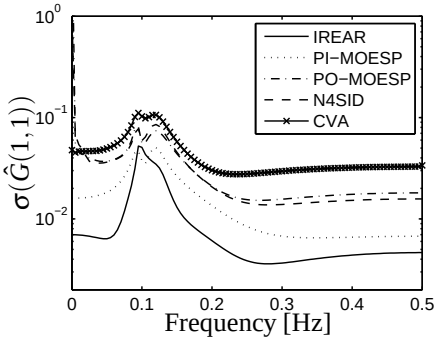

5 Conclusions

An algorithm was presented for the estimation of impulse response matrices in a statistically strongly consistent way. As a result, if this algorithm is combined with a realization algorithm, the latter is also strongly consistent. From the numerical experiment, it is clear that this approach, notwithstanding its conceptual simplicity, yields promising results, especially for the identification of systems with uncoupled deterministic and stochastic dynamics.

References

[1] I. Markovsky, J. Willens, P. Rapisarda, and B. De Moor. Algorithms for deterministic balanced subspace identification. *Automatica*, 41:755–766, 2005.

[2] E. Reynders, R. Pintelon, and G. De Roeck. Consistent impulse response estimation and system realization from noisy data. *IEEE Tr. Sign. Proc.*, Accepted.

Dynamic properties of a canine ventricular cell: model vs. myocyte

J. Heijman[1,2], D.M. Johnson[1], P.G.A. Volders[1], R.L.M. Peeters[2] & R.L. Westra[2]
[1] Dept. Of Cardiology; [2] Dept of Mathematics Maastricht University
P.O. Box 616 6200 MD Maastricht The Netherlands
Email: jordi.heijman@micc.unimaas.nl

1 Introduction

Since the seminal work by Hodgkin and Huxley [1] various computational models have been developed for the simulation of the electrical activation of (heart) cells in numerous species [2]. Mathematically, these models consist in general of a set of nonlinear ordinary differential equations or differential algebraic equations. Typically these models receive a block input that triggers the generation of what is known as an action potential (AP) across the cellular membrane (see Figure 1). These type of models can be used to predict, for

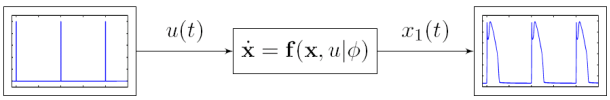

Figure 1: Input, output and mathematical structure of a canine ventricular cell model

example, the electrophysiological effects of pharmacological interventions or congenital conditions [2]. To assess the dynamic behavior and range of these models, the output of the Hund-Rudy dynamic (HRd) ventricular cell model [3] is compared here to the electrical activation of canine ventricular myocytes under an alternative pacing protocol that uses sinusoidal stimuli instead of a block stimulus. The HRd model employs standard forward Euler integration to solve the system of ODEs.

2 Methods & Results

Canine ventricular myocytes were stimulated with a sinusoidal stimulus current: $u(t) = \alpha \cdot \sin(2\pi \cdot \omega \cdot t)$ with various frequencies ω (0.5, 1.0, 2.0 and 5.0 Hz) and amplitudes α $(1.0 \cdot 10^{-2}, 5.0 \cdot 10^{-2}, 1.0 \cdot 10^{-1})$. With these settings, three types of qualitative behavior can be observed experimentally: 1) there is not enough driving force to trigger an AP, the membrane potential oscillates around the resting potential; 2) an AP is triggered when the stimulus reaches a threshold; 3) The stimulus is too large for the cell to respond with a normal AP. The HRd model displays similar types of qualitative behavior.

To quantify the effects of α and ω, the output of the HRd model and the experimental recordings were fit with a single sine function: $v(t) = \alpha' \cdot \sin(2\pi \cdot \omega' \cdot t + \phi') + \beta'$. Figure 2 shows the main input/output characteristics of both types of data. The frequency of the output is completely determined by the frequency of the input ($\omega' = \omega$; not shown). Furthermore, it can be seen that there is a critical threshold in the amplitude of the input that controls the qualitative behavior of the output and the frequency of the input only has effect on the output amplitude above this threshold. Below the threshold, the phase shift ϕ' is approximately half a period, with no influence of amplitude. Although there is a high similarity between the model and the experimental data, it appears that the threshold for AP generation is frequency dependent in canine ventricular myocytes and not in the HRd model.

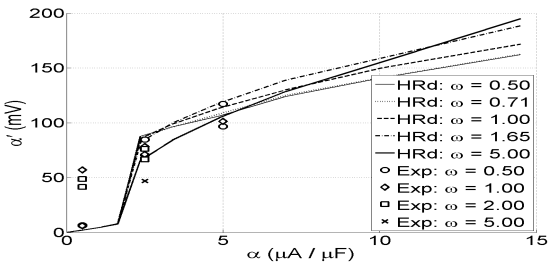

Figure 2: Amplitude dependence of output

3 Conclusions

A close resemblance between model and reality is required if one would like to use a model to make predictions about conditions for which the model is not explicitly designed. Realistic dynamic properties of ventricular cell models are particularly important in 2D or 3D tissue simulations where, for example due to reentry, the stimulation of each cell is more dynamic than in single cell simulations. The presented research shows that the HRd model has the same qualitative behavior as the canine ventricular myocytes. However, further research is still required to make a more detailed quantitative comparison between the model and actual ventricular myocytes.

References

[1] A.L. Hodgkin and A.F. Huxley. 1952. "A quantitative description of membrane current and its application to conduction and excitation in nerve," *J. Physiol.* 117:500-544.

[2] Y. Rudy and J.R. Silva. 2006. "Computational biology in the study of cardiac ion channels and cell electrophysiology." *Q. Rev. Biophysics* 39:57-116.

[3] T.J. Hund and Y. Rudy. 2004. "Rate dependence and regulation of action potential and calcium transient in a canine cardiac ventricular cell model" *Circulation* 110:3168-3174.

Dynamical phenomena in pulse-coupled networks of firing integrators

Alexandre Mauroy, Rodolphe Sepulchre
Departement of Electrical Engineering and Computer Science,
University of Liège, B-4000 Liège, Belgium
Email: alexandre.mauroy@ulg.ac.be, r.sepulchre@ulg.ac.be

1 Introduction

Synchronization and clustering phenomena are omnipresent in nature. They have attracted a lot of attention in the dynamical systems literature. In particular, they have become a topic of growing interest in neuroscience, where they play a key role in the understanding of brain mechanisms and disorders.

We are here interested in an integrate-and-fire model introduced in [2] for the study of pacemaker cells in the heart. This model was later analysed in [1] where it was adapted to neuronal networks. For each neuron, the state variable — the membrane potential — evolution is determined by a differential equation which is linear (LIF model) or quadratic (QIF model). Besides, it is a hybrid model because the potentiel only evolves between two threshold values. When the high threshold level is reached, the variable is reset to the low one.

The coupling between the neurons is impulsive : if a reset occurs, the membrane potential of every connected neurons will be increased by a discrete value. Impulsive coupling applied to the QIF model is an original feature of the present work as literature is poor on the subject. A distinct characteristic of the QIF model is that it allows to study the behaviour of populations including both oscillatory and excitable neurons.

Mirollo and Strogatz [1] introduced a map, the so-called *firing map*, which gives the successive state of all the variables at each firing of any neuron. The characterization of this map, especially its fixed points and their stability, is used to study the global behaviour of the network.

2 Synchronization and clustering behaviour

The main result in [1] is to provide a complete mathematical analysis of synchronization in a network of identical LIF neurons. In the present work, we extend the study to a more general case and show that the LIF model can only exhibit two opposite behaviours : synchronization and clustering. For the second one, it can be proved that there exists a finite number of clustering configurations, all of which are asymptotically stable.

The synchronization behaviour of the model is qualitatively similar to the one studied in the Kuramoto model [3]. In contrast, the clustering behaviour of the present model has no direct analogy in Kuramoto model and seems to offer tractable features of interest.

In case of the QIF model with identical neurons, a simple condition based on the evolution interval of the state variables allows to predict whether the network will synchronize or form clusters. Thanks to this, a strong link between the QIF and LIF models is underlined.

When a distribution in the neuron frequencies is allowed, the system exhibits some noticeable phenomena. In particular, exchanges between the clusters may trigger periodic evolutions characterized by very long periods.

We will report both on prospective simulation results and on preliminary mathematical results.

References

[1] R. E. Mirollo and S. H. Strogatz, *Synchronization of pulse-coupled biological oscillators*, Siam J. Appl. Math., Vol. 50, No. 6, pp. 1645-1662, December 1990

[2] C. S. Peskin, *Mathematical Aspects of Heart Physiology*, Courant Institute of Mathematical Sciences, New York University, New York, pp. 268-278, 1975

[3] Y. Kuramoto, *Int. Symp. on Mathematical Problems in theoretical physics*, edited by H. Araki (Springer New York), Vol. 39 of Lect. N. Phys., pp. 420-422, 1975

Effect of transient response of PID pressure control loop on cascade position control of a pneumatic artificial muscle

Tri Vo-Minh
Email: tri.vominh@student.kuleuven.be
Prof. Herman Ramon
Faculty of Bioscience Engineering
Department of Biosystems (BIOSYST)
KULeuven
Kasteelpark Arenberg 30 - bus 2456, 3001
(Heverlee), Belgium
Email: Herman.Ramon@biw.kuleuven.be

Prof. Hendrik Van Brussel
Faculty of Engineering
Department of Mechanical Engineering
Division of Production Engineering, Machine
Design & Automation (PMA)
Celestijnenlaan 300B, B-3001 Leuven
(Heverlee), Belgium
Tel : (+32)16 32 26 47
Hendrik.VanBrussel@mech.kuleuven.ac.be

1. Introduction

A pneumatic artificial muscle (PAM) or Mckibben pneumatic artificial muscle has some advantages apparently known as high power/weight ratio, variable stiffness and compactness. Those advantages encourage researchers toward applications in humanoid robots. However, air compressibility, hysteresis due to elasticity and dry friction in structural materials of its shell make such muscle difficult to control position accurately. Currently there exist both trends of research interest; one has been dealing with improving muscle models and other dealing with finding new strategies for positioning control. The latter is my interest and one of PAM position control aspects is the regulation of pressure which serves as a system input. In this study, different methods for controlling pressure are investigated and in each method the dynamic response was analyzed. The results were compared and figured out conclusions which help further step in PAM applications.

2. Pressure Regulation Problem

For regulating pressure, a pneumatic proportional directional (PPD) valve with PID (Proportional, Integral, Derivative) controller was used to analyze the dynamic response, and a pneumatic fast switching (PFS) valve with PWM (Pulse Width Modulation) regulator was also used as a counterpart in order to compare and select a good regulation method. The response of PID pressure control loop is limited to the time constant of a given pneumatic system. This constant depends on sonic conductance, critical pressure ratio, upstream/downstream pressure and media volume. The faster response requires a higher loop gain which brings the control valve to maximum flow. The high gain causes control valve to saturation and the inertia of mass flow causes over charge or discharge. This leads to a potential of overshoot in transient state of PID pressure control loop. Tuning parameters for PID controller is always a compromise. However, any potential overshoot in pressure loop will easily amplify in outer loop of a cascade position control. Unlike using PID control method, the PWM regulator gives the means pressure based on a given duty circle. There is no need to amplify in transient response state and therefore the potential overshoot is eliminated.

3. Results and Discussion

The PID pressure regulator using PPD valve is slow response and existing potential overshoot that decreases the stability in cascade position control of a PAM. Using PPD valve for pressure regulation is always put in a closed loop since leakage, dead zone and flow saturation are inevitable. Meanwhile using PFS valve for pressure regulation can not only avoid potential overshoot but also run on an open loop. However, using PFS valve with PWM technique make very noisy, power loss and pressure ripple comparable to those of using PPD valve. The stability of a whole system should be also proved in further study.

ACKNOWLEDGEMENTS

The author gratefully acknowledges the DGDC (Directorate- General for Development Cooperation), from Belgium Government for awarding scholarship and funding this research.

Variable selection for dynamic treatment regimes

Raphael Fonteneau
University of Liège
raphael.fonteneau@ulg.ac.be

Louis Wehenkel
University of Liège
L.Wehenkel@ulg.ac.be

Damien Ernst
University of Liège
dernst@ulg.ac.be

Nowadays, many illnesses as for example HIV/AIDS, cancer or psychological diseases are seen by the medical community as being chronic-like diseases. For treating such diseases, physicians often adopt explicit, operationalized series of decision rules specifying how treatment level and type should vary overtime. These rules are referred to in the medical community as dynamic treatment regime or DTR in short. Designing DTR for such diseases is a challenging issue. Among the difficulties encountered, we can mention the poor compliance to treatments due to the side effects associated to some drugs (e.g., chemotherapies can decrease significantly the quality of life of some patients), the decrease of treatment efficiency with time (e.g., apparition of drug-resistant HIV viruses after several years of treatment) and the enormous cost of administrating drugs to patients over periods ranging sometimes to tens of years. To a large extent DTR are nowadays based on clinical judgment and medical instinct rather than on a formal and systematic data-driven process that could reveal itself to be more efficient. These latter ten years, one has seen the emergence among the biostatistics community of a research field addressing specifically problems of inference of DTR from clinical data. While this research field is still young, encouraging results have already been published. We mention for example [1] where the authors propose such an approach for designing treatments for psychotic patients.

One common approach in biostatistics to infer DTR from the data collected through some (randomized multi-stage) clinical trials is to formalize this inference problem as an optimal control problem for which most of the information available on the 'system dynamics' (the system is here the patient and the input of the system is the treatment) is contained in the clinical data. This problem of inference of (close-to) optimal policies from real-life data has been vastly studied in Reinforcement Learning (RL), a subfield of machine learning (see e.g., [2]). The common approach in RL is to process these data to output closed-loop policies which usually take their values on the clinical indicator space which can be large-dimensional (for example, the clinical data analysed in [1] contain around 60 indicators). Using policies outputted by these RL algorithms as such can thus be non-practical for the physicians who prefer to have DTR based on a few indicators rather than on the large set of variables monitored through the clinical trial. In this research, we address the problem of inference of good policies defined on a small subset of indicators, a problem that we have chosen to refer to as variable selection for policy representation in RL.

The problem of variable selection has already been considered by many authors in the machine learning community but mostly for Supervised Learning (SL). For example, in [3] the authors propose a Bayesian approach for selecting the most informative variables, while decision or regression trees are used in [4]. Only a handful of papers address this problem in the RL context (see e.g., [5]) and mostly for reducing the input space for RL algorithms in order to leverage their generalization capabilities rather than for finding policies defined on a small number of indicators.

Our approach for variable selection is based on a new class of RL algorithms named fitted Q iteration which reformulates the problem of inference of good policies from data as a sequence of supervised learning problems [2]. While not entering into the details, this reformulation of the problem is then exploited by our approach to use state-of-the-art techniques in variable selection in SL for the RL problem. The approach is validated on several examples and the results found are encouraging.

References

[1] S. Murphy, "An experimental design for the development of adaptative treatment strategies," *Statistics in Medicine*, vol. 24, pp. 1455–1481, 2005.

[2] D. Ernst, P. Geurts, and L. Wehenkel, "Tree-based batch mode reinforcement learning," *Journal of Machine Learning Research*, vol. 6, pp. 503–556, 2005.

[3] E. George and R. McCulloch, "Approaches for Bayesian variable selection." *Statistica Sinica*, vol. 7, 2, pp. 339–373, 1997.

[4] C. Strobl, "Variable selection in classification trees based on imprecise probabilities," in *4th International Symposium on Imprecise Probabilities and Their Applications, Pittsburgh, Pennsylvania*, 2005. [Online]. Available: http://www.sipta.org/isipta05/proceedings/022.html

[5] L. Gunter, J. Zhu, and S. Murphy, *Artificial Intelligence in Medicine.* Springer Berlin / Heidelberg, 2007, vol. 4594/2007, ch. Variable Selection for Optimal Decision Making, pp. 149–154.

Relating human lung pathology with non-integer orders model

C.M. Ionescu, R. De Keyser
Department of Electrical energy, Systems and Automation
Ghent University, Technologiepark 913, Gent B9052, Belgium
Email: clara@autoctrl.UGent.be

This paper relates the non-integer orders in a lumped parametric model of input respiratory impedance to lung pathology. The data is obtained with the non-invasive Forced Oscillation Technique (FOT) lung function test [1]. Changes in respiratory mechanics from healthy and chronic obstructive pulmonary disease diagnosed patients are observed from the identified model parameters. The observations show that the proposed model may be used to detect changes in respiratory mechanics and offers a clear-cut separation between the healthy and COPD subject groups. These changes are then related to the pathophysiology of the human lungs in the two groups of subjects.

The mathematical basis of fractional-order models is highly related to fractal geometry and its repetitive / recursive property. A correlation between the model structure and the dichotomous branching in the anatomical structure of the human lung might exist. Research has shown that the choice of a lumped fractional-order model can be correlated with soft tissue viscoelasticity and dissipative effects of mechanical properties [2]. Respiratory system is a quasi-symmetric branching tree with repetitive geometry, leading to recursive relations between mechanical properties in consequent depths (trachea, bronchi, bronchiole,). Empirical studies [3] have shown that the frequency-dependent impedance must comprise two fractional-orders: a derivative and an integral one. The original contribution of this study is the non-integer order model parameter analysis on two groups of subjects with various mechanical properties of respiratory input impedance. The aim of the study was to verify if the parameters are sensitive to the different mechanical properties expected in healthy vs. COPD diagnosed patients. The results show that a clear-cut separation is possible. Furthermore, we relate the interpretation of the model parameters to respiratory mechanics by analyzing phenomena such as energy absorption, damping, elastance (hysteresivity as shown in figure 1) and permittivity (as shown in figure 2).

Results indicate significant differences between healthy and COPD group of subjects in the model parameter values and therefore can give useful information when classification is envisaged. Thanks to the relation to propagation phenomena in electrical networks, insight on mechanical properties is achieved.

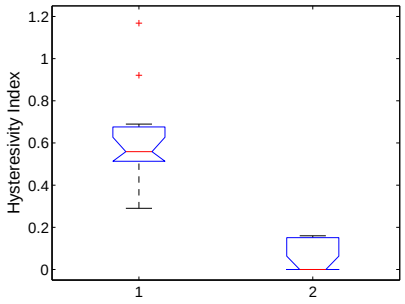

Figure 1: Boxplot for the computed hysteresivity index, in the two groups: 1: COPD and 2: Healthy subjects.

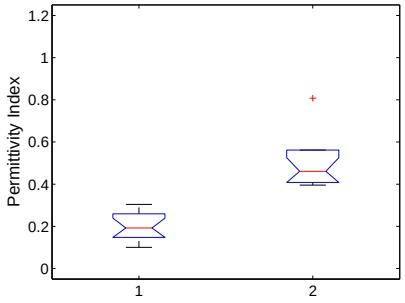

Figure 2: Boxplot for the computed permittivity index, in the two groups: 1: COPD and 2: Healthy subjects.

References

[1] E. Oostveen, D. Macleod, H. Lorino, R. Farré, Z. Hantos, K. Desager, F. Marchal, "The forced oscillation technique in clinical practice: methodology, recommendations and future developments", *Eur Respir J*, **22**, 1026-1041, (2003)

[2] B. Suki, H. Yuan, Q. Zhang, K. Lutchen, "Partitioning of lung tissue response and inhomogeneous airway constriction at the airway opening", *J Appl Phys*, **82**, 1349-1359, (1997)

[3] C.M. Ionescu, R. De Keyser, "On the potential of using fractional-order systems to model the respiratory impedance", *Annals of University of Galati*, Fasc III, 57-62, (2006)

Detection of filamentous bulking problems: evaluation of different modeling/classification approaches

J. Vanlaer, G. Gins, I.Y. Smets and J.F. Van Impe*
BioTeC, Department of Chemical Engineering, Katholieke Universiteit Leuven,
W. de Croylaan 46, B-3001 Leuven, Belgium.
{jef.vanlaer, geert.gins, ilse.smets, jan.vanimpe}@cit.kuleuven.be
* Corresponding author

1 Introduction

To prevent overloading of the natural purification capacity of streams and rivers, the huge amount of wastewater produced daily in modern industry and households, must be treated before discharge. The most widely used system for this purpose is the *activated sludge installation*. In the aeration tank of such installations, the activated sludge, a complex mixture of floc- and filament-forming micro-organisms, digests the organic components in the incoming water. A well-balanced ratio of flocs to filaments is necessary to assure a good separation of clarified water and biomass in the sedimentation tank. An overabundance of filamentous organisms results in an improper sedimentation and, eventually, in loss of treatment capacity. The difficulties in solving these *filamentous bulking* problems have resulted in a search for mathematical models to predict the onset of bulking, lately more and more based on objective image analysis parameters (e.g., [1, 2]). However, bad validation results hamper the development of an early warning tool for bulking sludge.
In this work, *partial least squares* (PLS) black box models to predict the sedimentation properties of the activated sludge starting from image analysis results are constructed and validated using experimental data. In addition, the input scores are used to construct a classification function distinguishing between bulking and non-bulking situations. This classification function is evaluated and compared to a simple linear classifier and a highly nonlinear one, based on a *least squares support vector machine* (LS-SVM).

2 PLS modeling

A dataset originating from four lab-scale experiments and consisting of 200 measurements is used for the training and validation of PLS models. Inputs are normalized and mean-centered before processing. Optimal input combinations and model order are determined using a forward branch-and-bound technique and a ten-fold cross-validation.
The identified models seem unable to accurately describe the sedimentation properties of the sludge in all four experiments and bad validation results are obtained. However, for automated monitoring purposes, correctly distinguishing bulking from non-bulking sludge is more important than the actual prediction of the sedimentation properties.

3 Classifier construction

A classification function based on the input scores of a PLS model is compared to a simple linear classifier and a highly nonlinear LS-SVM-based one. Threshold values are selected based on values of sensitivity and specificity.
All three classifiers achieve a good separation between bulking and non-bulking events. High values of the area under the ROC-curve are obtained, indicating a good classification performance. A double-threshold classification reduces the amount of misclassifications, but introduces an uncertainty area in which no classification can be made. The nonlinear classifier slightly outperforms the other classifiers, but also requires the identification of a higher amount of parameters.

4 Conclusions & future work

In this work, both a black box PLS modeling and a classifier approach are presented to predict the sedimentation properties of activated sludge from image analysis information. The classifiers, that merely distinguish between bulking and non-bulking situations, range from linear to highly nonlinear LS-SVM ones. They all achieve a good separation and outperform the constructed PLS models. The LS-SVM classifier yields slightly better results than the others.
Presently, additional experiments are performed for validation purposes. Future work will consist of validation of the developed classifiers on full scale activated sludge plants.

Acknowledgements. Work supported in part by Projects OT/03/30 and EF/05/006 (Center-of-Excellence Optimization in Engineering) of the Research Council of the Katholieke Universiteit Leuven and the Belgian Program on Interuniversity Poles of Attraction, initiated by the Belgian Federal Science Policy Office. The scientific responsibility is assumed by its authors.

References

[1] A.L. Amaral and E.C. Ferreira. 2005. Activated sludge monitoring of a wastewater treatment plant using image analysis and partial least squares regression. *Analytica Chimica Acta*, 544(1-2):246-253.

[2] I.Y. Smets, E.N. Banadda, J. Deurinck, N. Renders, R. Jenné and J.F. Van Impe. 2006. Dynamic modeling of filamentous bulking in lab-scale activated sludge processes. *Jounal of Process Control*, 16:313-319.

Modelling the temporal evolution of *Drosophila* gene expression

A. Haye
Unit of Genomic and Structural Bioinformatics
ahaye@ulb.ac.be

Y. Dehouck
Unit of Genomic and Structural Bioinformatics
ydehouck@ulb.ac.be

J.-M. Kwasigroch
Unit of Genomic and Structural Bioinformatics
jkwasigr@ulb.ac.be

Ph. Bogaerts
Unit of Biomodelling and Bioprocesses
philippe.bogaerts@ulb.ac.be

M. Rooman
Unit of Genomic and Structural Bioinformatics
mrooman@ulb.ac.be

Université Libre de Bruxelles
Department of General Chemistry and Biosystems
Av. F.-D. Roosevelt 50 C.P. 165/61
B-1050 Brussels

1 Context

The DNA microarray technology allows measuring simultaneously the expression levels of several thousands of genes in a cell sample. Time series, obtained by considering cells at different moments of their development or the development of their host organism, give the possibility to analyze the temporal evolution of gene expression.

2 Main contribution

We studied the gene expression pattern of drosophila, on the basis of a microarray time series involving the expression levels of 4028 genes over 67 time points, covering the embryonic to adult development phases. The genes presenting a similar temporal evolution of their expression levels were clustered together using the Smoothing Spline Clustering method, which led to the definition of a small number of representative classes. To model the network interactions responsible for the dynamic behavior of gene expression, we used a system of linear differential equations with time-invariant coefficients. The parametric estimation of this model is performed in two stages: a first stage of linear parametric estimation allowing the analytical approach to the solution, and a second stage of nonlinear parametric optimization which refines this solution. This model is shown to reproduce the experimental curves with a fairly good precision. Moreover, the application of parameter reduction techniques leads to drop more than 60% of the model's parameters with almost no loss of precision. This result suggests that each gene class influences the transcription of only a few gene classes, and thus that the gene transcription network is sparsely connected.

Hurdles and challenges in parameter estimation for individual based models

A.J. Verhulst[1], A.R. Standaert[1,2], K. Bernaerts[1] and J.F. Van Impe[1]
[1]Chemical and Biochemical Process Technology and Control, Dept. of Chemical Engineering, Katholieke Universiteit Leuven, W. de Croylaan 46, B-3001 Leuven (Belgium)
anke.verhulst@cit.kuleuven.be - jan.vanimpe@cit.kuleuven.be
[2]Current affiliation: Flemish Institute of Technological Research (Vito), Boeretang 200, B-2400 Mol (Belgium)

1 Introduction

Individual based modeling (IbM) is widely applied in a number of disciplines, such as economy, astronomy, and ecology. Recently, IbM has been introduced in the field of predictive microbiology. Predictive microbiology is a scientific discipline that aims to condense mathematical and biological knowledge into models describing microbial growth in a wide range of environmental conditions. Traditionally, microbial growth is modeled from a macroscopic viewpoint by describing the dynamics of a population parameter in function of time. These models are able to predict microbial dynamics under uncomplicated environmental conditions, but fail to provide accurate predictions when more complex situations occur. Individual based modeling considers the individual cell as the modeling unit, circumventing some of these limitations and complementing the traditional approach. Nevertheless, the IbM methodology still lacks a generic set of tools for model analysis.

2 Hurdles and challenges

One of the elements often neglected in IbM studies is the issue of validation and parameter identification with regard to macroscopic, population-level data [1]. This is especially apparent in microbiological applications, where adequate parameter identification techniques would provide a way to estimate experimentally inaccessible cell properties. Parameter estimates are usually derived from independent data or based on educated guesswork. There are several reasons for this. First, the structure of IbM models is often highly non-linear and analytical tools for model analysis are scarce. Second, classical parameter estimation techniques usually require a large number of objective function evaluations, which is not always practical given the duration of individual IbM simulation runs.

The need for parameter identification techniques is emphasized in IbM models of microbiological systems, which often lack knowledge of biological mechanisms governing individual cell behavior. Formal estimation procedures to identify microscopic cell characteristics based on macroscopic experimental data can compensate for this and also provide a basis for the development of experimental measurement techniques for studying individual cells. A clear 1-1 mapping between the microscopic and macroscopic levels will be unlikely as multiple combinations of IbM parameter values can give rise to the same macroscopic behavior. Macroscopic data alone are insufficient in such cases, and additional experimental evidence on cellular mechanisms is required for IbM parameter estimation. The combination of macroscopic and microscopic measurements guarantees that as much information as possible is included in the parameter estimates. This fits into the concept of pattern-oriented modeling, and corresponds with [2] who state that bottom-up models benefit most from including information from different scales and hierarchical levels.

In this presentation, hurdles and challenges in parameter estimation for IbM models are illustrated with examples from predictive microbiology.

3 Acknowledgements

This research is supported in part by OT/03/30 of the Research Council of the Katholieke Universiteit Leuven, the Belgian Program on Interuniversity Poles of Attraction, initiated by the Belgian Federal Science Policy Office and by the K.U.Leuven-BOF EF/05/006 Center-of-Excellence Optimization in Engineering. K. Bernaerts is a Postdoctoral Fellow with the Fund for Scientific Research Flanders (FWO-Vlaanderen).

References

[1] B. LeBaron. Agent-based computational finance: Suggested readings and early research. *Journal of Economic Dynamics and Control*, 24(5-7):679-702, 2000.

[2] V. Grimm, E. Revilla, U. Berger, F. Jeltsch, W.M. Mooij, S.F. Railsback, H.-H. Thulke, J. Weiner, T. Wiegand, and, D.L. DeAngelis. Pattern-oriented modeling of agent-based complex systems: Lessons from ecology. *Science*, 310:987-991, 2005.

Analysis of Nonlinear Software Sensors Applied to Bioprocesses : Particle Filtering and Unscented Kalman Filtering

J. Mailier, G. Goffaux, A. Vande Wouwer
Service d'Automatique
Faculté Polytechnique de Mons
Boulevard Dolez 31, B-7000 Mons
Johan.Mailier, Guillaume.Goffaux, Alain.VandeWouwer@fpms.ac.be

Abstract

Kalman filtering is one of the most popular state estimation methods in process control applications. However, as biochemical process models are nonlinear, the extended Kalman filter requires a first-order linearization along the state estimate trajectory, and convergence is no longer guaranteed, especially with uncertainties on model parameters and measurements.

In recent times, modern state estimation techniques such as particle filtering [1] and unscented Kalman filtering [5, 7], or a combination of both approaches (the unscented particle filter [6]), have been developed in different areas of science and engineering, but have received relatively little attention in bioprocess applications so far [3].

The purpose of this study is to test and compare the performance of these several estimation methods (particle filter, unscented Kalman filter and unscented particle filter) in the context of microalgae cultures operated in chemostat mode. These tests are performed both in simulation, using Droop model [2] and Pawlowski model [4], as well as with real experimental data from continuous cultures of chlorophycae *Dunaliella tertiolecta*. In particular, performance is focused on robustness with respect to uncertainties.

Figure 1: Microalgae cultures in chemostat.

Acknowledgment

This paper presents research results of the Belgian Network DYSCO (Dynamical Systems, Control, and Optimization), funded by the Interuniversity Attraction Poles Programme, initiated by the Belgian State, Science Policy Office. The scientific responsibility rests with its authors.

References

[1] A. Doucet, N. de Freitas, and N. Gordon. *Sequential Monte Carlo Methods in Practice*. Springer-Verlag, New-York, January 2001.

[2] M. Droop. Vitamin B12 and marine ecology IV : The kinetics of uptake growth and inhibition in monochrisis lutheri. *Journal of the Marine Biological Association*, 48(3):689–733, 1968.

[3] G. Goffaux and A. Vande Wouwer. *Bioprocess State Estimation : Some Classical and Less Classical Approaches*, pages 111–128. Control and Observer Design for Nonlinear Finite and Infinite Dimensional Systems. Springer - Verlag Berlin Heidelberg, 2005.

[4] L. Pawlowski, O. Bernard, E. Le Floc'h, and A. Sciandra. Qualitative behaviour of a phytoplankton growth model in a photobioreactor. In *Proceedings of the 15th IFAC World Congress, Barcelona*, 2002.

[5] S. Särkkä. On unscented kalman filtering for state estimation of continuous-time nonlinear systems. *IEEE Transactions On Automatic Control*, 52(9):1631 – 1641, 2007.

[6] R. Van der Merwe, A. Doucet, N. de Freitas, and E. Wan. The unscented particle filter. Technical report, Cambridge University Engineering Department, 2000.

[7] E.A. Wan and R. Van der Merwe. The unscented kalman filter for non-linear estimation. In *Symposium 2001 on Adaptative Systems for Signal Processing, Communications and Control*, Lake Louise, Alberta, Canada, October 2000.

Two-step identification procedure for biological reaction schemes when stoichiometry and kinetics can not be decoupled

V. Vastemans M. Rooman Ph. Bogaerts

Unit of Biomodelling and Bioprocesses
Unit of Genomic and Structural Bioinformatics
Unit of Biomodelling and Bioprocesses
Université Libre de Bruxelles
Department of General Chemistry and Biosystems
Av. F.-D. Roosevelt 50 C.P. 165/61
B-1050 Brussels
vincent.vastemans@ulb.ac.be mrooman@ulb.ac.be philippe.bogaerts@ulb.ac.be

1 Context

Modelling of bioreactor cultures allows the design of control, state observation, and fault detection tools for industrial bioprocesses. The global context of this work aims at proposing original methods for the systematic determination of bioprocess reaction schemes using as little structural knowledge as possible. An existing approach of systematic generation of C-identifiable reaction schemes (whose stoichiometric parameters can be estimated independently of the kinetics) can be extended to non C-identifiable schemes, which make up a much broader structural class of reaction schemes. This requires the definition of a C-identifiable equivalent scheme, and the identification of a projection matrix which allows recovering any reaction scheme from a C-identifiable equivalent one

2 Main contribution

In this context, a 2-step identification procedure is proposed. The first one consists, through some mathematical transformation of the mass balance equations, in determining a first estimation of the kinetic parameters independently of any stoichiometric parameter knowledge. An additional result of this first step is the estimation of the corresponding stoichiometric parameters. As this first step uses estimates of the time derivative of the states (component concentrations), it has to be questioned in a second step. The latter consists in identifying jointly the stoichiometric and kinetic parameters, starting from initial estimates which are the results of the first step and by using only the discrete measurements of the state (and no more time derivatives). This two-step procedure proves to be more robust with regard to errors on the initial estimates of the parameters than direct identification, in one step, of both the projection matrix and the kinetic parameters. A general example is developed, showing clear superiority of the two-step procedure.

Analysis of a Variable Geometry Active Suspension

Willem-Jan Evers[⋆∗], Albert van der Knaap[◇], Igo Besselink[⋆], Henk Nijmeijer[⋆]

[⋆] Eindhoven University of Technology,
Department of Mechanical Engineering,
5600 MB Eindhoven, The Netherlands
Fax: +31 402461418
Email: W.J.E.Evers@tue.nl
Email: I.J.M.Besselink@tue.nl
Email: H.Nijmeijer@tue.nl

[◇] TNO Automotive,
Advanced Chassis and Transport Systems,
5700 AT Helmond, The Netherlands
Fax: +31 4925665666
E-mail: albert.vanderknaap@tno.nl

∗ Corresponding author.

Abstract

The use of actuators in vehicle suspensions is not very common. When looking at passenger cars, it can be seen that the majority uses suspensions with passive spring and damper elements. However, the benefits of active suspension systems over passive systems are clear, [1]. They can be used to both increase the driver comfort and handling behavior of the vehicle.
In this study a model is presented of the variable geometry force actuator as described in [3]. Furthermore, the concept of the variable geometry force actuator is evaluated with respect to power consumption and disturbance reduction properties. Hereto, a comparison is given with a passive spring-damper suspension; a spring-damper suspension with either a hydraulic or electric actuator parallel; and a spring-damper suspension with either a hydraulic or electric actuator in series with the spring. Similar results as those presented here can be obtained using a quarter car model (two mass-spring-damper system). However, a single suspended mass is chosen here for simplicity.

The variable geometry force actuator under consideration is inspired by the *Delft Active Suspension* [4], with the modification that it has a fixed spring [3], see Fig. 1. The benefits of this configuration over the conventional system with rotating spring include a higher achievable bandwidth (due to the lower inertia) and better packaging (more compact system). The actuator uses a spring with stiffness c_a and a certain pre-tension F_s^0. The force within this spring gives rise to a force F_{act} at the end of the wishbone. This is the actuator force, which varies for different values of α and γ. Herein, α can be seen as the suspension deflection and γ is the controlled orientation of the actuator arm with length l_b.

The direction of motion of the electric motor, γ, lies perpendicular to the direction of force. As such, a fictitional cone is created with height h_0 and radius l_b, similar to that obtained by the *Delft Active Suspension* [4]. The advantage of this concept lies in the fact that with a limited amount of power (acceleration of the electric motor) a large actuator force variation can be obtained. However, this only holds as long as the wishbone (with length l) remains horizontal. For any $\alpha \neq 0$ a disturbance moment induced by the spring force acts on the electric motor.

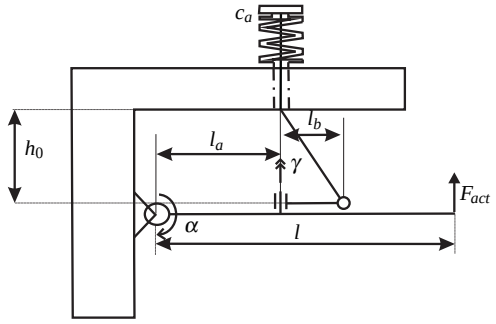

Figure 1: Schematic representation of the variable geometry force actuator.

The (idealized) simulation results, using a skyhook control strategy as proposed in [2] on a stochastic road, show that the performance increase with variable geometry force actuator is about the same as that of the active benchmark systems. However, the peak required power is significantly lower. As such, it is expected that the variable force actuator is (by far) more energy efficient than the active reference systems.

References

[1] Fischer, D. and Isermann, R. ”Mechatronic semi-active and active vehicle suspensions”. *Control Engineering Practice*, 12, pp 1353 – 1367, 2004.

[2] Hrovat, D. ”Survey of advanced suspension developments and related optimal control applications”. *Automatica*, 33(10), pp 1781 – 1817, 1997.

[3] Nederlandse organisatie voor toegepast natuurwetenschappelijk onderzoek TNO, ”Anti-roll/pitch system for use in a vehicle and vehicle equiped with such system”. *International patent, number WO 2006/019298 A1*, February, 2007.

[4] Venhovens, P.J.Th. and Knaap, A.C.M. van der ”Delft Active Suspension (DAS). Background Theory and Physical Realization”. *Smart Vehicles*, ed. Pauwelussen, J.P. and Pacejka, H.B., pp 139 – 165, Taylor & Francis 1995.

Automatic control code generation for mechatronic systems[1]

Ö. Aydın Tekin Robert Babuška Bart De Schutter
Delft Center for Systems and Control, Delft University of Technology
o.a.tekin@tudelft.nl r.babuska@tudelft.nl b@deschutter.info

1 Introduction

Software development for mechatronic machines in industry still suffers from the following problems: lack of integration, lack of verification, lack of automation, and the fact that the physical world of mechatronic systems, irregular situations, and service functions are often insufficiently taken into account. To address these problems, we will develop a set of prototype tools and a framework with which an interdisciplinary product development team can (almost) automatically generate control software for mechatronic machines.

2 New design methodology

Design approaches for mechatronic systems have traditionally been sequential (see Fig. 1, http://zone.ni.com). Possible errors in machine design can then only be detected after the physical prototyping, and it may be really expensive to restart the design from the beginning. Therefore, we will adopt a parallel design approach (see Fig. 2), which will save time and money, decrease the risk of errors in the design phase, and allow to include new prototyping techniques. However, using parallel design methods will require a top level framework to integrate all the separate design phases, since each discipline has its own self-contained design tools. Building such a high-level integration framework and integration of each design phase within this framework will be the main challenge part of this methodology.

Some first steps towards such a high-level integration framework have already been taken. For instance, in [1], a rapid controller prototyping system based on Matlab, Simulink, and the Real-Time Workshop toolbox is presented. Executable code is automatically generated for Linux RTAI which is a hard real-time extension of the Linux Operating System. In [2], a novel object-oriented integration design environment based on UML is used for the integration of a control system tool (Simulink) and a process control notation (IEC 61131-3) within a new control software design environment.

3 Approach

The development of the high-level integration framework and integration of each design phase within this framework will be handled in three parts within a big interdisciplinary development group: one subgroup will be dealing with the main framework, another subgroup will be dealing with the mechatronics design and its integration with the main frame, and we will be dealing with the electronics and control design methods and their integration into the main framework. The resulting prototype will demonstrate generation of control software beginning with functional information defined at a very early stage of the development before having the block diagrams, quantified ladder diagrams, or state transition diagrams. For this, we have to investigate

- model-based representation systems for functional and behavioral modeling,
- model-based qualitative behavior generation system from functional information,
- multiple model management systems.

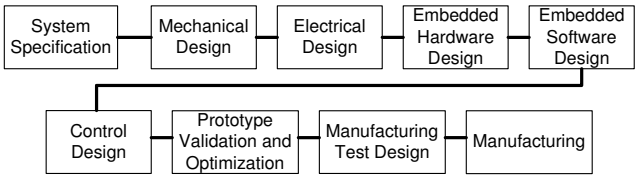

Figure 1: Traditional sequential design approach for mechatronic systems (source: National Instruments).

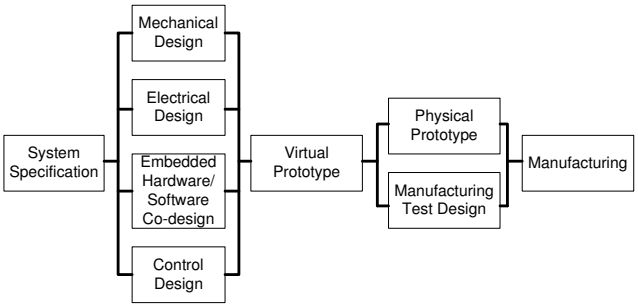

Figure 2: Parallel design approach (source: National Instruments).

References

[1] R. Bucher and S. Balemi, "Rapid controller prototyping with Matlab/Simulink and Linux," *Control Engineering Practice*, vol. 14, pp. 185–192, 2006.

[2] D. N. Ramos-Hernandez, P. J. Fleming, and J. M. Bass, "A novel object-oriented environment for distributed process control systems," *Control Engineering Practice*, vol. 13, pp. 213–230, 2005.

[1] Research supported by the IOP project "Automatic Generation of Control Software for Mechatronic Systems" (IOP IPCR0602A).

A Linear Programming Reformulation of Input Shaping

Lieboud Van den Broeck, Goele Pipeleers, Jan De Caigny, Bram Demeulenaere,
Jan Swevers and Joris De Schutter
Katholieke Universiteit Leuven, Division PMA, Celestijnenlaan 300b, 3001 Heverlee, Belgium
lieboud.vandenbroeck@mech.kuleuven.be

1 Introduction

Input shaping is an established technique to generate prefilters that move flexible mechanical systems with little or no residual vibration. While traditional input shaping design strategies are often analytical, the presented work introduces a design method based on numerical optimization. It is shown that, through a careful selection of the optimization variables, objective function and constraints, it is possible to obtain a linear optimization problem. The presented optimization framework is able to handle higher-order, linear time-invariant dynamic systems, as opposed to traditional input shapers, which are mainly based on second-order systems. Moreover, constraints on input, output and state variables are easily accounted for, as well as robustness against parametric uncertainty.

2 The Linear Programming Framework

The linear programming framework generates a finite impulse response (FIR) filter, which is based on generalizing the zero vibration conditions for second order systems for traditional input shapers as presented in [1]. The generalization is based on the following expression of the output $y(t)$ of a linear time invariant system described by its impulse response $p(t)$:

$$y(t) = r(t) \otimes f(t) \otimes p(t), \tag{1}$$

where $\otimes$ denotes the convolution operator. $f(t)$ and $r(t)$ denote the impulse response of the input shaping prefilter F and the reference trajectory respectively. Hence, if $r(t)$ is constant for $t \geq t_v$, the output $y(t)$ is constant for $t \geq t_K + t_v$, if:

$$f(t) \otimes p(t) = 0 \text{ for } t \geq t_K, \tag{2}$$

This is the desired generalization and the basic zero vibration condition. If the system is known, this can be written as a linear constraint on the filter parameters f.

However, the developed prefilter introduces a move time penalty t_K. By using a bisection-algorithm, the developed framework makes the time penalty introduced by the filter as small as possible.

This basic approach can easily be extended to include robustness (by considering multiple systems), input constraints (by imposing linear constraints on the filter parameters) and output constraints (by imposing linear constraints on the resulting total impulse response). All these extensions can be applied regardless of the order of the system.

3 Validation

The developed framework is validated numerically and experimentally. Benchmark results in [1] and [2] are exactly reproduced.
Experimental results have validated the potential for higher-order systems. Tests on a fifth-order mass-spring-damper-system, show the capability of handling these higher order systems. These tests also show the necessity to include robustness in the prefilterdesign.

4 Acknowledgement

L. Van den Broeck and G. Pipeleers are funded by a Ph.D. fellowship of the Research Foundation - Flanders (FWO - Vlaanderen), while B. Demeulenaere is a Postdoctoral Fellow of the Research Foundation - Flanders. This work benefits from FWO projects G.0446.06 and G.0462.05, K.U.Leuven-BOF EF/05/006 Center-of-Excellence Optimization in Engineering and the Belgian Programme on Interuniversity Attraction Poles, initiated by the Belgian Federal Science Policy Office (DYSCO).

References

[1] N. C. Singer and W. P. Seering. Preshaping command inputs to reduce system vibration. *Transactions of the ASME, Journal of Dynamic Systems, Measurement, and Control*, 112:76–82, 1990.

[2] W.E. Singhose, W. P. Seering, and N.C. Singer. Residual vibration reduction using vector diagrams to generate shaped inputs. *Journal of Dynamic Systems Measurement and Control-Transactions of the Asme*, pages 654–659, 1994.

Non-centralized model predictive control of power networks

A.C.R.M. Damoiseaux, A. Jokic, M. Lazar, P.P.J. van den Bosch
Department of Electrical Engineering
Eindhoven University of Technology
P.O. Box 513, 5600 MB Eindhoven
The Netherlands
Email: a.c.r.m.damoiseaux@student.tue.nl

1 Introduction

Current power networks consist of large scale power generating units and automatic generation control (AGC) is used for real-time control of the system frequency and tie line interchange among control areas in the system. However, there is a strong tendency to implement an increasing amount of decentralized power generating units and to liberalize power markets. Distributed generation introduces uncertainties and therefore complicates control. Large unpredictable power fluctuations from renewable energy sources, e.g. wind power, require efficient and fast acting controllers.

2 Model Predictive Control

Recently, it was observed that model predictive control (MPC) has a potential for solving the above mentioned problems that will appear in future electrical power networks. The reason for this lies in the capability of MPC to guarantee optimality with respect to a desired performance objective, while explicitly taking constraints into account. Furthermore, MPC allows the usage of disturbance models which can be employed to counteract the uncertainties introduced by renewable energy sources.

Nevertheless, the fact that model predictive control is a global centralized control technique is a considerable drawback when power system control is considered. Centralized control implies that a single controller is able to perform the following sequence of operations within a time sample: measure all outputs of the system, compute an optimal control action and apply this control action to all actuators in the power system. As power networks are large scale systems, computationally as well as geographically, it is practically impossible to implement a centralized MPC controller.

3 Non-centralized Model Predictive Control

The problems of centralized MPC for control of power networks is one of the reasons for which the non-centralized formulation and implementation of MPC receives more and more interest. Roughly speaking, non-centralized MPC schemes can be divided into two categories: decentralized techniques, where there is no communication in between different controllers, and distributed techniques, where communication between different controllers is allowed. Furthermore, distributed MPC techniques can be categorized as techniques that require communication with all the controllers in the network and techniques that require communication solely with directly neighboring controllers.

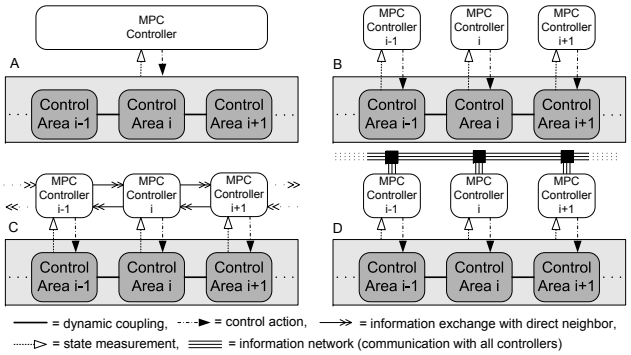

Figure 1: A schematic representation of: Centralized MPC (A), Decentralized MPC (B), Distributed MPC with communication with solely neighbors (C), Distributed MPC with communication with all subsystems (D).

In this talk, three non-centralized MPC techniques [1,2,3] are investigated and the suitability for use in power networks is critically assessed with respect to relevant characteristics: performance of the closed loop system, the extent of decentralization, and the computational complexity. Furthermore, important issues such as feasibility, convergence and stability are addressed.

References

[1] A.N. Venkat, "Distributed Model Predictive Control: Theory and applications," Ph.D. dissertation, University of Wisconsin-Madison, Wisconsin Madison, 2006.

[2] A. Alessio, A. Bemporad, "Decentralized model predictive control of constrained linear systems," in Proceedings European Control Conference, Kos, Greece, 2007, pp.2813-2818.

[3] E. Camponogara, D. Jia, B.H. Krogh, and S. Talukdar "Distributed model predicitve control," IEEE Control Systems Magazine, vol 22, no. 1, pp. 44-52, 2002.

A rare-event approach for analyzing power system reliability

Florence Belmudes
University of Liège
Florence.Belmudes@ulg.ac.be

Damien Ernst
University of Liège
dernst@ulg.ac.be

Louis Wehenkel
University of Liège
L.Wehenkel@ulg.ac.be

Blackouts in power systems are rare, but they have such tremendous societal consequences that decreasing their likelihood of occurrence is of paramount importance. It is of common use among the Transmission System Operators (TSOs) to design and operate their systems to make them robust with respect to some events such as the sudden loss of transmission elements, short-circuits, fast variations in the generation patterns, etc. The events they consider in their studies, or the combination of events, have in general a probability of occurrence high enough to be judged as being likely to occur. On a reliability point of view, the motivation behind their approach to design and to operate power systems is twofold. First, by focusing on the events that are the most likely to occur they can reduce the complexity that would otherwise be associated with studying a much larger set of events. Second, they assume that by making the system robust with respect to the selected events, they will automatically ensure the reliability of their system for many other events which have not been taken into account in their analysis.

The increasing rates of blackouts observed over the last ten years may however question whether such an approach for assessing the security of a power system is still relevant. The main goal of this research is to show the weaknesses of these approaches, especially when facing complex systems, and to propose a general framework, to identify in a "right way" the events that should be considered by the TSOs in their stability studies. Before developing further the motivation behind this new approach, we remind here the causes of two major blackouts that have happened recently. One is the August 14th, 2003 blackout that has plunged the North-East part of the USA in the dark for several hours and the other is the November 4th, 2006 which has affected West Germany as well as some areas in France and Belgium. As for the first aforementioned blackout, the event having lead to the collapse of the system is the following. First, some transmission lines have been lost due to some poor vegetation management under the lines. Second, this information has not been correctly displayed on the screen of an operator, who did not take appropriate actions. And then, the failure for other dispatchers to response adequately to this dangerous situation lead to a sequence of cascading failures causing a major blackout [1]. The event behind the German blackout was from another but still puzzling nature. In order to allow a boat to cross a river, a transmission line above the river had to be switched off. A system operator gave the green light for carrying this manoeuvre though the load on the power network at the time of the manoeuvre had significantly increased with respect to the load at the time at which the stability study took place. When the line was disconnected, several lines became saturated and, because of insufficiently accurate stability studies, a local change in the electrical operating topology triggered many line trippings in Germany and in neighbouring countries, splitting the European network into three unconnected areas [2].

It is intriguing to observe that the two events having lead to these major blackouts have really an "unfortunate nature". Their probability of inception is indeed extremely low, which is also why the TSOs did not consider them in their stability studies. Actually, our main motivation behind the newly developed approach in this paper is that the power system integrity is not nowadays mainly jeopardized by some high-probability events but by the multitude of (extremely) low-probability ones whose degree of severity is not necessarily correlated to the degree of severity of the high-probability events which are studied by the TSOs. The continual increase in complexity in power systems (e.g., new interconnections, coupling of the grid with the gas transmission system and market platforms) generates also new low-probability dangerous events which will make current practices for studying power system reliability more irrelevant.

Our new approach for power system analysis will not, as it is currently the case, focus on high probability events as candidate interesting ones for stability studies. It will rather identify in an efficient manner (at least on a computational point of view), within an a priori defined extremely large set of events, those which have the potential to endanger the integrity of the system and give also some good estimates of reliability indices. The approach is based on a reformulation of the problem of assessing the reliability of a power sytem as a rare-event problem, which is then solved by using cross-entropy based techniques [3].

References

[1] H. Laffaye, "Les Blackouts Récents : Enseignements et Expérience RTE," RTE, Tech. Rep., 2004.

[2] "Final Report, System Disturbance on 4 November 2006," UCTE, Tech. Rep., 2007.

[3] R. Rubinstein and D. Kroese, *The Cross-Entropy Method : a Unified Approach to Combinatorial Optimisation, Monte-Carlo Simulation and Machine Learning*. Springer, 2004.

Global Aerodynamic Modeling with Multivariate Splines

C.C. de Visser, J.A. Mulder, Q.P. Chu
Devision of Control and Simulation
Faculty of Aerospace Engineering
Delft University of Technology
2600 GB Delft
The Netherlands
Email: c.c.devisser@tudelft.nl

1 Introduction

Detailed aerodynamic models play a crucial role in modern flight control law designs based on nonlinear dynamic inversion or feedback linearization [1]. These aerodynamic models are implemented either in the form of lookup tables or in the form of polynomial models. Lookup tables hold numerical data based upon which the force and moment coefficients are reconstructed. Lookup tables are used mostly in high performance (fighter) aircraft with large flight envelopes and non-linear aerodynamic characteristics. An inherent limitation of a lookup table is its finite resolution, which means that some interpolation scheme must always be used to interpolate between table values. Polynomial models are used in aircraft with a more linear aerodynamic behavior. The polynomial model is obtained by performing a Taylor series expansion around some linearization point. The polynomial model is therefore valid only in a small region around the linearization point. We present a new method for global aerodynamic modeling using multivariate (i.e. multidimensional) spline functions. The multivariate spline functions make it possible to create a phenomenological model of aircraft aerodynamics from an aerodynamic data set that is based on wind tunnel and flight test data. A phenomenological model requires no a-priori model structure; it simply fits the aerodynamic data set in some optimal way. In theory this can lead to the modeling of 'false' dynamics such as measurement biases and sensor artifacts. Current practice in state estimation techniques however, produce estimated aircraft states that are of such a high quality that state estimation errors may assumed to be negligible [2].

2 Multivariate Simplex B-splines

The idea of using multivariate splines for the modeling of aircraft aerodynamics is not new. In the past multivariate tensor product B-splines were used for global aerodynamic modeling, although their application was limited to the bivariate case [4]. Our method is new in the sense that we use multivariate simplex B-splines together with a transparent multivariate spline scheme to model aerodynamic data sets created from wind tunnel or flight test data. Simplex B-splines are spline functions that are defined locally on a per-simplex basis and which can be written in the B-form. The theory of the multivariate simplex B-spline has been around for some time [6] but was only recently developed into a transparent and efficient spline scheme [5, 3]. Multivariate simplex B-splines have a number of properties that make them especially suited for global aerodynamic modeling, such as the ability to fit scattered data and to be defined on non-rectangular domains.

3 A Spline Model for the F-16 Pitching Moment Coefficient

A global multivariate spline model for the aerodynamic pitching moment coefficient (C_m) of the F-16 fighter aircraft was created based on a five-dimensional NASA windtunnel data set. It was shown that the model fit was better than 99.9% over the entire flight envelope. Confidence bounds for the multivariate spline model for C_m were generated based on a model residue analysis. The confidence bounds were also expressed in the form of multivariate spline functions.

References

[1] B. L. Stevens and F. L. Lewis, "Aircraft Control and Simulation", Wiley, 2003.

[2] J. A. Mulder, Q. P. Chu, J. K. Sridhar, J. H. Breeman and M. Laban, "Non-Linear Aircraft Flight Path Reconstruction Review and New Advances", Progress in Aerospace Sciences, vol. 35, pages 673-726, 1999.

[3] M. J. Lai and L. L. Schumaker, "Spline Functions over Triangulations", Cambridge University Press, 2007.

[4] V. Klein and J. G. Batterson, "Determination of Airplane Model Structure From Flight Data Using Splines and Stepwise Regression", NASA Tech. Rep. 2126, 1983.

[5] G. Awanou, M. J. Lai and P. Wenston, "The Multivariate Spline Method for Scattered Data Fitting and Numerical Solutions of Partial Differential Equations", Wavelets and Splines, 2005.

[6] C. de Boor, "B-form Basics", SIAM Geometric modeling: algorithms and new trends, 1987.

Nonlinear analysis of flutter

Mattijs Van de Walle, Johan Schoukens, Steve Vanlanduit

Vrije Universiteit Brussel, Pleinlaan 2, 1050 Brussels, Belgium
Department of Fundamental Electricity and Instrumentation (ELEC),
Email: mattijs.van.de.walle@vub.ac.be

1 Introduction

Flutter is an aerolastic phenomenon that makes structures oscillate when surrounded by a moving fluidum. Flutter can lead to fatigue and/or failure on the wings, flaps and fuselage of an airplane. Laborious testing needs to be done on aircraft to ensure safe operation within a certain flight envelope. While flutter is inherently nonlinear, most models use a linear framework to predict the critical speed at which oscillations might occur. The aim of this work is the construction of a nonlinear model to more accurately predict the onset of oscillatory behaviour.

2 Experimental setup

Depicted in figure 1 is a schematic representation of the current two degree-of-freedom setup used for wind tunnel testing. Rigid airfoil sections are being used for simplicity. The plunge spring represents the bending stiffness of a real wing and the pitch spring represents the torsional stiffness. The test setup allows arbitrary adjustments to the stiffness in both the pitch and the plunge direction.

3 Excitation methods

What sets this project apart from other flutter-related research (linear analysis), is the necessity to impose an excitation signal upon the structure [1]. This signal needs to have a user- defined spectrum and insert an amount of power of the same order of magnitude (preferably bigger) as the power inserted through turbulence and unsteady airflow during wind tunnel tests. Several methods are currently considered to be viable:

- Electro dynamic shaker (fixed): while possibly the most straightforward and obvious means of excitation (the shaker being fixed, exciting the airfoil through a stinger), caution needs to be taken not to let the often violent behavior of the wing harm the shaker.
- Electro dynamic shaker (inertial): a shaker can be mounted on the structure and exert force inertially. This technique implies stringent constraints upon the weight and size of the device and also still involves considerable risk to damage the device.
- Electro dynamic shaker (inertial + pneumatic/ hydraulic): to alleviate the two above mentioned techniques from the constraints they impose, a dedicated wing structure can be built that holds only the mass (not the shaker) for inertial excitation. This mass can be controlled through an internal pneumatic or hydraulic system. In this way, an optimal, external shaker can be used. Even though being the most involved means of excitation, this method is expected to insert the most power into the structure within the bandwidth of interest.
- Compressed air: it has been shown that a jet of air, aimed at the structure can be used as means of excitation and that, albeit being dependent upon the type of valve used, a close to linear relation exists between pressure and force exerted on the structure [2]. Furthermore, both proportional and on-off type valves can be used to produce signals with controlled spectral content [3]. Pitfalls with this technique are the high pressure needed for a given amount of input power and the inherent, hard to model, interaction between the airflow in the wind tunnel and the controlled excitation.
- Flap: a dedicated wing can be built that incorporates a moving flap either on top of the wing or at the trailing edge. The flap can be controlled with a piezoelectric actuator and, through the use of a pulse width modulated control signal, an excitation in the bandwidth of interest is achieved.

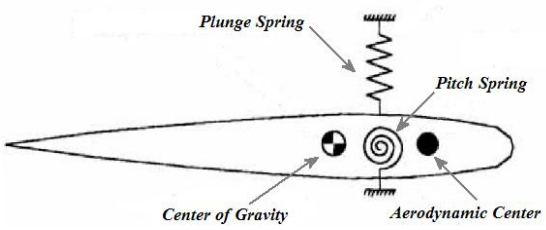

Figure 1: Experimental setup 2DOF

4 Conclusion

At the moment of writing the best suited of the above mentioned techniques has yet to be chosen. Preliminary testing with compressed air seems to indicate a need for excessive pressure. Other excitation techniques have not yet been undertaken.

References

[1] R. Pintelon and J. Schoukens, System Identification: a Frequency Domain Approach, IEEE Press, 2001.
[2] S. Vanlanduit, F. Daerden, P. Guillaume, Experimental modal testing using pressurized air excitation, Journal of Sound and Vibration, 299, 83–98, 2007.
[3]K. Godfrey, Perturbation Signals for System Identification, Prentice Hall, 1993.

Fault Tolerant Flight Control using Nonlinear Dynamic Inversion

Thomas Lombaerts, Ping Chu, Bob Mulder and Diederick Joosten
Faculty of Aerospace Engineering and Delft Center for Systems and Control, faculty 3ME
Delft University of Technology
Kluyverweg 1, 2629 HS Delft
the Netherlands
e-mail: {t.j.j.lombaerts,q.p.chu,j.a.mulder,d.a.joosten}@tudelft.nl

1 Introduction

Thanks to the advent of fly-by-wire aircraft control and the ever increasing computational power of on-board computers, it is possible to design new autopilot control techniques which include more fault tolerant flight control properties. One version of these relies on model based control routines. This setup involves a suitable FDI/identification strategy as well as a reconfiguring controller.

2 Real Time Damaged Aircraft Model Identification

The identification routine which is used for the above mentioned reconfiguring control purpose is the so-called two step method, which has been continuously under development at Delft University of Technology over the last 20 years. Key concept of the two step method, is that the identification procedure has been split into two consecutive steps, as substantiated in ref. [1]. The aim is to update an a priori aerodynamic model (obtained by means of windtunnel tests and CFD calculations) by means of on line flight data. More information can be found in ref. [2] and [3].

3 Fault Tolerant Flight Control

By making use of Nonlinear Dynamic Inversion (NDI), the nonlinear aircraft dynamics can be cancelled out such that the resulting system behaves like a pure single integrator. For this, the physical control input u is defined as follows:

$$u = b^{-1}(\underline{x})\,(\nu - a(\underline{x})) \tag{1}$$

where ν is the outer loop control input. Furthermore, $a(\underline{x})$ is representing the airframe/engine model and $b(\underline{x})$ is the so-called effector blending model. The classical weakness of NDI, its sensitivity for modelling errors which leads to erroneous inversion and thus a possibly unstable result in case of failures, is circumvented here by making use of the real time identified physical model, which allows reconfiguring for the failure in real time. The NDI routine is composed of two loops, relying on the time scale separation principle.

4 Application on a Boeing 747 simulation model

This control strategy has been applied on a high-fidelity nonlinear simulation model of a Boeing 747 based on realistic failure scenarios validated against flight data, such as the Bijlmermeer scenario. Simulation results have shown that this method is very well capable to handle structural failures as well as control surface failures, on the condition that the boundaries of the safe flight envelope are not violated and a minimal subset of control surfaces is still operational.

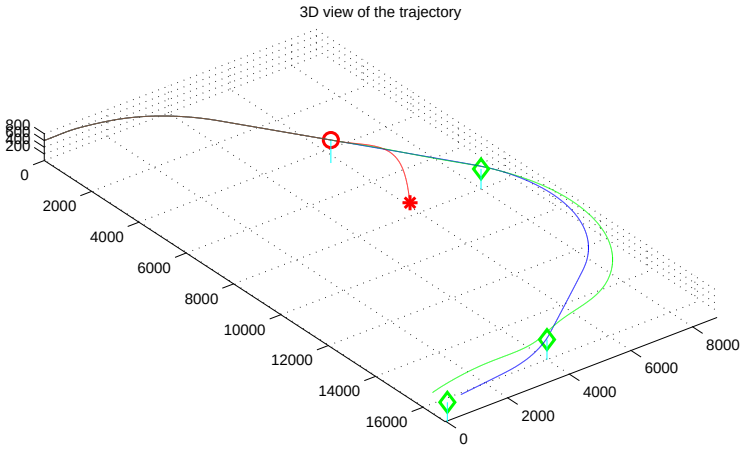

Figure 1: Comparison of the trajectories flown by autopilot along 3 waypoints for classic failed (stops halfway), NDI unfailed (small turn radius), NDI failed (larger turn radius). Due to the damage, the NDI failed aircraft has a restricted bank angle and thus a larger turn radius.

References

[1] Q.P. Chu, J.A. Mulder, and J.K. Sridhar. Decomposition of Aircraft State and Parameter Estimation Problems. *Proceedings of fhe 10th IFAC Sympium on System Identifiation*, Vol. 3, pp. 61-66, 1994.

[2] T.J.J. Lombaerts, Q.P Chu, and J.A. Mulder. Computer based real time aircraft model identification. In *Book of Abstracts* 26^{th} *Benelux Meeting on Systems and Control*, Lommel, Belgium, March 13-15 2007.

[3] T.J.J. Lombaerts, Q.P. Chu, J.A. Mulder, and D.A. Joosten. Real time damaged aircraft model identification for reconfiguring control. In *Proceedings of the AIAA AFM conference*, number AIAA-2007-6717, Hilton Head, SC, August 2007.

Dynamic inversion and model-predictive control applied to an aerospace benchmark for fault-tolerant control purposes

D.A. Joosten*, T.J.J. Lombaerts†, T.J.J. van den Boom*
*Delft Center for Systems and Control, faculty 3ME
†Control and Simulation Division, faculty of Aerospace Engineering
Delft University of Technology, Delft, The Netherlands
{d.a.joosten, t.j.j.lombaerts, a.j.j.vandenboom}@tudelft.nl

1 Introduction

Physical damage to an aircraft, like the blockage of a control surface can lead to loss of controllability and/or stability. Such failures create a very challenging situation for the pilots, since these make it vastly more difficult to pilot the aircraft. An example of such a situation, that was not survived by the crew, is the disaster that involved the El Al Boeing 747 freighter that crashed in the Bijlmermeer, near Amsterdam, The Netherlands, in 1992. A simulation study by Smaili [5] has shown that the failure was likely to be survivable, given the correct control inputs and a wisely chosen trajectory.

2 Fault-tolerant control through model inversion and model-predictive control

Fly-by-wire systems offer the possibility to redistribute control effort over the actuators in an automated fashion. Actuator redundancy in such flight control systems allows for the investigation of fault-tolerant flight control (FTFC) techniques. An overview of control methods that can be applied for FTFC purposes, has been compiled by [1]. One control method that is deemed very suitable for FTFC is model-predictive control. Here, we apply a combination of two different control techniques, model predictive control (MPC) and feedback linearisation (FBL), to obtain FTFC capabilities.

The first control method that is applied is MPC. MPC is selected because of its ability to cope with constraints on the input, state, or output of the system. Furthermore, since this is a discrete-time control method, it is possible to change the model in between the discrete time steps. Both of these properties makes it a serious candidate for FTFC of systems that feature a failure detection (FDI) mechanism.

MPC methods, do however, rely upon optimisation and require linear models in order for the solution of the optimisation problem to converge to a solution that is a global minimum. Feedback linearisation (FBL) offers the possibility to find a nonlinear feedback law, such that given certain assumptions, the closed loop of the system and FBL controller has linear and time-invariant behaviour.

The concept of a combination between FBL and MPC as to form a reconfigurable, globally valid, nonlinear, and constrained controller therefore seems intuitive, but there are several interconnection issues that require attention. Such issues are caused by the fact that the number of system inputs is in general much larger than the number of states that are to be controlled, which is actually a prerequisite for FTFC. Furthermore, it is not a priori clear how the constraints on the inputs relate to the constraints of the MPC controller. A more detailed investigation of the synthesis of MPC and FBL for FTFC purposes is to be found in [2]

3 Application to the GARTEUR AG16 benchmark

The previously introduced methodology has been incorporated into the benchmark model of action group 16 of the Group for Aeronautical Research Europe (GARTEUR). This detailed and life-like model represents the full dynamics of a Boeing 747/100. Several failures, e.g. stabiliser runaway, loss of vertical fin, have been evaluated using this model and the proposed control methodology. More details are to be found in [3]

4 Conclusion

It has been shown in simulation that the proposed methodology is suitable for FTFC purposes in a life-like setting. The computational cost of the method is large though. Future work will focus on variations upon this method that allow for a formal proof of stability for the closed loop.

References

[1] C.N. Jones. Reconfigurable flight control. Technical report, Engineering Dept, University of Cambridge, 2002.

[2] D.A. Joosten and T.J.J. van den Boom. Towards fault tolerant flight control using model predictive control. In *25th Benelux meeting on systems and control*, page 137, 2006.

[3] D.A. Joosten, T.J.J. van den Boom, and T.J.J. Lombaerts. Fault-tolerant control using dynamic inversion and model-predictive control applied to an aerospace benchmark. In *the Proceedings of the 17th IFAC world congress*, 2008. accepted for presentation at the IFAC world congress.

[4] J.M. Maciejowski and C.N. Jones. MPC fault-tolerant flight control case study: flight 1862. In *Proceedings of the IFAC SAFEPROCESS*, 2003.

[5] M.H. Smaili. Flight data reconstruction and simulation of El Al flight 1862. Master's thesis, Delft University of Technology, Delft, The Netherlands, 1997.

New Approach for Nonlinear Aircraft Trim using Interval Analysis

E. van Kampen, Q. P. Chu, J. A. Mulder
Delft University of Technology, Department of Control and Simulation
P.O. Box 5058, 3600 GB Delft, The Netherlands
E.vanKampen@TUDelft.nl, Q.P.Chu@TUDelft.nl, J.A.Mulder@TUDelft.nl

1 Abstract

A new algorithm is proposed for finding the equilibrium or trim conditions of an aircraft, which is an important tool in flight control system design and flight simulation. The algorithm is based on Interval Analysis (IA), which deals with computations on intervals of numbers as opposed to computations on crisp numbers in ordinary arithmetic[1, 2, 3]. Interval analysis generates lower and upper bounds for the result of a computation and is an excellent tool for global nonlinear optimization problems. The basic rules of interval arithmetic are shown in eqs.1 to 4.

The advantage of optimization algorithms using interval analysis over classical optimization algorithms is that they will detect all minima and maxima within a search space, compared to the classical algorithms that only find a local optimum closest to some initial point. In this paper we show how interval analysis can be used to find all solutions to the steady state equations of motion for any type of aircraft model to any desired accuracy. No other numerical method exists that is guaranteed to find all the solution and although analytical methods are capable of this[4], they pose significant restrictions on the type of aircraft model. Important concepts in interval analysis such as box consistency and box splitting methods are applied in the trim algorithm.

$$[a,b]+[c,d]=[a+c,b+d] \tag{1}$$
$$[a,b]-[c,d]=[a-d,b-c] \tag{2}$$
$$[a,b]\cdot[c,d]=[\min(ac,ad,bc,bd),\max(ac,ad,bc,bd)] \tag{3}$$
$$\frac{[a,b]}{[c,d]}=[a,b]\cdot[1/d,1/c] \qquad if\, 0\notin[c,d] \tag{4}$$

Simulation results for trimming in horizontal flight of a six degrees of freedom fighter aircraft model show that the interval analysis trim algorithm can find all the trim points with any specified accuracy. Trimming for fixed thrust in horizontal and level flight results in multiple equilibrium points that are all found by the algorithm (see fig.1), something that conventional trim algorithms such as sequential quadratic programming (SQP [5]) cannot do. Application to a nonlinear model with multiple simultaneous equilibrium points

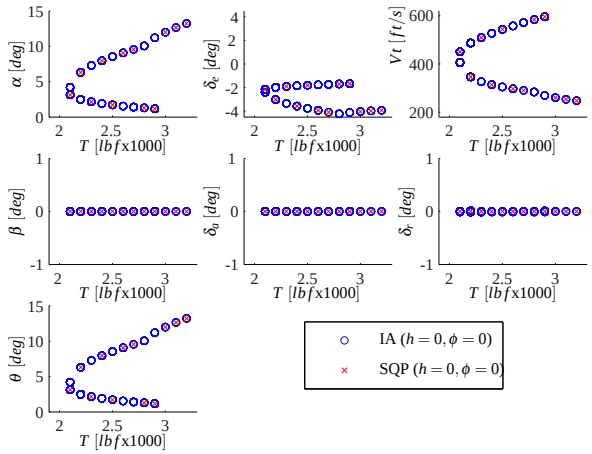

Figure 1: Trim for fixed thrust level horizontal flight at sea-level altitude.

demonstrates the advantages of the algorithm over classical algorithms.

The trim algorithm decribed here will be particularly useful when multiple trimpoints exist, for example due to flexible structure modes or redundant controls.

References

[1] Ramon E. Moore. *Interval Analysis*. Prentice-Hall, Inc., 1966.

[2] Eldon Hansen and G. William Walster. *Global Optimization using Interval Analysis*. Marcel Dekker, Inc., second edition, 2004.

[3] L. Jaulin, M. Kieffer, O. Didrit, and E. Walter. *Applied Interval Analysis*. Springer-Verlag, 2001.

[4] Michael R. Elgersma and Blaise G. Morton. Nonlinear six-degree-of-freedom aircraft trim. *Journal of Guidance, Control, and Dynamics*, 23:305–311, March-April 2000.

[5] K. Schittkowski. Nlqpl: A fortran-subroutine solving constrained nonlinear programming problems. *Annals of Operations Research*, 5:485–500, 1985.

Black box modeling of a continuously variable semi-active damper

Maarten Witters , Jan Swevers
K.U.Leuven, Department of Mechanical Engineering, PMA - Celestijnenlaan 300B, B-3001 Heverlee
maarten.witters@mech.kuleuven.be

1 Introduction

This paper describes the identification of a black box dynamic model for a continuously variable, semi-active damper for a passenger car. The modeled damper is a telescopic, hydraulic damper equipped with a current controlled, electromagnetic servo-valve. Figure 1 gives a schematic representation of the device. It corresponds to a passive damper in which the piston and base valve are each replaced by a check valve. In addition, the rebound and reserve chamber are connected with a current controlled *cvsa*-valve [1], that controls the damping ratio.

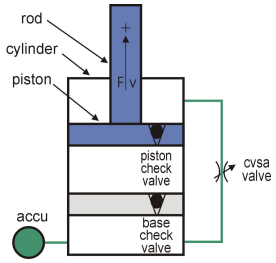

Figure 1: Schematic representation of the semi-active damper.

It is shown that a neural network based, output error model (nnoe) [1] is able to accurately describe the damper dynamics, including saturation and hysteresis. The obtained model has been integrated in a multi-body simulation model of a passenger car. This full-vehicle model can then be used to optimize the parameters of the suspension controller, such that the expensive road tests needed to fine tune the controller can be reduced to a minimum [2].

2 Neural network output error model

The damper dynamics are complex and non-linear, which makes the use of first principles based models cumbersome. Therefor, a black box modeling approach is applied, since this requires only limited insights in the damper dynamics. The output error model maps the regression vector $\varphi(t_n)$ at time instant t_n, to the damper force $F_d(t_n)$ using a nonlinear function g:

$$F_d(t_n,\theta) = g(\varphi(t_n),\theta) \tag{1}$$

Where θ represents the parameter vector of the function. The regression vector consists of previous values of the simulated damper force and the input up to time t_{n-1}. The input vector u includes the damper displacement, velocity and the control current. For the non-linear function g, a neural network with one hidden layer of tangent hyperbolic nodes f, and a linear output layer, is used:

$$\widehat{F}_d(t) = \sum_{j=1}^{q}\left(W_j f(\sum_{i=1}^{m} w_{ji}\varphi_i + w_{j0}) + W_0\right) \tag{2}$$

The developed identification procedure consists of following steps:

- experiments: broad band excitation (0-30 Hz) of the damper on a position controlled hydraulic test rig,
- selection of model structure: number of hidden nodes and the variables included in the regression vector,
- estimation of the model parameters W_j and w_{ji},
- validation of the obtained model.

3 Results

Figure 2 shows a simulation result obtained with the identified model. The relative RMS error of the simulated damper force for this validation measurement is about 5 %.

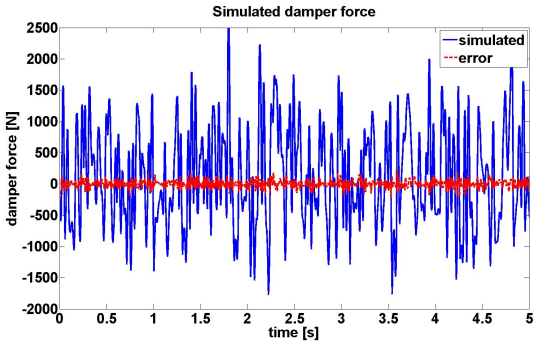

Figure 2: Validation of the identified damper model.

References

[1] M. Nørgaard, O. Ravn, N.K. Poulsen, L.K. Hansen, *Neural networks for Modelling and Control of Dynamic Systems*, Springer-Verlag, London, UK, 2000.

[2] J. Swevers, C. Lauwerys, B. Vandersmissen, M. Maes, K. Reybrouck, P. Sas, *A model-free control structure for the on-line tuning of the semi-active suspension of a passenger car*, Mechanical Systems and Signal Processing, vol. 21, 2007, pp. 1422-1436.

[1] *cvsa*: continuously variable semi-active valve

Identifiability of geological parameters in large-scale models for reservoir engineering

Jorn Van Doren, Paul Van den Hof and Okko Bosgra
Delft Center for Systems and Control
Delft University of Technology
2628 CD Delft
The Netherlands
Email: j.f.m.vandoren@tudelft.nl

Jan Dirk Jansen
Dept. of Geotechnology, CiTG
Delft University of Technology
2628 CN Delft
The Netherlands

1 Introduction

In reservoir engineering large-scale, physical models of subsurface reservoirs are constructed (see Figure 1), which are used for prediction and control of water, oil and gas flows over a period of years to decades. One of the model parameters that is of paramount importance for an accurate prediction of the flows is the permeability in each grid block of the spatially discretized model. Permeability indicates how easy the fluid can flow through the porous medium. A prior estimate of the grid block permeability originates mainly from geological insight and geophysical measurements. This estimate is subsequently updated using dynamic measurements in the wells. Estimating these parameters from well measurements is challenging, mainly because of the discrepancy between the number of parameters to be estimated and the number of available wells, and the requirement that the estimated parameters preserve the prior geological and geophysical knowledge. Therefore, before actually estimating the grid block permeabilities from well measurements it is wise to examine the structural identifiability.

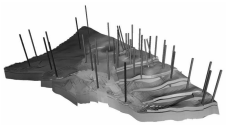

Figure 1: Example of a spatially discretized 3D reservoir simulation model with vertical wells.

2 Structural identifiability

Local structural identifiability analysis gives an answer to the question if it is at all possible to distinguish two given parameters sets from the outputs, provided the inputs are chosen the best possible way. For single-phase reservoir models with multiple inputs and outputs the state observability, state controllability and local structural identifiability of the grid block permeabilities is analyzed in [1] and [2]. From this analysis we were able to extract the parameters and combinations of parameters that are best identifiable, i.e. a parameterization to which the input-output behavior is most sensitive. An example with 2025 parameters is given in Figure 2.

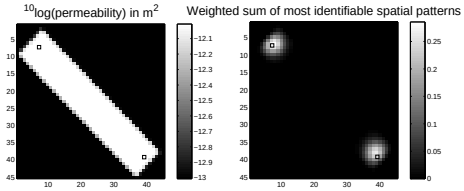

Figure 2: Top view of reservoir with grid block permeabilities (left) and the weighted sum of most identifiable spatial patterns of grid block permeabilities (right). Black rectangles indicate the well position.

3 Structural identifiability of geological parameters

In this work the structural identifiability of a geological parameterization of the permeability is investigated. The main idea of a geological parameterization is that the number of parameters is reduced and that an updated parameter estimate preserves the geological knowledge. To this end a deterministic, 2-dimensional channel/barrier modeling method is developed where channels with a higher permeability or barriers with a lower permeability are positioned in a homogeneous background. Each channel/barrier is parameterized by only six geological parameters: width, length, position in x and y direction, angle and permeability of the channel. The permeability of the background is given by one parameter. The 7 parameters in the example are all structurally identifiable, which means that (in theory) with a geological parameterization the high permeable channel can be identified.

References

[1] M.J. Zandvliet, J.F.M. Van Doren, O.H. Bosgra, J.D. Jansen, P.M.J. Van den Hof, “Controllability and Observability in Reservoir Engineering”, Submitted to a journal, 2008.

[2] J.F.M. Van Doren, P.M.J. Van den Hof, J.D. Jansen, O.H. Bosgra, “Determining Identifiable Parameterizations for Large-scale Physical Models in Reservoir Engineering”, To be presented at IFAC, Seoul, Korea, 2008.

Climate reconstruction based on archaeological shells: a non-linear multi-proxy approach

Maite Bauwens[1] Veerle Beelaerts[2], Kurt Barbé[2], Johan Schoukens[2] and Frank Dehairs[1]
[1] Department of Analytical and Environmental Chemistry, [2] Department of Fundamental Electricity and Instrumentation
Vrij Universiteit Brussel, Pleinlaan2, 1050 Brussel, Belgium
e-mail: Maite.Bauwens@vub.ac.be

In accordance with the trends seen in previous years, also 2007 beaded some temperature records. We just lived the warmest winter and the warmest spring since the beginning of all temperature measurements. This seems to be convincing evidence for most people to begin to believe in global warming. The question remains: what do we know about the temperature before the start of the measurements? Not too much to be honest.[1] To know more about it, we need on one hand good proxy-archives (= sensors) in which a clear proxy-signal is seen and on the other hand a good interpretation of the signal to reconstruct the paleoclimate.

Several years of biogeochemical research on bivalve shells resulted in clear proxy-signals with the promising potential for reconstruction of yearly variations in the paleoclimate around estuarine systems.[1, 2] But the interpretation of the different proxy signals is still problematic. The classical linear transfer function from proxy to environmental parameter failed for most proxies, and if they seem to work (e.g. for $\delta^{18}O$ in relation to temperature) the signal-to-noise ratio is so high that the uncertainty on the reconstructed temperature is higher than the recent temperature changes.[2]

This is why we developed a non-linear multi-proxy approach. This approach consists in the construction of a manifold in a multi-dimensional space, as an intermediate step, from which in a second step a temperature is obtained. At this moment two types of models are used to describe the manifold; (1) a spline model and (2) a polynomial model. Both models describe the variations in the chemical signature of the shell during a one year cycle. The shortest distance from another measurement (e.g. in an archeological shell) to the model will give a time estimation, which can be linked to several environmental parameters. Initial temperature reconstructions were promising, and after some ameliorations on the basic principals (normalization, time-basis movements and weighting factor for proxies) the reconstruction can even be called good.

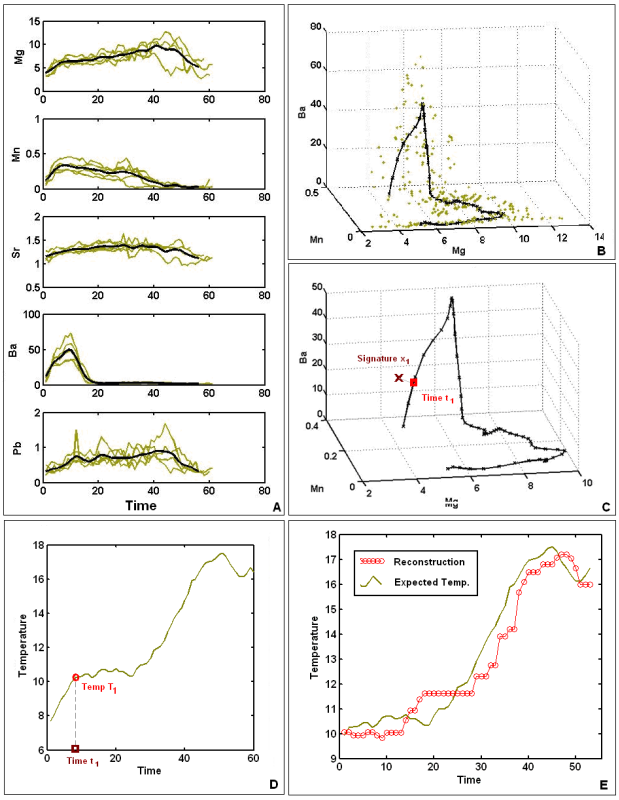

Figure: A.: Initial estimation of a non-linear transfer function for every proxy over time. B.: rewriting the transfer functions in a multi-dimensional function (there are as many dimensions as proxies). C. Linking of a measurement (chemical signature) to a unique time-position. D. Linking of the time-position to the corresponding environmental parameter(s). E. Validation of the method, comparing the measured environmental parameter(s) to the predicted environmental parameter(s).

References

[1] Gillikin, D. P. et all., 2005 . Assessing the reproducibility and reliability of estuarine bivalve shells for sea surface temperature reconstruction: implications for paleoclimate studies. *Palaeogeography Palaeoclimatology Palaeoecology* 228: 70-85.
[2] Lazareth C.E., E. Vander Putten, L. André and F. Dehairs, 2003. High-resolution trace element profiles in shells of a mangrove bivalve (*Isognomon ephippium*): A record of environmental spatio-temporal variations? *Estuarine, Coastal and Shelf Science*, 57, 1103-1114.

This research was funded by a grand of the Vrije Universiteit Brussel (HOA-9) and a grand of the the Flemish government (CALMAR's)

Estimating Cutting forces in Micromilling by Input estimation from Closed-loop Data

Rogier S. Blom [a,b,*], Paul M.J. Van den Hof [b]

[a] Precision and Microsystems Engineering, [b] Delft Center for Systems and Control,
Delft University of Technology

[*] Corresponding author, email: r.s.blom@tudelft.nl

1 Introduction

The topic of this presentation concerns an application in the area of micro-manufacturing. In particular micromilling is considered, which entails the scaling of conventional milling into the microdomain. Tools with diameters of less than $0.5mm$ are used to manufacture components with arbitrary 3D features in a range of materials. More than in conventional milling, it is important in micromilling to monitor the cutting forces during the milling process in order to maintain a stable cutting process. These forces can be measured directly with force transducers, however commercially available systems are limited by their bandwidth and the additional space needed in the machine.

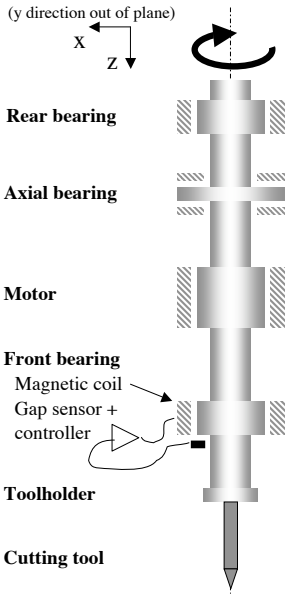

Figure 1: Schematic of an AMB spindle

When the milling is performed by a spindle with Active Magnetic Bearings (AMBs), the active nature of the bearings can be employed to observe the cutting forces from the signals of the bearings. In AMB spindles, the rotor is levitated by generating electromagnetic forces at the front and rear side of the rotor, as well as in the axial direction

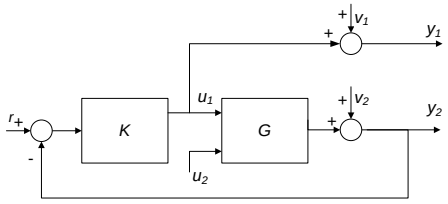

Figure 2: Block diagram of closed-loop input estimation problem

(see figure 1). A stable system is obtained by using position measurements in a closed-loop to control the currents of the electromagnets. Force estimation based on the current and position signals is favorable as it eliminates the need for additional sensors, thus saving cost and space.

2 Input estimation from closed-loop data

The problem of observing cutting forces from the signals of an AMB spindle can be considered an input estimation problem. The cutting forces constitute an unknown input to a partially closed loop dynamical system (see figure 2). Measurements of the control input y_1 and the outputs y_2 are available, viz. the currents through the coils and the displacement of the rotor respectively, which are used to estimate the unknown input u_2, representing the cutting forces.

Optimal estimates $\hat{u}_2$ can be obtained by minimizing the mean square error $\mathbb{E}|\hat{u}_2(t) - u_2(t-N)|^2$, where $N \geq 0$ is some fixed time-lag. When the unknown input sequence is treated as white noise filtered by known dynamics, and full knowledge on the controller K is available, the optimal estimator will have a Wiener filter structure. It will be shown that controller knowledge can be replaced by a perfect measurement of the control signal u_1. The adjustable delay N allows to trade off the estimation error against the lag in the estimation results. It will be demonstrated that given the dynamics of the plant and the noise characteristics, a minimum delay exists that can be attained.

3 Acknowledgement

This research is supported by MicroNed and the Delft Center for Mechatronics and Microsystems.

Velocity and acceleration estimation for optical incremental encoders using time stamping

Roel Merry*, René van de Molengraft, and Maarten Steinbuch
Eindhoven University of Technology, Department of Mechanical Engineering
P.O. Box 513, 5600 MB Eindhoven, The Netherlands
Email: *r.j.e.merry@tue.nl

1 Introduction

Optical incremental encoders are widely used to apply feedback control on motion systems where the position is measured at a fixed sample frequency. The accuracy is limited by the quantized measurement of the encoder. Velocity and acceleration information from incremental encoders can be obtained using only the position information [1], thus disregarding the variable rate of occurrence of the encoder events, or using model based methods such as observers [2].

This research employs the time stamping concept, in which both encoder counts and their time instants are used for the position estimation [3]. To obtain accurate velocity and acceleration estimations, the time stamping concept is extended with a skip option.

2 The skip option in time stamping

The time stamping concept stores encoder events (t_i, x_i), consisting of the encoder positions x_i and the time instants t_i the transition occurs, captured at a high resolution clock. Position information is obtained using polynomial fitting through n encoder events and extrapolation to the desired time instant.

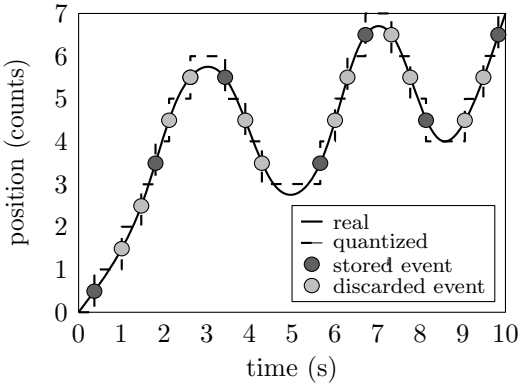

Figure 1: Visualization of the skip option for σ=2 counts.

The encoder events suffer from errors due to encoder imperfections, which act as a disturbance on the position estimation. The errors are amplified in the velocity and acceleration estimations. A skip option is proposed to skip σ events in between two stored events. This extends the time span covered by the events in the fit without the need for more events. The skip option is shown in Fig. 1 for $\sigma = 2$ counts.

3 Experimental results

The velocity and acceleration estimations of time stamping without skip and with $\sigma = 3$ are shown in Fig. 2 for a sinusoidal reference signal $r(t) = \pi/2\sin(2\pi t)$. The estimation error of the velocity (Fig. 2(a)) with $\sigma = 3$ is 74% more accurate than without skip, i.e. $\sigma = 0$. For the acceleration, the estimation with $\sigma = 3$ is 92% more accurate than with $\sigma = 0$.

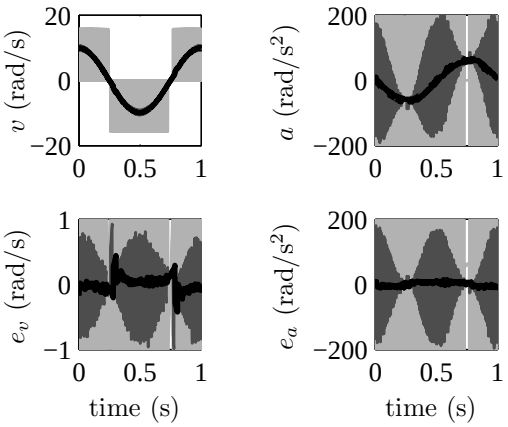

(a) Velocity estimation (b) Acceleration estimation

Figure 2: Experimental results, quantized measurement (light grey), σ=0 (dark grey) and σ=3 (black).

References

[1] G. Liu. On velocity estimation using position measurements. *American Control Conference*, 2:1115–1120 vol.2, 2002.

[2] L. Kovudhikulrungsri and T. Koseki. Precise speed estimation from a low-resolution encoder by dual-sampling-rate observer. *IEEE/ASME Transactions on Mechatronics*, 11(6):661–670, 2006. 1083-4435.

[3] R. H. Brown and S. C. Schneider. Velocity observations from discrete position encoders. *IEEE conf. of the Industrial Electronics Society*, pages 1111–1118, 1987.

Studying the Properties of Unimodular Maps and Interconnected Behaviors by means of Galois Connections

Tzvetan Ivanov
Université Catholique de Louvain
Department of Mathematical Engineering
Bâtiment Euler, Av. Georges Lemaître, 4
B-1348 Louvain-la-Neuve, Belgium
Email: tzvetan.ivanov@uclouvain.be

1 Introduction

A large class of linear and time-invariant (LTI) behaviors [1] can be described by a finite number of equations[1]

$$a_i(\tfrac{\mathrm{d}}{\mathrm{d}t})w(t) = 0 \quad (i = 1,\ldots,m), \tag{1}$$

with $w \in C^\infty(\mathbb{R},W)$ and $a_i \in W^*[z]$, where W can be $\mathbb{R}^n$, or any other finitely generated linear space, $C^\infty(\mathbb{R},W)$ denotes the set of smooth functions from the time axis $\mathbb{R}$ to W, and W^* denotes the dual of W.[2] Given the solution set $\mathcal{B} \subseteq C^\infty(\mathbb{R},W)$ of (1) one defines the annihilator submodule $\mathcal{B}^\perp \subseteq W^*[z]$ to consist of all derivations which annihilate all trajectories in $\mathcal{B}$, i.e., all $a \in W^*[z]$ with $a(\frac{\mathrm{d}}{\mathrm{d}t})w(t) = 0$ for all $w \in \mathcal{B}$. Then $\mathcal{B}^\perp$ is precisely $S = \sum_{i=1}^m a_i\mathbb{R}[z]$, i.e., the submodule spanned by the a_i's. On the other hand one defines $S^\top$ to denote the set of all trajectories $w \in C^\infty(\mathbb{R},W)$ which are annihilated by all derivations in S. The pair $(\perp,\top)$ which connects the lattice $\mathscr{D}^*(W)$ of submodules in $W^*[z]$, i.e., the arithmetic perspective, with the lattice of LTI behaviors $\mathscr{D}(W)$, i.e., the geometric perspective, forms a Galois connection with $S^{\top\perp} = S$. We propose methods exploiting this Galois connection in order to discuss properties of unimodular maps as well as to establish a new way of interconnecting behaviors.

2 Properties of Unimodular Maps

Let $\mathrm{L}(V_1,V_2)$ denote the set of all linear maps from V_1 to V_2 and $\mathrm{L}(W) = \mathrm{L}(W,W)$. A polynomial matrix $U \in \mathrm{L}(W)[z]$ is called *unimodular* if it possesses a polynomial inverse. It has been shown in [2, p.21 Theorem 15] that

$$\begin{cases} U^* \circ (\perp \circ U(\frac{\mathrm{d}}{\mathrm{d}t}) \circ \top) &= \mathrm{Id}_{\mathscr{D}^*(W)} \\ U(\frac{\mathrm{d}}{\mathrm{d}t}) \circ (\top \circ U^* \circ \perp) &= \mathrm{Id}_{\mathscr{D}(W)}, \end{cases} \tag{2}$$

iff U is unimodular, where $U^* \in \mathrm{L}(W^*)[z]$ denotes the *dual map* of U given by $U^*a := a \circ U$ for all $a \in W^*[z]$.[3]

3 Interconnecting Behaviors

Given two LTI behaviors $\mathcal{B}_1,\mathcal{B}_2 \in \mathscr{D}(W)$ it is natural to define their interconnection as $\mathcal{B}_1 \cap \mathcal{B}_2$, i.e., the solution set of $\mathcal{B}_1^\perp + \mathcal{B}_2^\perp$.[4] However in many situations the controller has only access to a subspace $V \subseteq W$, i.e., $\mathcal{B}_2 \in \mathscr{D}(V)$. An approach that deals with this *partial information* case from the start has been proposed in [2, p.78 Definition 124] where one assumes $\mathcal{B}_i \in \mathscr{D}(W_i)$ $(i = 1,2)$, $\imath_i : W_i^* \hookrightarrow W^*$ are linear inclusions and defines the *interconnection of* $\mathcal{B}_1$ *and* $\mathcal{B}_2$ *w.r. to* $(\imath_1,\imath_2)$, denoted by $\mathcal{B}_1[\imath_1|\imath_2]\mathcal{B}_2 \in \mathscr{D}(W)$, in terms of its annihilator, i.e.,

$$\mathcal{B}_1[\imath_1|\imath_2]\mathcal{B}_2 = (\imath_1(\mathcal{B}_1^\perp) + \imath_2(\mathcal{B}_2^\perp))^\top. \tag{3}$$

The interconnection is said to be *regular* if the sum in (3) is direct, i.e., $\imath_1(\mathcal{B}_1^\perp) \cap \imath_2(\mathcal{B}_2^\perp) = \{0\}$. The full information case is given by $W_i = W$ and $\imath_i = \mathrm{Id}_W$ $(i = 1,2)$ without the need to "copy" trajectories as in [3].

References

[1] J. C. Willems and J. W. Polderman, *Introduction to Mathematical Systems Theory – A Behavioral Approach*. Springer-Verlag New York, Inc., 1998.

[2] T. Ivanov, "A polynomial approach to behaviors and control of dynamical systems," Master's thesis, Munich University of Technology - Associate Institute for Signal Processing, July 2007.

[3] M. N. Belur and H. L. Trentelman, "Stabilization, pole placement, and regular implementability," *IEEE Transactions on Automatic Control*, vol. 47, pp. 735–743, 2002. [Online]. Available: http://www.math.rug.nl/~trentelman/psfiles/StabPole.pdf

[1] The discrete time case, where the time axis $\mathbb{R}$ is replaced by $\mathbb{Z}_{\geq 0}$, can be handled analogously by substituting $(\frac{\mathrm{d}}{\mathrm{d}t})$ by the *truncated* left shift σ defined by $(\sigma w)(t) = w(t+1)$ and $C^\infty(\mathbb{R},W)$ by $W^{\mathbb{Z}_{\geq 0}}$.

[2] Informally speaking the elements in $W^*[z]$ are polynomials whose coefficients are functionals, i.e., elements of W^*. Formally one utilizes the tensor product $\mathbb{R}[z] \otimes W^*$ to define $W^*[z]$ as a linear space and endows it with a $\mathbb{R}[z]$-module structure defined by linear extension of $p \cdot (q \otimes w^*) := (pq) \otimes w^*$ for all $p,q \in \mathbb{R}[z]$ and all $w^* \in W^*$. Every element in $W^*[z]$ is of the form $\sum_{\text{finite}} z^i \otimes w_i^*$ with $w_i^* \in W^*$. One tends to write this sum as $\sum w_i^* z^i$.

[3] Thus, in this sense, unimodular matrices satisfy $UU^* = 1$ and $U^*U = 1$ forming the categorical pendant to orthogonal matrices, i.e., those well studied maps in the theory of Hilbert spaces where $\perp$ and $\top$ are both given by the "take the orthogonal complement"-operation.

[4] Think of $\mathcal{B}_1$ as the plant, $\mathcal{B}_2$ as the controller and $\mathcal{B}_1 \cap \mathcal{B}_2$ as the desired sub-behavior of the plant.

The positive LQ-problem for linear continuous time systems

Charlotte Beauthier and Joseph J. Winkin
University of Namur (FUNDP), Department of Mathematics
Rempart de la vierge, 8, 5000 Namur – Belgium
charlotte.beauthier@fundp.ac.be, joseph.winkin@fundp.ac.be

Abstract

Positive linear systems constitute an important class of controlled linear systems. These systems encompasse dynamical models where all the variables, i.e. the state and output variables, should remain nonnegative for any nonnegative initial conditions and input functions. An overview of the state of the art in positive systems theory is given e.g. in [3] and [8].

Here we report some results concerning the finite-horizon positive linear quadratic (LQ) problem for positive linear continuous time systems. The infinite horizon LQ problem was studied in [6], by means of a Newton-type iterative scheme.

More specifically, the (normalized) LQ positive problem consists of minimizing the following quadratic functional :

$$\frac{1}{2}\left(\int_0^{t_f}(\|u(t)\|^2+\|Cx(t)\|^2)\,dt+x^T(t_f)Sx(t_f)\right)$$

for a given positive linear system $\dot{x}(t)=Ax(t)+Bu(t)$, $t\in[0,t_f]$ where $x(0)=x_0$, u is a piecewise-continuous function, $A\in\mathbb{R}^{n\times n}$ is a Metzler matrix (i.e. each off-diagonal entry is nonnegative), $B\in\mathbb{R}^{n\times m}$ is a nonnegative matrix (i.e. each entry is nonnegative) and $S\in\mathbb{R}^{n\times n}$ is a symmetric positive semidefinite matrix, under the constraints that the state trajectories $x(t)$ be nonnegative for all time.

By applying the maximum principle in continuous time to this problem (see e.g. [4]), it can be shown that the LQ optimal control u is of the state feedback type, as in the classical theory of the LQ problem, i.e. without the nonnegativity constraints on the state trajectories (see [2]). More precisely, $u(t)=K(t)x(t)=-B^TP(t)x(t)$, where $P(\cdot)=P(\cdot)^T$ is the positive semidefinite matrix solution of the following matrix differential Riccati equation :

$$-\dot{P}(t)=A^TP(t)+P(t)A-P(t)BB^TP(t)+C^TC,$$

with $P(t_f)=S$, such that $A+BK(t)=A-BB^TP(t)$ is a Metzler matrix for all time t. The last condition is obtained by applying the characterization of the positivity of homogeneous time-varying linear systems in continuous time, see e.g. [1] and [5].

Sufficient conditions are reported for the positivity of the closed-loop system in terms of $P(t)$ by the study of an upper bound of this matrix. Using an approach similar to the one developed in [7] it can be shown that $P(t)\leq F(t)$, that is the matrix $F(t)-P(t)$ is nonnegative for all time, where $F(t)$ is the solution of the matrix Lyapunov differential equation,

$$\dot{F}(t)=-A^TF(t)-F(t)A-C^TC,\quad F(t_f)=S.$$

Then, by using the fact that $A-BB^TF(t)$ is a Metzler matrix implies that $A-BB^TP(t)$ is also a Metzler matrix, a criterion can be derived for the positivity of the LQ-optimal closed-loop system.

We have also studied the particular problem of minimal energy control with penalization of the final state. By computing the expression of $P(t)$ in terms of the matrix solution of the Hamiltonian system, where $C=0$, sufficient positivity conditions have been obtained under the form of inequalities involving the spectral radius of S and the final time t_f. This analysis reveals a tradeoff between positivity and stability of the closed-loop system (in a receding horizon approach).

These results are illustrated by some numerical experiments.

References

[1] D. Angeli, E.D. Sontag, *Monotone control systems*, IEEE Transactions on Automatic Control, Vol. 48, No. 10, pp. 1684-1698, 2003.

[2] F. M. Callier, C. A. Desoer, *Linear System Theory*, Springer-Verlag New-York, 1991.

[3] L. Farina, S. Rinaldi, *Positive Linear Systems : Theory and applications*, Wiley, New York, 2000.

[4] R. F. Hartl, S. P. Sethi, R. G. Vickson, *A survey of the maximum principles for optimal control problems with state constraints*, SIAM Review, Vol. 37, No. 2, pp. 181-218, 1995.

[5] T. Kačzorek, *Externally and internally positive time-varying linear systems*, Int. J. Appl. Math. Comput. Sci., 2001, Vol. 11, No. 4, pp. 957-964.

[6] M. Laabissi, J. Winkin, Ch. Beauthier, *On the positive LQ-problem for linear continous-time systems*, Positive systems (Proceedings of the 2nd Multidisciplinary International Symposium on Positive Systems : Theory and Applications (POSTA06), Grenoble, France), Lecture Notes in Control and Information Sciences, Springer Verlag, pp. 295-302, 2006.

[7] K. N. Murty, K. R. Prasad, M. A. S. Srinivas, *Upper and lower bounds for the solution of the general matrix riccati differential equation*, Journal of mathematical analysis and applications, Vol. 147, pp. 12-21, 1990.

[8] J. H. Van Schuppen, *C*ontrol and System Theory of Positive Systems, Lecture Notes, 2007.

Bisimulation for switching linear systems with inequality constraints

F.J. Kerber*, A. J. van der Schaft, M. K. Camlibel
Institute for Mathematics and Computing Science
University of Groningen
P.O. Box 407, 9700 AK Groningen
The Netherlands
Email: florian@math.rug.nl*

1 Introduction

The use of bisimulation techniques originates from computer-aided verification, [3]. To facilitate the automated use of formal methods like temporal logics or process algebras, the complexity of the programs to be checked often has to be reduced. Bisimulations are equivalence relations with respect to the externally visible behavior of state transition systems potentially giving rise to an approximation which can be verified with less computational efforts.

2 Bisimulation relations for dynamical systems

The usefulness of bisimulation equivalences in the context of dynamical systems has been shown when applying this concept to linear continuous-time systems, see [1]. Existence conditions as well as constructive algorithms to compute maximal bisimulations were developed. It proved to be an important observation that the problem to find a bisimulation relation between two linear time invariant systems can be reformulated as a modified disturbance decoupling problem as arising in geometric control theory.
Another class of dynamical systems for which bisimulation equivalences have been studied are switching linear systems. For this special class of non-deterministic hybrid systems, the state evolution depends on input driven mode switches. Separating discrete and continuous dynamics by means of graph theoretic concepts, a bisimulation relation could be established in [2].

3 Application to switching linear systems with inequality constraints

It is the aim of this work to extend the available techniques to a more general class of hybrid systems, switching linear systems with location invariants. In addition to the influence of the discrete dynamics on the evolution of the continuous state, such kind of systems incorporate reciprocal dependencies of discrete and continuous dynamics by means of location invariants. These location invariants are represented by affine inequality constraints on the states.
In a first step, bisimulation relations for the constrained continuous-time dynamcis should be analyzed using Farkas' Lemma. The final goal is to develop an algorithm to compute the maximal bisimulation for switching linear systems with inequality constraints. This could be used to reduce a given system to an equivalent bisimilar system of minimal state space dimension.

References

[1] A.J. van der Schaft, "Equivalence of dynamical systems by bisimulation," IEEE Transactions on Automatic Control, 49, pp. 2160-2172, 2004.

[2] G. Pola and A. J. van der Schaft and M. D. Di Benedetto, "Equaivalence of switching linear systems by bisimulation," International Journal of Control, 79, No.1, 74-92, 2006.

[3] R. Milner, "Communication and Concurrency", Prentice Hall, 1989

Temporal linear system structure

Gerard van Willigenburg
Systems and Control Group
Wageningen University
P.O. Box 17, 6700 AA Wageningen
The Netherlands
Email: gerard.vanwilligenburg@wur.nl

Willem de Koning
Kroeskarper 6
2318 NG Leiden
The Netherlands
Email: wilros@planet.nl

1 Introduction

Piecewise constant rank systems and the *differential Kalman decomposition* are introduced. Together these enable the detection of temporal uncontrollability/unreconstructability of linear continuous-time systems. These temporal properties are not detected by any of the four conventional Kalman decompositions. Moreover piecewise constant rank systems admit the state dimension to be time-variable. It is demonstrated that linear continuous-time systems with variable state dimensions enable the well rounded realization theory suggested already by Kalman [1]. The differential Kalman decomposition is associated with differential controllability and differential reconstructability. The system structure obtained from the differential Kalman decomposition may be interpreted as the *temporal linear system structure*. It turns out that the difference between controllability and reachability as well as reconstructability and observability is entirely due to *changes* of the temporal linear system structure.

Figure 1: The main contributions

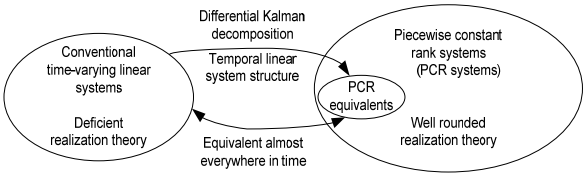

2 Illustrative example

Consider the following time-varying linear system,

$$\begin{aligned} \dot{x}(t) &= A(t)x(t) + B(t)u(t), \\ y(t) &= C(t)x(t),\ t \in [0,1], \end{aligned} \tag{1}$$

where

$$A(t) = \begin{bmatrix} 1 & 2 \\ 1 & 1 \end{bmatrix}, t \in [0, 0.25],$$

$$A(t) = \begin{bmatrix} 1 & 2 \\ 0 & 1 \end{bmatrix}, t \in (0.25, 0.5],$$

$$A(t) = \begin{bmatrix} 1 & 0 \\ 2 & 1 \end{bmatrix}, t \in (0.5, 0.75],$$

$$A(t) = \begin{bmatrix} 1 & 1 \\ 2 & 1 \end{bmatrix}, t \in (0.75, 1], \tag{2}$$

$$B(t) = \begin{bmatrix} 1 & 0 \end{bmatrix}^T, C(t) = \begin{bmatrix} 1 & 0 \end{bmatrix}, t \in [0,1].$$

If time in (1) would be restricted to $(0.25, 0.5)$ the system would be unreachable as well as uncontrollable. Similarly if time in (1) would be restricted to $(0.5, 0.75)$ the system would be unobservable and unreconstructable. If $t \in [0,1]$ then we might call the system temporarily uncontrollable/unreachable over $(0.25, 0.5)$ because over this time interval the second state variable is not influenced by the input. Similarly we might call the system temporarily unreconstructable/unobservable over $(0.5, 0.75)$ because over this time interval the second state variable does not influence the output. Since moreover the second state variable grows exponentially over $(0.25, 0.5)$ and over $(0.5, 0.75)$ it cannot be stabilized by a controller over these time intervals. If we apply a similarity transformation at every time $t \in [0,1]$ to the system then these temporal properties are unchanged but no longer obvious from the system description. None of the four conventional Kalman decompositions recovers these temporal properties because the system is controllable and reconstructable from any time as well as reachable and observable at any time. As demonstrated the differential Kalman decomposition retrieves the temporal system properties and structure by obtaining a system description similar to (2).

The total minimal systems introduced in [2] turn out to be piecewise constant rank systems that are not temporarily uncontrollable nor temporarily unreconstructable.

References

[1] Kalman R.E., Falb P.L., Arbib M., 1969, *Topics in Mathematical Systems Theory*, Mc Graw Hill, New York.
[2] Van Willigenburg L.G., De Koning W.L., 2006, "Total minimal systems", Book of Abstracts 25th Benelux Meeting on Systems and Control, March 2006, Heeze, The Netherlands

On the stabilization problem for a certain class of decentralized control systems

Ciprian Deliu
Department of Mathematics and Computer Science
Technische Universiteit Eindhoven
P.O. Box 513, 5600 MB Eindhoven
The Netherlands
Email: c.deliu@tue.nl

Anton A. Stoorvogel
Department of Applied Mathematics
University of Twente
P.O. Box 217, 7500 AE Enschede
The Netherlands
Email: a.a.stoorvogel@utwente.nl

1 Introduction

The stabilization problem for decentralized control systems has been an important subject of research starting from the 70's when Wang and Davison published their paper [1], where they establish necessary and sufficient conditions for stabilization of linear time-invariant decentralized control systems. Basically the stabilization relies on the fact that all the decentralized fixed modes of the system are located in the open left-half plane, although later it has also been proved that certain unstable fixed modes can be moved using time-varying controllers.

Clearly the decentralized structure imposes restrictive conditions on the controller design in the general case, and therefore many people have been looking to prove results for certain particular classes of decentralized systems.

2 Block-diagonal double integrator systems

Such a particular class of systems is the one where the system matrix is a block-diagonal double integrator, while the decentralized structure is appearing in the output matrix G:

$$\dot{x} = \begin{pmatrix} 0 & 1 & & & \\ 0 & 0 & & 0 & \\ & & \ddots & & \\ & & & 0 & 1 \\ & 0 & & 0 & 0 \end{pmatrix} x + \begin{pmatrix} 0 & & 0 \\ 1 & & \\ & \ddots & \\ & & 0 \\ 0 & & 1 \end{pmatrix} u$$
$$y = Gx.$$

This can be regarded as a system of ν independent vehicles (or agents), each having its own information about the positions and/or velocities of the others, while the aim is to globally stabilize the system using decentralized controllers for each agent.

Obviously the design of these controllers highly depends on the structure of the matrix G, where the decentralized information is lying, and the condition of the decentralized fixed modes being in the open left-half plane can be translated into a certain property of this matrix (see [2] for details).

3 Stabilization using static controllers

Also in [2] it is proved that stabilization using static decentralized controllers is possible if there exists a diagonal matrix K such that the eigenvalues of KG are in the open left-half plane. In this paper we will present necessary and sufficient conditions for the existence of such a matrix K:

Theorem 1. *Consider an arbitrary matrix $G \in \mathbb{R}^{\nu\times\nu}$. Then there exists a diagonal matrix $K \in \mathbb{R}^{\nu\times\nu}$ such that all the eigenvalues of KG have negative real part only if*

$\forall i \in \{1,\ldots,\nu\}$, *$G$ has at least one $i\times i$ principal minor $d_i \neq 0$.*

Theorem 2. *Consider an arbitrary matrix $G \in \mathbb{R}^{\nu\times\nu}$. Then there exists a diagonal matrix $K \in \mathbb{R}^{\nu\times\nu}$ such that all the eigenvalues of KG have negative real part if*

$$\exists\{i_1\} \subset \{i_1,i_2\} \subset \cdots \subset \{1,\ldots,\nu\}$$

such that the corresponding principal minors of G are all non-zero.

4 Conclusions

Decentralized control systems are often tough to handle in the general case, and therefore tools are developed for special classes of decentralized structure. In this paper we present some nice algebraic tools to test the stabilizability of a block-diagonal double integrator decentralized control system.

References

[1] S.H. Wang and E.J. Davison, "On the Stabilization of decentralized control systems", *IEEE Trans. Aut. Contr.*, 18(5):473-478, 1973.

[2] S. Roy, A. Saberi and K. Herlugson, "Formation and alignment of distributed sensing agents with double-integrator dynamics and actuator saturation", *Sensor Network Operations*, Wiley-IEEE Press, 2006.

Dynamic behaviour of the CSTR: a thermodynamic point of view

A. Favache
IMAP & CESAME, Université catholique de Louvain
1348 Louvain-la-neuve (Belgium)
audrey.favache@uclouvain.be

D.Dochain
IMAP & CESAME, Université catholique de Louvain
1348 Louvain-la-neuve (Belgium)
denis.dochain@uclouvain.be

B.Maschke
LAGEP, Université Claude Bernard, Lyon 1
69622 Villeurbanne (France)
maschke@lagep.cpe.fr

1 Abstract

Control theory is largely based on the concept of stability "a la Lyapunov" which was initially largely justified in terms of system energy. Because it was mainly considered in the context of mechanical and electrical systems, this had led to the use of quadratic functions as Lyapunov function candidates, since these can be easily justified as energy system functions. More generally speaking, stability analysis of nonlinear systems requires the use of abstract mathematical tools such as the two Lyapunov methods for instance. This can result in a loss of information stemming from the physics of the system. In most of the cases, the analysis of the dynamical behaviour and the control of a system are made by starting from the dynamical equations of the system and by considering them as a differential equation system. The further computations do not need any more links with the physics. But beside the equations expressing the dynamics of the system, the physics can give us more insightful information that can be useful for the analysis of its dynamical behaviour. This is particularly true for chemical reaction systems. For those systems, the dynamical equations are given by balance equations. But the laws of thermodynamics provide complementary information like the mass conservation that help us to exhibit invariants of the system, or the second thermodynamic law that provides a function that is always non-negative along the trajectories. Our aim is therefore to develop a new viewpoint and angle for the stability analysis and control design of chemical reactors that could more specifically be linked to and based on the physics.

In this work, a simple but comprehensive example of a chemical reactor is considered: a continuous stirred tank reactor (CSTR) with an exothermic reaction. Depending on the parameters of such a reactor, this system can exhibit multiple steady states. The objective is to interpret the stability, the region of attraction etc. of those steady states in terms of some thermodynamic functions. Contrary to most of the studies made on such reactors, we shall consider as few as possible assumptions when writing the dynamical models. For instance we shall not consider the usual hypothesis of constancy of the heat capacities or the heats of reaction. We shall also first consider all possible reaction rates, and discuss how this influences thermodynamics.

The aim of this work is to give a more physical insight of the dynamical behaviour of a chemical reactor in terms of the thermodynamic properties of the system. According to the second principle, entropy production is always non-negative along the system trajectories. Moreover, in some open systems the steady state is a minimum for entropy production. This seems to indicate that there could be a Lyapunov function related to entropy or entropy production. We shall also present analysis results about the influence of material exchange between the CSTR and the environments and of the chemical reactions occurring in the reactor on the entropy production and the use of entropy production as a Lyapunov function.

References

[1] R. B. Warden, R. Aris, and N. R. Amundson, "An analysis of chemical reactor stability and control–VIII : The direct method of Lyapunov. Introduction and applications to simple reactions in stirred vessels," *Chemical Engineering Science*, vol. 19, no. 3, pp. 149–172, 1964.

[2] ——, "An analysis of chemical reactor stability and control–IX : Further investigations into the direct method of Lyapunov," *Chemical Engineering Science*, vol. 19, no. 3, pp. 173–190, 1964.

[3] G. Beretta and E. Gyftopoulos, "Thermodynamic derivations of conditions for chemical equilibrium and of Onsager reciprocal relations for chemical reactors," *Journal of Chemical Physics*, vol. 121, pp. 2718–2728, 2004.

[4] J. M. Tarbell, "A thermodynamic Liapunov function for the near equilibrium cstr," *Chemical Engineering Science*, vol. 32, no. 12, pp. 1471–1476, 1977.

Robust Nonlinear Receding-Horizon Observer applied to continuous cultures of phytoplankton

G. Goffaux, A. Vande Wouwer
Service d'Automatique
Faculté Polytechnique de Mons
Boulevard Dolez 31, B-7000 Mons
Guillaume.Goffaux, Alain.VandeWouwer@fpms.ac.be

Introduction

Due to the lack of reliable on-line measurements of the key components of cell cultures, state estimation techniques (or software sensors) play an increasingly important role in bioprocess monitoring. A challenge to face in the design of software sensors is however the uncertainty associated with the underlying bioprocess model, which motivates in turn the development of robust state estimation techniques.

Receding-horizon estimation is a popular method where the most-likely initial conditions of a process model are estimated on the basis of data available in a moving time frame by solving a minimization problem. Using the estimated values and the process model, a state prediction can then be computed up to the next measurement time. Several applications of receding-horizon observers can be found in, e.g., [3], [1] and [5].

Contribution

In this study, the classical situation is considered, where a process model has been previously identified based on experimental data, and where parameter bounds have been evaluated. Our objective is to design a state estimation method, which would be robust to these parameter uncertainties. The formulation of this problem naturally leads to a nonlinear min-max optimization problem. The latter can either be solved numerically (at the price of expensive computation), or converted to a simpler minimization problem by using a model linearization along a nominal trajectory (defined by nominal parameter values and the most likely initial conditions) and recent results in linear robust receding-horizon estimation developed in [2].

In order to demonstrate the performance of the method, the culture of phytoplankton in a bioreactor operated in chemostat mode is considered. The tests are first conducted in simulation using Droop model [4], then using real-life experimental data.

Based on this application example, a comparison between the two numerical solution approaches to the min-max optimization problem is carried out. In order to reduce the computational expense required by the "brute-force" approach to the min-max optimization problem, advantage is taken from the monotonicity properties of the considered application example.

Results

Tests in simulation and with real-life experimental data show good performance of robust methods with respect to model uncertainties. Moreover, in the second version, linearization allows to significantly reduce the computational load. Tuning is easy because it is only related to the length of the time window and to the weighting matrix of the a priori initial estimation.

Acknowledgment

This paper presents research results of the Belgian Network DYSCO (Dynamical Systems, Control, and Optimization), funded by the Interuniversity Attraction Poles Programme, initiated by the Belgian State, Science Policy Office. The scientific responsibility rests with its authors.

References

[1] M. Alamir and J.P. Corriou. Nonlinear receding-horizon state estimation for dispersive adsorption columns with nonlinear isotherm. *Journal of process control*, 13 (6):517–523, 2003.

[2] A. Alessandri, M. Baglietto, and G. Battistelli. Robust receding-horizon state estimation for uncertain discrete-time linear systems. *Systems & Control Letters*, 54:627–643, 2005.

[3] P. Bogaerts and R. Hanus. On-line state estimation of bioprocesses with full horizon observers. *Mathematics and Computers in Simulation*, 56:425–441, 2001.

[4] M. Droop. Vitamin B12 and marine ecology IV : The kinetics of uptake growth and inhibition in monochrisis lutheri. *Journal of the Marine Biological Association*, 48(3):689–733, 1968.

[5] H. Valdéz-González, J. Flaus, and G. Acuña. Moving horizon state estimation with global convergence using interval techniques : Application to biotechnological processes. *Journal of Process Control*, 13:325–336, 2003.

Unravelling *E. coli* dynamics close to maximum growth temperature through heterogeneous modelling

Eva Van Derlinden, Ivan Lule, Kristel Bernaerts and Jan F. Van Impe
Chemical and Biochemical Process Technology and Control Section,
W. de Croylaan 46, B-3001 Leuven, Belgium
jan.vanimpe@cit.kuleuven.be - kristel.bernaerts@cit.kuleuven.be - eva.vanderlinden@cit.kuleuven.be

1 Introduction

Traditional microbial growth models applied in predictive microbiology are based on the assumption of sigmoidal growth curves. After an initial adaptation phase (the lag phase), microorganisms enter the exponential growth phase in which they grow at the maximum specific growth rate, determined by the environment. At a certain point, growth is slowed down and finally inhibited, e.g., by accumulation of a toxic metabolite or a shortage in nutrients (stationary phase). An extensive experimental study revealed that growth of *E. coli* K12 MG1655 in Brain Heart Infusion broth at elevated temperatures (close to its maximum temperature for growth of about 46°C) does not follow a typical sigmoidal growth curve characterized by a lag, exponential and stationary phase [4]. The exponential growth phase at 45°C is clearly disturbed. Based on plate count data and microscopic images, the existence of a more heat resistant subpopulation was hypothesized. This hypothesis is tested in this paper by means of a heterogeneous modelling approach (in analogy with [2]).

2 Materials and methods

The kinetics of *E. coli* K12 MG1655 were studied in Brain Heart Infusion broth at superoptimal temperatures in a temperature controlled environment. Cell density was determined based on plate counts.
Microbial growth is described by the model of Baranyi and Roberts (1994), in which temperature dependence of the maximum specific growth rate is incorporated by the Cardinal Temperature Model with Inflection (CTMI) [3]. This model encloses four parameters: the cardinal temperatures T_{min}, T_{opt} and T_{max} (the minimum, optimum and maximum growth temperature, respectively) and μ_{opt} (the specific growth rate at T_{opt}). Growth curves were simulated with Matlab (version 6.5, The Mathworks Inc.) and parameter estimates were acquired by minimization of the sum of squared errors (SSE), using lsqnonlin of the Matlab Optimization Toolbox. Simultaneously, parameter variances were calculated with the jacobian matrix.

3 Results and discussion

The postulated hypothesis considers two subpopulations: one sensitive population and another (very small) population with increased heat tolerance. A large fraction of the initial population density inactivates being unable to resist the inimical temperature. A remaining smaller fraction is able to resist the stressing temperature and multiplies. Superposition of the dynamics of these two subpopulations and taking into account experimental variability (inherent to the experimental set-up) enables accurate prediction of the experimental data).

4 Conclusion

A heterogeneous modelling approach enables accurate description of experimental data hereby confirming the existence of a small heat resistant subpopulation in typical inoculum culture of *E. coli* K12 MG1655. Additional dynamic experiments will be performed to give more insight in the microbial behavior within the superoptimal temperature region and in the temperature region between microbial growth and inactivation.

5 Acknowledgements

This research is supported in part by OT/03/30 and the K.U.Leuven-BOF EF/05/006 Center-of-Excellence Optimization in Engineering of the Research Council of the Katholieke Universiteit Leuven, the Belgian Program on Interuniversity Poles of Attraction, initiated by the Belgian Federal Science Policy Office. K. Bernaerts is a Postdoctoral Fellow with the Fund for Scientific Research Flanders (FWO-Vlaanderen).

References

[1] J. Baranyi and T.A. Roberts (1994). A dynamic approach to predicting bacterial growth in food. *International Journal of Food Microbiology* 23,277-294

[2] McKellar R.C. (1997) A heterogeneous population model for the analysis of bacterial growth kinetics. *International Journal of Food Microbiology* 36, 179-186

[3] L. Rosso, J.R. Lobry, S. Bajard and J.P. Flandrois (1995) Convenient model to describe the combined effects of temperature and pH on microbial growth. *Appl. Environ. Microbiol.* 61, 610-616

[4] Van Derlinden, E. , Bernaerts, K. B. and Van Impe, J.F. (2007) Dynamics of *Escherichia coli* at elevated temperatures: effect of temperature history and medium. *Journal of Applied Microbiology* (In press, available online 10.1111/j.1365-2672.2007.03592.x)

Global tracking for a plug flow tubular reactor

N. Beniich, D. Dochain
Université Catholique de Louvain,
4 Av G. Lemaître,
B-1348 Louvain-la-Neuve, Belgium,
Email: Nadia.Beniich@uclouvain.be

A. El Bouhtouri
Université Chouaib Doukkali
Faculté des Sciences
BP 20, El Jadida- Morocco

Abstract

This work present a relatively simple adaptive control (in the presence of the input constraints) for a class of plug flow tubular reactors. Our objective is to regulate the reactor temperature in a prespecified neighborhood of a given reference profile.

The dynamics of plug flow tubular reactors are described by nonlinear partial differential equations derived from mass and balances. Here, we consider exothermic chemical reaction $A \longmapsto bB$. The dynamics of this process has the form (see [1]):

$$\begin{aligned} \frac{\partial T(t,z)}{\partial t} &= -v\frac{\partial T(t,z)}{\partial z} + \alpha f(T(t,z),C(t,z)) \\ &\quad -k_0(T(t,z)-T_c(t,z)) \qquad (1) \\ \frac{\partial C(t,z)}{\partial t} &= -v\frac{\partial C(t,z)}{\partial z} - f(T(t,z),C(t,z)) \qquad (2) \end{aligned}$$

with the initial and boundary conditions:

$$\begin{aligned} T(0,t) &= T_{in}(t), \qquad C(0,t) = C_{in}(t) \qquad (3) \\ T(z,0) &= T_0(z), \qquad C(z,0) = C_0(z) \end{aligned}$$

In [2], a constrained adaptive control scheme has been developed with the objective to regulate the temperature of exothermic tubular reactors with axial dispersion in ball centred at the temperature profile x^* and of arbitrary prescribed radius $\lambda > 0$, where the inlet and coolant temperature as control actions. The convergence is local in the sense that the initial temperature is constrained to live in prefixed set. It may even be impossible to reduce the reaction temperature from such reference profile by any type of control of the temperature alone. To overcome this limitation, we introduce an additional input action which has a cooling effect. The considered input in this research is:

$$u(t) = \begin{pmatrix} u_1(t) \\ u_2(t) \\ u_3(t) \end{pmatrix} = \begin{pmatrix} T_{in}(t) \\ T_c(t,z) \\ C_{in}(t) \end{pmatrix} \qquad (4)$$

which means that our problem is a nonlinear boundary control problem. The first step of this work is to transform the model (1), (2) and the boundary conditions (3) in the context of the Fattorini model of boundary control see [3], [2].

For physical reasons, we assume that u_i (i = 1, 3) are constrained as follows: for all $t \geq 0$

$$\underline{u}_1 \leq u_1(t) \leq \bar{u}_1,\ \underline{u}_2 \leq u_2(t) \leq \bar{u}_2,\ 0 \leq u_3(t) \leq \bar{u}_3 \qquad (5)$$

where $\underline{u}_i$, $\bar{u}_i$ (i = 1, 2), $\bar{u}_3$ are positive constants.

we adopt an approach based on modified λ-tracking controllers, whereby prespecified asymptotic tracking accuracy, quantified by λ, is insured for all initial temperature. The adaptive control strategy does not require any knowledge of the system parameters and does not invoke an internal model, only a feasibility assumption in terms of the reference temperature and the input constraints is assumed.

Acknowledgements

This paper presents research results of the Belgian Network DYSCO (Dynamical Systems, Control, and Optimization), funded by the Interuniversity Attraction Poles Programme, initiated by the Belgian State, Science Policy Office. The scientific responsibility rests with its authors.

References

[1] I. Aksikas, J. Winkin and D. Dochain . Optimal LQ-feedback regulation of a nonisothermal plug flow reactor model by spectral factorization. *IEEE Transactions on Automatic Control*, 52 (10), 1179 - 1193, 2007.

[2] N. Beniich, A. El Bouhtouri and D. Dochain Input constrained adaptive local tracking for a nonlinear distributed parameter tubular reactor, *submitted to Automatica*.

[3] H.O. Fattorini. Boundary control systems. *SIAM Journal on Control*, 6, 349-385, 1968.

Dynamical Analysis of a Biochemical Reactor with Time Delay

A. K. Dramé[1,3], D. Dochain[1] and J. J. Winkin[2]

[1]CESAME, Université catholique de Louvain, 4-6 av. G. Lemaître, B-1348 Louvain-La-Neuve, Belgium. drame@inma.ucl.ac.be, dochain@csam.ucl.ac.be

[2] Department of Mathematics, University of Namur (FUNDP), 8 Rempart de la Vierge, B-5000 Namur, Belgium. joseph.winkin@fundp.ac.be

[3] Department of Mathematical Sciences, University of Nevada Las Vegas, Las Vegas, NV, USA. abdoukhadry.drame@unlv.edu

It has long been known that the classical models of growth response such as Monod or Haldane models, are not able to account for the oscillations in chemostat occuring under suitable operational conditions as it has been observed in many experimental studies (see [2], [3], [4] and references therein). The need of considering a time delay in the growth response, as a source of oscillations, has been therefore emphasized by many authors : see eg the references cited in [1]. The effect of delay in simple chemostat models was discussed e.g. in [2], [5] and [6]. Following the same idea, we consider here a biochemical reactor distributed parameter model with time delay, where the delay can be considered in the growth response for the same reasons as in the chemostat models.

Applying the mass balance principle to the limiting substrate concentration $S(\tau,\zeta)$ and the living biomass $X(\tau,\zeta)$ leads to the following partial differential equations, where $S_r(\tau,\zeta) := S(\tau-r,\zeta)$ and $X_r(\tau,\zeta) := X(\tau-r,\zeta)$:

$$\frac{\partial S}{\partial \tau} = D\frac{\partial^2 S}{\partial \zeta^2} - \nu\frac{\partial S}{\partial \zeta} - k\mu(S,X)X \tag{1}$$

$$\frac{\partial X}{\partial \tau} = -k_d X + \mu(S_r,X_r)X_r\,, \tag{2}$$

with the boundary conditions : for all $\tau \geq 0$,

$$D\frac{\partial S}{\partial \zeta}(\tau,0) - \nu S(\tau,0) + \nu S_{in} = 0 \quad \text{and} \quad \frac{\partial S}{\partial \zeta}(\tau,L) = 0\,, \tag{3}$$

and initial condition : for all $-r \leq s \leq 0$, $0 \leq \zeta \leq L$

$$S(s,\zeta) = S_0(s,\zeta), \quad X(s,\zeta) = X_0(s,\zeta). \tag{4}$$

In the equations above, D, ν, k, k_d, S_{in}, μ, r, L denote the diffusion coefficient, the superficial fluid velocity, the yield coefficient, the death coefficient of the biomass, the inlet limiting substrate concentration, the specific growth function or growth response, the delay parameter and the length of the reactor, respectively. The parameters D, ν, k, k_d, S_{in}, r and L are positive. In the right hand side of equation (1), the last term represents the growth response while the other terms represent the hydrodynamics (i.e. diffusion and transport terms). As the biomass is assumed to be fixed, there is no hydrodynamic term in the right hand side of equation (2). The first term in the right hand side of this equation represents the mortality of biomass and the last one represents the growth response with delay. The delay is considered in equation (2) only : it is assumed to be caused by memory effects of micro-organisms. The substrate is instantaneously consumed althought the biomass is produced with delay.

This model has been analyzed through a dimensionless semilinear infinite dimensional system description, [1]. Under suitable (smoothness and monotonicity) assumptions on the specific growth function and the initial data, the existence of global solutions of the system equations and their regularity are reported. The invariance (under the system dynamics) of the domain defined by physically feasible state variables is also proved as well as the relative compactness of the state trajectories. In addition, the system can have multiple equilibrium profiles and, as a consequence of time delay, periodic solutions bifurcating from the trivial equilibrium profile.

Acknowledgments This paper presents research results of the Belgian Network DYSCO (Dynamical Systems, Control, and Optimization), funded by the Interuniversity Attraction Poles Programme, initiated by the Belgian State, Science Policy Office. The scientific responsibility rests with its authors.

References

[1] A. K. Dramé, D. Dochain and J. Winkin, Dynamical Analysis of a biochemical reactor distributed parameter model with time delay, *Proceedings of ECC'07*, Kos, Greece, July 2-5, 2007, Cd-Rom paper ThC05.1, pp. 5003-5007.

[2] N. MacDonald ; Time Delay in Simple Chemostat Models ; *Biotechnology and Bioengineering*, Vol. XVIII, pp. 805-812, 1976.

[3] N. MacDonald ; Time delays in chemostat models, *in Microbial Population Dynamics, M. J. Bazin, ed., CRC Press, Boca Raton, FL,* 1982.

[4] T. Patarinska, D. Dochain, S. N. Agathos and L. Ganovski ; Modelling of continuous microbial cultivation taking into account the memory effects, *Bioprocess Engineering* 22 517-527, 2000.

[5] S. Ruan and G. S. K. Wolkowicz ; Bifurcation analysis of a chemostat model with a distributed delay, *J. Math. Anal. Appl.*, 204 (1996), pp. 786-812.

[6] T. F. Thingstad and T. I. Langeland ; Dynamics of chemostat cultutre : The effect of a delay in cell response, *J. Theor. Biol.,* 48 (1974), pp. 755-763.

Mechanics and control issues for piezo actuated positioning stages

J. van Hulzen[1,2], P.M.J. Van den Hof[1], J. van Eijk[2],G. Schitter[1]
[1]Delft Center for Systems and Control
[2]Precision and Microsystems Engineering Department, Mechatronics
Delft University of Technology, Delft, The Netherlands
Email: j.r.vanhulzen@tudelft.nl

1 Introduction

In positioning systems where high precision and high bandwidth operation is required piezo electric actuators (PEA) are often used. Typical examples are scanning tunnel or atomic force microscopes. PEA's are very stiff and have poorly damped resonant modes at high frequencies. These resonant modes can be excited leading to inaccuracy or even instability if feedback is used.

2 Methods of damping

Various methods of damping resonant modes in piezo actuated systems have been proposed. These methods exploit the fact that PEA's act as transducers. One idea is to dissipate energy originating in the mechanical domain in the electrical domain. A second use of the transducer property is to measure the voltage induced by the inertia forces associated with the load. As a third method of damping we can use velocity feedback using a separate sensor. All methods discussed so far deal with resonant modes in the mechanical domain by damping in the electrical domain or by using the transducer property. As an alternative to this we can deal with these problems directly in the mechanical domain. An advantage of this approach is that we avoid the amplification of noise associated with using sensor signals for velocity feedback.

3 Damping through load balancing

With careful design we can use the mechanical properties of the actuator-load configuration to deal with the resonant modes of the piezo-actuator. The goal is to shift the resonant modes towards the anti resonances associated with the PEA [1]. An effective way of doing this is by tuning the mass of the load and to a lesser extend the damping. In [1] a model of the mechanical behavior of a PEA has been derived. The PEA is modeled as a series connection of mass spring damper systems. The transfer function of the PEA is

$$y(s) = \frac{N_p(s)}{D_p(s)}\left(F_p(s) - F_s(s)\right) \tag{1}$$

$$N_p(s) = \prod_{i=1}^{\infty} \frac{m_p}{i^2\pi^2} + c_p s + k_p \tag{2}$$

$$D_p(s) = \prod_{i=1}^{\infty} \frac{4m_p}{(2i-1)^2\pi^2} + c_p s + k_p \tag{3}$$

Where m_p is the mass of the PEA and c_p and k_p its damping and stiffness. The system shown can be modeled as

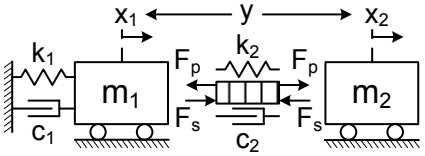

Figure 1: PEA in positioning system with frame m_1, stage m_2, frame stiffness/damping k_1/c_1, and pre-load spring and damping k_2/c_2

$$y(s) = \frac{N_s(s)}{D_s(s)}F_s(s) \tag{4}$$

$$N_s = (m_1+m_2)s^2 + c_1 s + k_1 \tag{5}$$

$$D_s = m_1 m_2 s^4 + (m_1 c_2 + m_2(c_1+c_2))s^3 + (m_1 k_2 + m_2(k_1+k_2) + c_1 c_2)s^2 + (c_2 k_1 + c_1 k_2)s + k_1 k_2 \tag{6}$$

Here we have frame stiffness k_1, frame mass m_1 and a pre-load spring k_2 in parallel with the PEA. The mass of the load is represented as m_2. Damping is represented by c_1 and c_2. Combining system and PEA we get

$$y(s) = \frac{N_p(s)N_s(s)}{N_s(s)D_p(s) + N_p(s)D_s(s)}F_p \tag{7}$$

From this last expression we can conclude that the closed loop zeros associated with the mechanics of PEA and load are invariant under the mechanical feedback introduced by mass, spring and damper. In contrast, for increasing load the poles of the closed loop system shift towards the zeros. Because a PEA has low mass and high stiffness, the most effective parameter for manipulating the closed loop poles is the mass of the load. If we increase the loading of the PEA, the resonant modes will shift to lower frequencies. Under high load the high resonant peaks will decrease to such an extend that cancelations occurs and a second order system remains. The first peak of the PEA will shift to a lower frequency and has to be dealt with using additional damping.

References

[1] H. J. M. T. A. Adriaens, W. L. de Koning, and R. Banning, Modeling piezoelectric actuators, IEEE/ASME Trans. Mechatron., vol. 5, no. 4, pp. 331 to 341, Dec. 2000.

Iterative Learning Control for wet-plate clutches

Gregory Pinte [1,2], Wim Symens [1], Jan Swevers [2]
[1]Flanders' Mechatronics Technology Center
[2]Department of Mechanical Engineering, Division PMA, Katholieke Universiteit Leuven
Celestijnenlaan 300 B/D, 3001 Heverlee, Belgium
Email: gregory.pinte@fmtc.be

1 Introduction

A wet-plate clutch (Fig. 1) is a mechanical device that transmits torque from its input axis to its output axis by means of friction. The input axis of the clutch is connected to a drum, which is a hollow cylinder with grooves on the inside. A first set of friction plates (clutch plates) with external toothing that can slide in those grooves are pressed against a second set of friction plates (clutch discs) with internal toothing that can slide over a grooved bus connected to the output axis. When the two sets of friction plates are pressed against each other by a piston, torque is transmitted. Initially, when the clutch is not engaged, the piston should be positioned as far as possible from the friction plates to avoid losses due to viscous friction of the oil between the plates. When the vehicle control unit gives the command to close the clutch, the distance between the piston and the plates should be decreased as fast as possible to zero, without the piston and the plates making brutal contact. Nowadays, this is achieved using feedforward control of the electro-hydraulic valve. However, long calibration procedures are necessary to find the optimal feedforward signal for a smooth clutch engagement. Furthermore, since the controlled system is time-varying (wear of the friction plates, variable temperature,...), regular recalibrations of the control signal are inevitable. To avoid these cumbersome calibrations, an ILC control system [1] is developed, which learns the appropriate control signal based on the quality of the previous engagements.

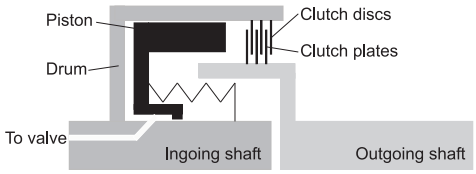

Figure 1: Design of a wet-plate clutch

2 ILC controller

To bring the piston close to the friction plates, a position reference trajectory is defined that has to be learned by the ILC controller. Afterwards, the final engagement of the clutch is realized using an additional feedforward action. Good tracking of the reference leads to a small feedforward action and consequently to a smooth and fast clutch engagement. The ILC scheme, used for the reference tracking, is added to a closed position loop. The performance of this closed loop with a linear feedback controller is low because of the time delay and the nonlinearity of the controlled system. However, this performance can be increased significantly by the ILC controller, which updates the control signal at each engagement based on the control signal and the reference error at the previous engagement. To take into account the wear of the friction plates, the reference trajectory of the ILC system is adapted online. Since it is too expensive to equip all clutches with a sensor to detect the piston's displacement, in a second part of the project, a pressure sensor is used as the only available sensor in a similar ILC control configuration.

3 Experimental results

The controllers are validated on a non-rotating wet-plate clutch. Fig. 2 shows the results for the ILC of the piston position with an adaptive reference. When the number of controlled engagements increases, the tracking response improves due to the ILC action and the engagement quality becomes better. After 5 engagements, the end point of the reference trajectory is adapted, which leads to a decrease of the feedforward action and a further improvement of the clutch engagement quality. Future work consists of an extension to a rotating set-up, where additional challenges are expected e.g. due to the centrifugal disturbing forces.

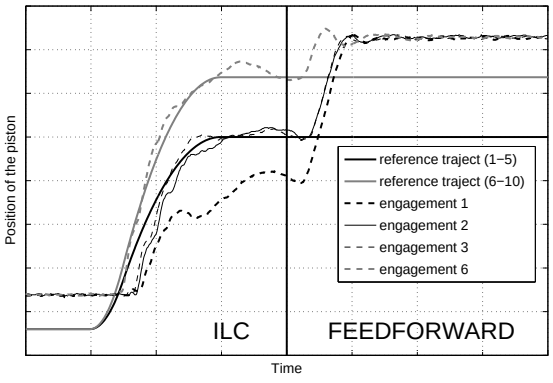

Figure 2: Effect of ILC on the piston position.

References

[1] D. A. Bristow, M. Tharayil, A.G. Alleyne. A Survey of Iterative Learning Control. *IEEE control systems magazine* vol. 26 (3), p. 96-114, 2006

Filtered-X LMS versus repetitive control for active structural acoustic control

Bert Stallaert[1], Gregory Pinte[1,2], Steven Devos[2], Wim Symens[2], Jan Swevers[1], Paul Sas[1]
[1] Department of Mechanical Engineering, Division PMA
Katholieke Universiteit Leuven
Celestijnenlaan 300B, 3001 Heverlee, Belgium
[2] Flanders' MECHATRONICS Technology Centre
Email: Bert.Stallaert@mech.kuleuven.be

1 Introduction

This presentation investigates Active Structural Acoustic Control (ASAC) of rotating machinery with high modal density, by placing actuators as close as possible to the noise source. For this purpose, an experimental set-up has been built, as discussed in [3]. The set-up consists of a shaft supported by two bearings, of which one is made "active" by mounting piezo-actuators around it, to influence the vibration transfer in the bearings. Sound is radiated by a flexible panel mounted on the set-up.

In [4], it has been shown that an adaptive repetitive controller is able to reduce noise radiation caused by a sinusoidal disturbance. The control design is based on a procedure presented in [2], which is adapted to systems with a high modal density, for which the identification of a parametric model is difficult. This presentation builds further on these results and compares them with a Filtered Reference Least Mean Squares (FXLMS) controller, commonly used in noise control.

2 Repetitive control versus FX-LMS

For the general repetitive control (RC) scheme, the stability criterion, for $Q(z) = 1$, simplifies to:

$$|1 - L(\omega)P_{sec}(\omega)| < 1$$

Although ideally L is the inverse of P_{sec}, this solution is often not feasible and prone to changes in the plant dynamics. Therefore, [2] proposes a design procedure for the repetitive controller in which the compensating filter L is designed such that the Nyquist plot of $L(\omega)P_{sec}(\omega)$ lies in the right half-plane and is constrained within the unit circle around the point 1. This implies that the phase of $L(\omega)P_{sec}(\omega)$ must lie between -90 and 90°.

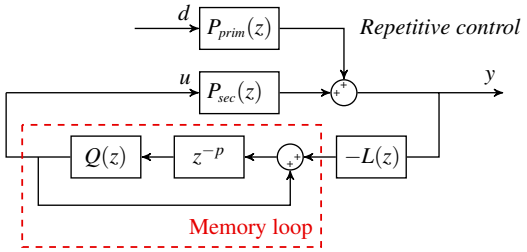

The FXLMS convergence criterion is similar to the RC stability criterion; ideally the plant model $\widehat{P}_{sec}$ exactly equals the plant P_{sec}. However, [1] shows that for an FXLMS algorithm to converge, it is necessary that the phase of P_{sec} does not differ more than 90° from the phase of the plant model $\widehat{P}_{sec}$.

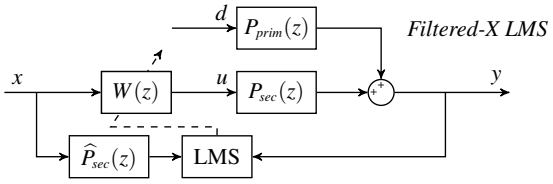

The similarity between the RC stability criterion, which results in the design of a "semi-inverse" of P_{sec} within a phase range of 90°, and the FXLMS convergence criterion, which states that $\widehat{P}_{sec}$ should equal P_{sec} within a phase range of 90°, shows the possibility to apply a similar design procedure for the FXLMS plant model as for the L-filter in RC. The procedure is evaluated based on simulation and experimental results.

Acknowledgment

Research funded by a Ph.D grant of the Institute for the Promotion of Innovation through Science and in Flanders (IWT-Vlaanderen).

References

[1] C.C. Boucher, S.J. Elliott, P.A. Nelson, "Effect of errors in the plant-model on the performance of algorithms for adaptive feedforward control," *IEE Proceedings-F Radar and Signal Processing,* 138(4):313-319, 1991.

[2] G. Pinte, R. Boonen, W. Desmet, P. Sas, "Active Structural Acoustic Control of repetitive impact noise," *Proceedings of the International Conference on Noise and Vibration Engineering, ISMA2006,* Leuven, Belgium, 2006.

[3] B. Stallaert, S.G. Hill, J. Swevers, P. Sas, "Design of active bearings for gearbox noise control," *25th Benelux meeting on systems and control,* Heeze, The Netherlands, 2006.

[4] B. Stallaert, G. Pinte, W. Symens, J. Swevers, P. Sas, "Design of a repetitive controller for gearbox noise," *26th Benelux meeting on systems and control,* Lommel, Belgium, 2007.

A Generalized Repetitive Controller Design

Goele Pipeleers, Bram Demeulenaere, Joris De Schutter, Jan Swevers
Katholieke Universiteit Leuven; Dept. of Mechanical Engineering,
Email: goele.pipeleers@mech.kuleuven.be

1 Introduction

Most of the current repetitive controllers (RCs), hereafter referred to as typical RCs (tRCs), apply the internal model principle by embedding a one-period delay into the control scheme. While being simple and often effective, the tRC structure involves a number of disadvantages: (i) in many applications, large memory buffers are needed; (ii) information about the input spectrum cannot be included and (iii) accounting for period-time uncertainty results in tRCs that are overly robust for lower harmonic frequencies. In order to overcome these disadvantages, the present paper proposes a novel type of RCs, called generalized RCs (gRCs), that sacrifices the simplicity of the tRC structure for the benefit of more design freedom. While tRCs are still encompassed as a special case, numerical results reveal that gRCs yield significantly better performance with the same amount of memory or, conversely, require substantially less memory to achieve equivalent performance.

2 Methodology

Figure 1(a) shows the structure of a tRC of order M, where N corresponds to the number of samples in one period of the input. In a proper tRC design, $L(z)$ compensates the transfer function from $u(k)$ to $e(k)$ in the original feedback system. To guarantee robust closed-loop stability, $Q(z)$ is designed as a low-pass zero-phase FIR filter with cut-off frequency sufficiently below the bandwidth ω_{BW} of the original feedback system. The design parameters W_m are computed such that the tRC yields an optimal trade-off between two performance indices, γ_{np} and $\gamma_{p,\Delta}$, that quantify its effect on the closed-loop performance for the non-periodic and the period-uncertain inputs, respectively. Δ corresponds to the relative uncertainty on the fundamental frequency of the periodic input.

Figure 1(b) shows the structure of a gRC. More design freedom is introduced by replacing $W(z)Q(z)$ of the tRC, which corresponds to a FIR filter with a particular structure, by an unstructured FIR-filter of the same order. $\tau > 0$ to overcome non-causality of $L(z)$. The design parameters X_k are computed such that the gRC yields a robustly stable closed-loop system and realizes an optimal trade-off between γ_{np} and $\gamma_{p,\Delta}$.

3 Results

To illustrate the potential of the gRC, it is compared to the tRC for an example with $N = 50$ and $\Delta = 2\%$. The RCs must

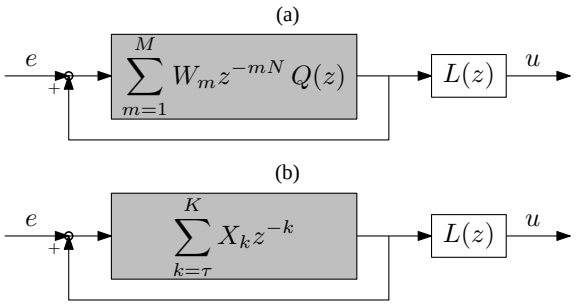

Figure 1: Structure of a tRC (a) and a gRC (b).

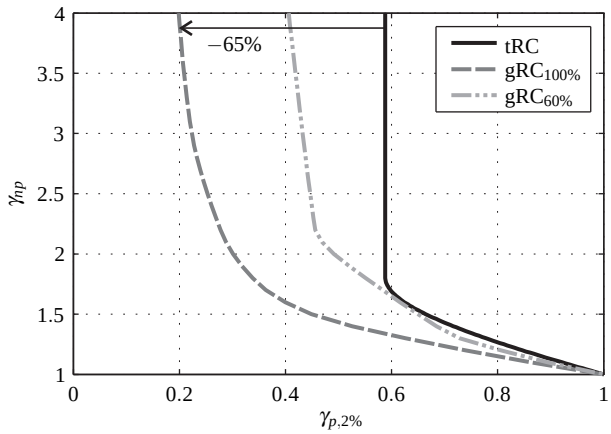

Figure 2: Tradeoff-curves between $\gamma_{p,2\%}$ and γ_{np}.

suppress the first five harmonics, while ω_{BW} corresponds to the eighth harmonic. In the tRC, $Q(z)$ is designed as the lowest-order FIR filter that fulfills the corresponding constraints.

Figure 2 compares for this example the trade-off curves between $\gamma_{p,2\%}$ and γ_{np} for the tRC and two gRCs, where the notation $\text{gRC}_{\mu\%}$ indicates that the gRC uses $\mu\%$ of the memory used by the tRC. These trade-off curves reveal that, with the same amount of memory and for the same level of non-periodic performance degradation γ_{np}, $\text{gRC}_{100\%}$ yields up to 65% better periodic performance $\gamma_{p,2\%}$ compared to tRC. Since $\text{gRC}_{60\%}$ always outperforms the tRC, a gRC allows saving at least 40% of memory without loss of performance.

Acknowledgement Goele Pipeleers is a Research Assistant of the Research Foundation - Flanders (FWO–Vlaanderen) and Bram Demeulenaere is a Postdoctoral Fellow of the Research Foundation - Flanders. This work benefits from K.U.Leuven-BOF EF/05/006 Center-of-Excellence Optimization in Engineering and from the Belgian Programme on Interuniversity Attraction Poles, initiated by the Belgian Federal Science Policy Office.

Nuclear fusion: principles and challenges

Gert Witvoet, Maarten Steinbuch
Department of Mechanical Engineering
Technische Universiteit Eindhoven
P.O. Box 513, 5600 MB Eindhoven
Email: G.Witvoet@tue.nl

Niek Doelman
TNO Science and Industry
Instrument Modeling and Control
P.O. Box 155, 2600 AD Delft
Email: Niek.Doelman@tno.nl

1 Introduction

Nuclear fusion is a very safe, clean and virtually inexhaustible energy source for the future. However, due to the large scientific and technological complexity it will take at least a few decades before fusion energy becomes available. This talk will give a short overview of the fusion principles and address some important control issues in nuclear fusion.

2 The fusion reaction

In fusion, two positively charged hydrogen nuclei, i.e. deuterium (D) and tritium (T), fuse together to form helium (He), a neutron and lots of energy (17,6MeV), see Figure 1. Due to the repulsive forces between nuclei, this reaction can only occur within very hot plasma's, typically with temperatures in the order of 10^8K.

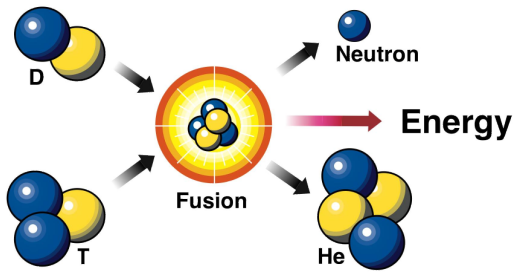

Figure 1: The fusion reaction

3 The tokamak

The best way to confine such extremely hot plasmas is by magnetic confinement. A very promising configuration is the toroidal *tokamak*, see Figure 2. Strong poloidal magnets create a large toroidal magnetic field inside the plasma, while transformator coils generate a current in the plasma which results in a poloidal field. The resulting helical field confines the charged plasma particles very well. Poloidal field coils can further shape the plasma inside the tokamak.

4 Control in nuclear fusion

Although confined within the magnetic field, the plasma inside the tokamak still faces various instabilities [1], e.g.

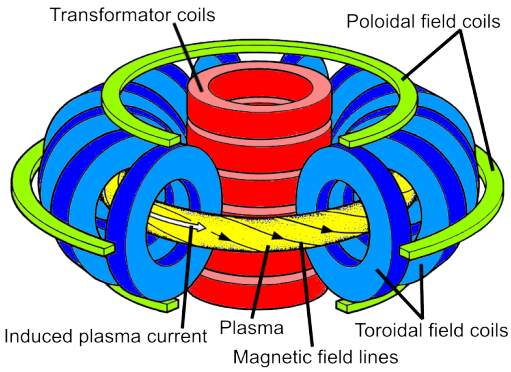

Figure 2: Schematic of a tokamak

- Neoclassical Tearing Mode (NTM), also known as magnetic islands,
- Edge Localized Mode (ELM),
- Resistive Wall Mode (RWM),
- Sawtooth instability.

Each instability diminishes the 'quality' of the plasma, or even destroys it, possibly resulting in disruptions which come with large forces on the tokamak. Hence control is necessary to suppress these instabilities. The 'performance' of the plasma can further be enhanced by advanced conditioning of the plasma via control of parameters like

- shape and position of the plasma
- plasma density and plasma pressure β
- q-profile and temperature profile
- plasma current

Unfortunately, for each control challenge only a limited amount of sensors and actuators is available.

5 Towards the future

At present, accurate input-output models considering these control challenges are scarce. Modeling and control of the above phenomena is clearly a necessity and opportunity on the way to realizing a stable fusion power plant.

References

[1] Control of Tokamak Plasmas, *IEEE Control Systems Magazine, special issues*, October 2005 & April 2006.

Modeling for control of an inflatable space reflector

Thomas Voß
University of Groningen, Faculty of Mathematics & Natural Sciences,
Nijenborgh 4, 9747 AG Groningen, The Netherlands
t.voss@rug.nl

1 Introduction

The goal of our research is to develop a controller which can be used for shape control of an inflatable reflector. Inflatable structures have very nice properties, suitable for aerospace applications. We can construct a huge light weight reflector for a satellite which consumes very little space in the rocket because it can be inflated when the satellite is in the orbit. So with this technology we can build telescopes which are about 100 times bigger then the current technology.

2 Modeling

Before we can design a controller which can be used to influence the shape of an inflatable structure we have to define a dynamical model of our structure. Unlike the standard modeling, used i.e. by physicists, we want to model the dynamics of our structure in the port-Hamiltonian frame work, see [1], in order to easily design a control based on the framework. We start with a simple one dimensional beam, which represents a cut through our inflatable structure, similar to [2]. A possible structure for such an inflatable can be seen in figure 1.

As sketched in the picture, we use a combination of two materials. The first is the so called base layer to which we bond piezo-electric patches. These patches are then used to influence the shape of the system. To model the system, we have to describe the potential and kinetic energy stored in it. The potential energy of the base layer can be described, see [3], as

$$P_{base} = \int_V \varepsilon^T \sigma dV,$$

where ε is the strain and σ is the stress in the base layer. The potential energy of the piezo-electric material is given as

$$P_{piezo} = \int_V \varepsilon^T \sigma + E^T D dV,$$

where E is the electrical field and D is the electrical displacement in the piezo-electric material. For both materials the kinetic energy can be stated as

$$K = \int_0^L \rho \dot{w}(x,t) dx,$$

where w is the displacement and ρ is the mass per length of the material. It is easy to see that the stored energy is given in a distributed fashion. Now we have two possibilities to achieve a discretized port-Hamiltonian model. We could either define a distributed port-Hamiltonian system and then discretize this model to achieve a lumped model. This is not trivial and the corresponding methods are not applicable to higher dimensions, see [4]. Or we discretize the stored energies and use the discretized form to get the port-Hamiltonian model. For our research we follow the second approach. The so achieved model is then be used to design a controller which will be able to alter the shape of the inflatable structure in the desired way.

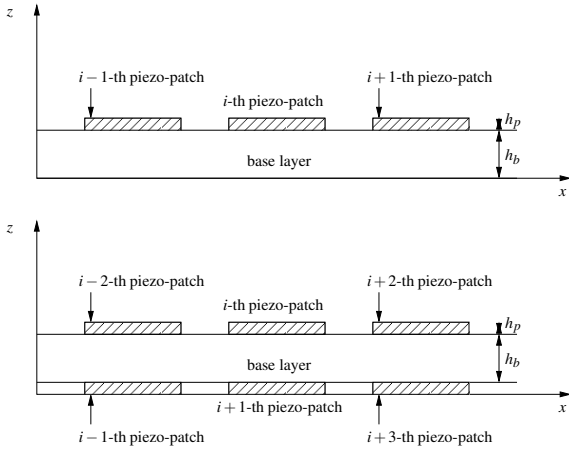

Figure 1: Two possible structures for an active membrane

3 Acknowledgements

I would like to thank my supervisor Jacqueline Scherpen for the support in my research and the MicroNed programme for the funding of the research.

References

[1] A.J. VAN DER SCHAFT & B.M. MASCHKE, *The Hamiltonian formulation of energy conserving physical systems with external ports,* Archiv für Elektronik und Übertragungstechnik, 49, pp. 362-371, 1995

[2] C.H. PARK, *Dynamics modeling of beams with shunted piezoelectric elements,* Journal of Sound and Vibration, 268, pp. 115-129, 2003

[3] S.P. TIMOSCHENKO & J.N. GOODIER, *Theory of Elasticity, Third Edition,* McGraw-Hill International Editions, 1970

[4] G. GOLO, V. TALASILA, A.J. VAN DER SCHAFT, B.M. MASCHKE, *Hamiltonian discretization of boundarycontrol systems,* Automatica, 40, pp. 757-771, 2004

ACC performance and design

G.J.L. Naus[a], J. Ploeg[b], M.J.G. v.d. Molengraft[a]

[a]Department of Mechanical Engineering, Control Systems Technology group,
Technische Universiteit Eindhoven, Eindhoven, The Netherlands
g.j.l.naus@tue.nl, m.j.g.v.d.molengraft@tue.nl

[b]Business Unit Automotive, Department of Integrated Safety,
TNO Helmond, The Netherlands
jeroen.ploeg@tno.nl

Abstract

Introduction
Adaptive Cruise Control (ACC) enables automatic following of a vehicle. The relative distance x_r is controlled (see Fig. 1). A driver dependent part determines the desired host vehicle acceleration $a_{h,d}$, while a vehicle dependent part controls the longitudinal dynamics via actuation of the throttle u_{th} and brake system u_{br} (see Fig. 2).

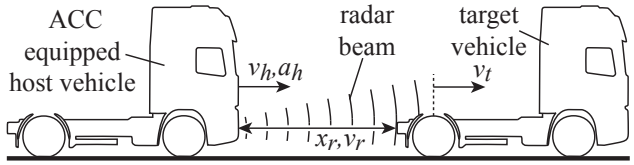

Fig. 1: *ACC system setup.*

Problem statement
Focusing on the driver dependent part, nonlinear (situation dependent) driver behaviour generally is accounted for in the controller design via scheduling gains and switching logic, while disregarding stability issues. Furthermore, the lack of appropriately defined performance metrics yields time-consuming tuning by trial-and-error. Hence, performance metrics as well as a structured control framework for ACC are required.

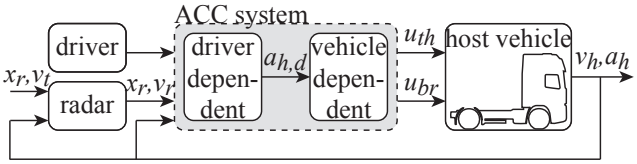

Fig. 2: *ACC control structure.*

ACC performance evaluation
On the basis of literature and on-the-road experiments, metrics are determined to enable objective performance evaluation of an ACC system in a qualitative manner. In case of a passenger car, both comfort and desirability have to be considered. Comfort is mainly related to vestibularly detectable variables, whereas desirability is mainly related to visually and auditorily detectable variables.

Regarding desirability, x_r, v_r and the so-called time-to-collision $TTC = x_r/v_r$ are the most promising metrics, yet some situation dependency seems inevitable. Regarding comfort, acceleration and jerk peak values are appropriate metrics enabling objective performance evaluation.

ACC design
Besides the control objective regarding x_r, the relative velocity v_r should be limited based on desirability and the acceleration and jerk should be limited out of comfort reasons. Furthermore, the nonlinear driver behaviour as well as safety considerations yield various (nonlinear) constraints on the control output $a_{h,d}$.

Model Predictive Control (MPC) is adopted as a suitable, structured framework for constrained, MIMO, nonlinear controller design. MPC minimizes a cost function J regarding the control output u over a user-defined prediction horizon; $\min_u J(u, \varepsilon, \mathscr{R})$, with ε the error with respect to the control objectives and $\mathscr{R}$ the performance related requirements. Adopting a closed-loop MPC synthesis enables explicit, offline optimization of the state-dependent controller gains. This yields a hybrid control synthesis, which prevents the need for significant online computational power.

Simulations as well as on-the-road experiments have been executed, showing appropriate behaviour of the ACC system.

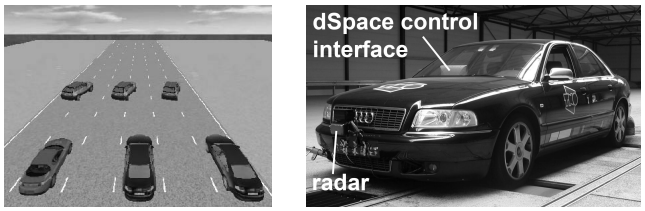

Fig. 3: *Screenshot of the simulation environment and the Audi S8 with which the ACC is tested.*

Future work
Current research focusses on further integration of the performance metrics in the tuning process and the possibly automated, driver-specific tuning.

Model-based traffic flow control for the reduction of fuel consumption and exhaust emissions

S. K. Zegeye, B. De Schutter[1], and J. Hellendoorn
Delft Center for Systems and Control
Delft University of Technology, Mekelweg 2, 2628 CD Delft, The Netherlands
Email: s.k.zegeye@tudelft.nl, b@deschutter.info, j.hellendoorn@tudelft.nl

1 Introduction

Road transport depends almost entirely on natural oil. In spite of the development of new high-quality, low-pollution fuels, the consumption of fuels derived from natural oil increases every year. This results in a negative effect on the environment. Moreover, in recent epidemiological studies of the effects of combustion-related (mainly traffic-generated) air pollution, NO_2 was shown to be associated with adverse health effects [2]. These problems can be addressed either by large-scale substitution of natural oil by alternative fuels, enhancing vehicle technology or/and reducing waste of fuels. The first option will be difficult to fully implement on the short to medium term. Therefore, reducing fuel consumption by reducing waste of fuel and enhancing vehicle technology are sensible strategies. This can be achieved by using different traffic flow control measures to minimize the impact of traffic.

2 Objective

Our objective is to use various traffic control measures (such as traffic signals, on ramp metering, variable speed limits, opening or closing shoulder lanes, route guidance) to reduce fuel consumption (e.g., due to idling and frequent acceleration and deceleration) and exhaust emission. Two possible control approaches will be investigated, infrastructure-based and integrated road-vehicle. In the first approach the control strategy will be driven by sensors and control equipment on the road side, while in the second the infrastructure-based framework will be integrated with the growing availability of in-car communication, sensing, and control systems to obtain an integrated road-vehicle control system, resulting in better and more sustainable mobility.

3 Approach

The above objectives will be addressed using a model-based control approach (also called model predictive control, or MPC for short). In this approach models are used to predict the emission and fuel consumption impact of various control measure settings on the traffic flow over a certain prediction horizon (see Figure 1). The most optimal settings are then selected using numerical optimization and applied to the traffic system. After a given fixed time period (control time step) the current traffic situation is assessed again through new measurements and updated predictions of demands, etc., and the whole process is repeated.

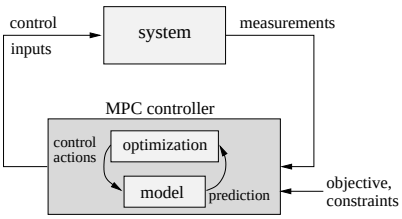

Figure 1: Schematic representation of MPC.

By assigning weights to the several, often conflicting, traffic control objectives (such as minimizing emissions and fuel consumption, minimizing travel times, minimizing the number of stops, maximizing throughput, etc.) a balanced trade-off between these objectives can be obtained. Furthermore, this optimization-based approach also allows to explicitly take into account various constraints such as hard limits on emission rates in certain areas, maximal queue lengths at some on-ramps or intersections, etc.

4 Acknowledgments

Research supported by the Shell/TU Delft Sustainable Mobility program, the BSIK project “Transition towards Sustainable Mobility (TRANSUMO)”, and the Transport Research Center Delft.

References

[1] J.M. Maciejowski. *Predictive Control with Constraints*. Prentice Hall, Harlow, England, 2002.

[2] WHO. Health aspects of air pollution, *Results from the WHO projects ”systematic review of health aspects of air pollution in Europe”*, June 2004.

[1] B. De Schutter is also with the Maritime and Transport Technology Department.

A Comparison of Adaptive Nonlinear Control Designs for an Overactuated Fighter Aircraft Model

E.R. van Oort, L. Sonneveldt, Q.P. Chu, J.A. Mulder
Aerospace Software and Technologies Institute
Delft University of Technology
{e.r.vanoort, l.sonneveldt, q.p.chu, j.a.mulder}@tudelft.nl

1 Introduction

The desire to improve safety and survivability of aircraft operation leads to a lot of ongoing research into the relatively young field of reconfigurable flight control design. The increase in available on-board computional power of modern and future aircraft opened possibilities for adaptive control designs with on-line model identification. In this paper, three such adaptive control designs based on the backstepping method are applied to a nonlinear over-actuated fighter aircraft model.

2 Control Approaches

The first approach is based on the backstepping method making use of tuning functions as introduced in [2] which will serve as the baseline controller. The second is based on the constrained adaptive backstepping method as introduced in [1, 3], and will be referred to as the *integrated* design due to the integration of the parameter identification process in the control design. The last control design, called *modular*, separates the control and identifier designs as in [4]. In this design, the parameter identification is performed with recursive least squares, and the control law design is based on a robust version of backstepping called Input-to-State Stable (ISS) backstepping.

3 Control Allocation

Aircraft often have redundant control surfaces each with their own position and rate limits, and therefore control allocation is used to distribute the desired control effect to the available control effectors. In the adaptive designs, the control allocation method allows for the reconfiguration of the available control effector such that the desired control effect is still obtained. Identification of the control effectiveness parameters plays a crucial role in this reconfiguration after a failure and therefore the choice of control allocation method can have drastic effects on the performance of (nonlinear) control designs, especially for adaptive designs. The control designs are combined with different control allocation methods: the pseudo-inverse, the weighted pseudo-inverse, and a direct control allocation method based on quadratic programming.

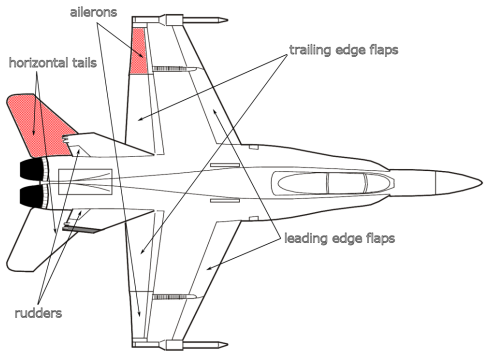

Figure 1: Control surface locations on the aircraft, hatching indicates a failure.

4 Controller Evaluation

The three control designs combined with the different control allocation methods are evaluated using numerical simulations of a simple fighter aircraft model. The stability, convergence and transient performance of the control law designs are evaluated for different, rather demanding, maneuvers and several types of locked and even hard-over aileron and horizontal stabilizer failures are considered. No explicit failure information is fed back to the flight control system.

References

[1] J. Farrell, M. Sharma, and M. Polycarpou. Backstepping based flight control with adaptive function approximation. *AIAA Journal of Guidance, Control and Dynamics*, 28(6):1089 – 1102, Jan. 2005.

[2] Miroslav Krstić, Ioannis Kanellakopoulos, and PetarV. Kokotović. *Nonlinear and Adaptive Control Design*. John Wiley & Sons, 1995.

[3] L. Sonneveldt, Q.P. Chu, and J.A. Mulder. Nonlinear Flight Control Design using Constrained Adaptive Backstepping. *Journal of Guidance, Navigation, and Dynamics*, 30(2):322 – 336, March - April 2007.

[4] E.R. van Oort, L. Sonneveldt, Q.P. Chu, and J.A. Mulder. Modular Adaptive Input-to-State Stable Backstepping of a Nonlinear Missile Model. In *AIAA Guidance, Navigation and Control Conference and Exhibit, Hilton Head, South Carolina, Aug. 20-23*, 2007.

Nonlinear Adaptive Flight Path Control Applied to a Damaged Fighter Aircraft Model

L. Sonneveldt, E. R. van Oort, Q. P. Chu and J. A. Mulder
Aerospace Software and Technologies Institute (ASTI), Delft University of Technology
{l.sonneveldt, e.r.vanoort, q.p.chu, j.a.mulder}@tudelft.nl

1 Introduction

The problem of trajectory tracking control for a damaged aircraft in three-dimensional space is considered. Automatic navigation and landing systems are important autopilot functions for both military and civil aircraft and the emerging field of unmanned air vehicles has only increased the interest in inertial trajectory tracking control systems. However, component failures or airframe damage can result in a degraded tracking performance or even in a total loss of control. Within the available computing power onboard nowadays an adaptive control law with online model identification can be designed that can online adapt to changes in the aircraft dynamics and/or failures of aircraft subsystems. The overall result of the application of such a reconfigurable flight control system will be an improvement of safety in operations, survivability and performance.

2 Nonlinear Adaptive Flight Path Control

A nonlinear adaptive autopilot based on Refs. [1, 2] is designed for the inertial trajectory control of an six-degrees-of-freedom, high-fidelity F-16 aircraft model. The control system is decomposed in four feedback loops constructed using a single control Lyapunov function. The aerodynamic force and moment functions of the aircraft model are assumed to be unknown during the control design phase and will be approximated online. To simplify approximation of the unknown aerodynamic force and moment functions the flight envelope is partitioned into multiple, connecting operating regions called 'hyperboxes'. In each hyperbox a locally valid linear-in-the-parameters nonlinear model is defined. The coefficients of these models can be estimated using the update laws of the adaptive control laws. In this study we use B-spline neural networks to interpolate between the local nonlinear models to ensure smooth model transitions. These update laws take state and input constraints into account so that they do not corrupt the parameter estimation process. The performance of the proposed control system has been assessed in numerical simulations of several types of trajectories at different flight conditions. Simulations with a locked control surface and uncertainties in the aerodynamic forces and moments are also included. The results demonstrate that the proposed control laws achieve closed-loop stability even in the presence of these uncertain parameters and actuator failures.

References

[1] J. Farrell, M. Sharma, and M. Polycarpou, "Backstepping based flight control with adaptive function approximation," *AIAA Journal of Guidance, Control and Dynamics*, vol. 28, pp. 1089–1102, Jan. 2005.

[2] L. Sonneveldt, Q. P. Chu, and J. A. Mulder, "Nonlinear flight control design using constrained adaptive backstepping," *Journal of Guidance, Control, and Dynamics*, vol. 30, pp. 322–336, Mar-Apr 2007.

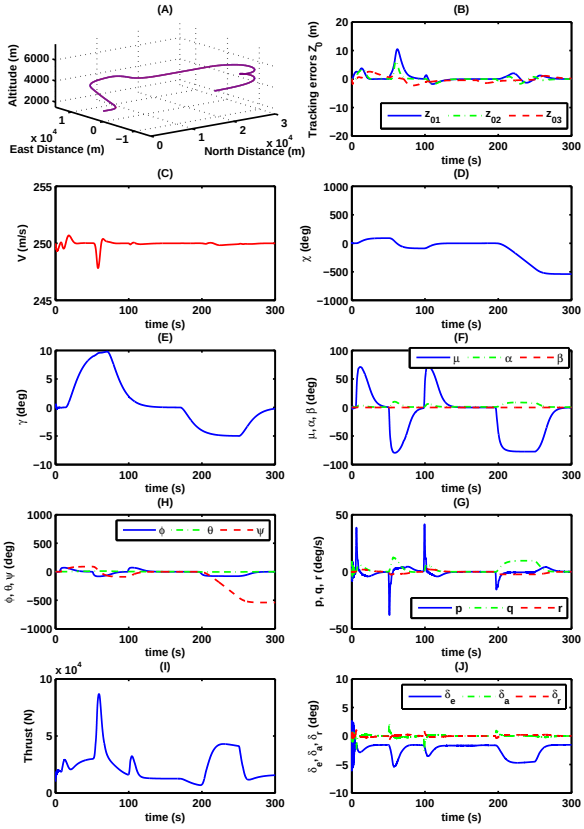

Figure 1: Reconnaissance and surveillance maneuver with −30% uncertainty in the aerodynamic coefficients.

Geometric dynamics analysis of humanoids — locked inertia

G. van Oort
Impact institute/University of Twente
g.vanoort@ewi.utwente.nl

S. Stramigioli
Impact institute/University of Twente
s.stramigioli@utwente.nl

1 Introduction

At the Control Engineering chair at the University of Twente, research is done on geometric dynamics analysis of humanoids. We strive to find mathematics that represent in an insightful, coordinate-free way the complex dynamics of humanoid robots. The basis of the geometric dynamics analysis is *screw theory* [1].

The advantage of geometric dynamics analysis over most classical 3D analysis is that the equations are coordinate-neutral: as long as all quantities are expressed in the same coordinate frame, the equations are correct. Contrary to for example euler angles, the dynamics equations are completely singularity-free. Moreover, equations for translations and rotations are combined, resulting in simple yet powerful equations.

2 The locked inertia tensor and locked inertia ellipsoid

A rigid body is characterized by its *inertia tensor*, which contains all inertia properties (mass m and moments of inertia I_x, I_y and I_z). The total inertia of a system of rigid bodies that are not moving relatively to each other (they are 'locked') —the *locked inertia* (also known as the *composite rigid body inertia* [2]) — can be found by simply summing the inertia tensors of the individual bodies.

The locked inertia enables us to regard the whole system as one single entity (as long as the joints are locked). This is very useful in humanoid robots, where the most important dynamics are the system as a whole pivoting around the contact point of the foot with the ground. Assuming that the internal motion of the system is negligible (see also section 4), the dynamics equations simplify from full multi-body equations of motion to those of an inverted pendulum.

The *locked inertia ellipsoid* is a visualization of the locked inertia tensor — its shape represents the inertial properties of the locked system (see figure 1). By analyzing it, we can visually judge how much the locked dynamics are influenced by changes of the internal configuration of the robot. This can be used both as an analysis tool (how much does an internal configuration disturbance influence the total dynamics) and as a control tool (deliberately changing the internal configuration in order to change the total dynamics).

To visualize the locked inertia ellipsoid, its properties (e.g. the three radii) need to be extracted from the inertia tensor.

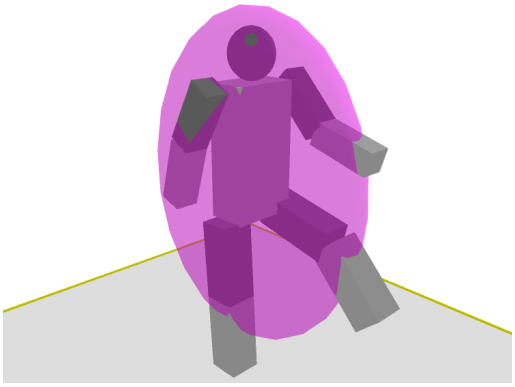

Figure 1: A screen shot of the simulation showing the locked inertia ellipsoid together with the system.

The equations we have found for this can be easily implemented in a simulation environment such as 20-sim, provided that SVD or eigenvalue decomposition algorithms are available.

3 Simulation

A system of interconnected rigid bodies was simulated in 20-sim and the equations for the locked inertia ellipsoid were implemented. The SVD algorithm was provided by creating a DLL-file in C++ that uses a freeware math library [3]. The simulations show that the locked inertia ellipsoid indeed matches the inertia properties of the locked system (figure 1).

4 Future work

The notion of locked inertia as explained above only makes sense when the joints in the system are locked, i.e. there is no relative motion between the bodies of the system. We are working on extending the theory to systems that do have dynamic internal movement.

References

[1] R. M. Murray, Z. Li, and S. S. Sastry, *A mathematical Introduction to Robotic manipulation.* Boca Raton: CRC Press, 1994.

[2] M. W. Walker and D. Orin, "Efficient dynamic computer simulation of robotic mechanisms," *ASME Journal of Dynamic Systems, Measurement, and Control,* vol. 104, pp. 205–211, Sept. 1982.

[3] *Newmat* C++ matrix library, `http://www.robertnz.net/nm_intro.htm`.

Distributed Surveillance by Swarms of Moving Agents

Jelmer van Ast Robert Babuška Bart De Schutter
Delft Center for Systems and Control, Delft University of Technology
j.m.vanast@tudelft.nl r.babuska@tudelft.nl b@deschutter.info

1 Introduction

In this research[1], it is investigated how a swarm of autonomous moving agents can be controlled to distribute the agents in an environment such that a certain spatial coverage is achieved. First, a general modeling framework for swarms is introduced. In this framework, each moving agent is viewed as *particle – dynamic agent* pair. A diagram of the framework is given in Fig. 1. The diagram shows N dynamic agents $A_1, \ldots, A_N$ interacting with an environment. The dynamic agents represent the intelligence of the moving agents. The particles $P_1, \ldots, P_N$ represent the physical part of the moving agents, such as their position and speed. Each dynamic agent, indexed by i, senses the environment by a vector $\mathbf{y}_i$ and produces an input $\mathbf{u}_i$ to the environment. Furthermore, each dynamic agent may send and receive messages $\mathbf{v}_i$ and $\mathbf{w}_i$.

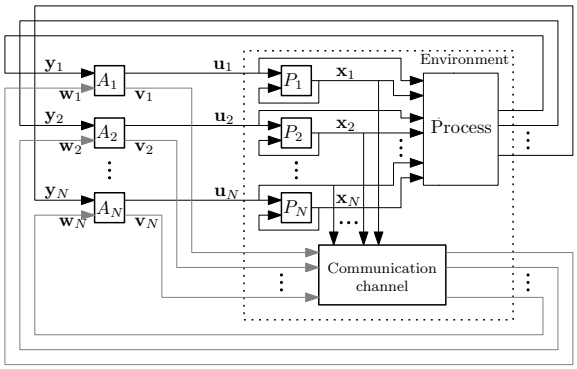

Figure 1: Block diagram of the modeling framework.

2 Control by Artificial Potential Functions

Artificial potential fields provide a method to control the moving agents. All objects in the environment, such as the particles and obstacles, are assigned a *potential function* that defines a virtual force acting upon a particle at a certain distance. The value of the artificial potential field is the sum of the values of all the potential functions. As in [1], the general class of attraction/repulsion functions considered is of the type:

$$g(\mathbf{y}) = -\mathbf{y}[g_{\mathrm{a}}(||\mathbf{y}||) - g_{\mathrm{r}}(||\mathbf{y}||)], \qquad (1)$$

where $g_{\mathrm{a}}, g_{\mathrm{r}} : \mathbb{R}^+ \to \mathbb{R}^+$ represent the magnitude of the attraction and repulsion term respectively and $\mathbf{y}$ is the distance between two particles, or between a particle and an obstacle. The function g is typically predefined and identical for all the moving agents. Dynamic agents may also infer g from observed physical properties of other moving agents. Parameters that define g may also be communicated by the signals $\mathbf{v}$ and $\mathbf{w}$. The influence of the environment on the coverage may be incorporated by including a term $\sigma(\mathbf{x}) : \mathbb{R}^n \to \mathbb{R}$ representing attractant and repellent parts of the environment. With O the number of obstacles, the input to particle i may then be defined as:

$$\mathbf{u}_i = -\nabla_{\mathbf{x}}\sigma(\mathbf{x}_i) + \sum_{j=1, j\neq i}^{N+O} g_i(\mathbf{x}_i - \mathbf{x}_j).$$

3 Simulation Results

A simulation of the motion of 40 particles and the coverage of the swarm in an environment with a quadratic profile and 10 obstacles is shown in Fig. 3. The goal for the particles is to avoid collisions and distribute themselves around the optimum in the environment.

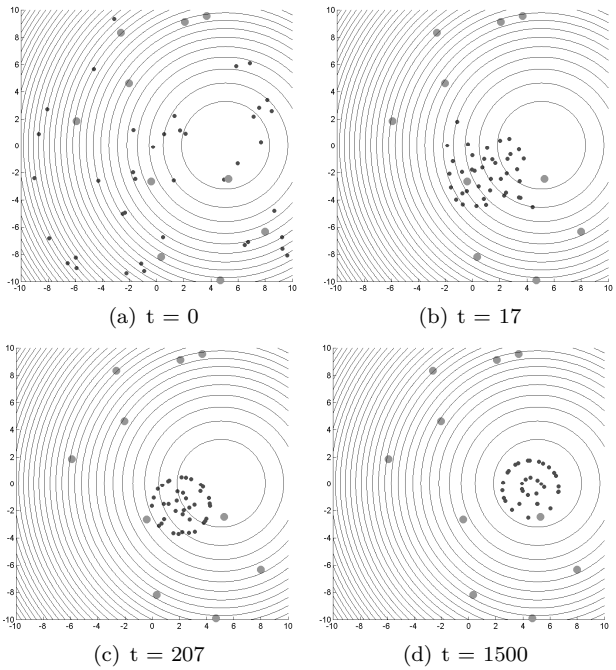

(a) t = 0 (b) t = 17

(c) t = 207 (d) t = 1500

Figure 2: Convergence of the swarm to an optimum in the environment while avoiding collisions.

[1] This research is financially supported by Senter, Ministry of Economic Affairs of The Netherlands within the BSIK-ICIS project "Self-Organizing Moving Agents" (BSIK03024).
Bart De Schutter is also with the department of Marine and Transport Technology, Delft University of Technology.

References

[1] V. Gazi and K. M. Passino, "A class of attractions/ repulsion functions for stable swarm aggregations," *International Journal of Control*, vol. 77, no. 18, pp. 1567–1579, December 2004.

Geometric framework for coordination on Lie groups

A.Sarlette
University of Liège
sarlette@montefiore.ulg.ac.be

S.Bonnabel
University of Liège
bonnabel@montefiore.ulg.ac.be

R.Sepulchre
University of Liège
r.sepulchre@ulg.ac.be

1 Context

The design of control laws for a set of interacting agents, with the objective of stabilizing a desired behavior for the overall swarm, has recently become a very popular subject in the control literature. A basic objective is the achievement of *coordination* or *coordinated motion*, where the agents move in such a way that relative positions among them remain constant.

Coordination of agents moving in the plane at unit speed is achieved in [1]. In the absence of any external reference, steering control laws coupling the individual agents' motions are designed to asymptotically stabilize different coordinated motions of the swarm. In [2], steering control laws are established to stabilize different coordinated motions for agents moving at unit speed in three-dimensional space. Another popular application is the coordinated rotation of spacecraft attitudes.

All these examples are coordination problems *on Lie groups*. The absence of external reference implies symmetry of the system with respect to absolute positions on the Lie group. Although control laws were successfully designed in this context for each individual application, the possibility to formulate a unified framework for coordination on Lie groups has not been explored yet. The goal of the authors' current work is to formulate general definitions of coordination objectives, and provide general design procedures for control laws achieving these coordination objectives, by exploiting the geometric properties of general Lie groups. The present contribution focuses on implications of the *geometric framework and different coordination objectives*. The issue of control law design will be addressed elsewhere.

2 Contributions

All concepts will be illustrated on simple examples for a better understanding; the presentation should be accessible to researchers which are not familiar with Lie groups.

After briefly recalling basic Lie group properties, two different types of relative positions — right-invariant and left-invariant — are defined on Lie groups. These lead to two types of coordination, right-invariant (for fixed right-invariant relative positions) and left-invariant (for fixed left-invariant relative positions). The motion of agents on Lie groups can be described in terms of right-invariant or left-invariant velocities. These are directly linked to the two types of relative positions. In particular, *equal right-invariant (resp. left-invariant) velocities corresponds to left-invariant (resp. right-invariant) coordination*. As a consequence, the coordination problem on Lie groups is reformulated as a consensus problem on the vector space of associated velocities.

Total coordination is defined as the situation where both types of coordination are satisfied simultaneously. Unlike left- and right-invariant coordination, total coordination imposes restrictions on possible values of the relative positions even for fully actuated agents. These restrictions involve eigenspaces of the adjoint representation of the Lie group.

A second part examines implications of underactuation on coordination possibilities. When the left-invariant velocities are constrained to some set $\mathscr{C}$, left-invariant coordination requires consensus on the *adjoint orbit* of $\mathscr{C}$. Conditions on $\mathscr{C}$ are presented to decide if coordination is feasible (in principle) from any initial positions; a link to controllability is established. Finally, controllability criteria by [3] are applied to the examples motivating the authors' research.

Acknowledgments

This paper presents research results of the Belgian Network DYSCO (Dynamical Systems, Control, and Optimization), funded by the Interuniversity Attraction Poles Programme, initiated by the Belgian State, Science Policy Office. The scientific responsibility rests with its authors. The first author is supported as an FNRS fellow (Belgian Fund for Scientific Research).

References

[1] R. Sepulchre, D. Paley, and N.E. Leonard. Stabilization of planar collective motion with all-to-all communication. *IEEE Transactions on Automatic Control*, 52(5):811–824, 2007.

[2] L. Scardovi, R. Sepulchre, and N.E. Leonard. Consensus based dynamic control laws for the stabilization of collective motion in three dimensional space. *Proc. 46th IEEE Conf. on Decision and Control*, pages 2931–2936.

[3] Y.L. Sachkov. Controllability of invariant systems on Lie groups and homogeneous spaces. *Lectures given at Trimester on Dynamical and Control Systems, Trieste*, 2003.

Active Ball Handling Mechanism for the Mid-Size RoboCup League

Jeroen de Best*, René van de Molengraft, Maarten Steinbuch
Technische Universiteit Eindhoven, Department of Mechanical Engineering
P.O. Box 5600 MB, Eindhoven
Email: *j.j.t.h.d.best@tue.nl

1 Abstract

This paper describes the practical implementation of an active ball handling mechanism which is used in the Tech United RoboCup team Eindhoven [1].

2 Introduction

In the middle size robot league of RoboCup different ways exist in order to keep posses of the ball. Most teams use passive systems with a more difficult trajectory planning problem whereas others use an active mechanism in which the ball is driven by wheels or rollers [2]. For each method the rules for ball manipulation state that the robot may enclose the ball only for one third of the balls diameter. Furthermore, during a movement of the robot, the ball should rotate in its natural direction of rotation. This paper describes a new active ball handling mechanism, where feedback of the balls position is incorporated and satisfies all rules mentioned above. The active ball handling mechanism is superior to the commonly used ones for multiple reasons. First of all, driving *backwards* while still possessing the ball is possible. Secondly, the balls position with respect to the robot can be adjusted. This property can be utilized during a kick. The ball can be pulled against the kicker, or can be placed slightly to the left or right which enables the opportunity to aim during a shot. Finally, the manoeuvres during a dribble can be much simpler since it is not necessary to constantly rotate around the vertical axis of the ball.

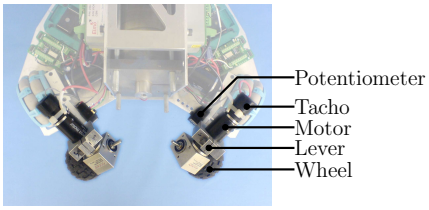

Figure 1: Top view ball handling.

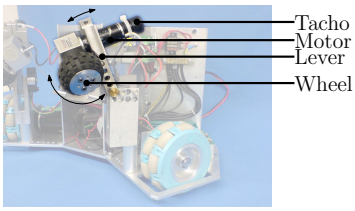

Figure 2: Side view ball handling.

3 Ball Handling Design

The mechanism is shown in Figures 1 and 2. The main part of the ball mechanism consists of two levers. At the end of each lever a wheel is mounted. These wheels can be actuated by DC motors and the velocities of these wheels can be measured with tachos. The levers can rotate around fixed points of the robot and the angles of the levers can be measured with potentiometers. The control architecture that is used is a hierarchical one. On the low level, it consist of two wheel velocity control loops, whereas on the high level it contains two position control loops which control the angles of the levers. All controllers are single-input single-output based controllers. This can be done if the levers are placed under an angle of 90° with respect to each other. In such a way a decoupled system is created on which you can apply single-input single-output control techniques. This is also justified by the relative gain array shown in Figure 3. Now a preferred distance from the ball to the front of the robot can be defined, which results in preferred angles of the two levers. If the levers are bending forward when the ball is in possess an error is introduced which is controlled towards zero by adjusting the velocities of the wheels and vice versa.

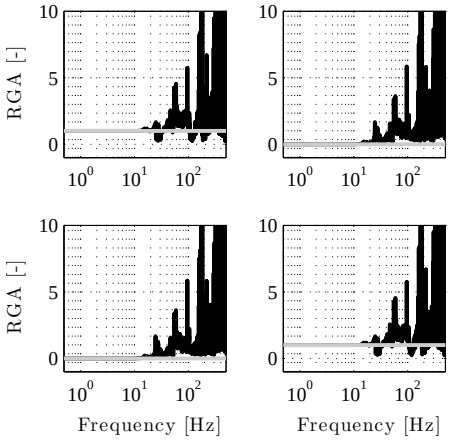

Figure 3: Measured relative gain array (black), perfectly decoupled (gray).

References

[1] Tech United Robocup Team Eindhoven Homepage, *www.techunited.nl*, 2007.

[2] Stancliff, S., *Evolution of Active Dribbling Mechanisms in RoboCup*, 16-471 Project, April 2005.

Master device optimization for a minimally invasive surgery bilateral teleoperation system

Jordi Martin Benet, Thomas Delwiche and Michel Kinnaert
Control Engineering Department
Université Libre de Bruxelles
50, Av F.D.Roosevelt, 1050 Brussels, Belgium
{Jordi.Martin.Benet,Thomas.Delwiche,Michel.Kinnaert}@ulb.ac.be

1 Introduction

Teleoperation is the manipulation in a remote environment through an electromecanical device. It is mainly used to accomplish tasks judged too hazardous or confined for a human operator (e.g. space extravehicular operations, submarine exploration). In a teleoperation setup, the operator manipulates the master robot while the slave robot tries to replicate the movements. For some applications, a feedback of the interaction forces between the environment and the slave robot helps in improving the system performance. When such feature is present, one talks about bilateral teleoperation.

In our case, the master manipulator will be used in a testbench to study force-feedback in Minimally Invasive Surgery (MIS). The range of the forces in MIS extends from $0.1\ N$ up to $70\ N$ [3]. In addition, the robot should be able to operate within a cone of vertex angle of 60° without singularites. For an accurate restitution of the haptic senses, the mechanical design of the robot must be considered carefully. This paper compares two possible parallel architectures derived from the delta robot that offer good performance in terms of stiffness, symmetry and low inertia.

2 Criteria and methods for the choice of architecture

The Linear Delta and the "Classical" Delta architectures are studied using the Performance-Chart based Design Methodology (PCbDM) [2] to assess which one yields the best results. The design parameters for the PCbDM method are those included within the Jacobian Matrix. A normalization, allows to reduce the number of parameters by one and ensures that the parameter space is finite while preserving performance similarities in the mechanism. The criteria used to analyze the kinematic characteristics of the mechanism are :

- the conditioning index (CI) of the Jacobian matrix; a measure of the manipulability and isotropy of a mechanism[1, 2]. The mean of the CI within the normalized workspace of the MIS is analyzed for each structure in order to evaluate the performance.
- the Euclidian norm of the Jacobian matrix ; a measure of the maximum amplification between the torques applied by the actuators and the resulting forces at the tip of the effector within the normalized workspace of the MIS.

Once the performance charts of the criteria are computed for the design parameters, an optimal point is selected and the real design parameters are calculated to match the real dimensions of the structure. A technological review is also critical as it will introduce design constraints for the joint angles, inertia and actuator limitation.

3 Perspectives

The study of the architectures is conducted to satisfy the kinematic criteria. It must be kept in mind that the dynamic study of the device may lead to different conclusions in terms of mechanism performance.

4 Acknowledgements

The work of Thomas Delwiche is supported by a FRIA grant. This paper presents research results of the Belgian Network DYSCO (Dynamical Systems, Control, and Optimization), funded by the Interuniversity Attraction Poles Programme, initiated by the Belgian State, Science Policy Office. The scientific responsibility rests with its authors.

References

[1] Jorge Angeles. *Fundamentals of robotic mechanical systems : theory, methods, and algorithms*. New York, Springer, 2nd ed. edition, 2003.

[2] Xin-Jun Liu and Jinsong Wang. A new methodology for optimal kinematic design of parallel mechanisms. *Mechanism and Machine Theory*, 42(9):1210–1224, 2007.

[3] Mitchell J.H Lum *et al.* Multidisciplinary approach for developing a new minimally invasive surgical robotic system. *IEEE International Conference on Biomedical Robotics and Biomechatronics*, 2006.

Control of Haptic Devices for Tele-Assembly

İlhan Polat and Carsten W. Scherer
Delft Center for Systems and Control (DCSC), TUDelft
Mekelweg 2, 2628 CD, Delft, The Netherlands
{i.polat,c.w.scherer}@tudelft.nl

1 Abstract

Haptics, in general, refers to the technology and devices thereof, that present the touch sense or force-feedback to a human operator from a remote site or from a simulated environment. This type of feedback is used for creating an artificial touching feel at the operator side so that tasks which are beyond human capabilities, not feasible to fully automate and/or necessitates exposure to harsh environments, are undertaken. The goal is to be as realistic as possible i.e. the user experiences the remote site as if he is on site. This is denoted as *Telepresence*.

Though the quality of telepresence is a performance problem, stability of the haptic devices is still the main limitation in achieving the desired performance levels. Since accurate modeling the operator and the environment is in general hard, a natural choice for synthesizing controllers is passivity based design techniques ([1],[2]). By this, the modeling of the human and environment is converted to energy (or power) relations with the haptic interface i.e. a system with power variables f, v is said to be passive if

$$\int_0^t f(\tau)^T v(\tau) d\tau + V(0) \geq 0$$

for all trajectories of f, v, where $V(t)$ denotes the generalized energy function. Hence, the system communicates with the environment via its input output ports. These techniques are proven to be very useful for assessing the stability but the problem of defining different performance objectives arise, due to the fact that converting time or frequency domain design specifications into passivity constraints is not a trivial task. Moreover, these specifications lead to a crude design trade-off between different scenarios both in terms of stability and performance, i.e. the device is tuned to be stable under all possible conditions and then fine-tuned for some manual operator feel. Thus, if the operating conditions of a haptic device are confined to a pre-defined region, the achievable performance levels are improved ([3]). This leads to the major difficulty of the haptic device design, namely *task specification*. The tasks are classified according to their working environment or specific fidelity and position/force ranges.

Common scenarios such as free-air motion and hard contact are simple examples for conflicting objectives. In the first case, the overall device should have as low inertia as possible to be able to render the voidness which leads to very lightweight and compliant device components, but in the latter case, to be able to transmit the hard contact feel to the operator side, the device should have low compliance to avoid cushioning type of behavior. It may seem that these conflicts are all hardware-related, but in fact, similar obstacles appear in control synthesis problems such as varying spectrum of the disturbance signals for different scenarios, noise significance in texture rendering etc. Hence, these devices are possible subjects for model-based control schemes ([4],[5]).

In this talk, we would like to give a brief overview of the current design paradigm, and elaborate on what the key limitations for assessing stability are and possible directions for improvement.

2 Acknowledgements

This work is supported by the MicroNed program (a part of the BSIK program of the Dutch government), The Netherlands.

References

[1] Hannaford, B. and Ryu, J.H., "Time-domain passivity control of haptic interfaces", *IEEE Transactions on Robotics and Automation*, Vol.18(1), pp.1–10,2002

[2] Mahvash, M. and Hayward, V., "Passivity-based high-fidelity haptic rendering of contact",*In Proc. IEEE International Conference on Robotics and Automation*, Vol.3, pp. 3722–3728, 2003

[3] MacLean, K. E., Hayward, V., "Do It Yourself Haptics, Part II: Interaction Design", *IEEE Robotics and Automation Magazine*, vol. 15(1), 2008

[4] Mahapatra, S. and Zefran, M., "Stable haptic interaction with switched virtual environments", *In Proc. IEEE International Conference on Robotics and Automation*, Vol.1, pp. 1241–1246, 2003

[5] Colgate, J. E., "Robust impedance shaping telemanipulation", *IEEE Transactions on Robotics and Automation*, Vol.9(4), pp. 374–384, 1993

A generalized eigenvalue approach to H_2 model order reduction

Ivo Bleylevens
Maastricht University
i.bleylevens@math.unimaas.nl

Ralf Peeters
Maastricht University
ralf.peeters@math.unimaas.nl

Bernard Hanzon
University College Cork
b.hanzon@ucc.ie

Consider a (real) continuous-time stable LTI system of order (McMillan degree) n and its associated proper rational transfer function $H(s)$. For a given value $k < n$, the H_2 model order reduction problem consists of finding a proper rational function $G(s)$ of order k, which minimizes the H_2-norm between $H(s)$ and $G(s)$. This norm is important as it provides a system theoretically meaningful way to measure the distance between two systems. However, it is also notorious for admitting local non-global optima, and for being hard to optimize especially when k is not small.

In [1] an algebraic method was developed to deal with the 'co-order 1 problem', i.e. for computing a *globally optimal* real approximation $G(s)$ of order $k = n-1$. When the co-order 1 technique is applied repeatedly to achieve a larger reduction of the model order, then the results are often not too satisfactory. This is in part due to the inability of the method to deal directly with complex conjugate pairs of poles. In the present paper we address the more difficult 'co-order 2 problem', in which $k = n-2$. We proceed by generalizing and extending the ideas of [1] for the co-order 1 case to the co-order 2 case, which has the benefit of providing us with additional insight into the co-order 3 case and beyond.

In the co-order 1 case the method proceeds as follows. First, a suitable reparameterization allows one to set up a quadratic system of n (complex) equations in n variables, which is in Gröbner basis form for any total degree monomial ordering and which admits a finite number of complex solutions. To solve it, one employs the Stetter-Möller matrix method [2] to transform it into an eigenvalue problem of size $2^n \times 2^n$. Then from its solutions, the corresponding feasible solutions for the real approximation problem are selected. The associated values of the H_2-approximation criterion can be calculated by evaluating a particular homogeneous polynomial of degree 3. This feature can be exploited to restrict the computation of eigenvalues to a much smaller set, see [3]. The best criterion value then yields the globally optimal approximation. In this way iterative local search methods are avoided and a global optimum is arrived at more directly.

For the co-order 2 case, a quadratic system of n equations in n variables is constructed analogous to the co-order 1 case, but the coefficients now involve an additional real variable, denoted by ρ, which shows up in a rational way. In addition, any feasible complex solution needs to satisfy an extra linear constraint of which the coefficients depend only on the given function $H(s)$. In conjunction with this linear condition, the Stetter-Möller matrix method now gives rise to a *polynomial eigenvalue problem* $A(\rho)v = 0$, of size $2^n \times 2^n$ and of degree $n-1$ in the variable ρ. Using a linearization technique it is transformed into an equivalent *generalized eigenvalue problem* $B(\rho)w = (B_0 - \rho B_1)w = 0$. The pencil $\{B_0, B_1\}$ is of size $(n-1)\,2^n \times (n-1)\,2^n$ and it happens to be singular.

Singular generalized eigenvalue problems are well-known to be numerically highly ill-conditioned. In general, the standard QZ-algorithm is not capable of handling such problems in a reliable way. Using exact arithmetic, however, it is possible to decompose the matrix pencil $\{B_0, B_1\}$ into a singular part and a regular part, as in the computation of the Kronecker Canonical Form (see [4]). The singular part relates to all the so-called *indeterminate* eigenvalues. The regular part is what we are interested in: it contains all the finite and the infinite (generalized) eigenvalues. Infinite eigenvalues correspond to singularity of the matrix B_1, zero eigenvalues correspond to singularity of the matrix B_0. For our purposes, the infinite and the zero eigenvalues cannot yield feasible solutions and must all be excluded. The associated Jordan block structure for these eigenvalues can be obtained with exact arithmetic too. In this way it is possible to arrive algebraically at a smaller sized regular matrix pencil $\{C_0, C_1\}$ in which both C_0 and C_1 are invertible. Its eigenvalues can then be computed reliably by standard numerical methods.

From the eigenvalues ρ and the corresponding eigenvectors of the matrix pencil $\{C_0, C_1\}$ all the feasible solutions for the approximation problem can be selected and constructed. To evaluate the H_2-approximation criterion, again a (modified) homogeneous polynomial of degree 3 is available. To demonstrate this technique, a worked example is presented where the repeated 'model order reduction by one' technique is compared against the 'model order reduction by two' technique. Also, some implications for the co-order 3 case are briefly discussed.

References

[1] B. Hanzon, J.M. Maciejowski, C.T. Chou, Optimal H2 order-one reduction by solving eigenproblems for polynomial equations, ArXiv e-prints 0706.1862, Volume 706, June 2007.

[2] H.M. Möller and H.J. Stetter, Multivariate polynomial equations with multiple zeros solved by matrix eigenproblems, *Num. Math.*, **70**, pp. 311-329, 1995.

[3] I. Bleylevens, R. Peeters and B. Hanzon, An nD-systems approach to global polynomial optimization with an application to H2 model order reduction, Proc. 44th IEEE CDC and the ECC 2005, Sevilla, Spain, 2005.

[4] F. Gantmacher, The Theory of Matrices, Vols. I and II, Chelsea, New York, 1959.

Component analysis for genome-wide association studies

Gilles Meyer and Rodolphe Sepulchre
Department of Electrical Engineering and Computer Science,
GIGA Bioinformatics Platform,
University of Liège, Belgium,
Emails : G.Meyer@ulg.ac.be, R.Sepulchre@ulg.ac.be

1 Introduction

This work illustrates the application of component analysis such as principal component analysis (PCA) and independent component analysis (ICA) to analyze SNP databases. The problems of association mapping and population stratification are both addressed with these methods.

2 Component analysis

In the general framework of component analysis, the data matrix $X \in R^{m\times n}$ is approximated by the product of two lower-rank matrices $A \in R^{m\times k}$ and $S \in R^{k\times n}$ with $k \leq m$:

$$X \approx AS \tag{1}$$

where S contains the reduced data and A's columns are the directions spanning the subspace of the reduced data.

If the directions are constrained to be mutually orthogonal and computed to retain as much variance as possible from the original data, the factorization (1) correspond to a principal component analysis of X.

Another possibility is to identify the directions that make the rows of S as statistically independent as possible. This objective is pursued in independent component analysis [1].

3 SNP databases

The human DNA sequence is about 3 billion base pairs of nucleotides (A-T-C-G) arranged into 23 chromosomes. Each individual has one pair of each chromosome, one is inherited from the maternal side and the other one from the paternal side.

In the world's population, there is about 10 million sites or loci that vary between individuals. Such loci referred as single nucleotide polymorphisms (SNPs) are natural candidates for the research of causal differences responsible for diseases or other phenotypes of interest.

At one particular SNP locus, there are usually two alleles (specific nucleotides) observed across the population. Thus, a SNP database can be represented as a matrix whose elements can take 3 discrete values : 2 if the arbitrary reference allele is carried on each chromosome, 1 if the two different alleles are observed and 0 if the non-reference allele is present on each chromosome. To date, an order of magnitude for these databases is the measurement of 10^6 SNPs for 10^3 individuals. These numbers are rapidly increasing with the development of cheaper technologies.

4 Association mapping

The analysis of SNP databases aim at finding loci biologically related to a measured phenotype, for example a particular disease.

The potential of ICA to perform such analysis has been illustrated in [2] on simulated data. In this work, the method is applied to a real database concerned about the identification of loci involved in Crohn disease.

5 Correction for population stratification

A problem encountered in association mapping is the presence of individuals coming from different populations. This is a source of bias into the observed allele frequencies leading to false discoveries in the mapping process.

In [3], PCA is used to correct for this effect by computing a component linked to the population structure and then by removing it from the data. The issue will be discussed in the context of a Crohn large database.

References

[1] A. Hyvärinen, J.Karhunen, and E. Oja. *Independent component analysis*. Wiley-Interscience, 2001.

[2] Z. Dawy, M. Sarkis, J. Hagenauer, and J. C. Mueller. A novel gene mapping algorithm based on independent component analysis. In *IEEE International Conference on Acoustics, Speech and Signal Processing (ICASSP)*, volume 5, pages 381–384, Philadelphia, March 2005.

[3] A. Price, N. Patterson, R. Plenge, M. Weinblatt, N. Shadick, and David. Reich. Principal components analysis corrects for stratification in genome-wide association studies. *Nature Genetics*, 38(8):904–909, July 2006.

Acknowledgments

This work was supported by the Belgian National Fund for Scientific Research (FNRS) through a Research Fellowship at the University of Liège. This paper presents research results of the Belgian Network DYSCO (Dynamical Systems, Control, and Optimization), funded by the Interuniversity Attraction Poles Programme, initiated by the Belgian State, Science Policy Office. The scientific responsibility rests with its author(s).

New algorithms for sparse principal component analysis

M. Journée*, P.-A. Absil† and R. Sepulchre*
*University of Liège, Department of Electrical Engineering and Computer Science, Belgium
†Université Catholique de Louvain, Department of Mathematical Engineering, Belgium

Principal component analysis (PCA) is a standard tool in many areas throughout science and engineering. It is mostly used for data analysis and dimensionality reduction. Given a multivariate data set, PCA identifies linear combinations of the variables, the *principal components*, that correspond to the directions of highest variance in the data. One key drawback of the approach is the fact that principal components are usually combinations of all variables. In applications where the original variables have a well-known physical interpretation, the principal components become difficult to interpret. It could be of interest to identify components that involve only a few variables but still explain a large amount of the variance. This tradeoff between statistical fidelity and interpretability is the goal of sparse principal component analysis.

Jolliffe *et al.* [1] were the first to address this issue in depth. Some further methods have been thereafter proposed [2, 3, 4, 5]. Most of these methods combine approaches to perform PCA with a criterion that favors the sparsity of the components. Let $\Sigma \in \mathbb{R}^{n\times n}$ be the symmetric covariance matrix of some multivariate data, the first principal component is computed by maximizing the Rayleigh quotient on the sphere $S^{n-1} = \{x \in \mathbb{R}^n | x^T x = 1\}$,

$$\max_{x\in S^{n-1}} x^T \Sigma x.$$

Since penalizing the L_1-norm of the variable is a well-known manner to force some sparsity, a simple algorithm for sparse PCA consists in solving the problem

$$\max_{x\in S^{n-1}} x^T \Sigma x - \rho \|x\|_1, \tag{1}$$

where ρ is a positive weight factor. Although the optimization of the Rayleigh quotient on the sphere is a well-posed problem, problem (1) presents many local minimizers.

Inspired by the work of [3], we propose to relax problem (1) by enlarging the dimension of the search-space,

$$\begin{array}{ll} \max\limits_{X\in R^{n\times p}} & X^T \Sigma X - \rho \|X\|_1 \\ \text{s.t.} & \text{trace}(X^T X) = 1, \end{array} \tag{2}$$

which is expected to reduce the impact of the local minimizers. Problems (1) and (2) are strictly equivalent once (2) has a rank-one solution. In any case, the dominant sparse principal component of Σ is computed as the rank-one approximation of the minimizer X_*, i.e, as its dominant left-eigenvector.

The relaxed problem (2) has been solved by using optimization methods over nonlinear matrix manifolds [6]. Numerical simulations indicate that the relaxation significantly reduces the effect of local minimizers. For a parameter p sufficiently large, the algorithm always converges towards the same sparse principal component, whatever the initialization.

References

[1] I. T. Jolliffe, N. T. Trendafilov, and M. Uddin. A modified principal component technique based on the LASSO. 12(3):531–547, September 2003.

[2] H. Zou, T. Hastie, and R. Tibshirani. Sparse principal component analysis, 2004.

[3] A. d' Aspremont, L. El Ghaoui, M. I. Jordan, and G. R. G. Lanckriet. A direct formulation for sparse PCA using semidefinite programming. Technical Report UCB/CSD-04-1330, EECS Department, University of California, Berkeley, 2004.

[4] B. Moghaddam, Y. Weiss, and S. Avidan. Spectral bounds for sparse PCA: Exact and greedy algorithms. In Y. Weiss, B. Schölkopf, and J. Platt, editors, *Advances in Neural Information Processing Systems 18*, pages 915–922. MIT Press, Cambridge, MA, 2006.

[5] A. d'Aspremont, F. R. Bach, and L. El Ghaoui. Full regularization path for sparse principal component analysis. In *ICML '07: Proceedings of the 24th international conference on Machine learning*, pages 177–184, New York, NY, USA, 2007. ACM.

[6] P.-A. Absil, R. Mahony, and R. Sepulchre. *Optimization Algorithms on Matrix Manifolds*. Princeton University Press, Princeton, NJ, January 2008.

Acknowledgments

Michel Journée is a research fellow of the Belgian National Fund for Scientific Research (FNRS). This paper presents research results of the Belgian Network DYSCO (Dynamical Systems, Control, and Optimization), funded by the Interuniversity Attraction Poles Programme, initiated by the Belgian State, Science Policy Office. The scientific responsibility rests with its authors.

Identification based model reduction using block structured models

Omar Naeem, Adrie E. M. Huesman and O.H. Bosgra
Delft Center for Systems and Control, Delft University of Technology,
Mekelweg 02, 2628CD Delft, the Netherlands.
Email: O.Naeem@tudelft.nl

1 Introduction

Computational effort (simulation time) has been one of the concerns of modern research. Large scale industrial process models require lot of computational effort, which is vital, if the model has to be used, in the real time setting, for the closed-loop control (process control) and optimization purposes. Model reduction has been considered as one of the method to achieve the acceptable computation effort. There are many different perspectives of model reduction for example, linear system theory (balancing & truncation), projection based (POD) model reduction, time scale based model reduction (singular perturbation) and identification based (block structured models). Block structure models have been used successfully for the model reduction of industrial processes such as distillation column, heat exchanger and reactors. [2]

2 Methodology

In this study, Hammerstein block structure has been adopted; the reason being the simplicity of the Hammerstein block structured model, as well as it is capable of identifying the non-linearities of the process. This model structure is particularly attractive for the process systems modeling and control, because the steady state information is often available for industrial processes from historical data. Hammerstein structure has been successfully applied for process control purposes to different fields including chemical engineering. [1], [2]

Hammerstein model structure consists of two blocks; A nonlinear block followed by, in series, a linear dynamic block. The NL (non-linear) block captures all the steady state characteristics of the original model, while the dynamics are added by the linear dynamic block. Figure 1 shows the Hammerstein block structure:

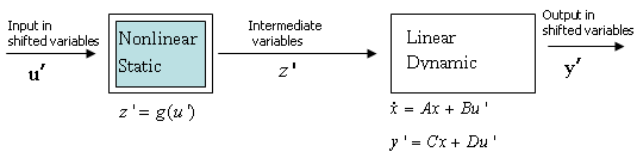

Figure 1: Hammerstein block structure

The objective is to identify the original model, using the Hammerstein structure such that the reduced model can be used for real time purposes. It has to be noted, that reduced model works with shifted variables (deviation variables). In the NL block, different NL maps have been used, such as artificial neural networks, sparse grid representations and interpolation tables [1]. In this study, the NL block has been identified by using interpolation tables. The linear dynamic block consists of *linearized original model (LTI model)* at nominal operating point.

3 Results & Future Perspective

The above mentioned methodology is implemented on continuous stirred tank reactor (CSTR). The implementation is done on single input single output (SISO) case, and then later extended to the multi-input multi-output (MIMO) case. In the SISO case, the input variable chosen is the coolant temperature (T_c) while the reactor temperature (T_R) is the output variable. For the MIMO case, coolant temperature (T_c) and flowrate of reactant (F_{in}) are considered as the input vector, whereas the output vector contains the reactor temperature (T_R) and output flowrate (F_{out}). Satisfactory results have been obtained as far as model reduction of CSTR example (SISO & MIMO) is concerned. Lately the methodology has been applied to a distillation column. The benchmark distillation column is high purity two cut splitter with 72 trays. Reduction related *separation index (SI) & effective cut point (ECP) change*, was satisfactory *partially*, but the methodology needs to be matured.

In future, the methodology has be to be established and developed such that reduced model should have explicit error bounds. Moreover the computational time has to be investigated. Later, the methodology has to be applied to complex industrial examples (multi-component distillation column). The influence of the operating envelope needs to be investigated as well.

References

[1] Gerrit Harnischmacher, Wolfgang Marquardt. "A multi-variate Hammerstein model for processes with input directionality." Journal of Process Control, Vol.17, 2007.

[2] Esref Eskinat, Stanley H. Johnson and William L. Luyben. "Use of Hammerstein Models in Identification of Nonlinear systems." AlChE Journal, Vol.37(2), 1991.

On the detection of bifurcations in dynamical systems using reduced order models

Satyajit K. Wattamwar
Department of Electrical Engineering
Eindhoven Univ. of Technology
P.O. Box 513, 5600 MB Eindhoven
s.wattamwar@tue.nl

Siep Weiland
Department of Electrical Engineering
Eindhoven Univ. of Technology
P.O. Box 513, 5600 MB Eindhoven
s.weiland@tue.nl

1 Introduction

Solutions of distributed parameter systems are usually simulated by means of finite element or finite volume methods. Depending on the required accuracy, such simulation models are typically of high order. Model approximation is then an important step towards simplification of such models. However, most model reduction methods hardly take model uncertainties and parameter variations into account. As such, reduced order models are not well equipped to describe or analyse uncertainties or parameter variations in distributed parameter models.

It is shown in this presentation that the performance of reduced order models that are inferred from Galerkin projections and proper orthogonal decompositions [2, 3] can deteriorate substantially when system parameters vary over bifurcation points.

Motivated by these observations, we propose a detection mechanism based on reduced order models and proper orthogonal decompositions that allows to characterize the influence of parameter variations around a bifurcation value. For this, a hybrid model structure is proposed for an observer that is driven by residuals of reduced order models.

2 Example

The ideas are applied on the example of a tubular reactor with both diffusion and convection phenomena and a nonlinear heat generation term. See Figure 1.

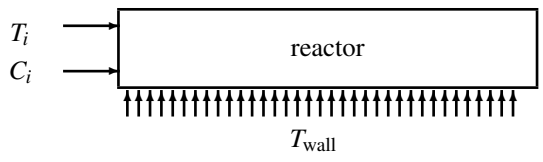

Figure 1: Tubular reactor

The model is governed by the partial differential equations

$$\frac{\partial T}{\partial t} = \frac{1}{P_{\text{eh}}}\frac{\partial^2 T}{\partial z^2} - \frac{1}{L_e}\frac{\partial T}{\partial z} + \nu C e^{\gamma\left(1-\frac{1}{T}\right)} + \mu(T_{\text{wall}} - T) \tag{1a}$$

$$\frac{\partial C}{\partial t} = \frac{1}{P_{\text{em}}}\frac{\partial^2 C}{\partial z^2} - \frac{\partial C}{\partial z} - D_{\text{a}} C e^{\gamma\left(1-\frac{1}{T}\right)} \tag{1b}$$

which are subject to the mixed boundary conditions

$$\text{left side: } \begin{cases} \frac{\partial T}{\partial z} = P_{\text{eh}}(T - T_i) \\ \frac{\partial C}{\partial z} = P_{\text{em}}(C - C_i) \end{cases} \qquad \text{right side: } \begin{cases} \frac{\partial T}{\partial z} = 0 \\ \frac{\partial C}{\partial z} = 0 \end{cases}$$

See, e.g., [1]. $T(z,t)$ and $C(z,t)$ are dimensionless temperature and concentration variables, respectively, which are functions of time t and position z.

The Damkohler number D_{a} is viewed as uncertain parameter of the model and varies close to one of its bifurcation values. The parameter variation was chosen so as to exhibit a discontinuous dependence of the dynamical responses as function of the Damkohler number. Changes of the Damkohler number correspond to the transition of the reactor from lower (extinction) to higher (ignited) states.

In the presentation we discuss the difficulties in approximating the transition from extinction to ignited state in this tubular reactor. In addition we describe a method to detect the Damkohler number from observed data.

References

[1] Zheng, D. and Hoo, K. A., "Low-order model identification for implementable control solutions of distributed parameter systems," Computers and Chemical Engineering, 2002, vol. 26, nr. 7:8, pp. 1049-1076.

[2] Romijn, R. and Ozkan, L. and Weiland, S. and Marquardt, W. and Ludlage J., "A hybrid modeling approach for the reduction of nonlinear systems," Procedings of DYCOPS, 2007.

[3] Shvartsman, S. Y. and Kevrekidis, I.G., "Nonlinear model reduction for control of distributed parameter systems: A computer assisted study," AIChE Journal, 1998, vol. 44:7, pp. 1579-1595.

Analysis and Approximation of Multi-way Arrays through Singular Value Decompositions

Femke van Belzen
Department of Electrical Engineering, Technische Universiteit Eindhoven
PO Box 513, 5600 MB Eindhoven, The Netherlands
Email: f.v.belzen@tue.nl

Introduction

Data objects which are indexed with more than two indices, multi-way arrays, occur very frequently. Examples include the MRI data of a body part, flow patterns in fluid dynamics and in general measurements of N-d systems. The analysis and approximation of multi-way arrays is relevant in many applications, such as data compression, control design and model reduction. More specifically, when using the method of Proper Orthogonal Decompositions for model reduction, the first step is the computation of coherent patterns from a representative set of measurement data of the process. Computation of basis functions is usually done by rearranging the measurement data into a matrix and then computing its Singular Value Decomposition (SVD), instead of directly analyzing the multi-way array.

Singular Value Decompositions and Approximation of Tensors

A powerful way to describe multi-way arrays is using tensors. A tensor is a multi-linear functional $T : \mathscr{W}_1 \times \cdots \times \mathscr{W}_N \to \mathbb{R}$ defined on N inner product spaces $(\mathscr{W}_n, \langle \cdot, \cdot, \rangle)$ of dimension L_n. After choosing suitable bases for the inner product spaces the tensor is represented by the N-way array $[[t_{\ell_1,\ldots,\ell_N}]] \in \mathbb{R}^{L_1 \times \cdots \times L_N}$. Unfortunately there is no straightforward generalization of the SVD for matrices to tensors. There are several possibilities, two will be considered here [1, 2]. We propose a notion of singular value decomposition (SVD) for a tensor T by defining singular vectors for each of the inner product spaces $\mathscr{W}_n$. The singular vectors $\{w_n^{(1)}, \cdots, w_N^{(L_n)}\}$ form an orthonormal basis for $\mathscr{W}_n$. The singular value decomposition of a tensor T is then the representation of T with respect to these bases.

Example

Consider the following two-dimensional heat transfer process:

$$\rho c_p \frac{\partial w}{\partial t} = \kappa_x \frac{\partial^2 w}{\partial x^2} + \kappa_y \frac{\partial^2 w}{\partial y^2} + u \qquad (1)$$

where $w(x,y,t)$ denotes the temperature on position (x,y) and time t. The PDE is defined on a rectangular plate. A finite element implementation of this PDE is computed using a grid size of $L_1 = 50$ and $L_2 = 100$ and 500 time samples, i.e. $L_3 = 500$. Singular vectors for this implementation of the PDE are computed using two different methods, the HOSVD [1] and the tensor SVD [2]. Results are displayed in Figure 1.

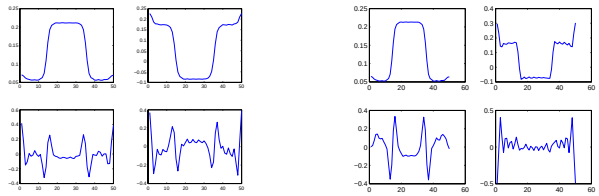

Figure 1: First basis functions for $\mathscr{X}$, using HOSVD (left) and tensorial SVD (right)

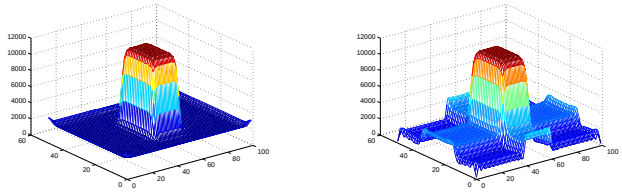

Figure 2: Time slice of the original data (left) and time slice of the rank$-(5,5,9)$ approximant(right)

To approximate a tensor T first a vector of integers $r = (r_1, \ldots, r_N)$ has to be chosen. An approximant is then defined by the restriction $T_r^* := T|_{\mathscr{M}_1^{(r_1)} \times \ldots \times \mathscr{M}_N^{(r_N)}}$ where $\mathscr{M}_n^{(r_n)} = \text{span}(w_n^{(1)}, \cdots, w_n^{(r_n)})$ spans first r_n singular vectors in $\mathscr{W}_n$. An approximant of the example is shown in Figure 2.

References

[1] L. de Lathauwer et al., "A Multilinear Singular Value Decomposition," SIAM J. Matrix Anal. Appl., vol. 21 (4), 2000.

[2] Belzen, F. van, Weiland, S., de Graaf, J. "Singular value decompositions and low rank approximations of multi-linear functionals", Proc. 46th IEEE Conf. on Decision and Control, 2007.

Modeling and experimental validation of batch settling

Robert David and Alain Vande Wouwer
Service d'Automatique
Faculté Polytechnique de Mons
7000 Mons Belgium
Email: alain.vandewouwer@fpms.ac.be

Jean-Luc Vasel
Service Environnement
Université de Liège
6700 Arlon Belgium
Email: jlvasel@ulg.ac.be

The secondary settler is an important process unit in a wastewater treatment plant as it allows the separation of the solid and liquid phases. The solids particles arriving in the tank fall to the bottom with a sedimentation velocity ν_s, and part of the sludge accumulating in the lower part of the tank is recirculated to the activated sludge process. The design of secondary settlers has long been based on empirical considerations. A first physical model of batch settling was developed by George Kynch in 1952 [2], in which the sludge transport is described by a mass balance partial differential equation. Further modelling studies introduced additional refinements to this basic model in order to reproduce experimental observations: continuous settling (Petty model), limitation of the sedimentation flux from layer to layer (Takács model [3]), consideration of a diffusion term (Hamilton model).

Despite these efforts, recent studies show several drawbacks of these models: unrealistic profiles produced by the basic model of Petty, influence of the number of layers on the numerical results obtained with the popular model of Takács, and the interaction with the model formulation.

In this work, we first review some of these models and show how inconsistent the numerical results can be. Then, we reformulate the model, highlighting the importance of the boundary conditions (i.e. the conditions imposed at the secondary settler inlet and outlets, which are usually defined in an implicit way in standard models). On this basis, we develop a numerical solution procedure, based on the method of lines [4], thus avoiding the use of the standard "tanks-in-series" approach which is quite limitative. This solution procedure is general and avoids the coupling between model formulation and numerical solution, which is inherent in Takács' modelling approach. Finally, we estimate physical parameters from experimental data collected on a batch pilot plant [1] and demonstrate the good predictive capability of the proposed model (Fig. 1).

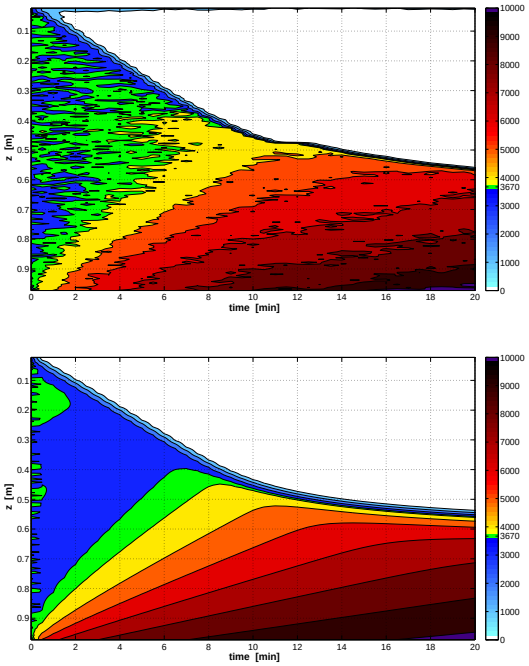

Figure 1: *Experimental iso-concentration curves for $C_0 = 3670$ $^{g}/_{m^3}$ (above), and simulation results (below).*

Acknowledgements. This paper presents research results of the Belgian Network DYSCO (Dynamical Systems, Control, and Optimization), funded by the Interuniversity Attraction Poles Programme, initiated by the Belgian State, Science Policy Office. The scientific responsibility rests with its authors. The authors are very grateful to Prof. Peter Vanrolleghem and Dr. Jeriffa De Clercq for providing the experimental data.

References

[1] J. De Clercq. *Batch and Continuous Settling of Activated Sludge: In-Depth Monitoring and 1D Compression Modelling.* PhD thesis, Universiteit Gent, Faculteit Ingenieurswetenschappen, 2006.

[2] G.J. Kynch. A theory of sedimentation. *Trans. Faraday Soc.*, 48:166–176, 1952.

[3] I. Takács, G.G. Patry, and D. Nolasco. A dynamic model of the clarification-thickening process. *Wat. Res.*, 25(10):1263–1271, 1991.

[4] A. Vande Wouwer, P. Saucez, and W.E. Schiesser. *Adaptive method of lines.* Chapman Hall/CRC Press, USA, 2001.

Multiple objective optimisation of jacketed tubular reactors with dispersion

Filip Logist, Peter M.M. Van Erdeghem, Ilse Y. Smets and Jan F. Van Impe
BioTeC, Department of Chemical Engineering
Katholieke Universiteit Leuven
W. de Croylaan 46, B-3001 Leuven, Belgium
Email: {filip.logist, peter.vanerdeghem, ilse.smets, jan.vanimpe}@cit.kuleuven.be

1 Introduction

This paper deals with the optimal and safe operation of dispersive jacketed tubular reactors. Despite the existence of advanced distributed controllers (e.g., [1, 2]), optimal steady-state reference profiles to be tracked are often unknown. In addition, multiple and conflicting objectives may often be present.

2 Procedure

In [3, 4] a four step procedure which is based on a weighted sum approach and a combination of analytical and numerical optimal control techniques, has been applied successfully to plug flow reactors with conflicting conversion and energy costs.

In step 1, analytical expressions for all possible optimal control arcs are calculated using analytical techniques from, e.g., [5]. The derivation of possible optimal controls inside the feasible region is performed by eliminating the costates from the necessary conditions for optimality. Control arcs which keep a constraint active, as well as the corresponding tangency conditions, are found by differentiating the active constraint with respect to the independent variable, and substituting the system equations until the control appears explicitly. In step 2, approximate optimal control profiles are determined numerically for a coarse grid of weights. Hereto, a numerical optimal control approach with a piecewise constant control parameterisation is adopted. In step 3, the optimal arc sequences present in the numerically obtained optimal control profiles are identified. Finally, in step 4, the control parameterisation is refined based on the identified optimal sequence using the analytical expressions. These analytical parameterisations with the switching positions between the different arcs as degrees of freedom, are then optimised on a refined grid.

3 Results and discussion

The aim is to illustrate the general applicability of the procedure by allowing dispersion. As dispersion significantly complicates a possible solution process (due to second-order derivatives and split boundary conditions), hardly any generic results are known. Nevertheless, the dispersive plug flow reactor model is important for practice, since varying the dispersion level allows to mimic an entire reactor range, i.e., from plug flow to perfectly mixed reactors. Also obtaining the set of Pareto optimal solution yields valuable information in view of changing economic situations.

As an example a jacketed tubular reactor in which an exothermic irreversible first-order reaction takes place is adopted. It is shown that the proposed procedure yields generic reference solutions for (*i*) different cost criteria, and (*ii*) different dispersion levels. Here, all criteria involve a trade-off between conversion and energy costs, which can all be interpreted in view of sustainable development. Each time the Pareto set is found, which yields solutions for possibly highly different economic situations, i.e., from worthless reaction products to freely available energy.

4 Acknowledgements

Work supported in part by Projects OT/03/30 and EF/05/006 (Center-of-Excellence Optimization in Engineering) of the Research Council of the Katholieke Universiteit Leuven, and by the Belgian Program on Interuniversity Poles of Attraction, initiated by the Belgian Federal Science Policy Office. The scientific responsibility is assumed by its authors.

References

[1] P.D. Christofides. Robust control of parabolic PDE systems. *Chemical Engineering Science*, 53:2949–2965, 1998.

[2] P.D. Christofides and P. Daoutidis. Robust control of hyperbolic PDE systems. *Chemical Engineering Science*, 53:85–105, 1998.

[3] F. Logist, I.Y. Smets, and J.F. Van Impe. Derivation of generic optimal reference temperature profiles for steady-state exothermic jacketed tubular reactors. *Journal of Process Control*, 18:92–104, 2008.

[4] F. Logist, P. Van Erdeghem, I.Y. Smets, and J.F. Van Impe. Multiple-objective optimisation of a jacketed tubular reactor. In *Proceedings of the European Control Conference*, pages 963–970, 2007.

[5] B. Srinivasan, S. Palanki, and D. Bonvin. Dynamic optimization of batch processes I. Characterization of the nominal solution. *Computers and Chemical Engineering*, 27:1–26, 2003.

Unravelling *E. coli* dynamics close to maximum growth temperature through heterogeneous modelling

Eva Van Derlinden, Ivan Lule, Kristel Bernaerts and Jan F. Van Impe
Chemical and Biochemical Process Technology and Control Section,
W. de Croylaan 46, B-3001 Leuven, Belgium
jan.vanimpe@cit.kuleuven.be - kristel.bernaerts@cit.kuleuven.be - eva.vanderlinden@cit.kuleuven.be

1 Introduction

Traditional microbial growth models applied in predictive microbiology are based on the assumption of sigmoidal growth curves. After an initial adaptation phase (the lag phase), microorganisms enter the exponential growth phase in which they grow at the maximum specific growth rate, determined by the environment. At a certain point, growth is slowed down and finally inhibited, e.g., by accumulation of a toxic metabolite or a shortage in nutrients (stationary phase). An extensive experimental study revealed that growth of *E. coli* K12 MG1655 in Brain Heart Infusion broth at elevated temperatures (close to its maximum temperature for growth of about 46°C) does not follow a typical sigmoidal growth curve characterized by a lag, exponential and stationary phase [4]. The exponential growth phase at 45°C is clearly disturbed. Based on plate count data and microscopic images, the existence of a more heat resistant subpopulation was hypothesized. This hypothesis is tested in this paper by means of a heterogeneous modelling approach (in analogy with [2]).

2 Materials and methods

The kinetics of *E. coli* K12 MG1655 were studied in Brain Heart Infusion broth at superoptimal temperatures in a temperature controlled environment. Cell density was determined based on plate counts.
Microbial growth is described by the model of Baranyi and Roberts (1994), in which temperature dependence of the maximum specific growth rate is incorporated by the Cardinal Temperature Model with Inflection (CTMI) [3]. This model encloses four parameters: the cardinal temperatures T_{min}, T_{opt} and T_{max} (the minimum, optimum and maximum growth temperature, respectively) and μ_{opt} (the specific growth rate at T_{opt}). Growth curves were simulated with Matlab (version 6.5, The Mathworks Inc.) and parameter estimates were acquired by minimization of the sum of squared errors (SSE), using lsqnonlin of the Matlab Optimization Toolbox. Simultaneously, parameter variances were calculated with the jacobian matrix.

3 Results and discussion

The postulated hypothesis considers two subpopulations: one sensitive population and another (very small) population with increased heat tolerance. A large fraction of the initial population density inactivates being unable to resist the inimical temperature. A remaining smaller fraction is able to resist the stressing temperature and multiplies. Superposition of the dynamics of these two subpopulations and taking into account experimental variability (inherent to the experimental set-up) enables accurate prediction of the experimental data).

4 Conclusion

A heterogeneous modelling approach enables accurate description of experimental data hereby confirming the existence of a small heat resistant subpopulation in typical inoculum culture of *E. coli* K12 MG1655. Additional dynamic experiments will be performed to give more insight in the microbial behavior within the superoptimal temperature region and in the temperature region between microbial growth and inactivation.

5 Acknowledgements

This research is supported in part by OT/03/30 and the K.U.Leuven-BOF EF/05/006 Center-of-Excellence Optimization in Engineering of the Research Council of the Katholieke Universiteit Leuven, the Belgian Program on Interuniversity Poles of Attraction, initiated by the Belgian Federal Science Policy Office. K. Bernaerts is a Postdoctoral Fellow with the Fund for Scientific Research Flanders (FWO-Vlaanderen).

References

[1] J. Baranyi and T.A. Roberts (1994). A dynamic approach to predicting bacterial growth in food. *International Journal of Food Microbiology* 23,277-294

[2] McKellar R.C. (1997) A heterogeneous population model for the analysis of bacterial growth kinetics. *International Journal of Food Microbiology* 36, 179-186

[3] L. Rosso, J.R. Lobry, S. Bajard and J.P. Flandrois (1995) Convenient model to describe the combined effects of temperature and pH on microbial growth. *Appl. Environ. Microbiol.* 61, 610-616

[4] Van Derlinden, E. , Bernaerts, K. B. and Van Impe, J.F. (2007) Dynamics of *Escherichia coli* at elevated temperatures: effect of temperature history and medium. *Journal of Applied Microbiology* (In press, available online 10.1111/j.1365-2672.2007.03592.x)

Predicting the quality of a batch process using an inferential sensor

G. Gins, I.Y. Smets and J.F. Van Impe*
BioTeC, Department of Chemical Engineering, Katholieke Universiteit Leuven,
W. de Croylaan 46, B-3001 Leuven, Belgium.
{geert.gins, ilse.smets, jan.vanimpe}@cit.kuleuven.be
* Corresponding author

B. Pluymers and W. Van Brempt
IPCOS - ISMC office,
Technologielaan 11/0101, B-3001 Leuven, Belgium.
{bert.pluymers, wim.vanbrempt}@ipcos.com

1 Introduction

In chemical process industry, batch processes are commonly used for the production of products with a high added value (e.g., high-performance polymers, pharmaceuticals, and biochemicals). However, a close online monitoring of these batch processes is required to achieve a constant satisfactory product quality. Hereto, multivariate statistical methods have been extended from continuous to batch processes [2, 3].
In this work, an inferential sensor is constructed for the prediction of the batch-end quality of an industrial polymerization process. The sensor is obtained by combining a *derivative dynamic time warping* (DDTW) measurement alignment procedure with a *partial least squares* (PLS) black box model, and provides estimates of the final product quality, which cannot be measured during the process, well before the production run is completed. Hence, batches with a faulty quality can be detected in an early stage, and actions can be taken to correct the product quality.

2 Model structure

The available data set consists of 83 batch production runs (73 used for training and 10 for validation), during which 30 measurement variables are sampled. First, the measurement profiles are preprocessed by means of a DDTW data alignment [1]. This brings all measurement profiles to an identical length and aligns the major production events. Next, the full PLS model is trained and validated.
This identified PLS model is only capable of estimating the product quality after the completion of the batch process. Therefore, an online adaptation of the DDTW data alignment procedure is combined with an online implementation of the full PLS model. This inferential sensor provides true online estimates of the final product quality.

3 Results

The inferential sensor provides stable and accurate predictions of the final product quality during the whole batch production process. As the batch run progresses, the quality estimates become more reliable, until the maximum accuracy of the sensor is reached approximately halfway throughout the batch operation.

4 Conclusions & future work

In this work, an inferential sensor for the prediction of batch-end quality parameters has been developed. Hereto, an online *derivative dynamic time warping* data alignment has been combined with an online implementation of a *partial least squares* black box model. The obtained sensor provides stable and accurate estimates of the final product quality for an industrial polymerization process.
Future research will consist of further industrial validation, refinement of the developed inferential sensor, and application of the developed methodology to other batch production processes.

Acknowledgements. Work supported in part by IWT Project 040363 and Projects OT/03/30 and EF/05/006 (Center-of-Excellence Optimization in Engineering) of the Research Council of the Katholieke Universiteit Leuven and the Belgian Program on Interuniversity Poles of Attraction, initiated by the Belgian Federal Science Policy Office. The scientific responsibility is assumed by its authors.
The authors would like to thank J. De Wilde of CYTEC (Drogenbos, Belgium) for the data sets provided for this study.

References

[1] E.J. Keogh and M.J. Pazzani. 2001. Derivative Dynamic Time Warping. *First SIAM International Conference on Data Mining* (Chicago, IL).

[2] J.H. Lee, and A.W. Dorsey. 2004. Monitoring of batch processes through state-space models. *AIChE J.*, 50(6):1198-1210.

[3] P. Nomikos, and J.F MacGregor. 1994. Monitoring batch processes using multiway principal component analysis. *AIChE J.*, 40(8):1361-1375.

Productivity optimization of yeast fed-batch cultures using an extremum-seeking strategy

Laurent Dewasme and Alain Vande Wouwer
Laboratoire d'Automatique, Faculté Polytechnique de Mons,
7000 Mons, Belgium
{Laurent.Dewasme, Alain.VandeWouwer }@fpms.ac.be

Yeasts are one of the most important host microorganisms in manufacturing of biopharmaceuticals. Industrial vaccine production is usually achieved using fed-batch cultures of genetically modified yeast strains, which can express different kinds of recombinant proteins.

From an operational point of view, it is necessary to determine an optimal feeding strategy (i.e. the time evolution of the input flow rate to the fed-batch culture) in order to maximize productivity. The main problem that can be encountered at this stage is the presence of an overflow metabolism. The fermentation of an excess of substrate (glucose) can lead to the accumulation of ethanol in the culture medium, and in turn to the inhibition of the cell respiratory capacity.

To avoid this undesirable effect, a closed-loop optimizing strategy is required, which could take various forms ([1], [2], [3]). In particular, the use of extremum seeking strategies for bioprocess optimization has received an increasing attention in recent years ([4]).

In this study, we develop an adaptive extremum-seeking strategy based on Lyapunov stability arguments, in a way similar to [1]). However, the switch between a respirative regime and a respiro-fermentative regime, depending on the yeast respiratory capacity and the substrate concentration in the culture medium (i.e. the bottleneck assumption of [5]), as well as the inhibitory effect of ethanol on the yeast respiratory capacity, complicates the study. The main challenge is actually not to control the substrate concentration at a constant value but to maximize the respiratory capacity while maximizing the substrate uptake rate, resulting finally in a productivity optimization.

Two original adaptive laws are proposed based on substrate or ethanol regulation, and the on-line estimation of unknown kinetic parameters. Moreover, the use of an asymptotic observer is considered so as to limit the number of required on-line measurements ([6]). Simulation results presented in Figure 1 show the application of the controller to a simulated case-study corresponding to classical small-scale (20 l bioreactor) culture conditions. Figure 1 also shows the evolution of the feed rate F_{in}. The adaptation parameters θ and α converges to their true values through a judicious choice of the tuning parameters values. The selection of an appropriate dither signal is based on a persistence of excitation (PE) condition ([1]) which, once fulfilled, ensures the asymptotic convergence of the parameter estimates. The

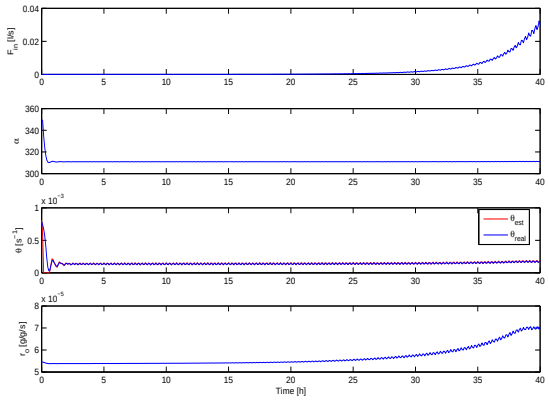

FIG. 1: Feed rate (F_{in}), two unknown kinetic parameters (θ and α), and respiratory capacity (r_o) evolutions.

productivity is quite satisfactory as more than $150 g/l$ of biomass are obtained within less than 40 hours. In order to ease the procedure and facilitate the tuning, an alternative strategy is finally proposed in which the control variable is based on the ethanol concentration.

Acknowledgements

This work presents research results of the Belgian Network DYSCO (Dynamical Systems, Control, and Optimization), funded by the Interuniversity Attraction Poles Programme, initiated by the Belgian State, Science Policy Office.

References

[1] M. Titica, D. Dochain, and M. Guay. Adaptive extremum seeking control of enzyme production in filamentous fungal fermentation. *CAB9, Nancy - France*, pages CD–ROM paper 062, 2004.

[2] L. Chen, G. Bastin, and V. van Breusegem. A case study of adaptive nonlinear regulation of fed-batch biological reactors. *Automatica*, 31(1) :55–65, 1995.

[3] F. Renard and A. Vande Wouwer. Robust adaptive control of yeast fed-batch cultures. *Computers and Chemical Engineering*, May 2007.

[4] K. B. Ariyur and M. Krstic. *Real-Time Optimization by Extremum-Seeking Control*. John Wiley & Sons, INC., publication, wiley-interscience edition, 2003.

[5] B. Sonnleitner and O. Käppeli. Growth of s*accharomyces cerevisiae* is controlled by its limited respiratory capacity : Formulation and verification of a hypothesis. *Biotechnol. Bioeng.*, 28 :927–937, 1986.

[6] G. Bastin and D. Dochain. *On-line estimation and adaptive control of bioreactors*. Elsevier, Amsterdam, 1990.

Convex Analysis Tools Applied to Underdetermined Reaction Networks

Francisca Zamorano, Alain Vande Wouwer
Service d'Automatique, Faculté Polytechnique de Mons, Boulevard Dolez 31, B-7000 Mons

Georges Bastin
CESAME, Université Catholique de Louvain, Avenue Georges Lemaitre 4, B-1348 Louvain-La-Neuve

The derivation of minimal dynamic representation of detailed metabolic reaction networks has been established in several publications [4, 3, 1]. This approach is based on the *a priori* knowledge of a detailed underlying metabolic network and the use of the fundamental assumption that internal metabolites are in quasi-steady state. The resulting equilibrium mass balance conditions can be completed using available measurements of the time evolution of some extracellular species (uptake and production rates). However, this additional information is usually not sufficient to provide a unique solution for the metabolic fluxes, so that the resulting mass balance system is underdetermined. Depending on the metabolic phase under consideration (for instance the growth phase), reactions can be assumed irreversible (even if in another metabolic phase the reactions are indeed occurring in the reverse way) and the corresponding fluxes non-negative, so that tools of non-negative linear algebra, or convex analysis, can be exploited to compute the set of admissible solutions.

In this study, a detailed metabolic network of animal cell cultures, namely cultures of CHO-320 cells, has been built to further test the methodology and unveil the information content in the inherent network level of interconnection and detail. Nevertheless, as we usually deal with underdetermined systems due to the lack of sufficient measurement, it is not possible to achieve an unique solution (flux distribution) by the common methodology of Metabolic Flux Analysis.

In [2] a new concept has been proposed, defined as the Flux Spectrum Space. This approach allows obtaining a range of possible (non-negative) values for each flux. Interestingly, the intervals obtained for the intracellular fluxes appear to be quite limited, especially for the fluxes surrounding the central metabolism. In addition, the flux distribution intervals barely change when considering additional constraints based on intracellular products. Thus, independently of the constraints added to the system, the flux distribution intervals depend mostly on the structure of the underlying metabolic network.

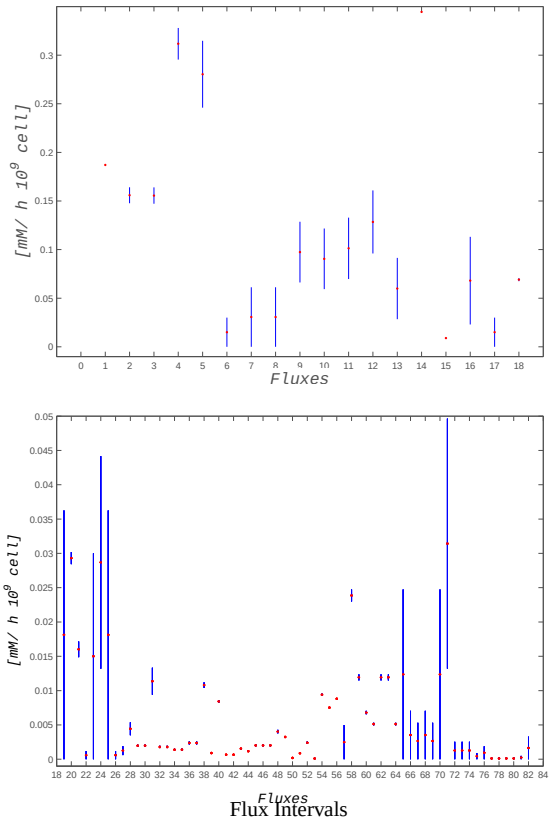

Flux Intervals
Top: Central Metabolism. Bottom: Amino Acids metabolism, Protein, Nucleic acids and Lipids Synthesis

Acknowledgements

This work presents research results of the Belgian Network DYSCO (Dynamical Systems, Control, and Optimization), funded by the Interuniversity Attraction Poles Programme, initiated by the Belgian State, Science Policy Office. The authors also gratefully acknowledge Professor Yves-Jacques Schneider for his insightful comments and providing experimental data.

References

[1] Hendrik P. J.Bonarius, V. Hatzimanikatis, K.P.H. Meesters, C.D. de Goojier, G. Schimd, and J. Tramper. Metabolic flux analysis of hybridoma cells in different culture media using mass balances. *Biotechnology and Bioengineering*, 50:299–318, 1996.

[2] F. Llaneras and J. Picó. An interval approach for dealing with flux distributions and elementary modes activity patterns. *Journal of Theoretical Biology*, 246:290–308, 2007.

[3] A. Provost. *Metabolic Design of Dynamic Bioreaction Models*. PhD thesis, Catholic University of Louvain, 2006.

[4] A. Provost and G. Bastin. Dynamic metabolic modelling under the balanced growth condition. *Journal of Process Control*, 14:717–728, 2004.

An Adaptive Sub-Optimal Energy Management Strategy for Hybrid Drive Trains

Thijs van Keulen, Bram de Jager, Maarten Steinbuch
Control Systems Technology Group
Technische Universiteit Eindhoven
P.O. BOX 513, 5600 MB, Eindhoven, The Netherlands
Tel: +31 40 247 4828; e-mail: t.a.c.v.keulen@tue.nl

1 Introduction

Hybridization of drive trains is an often proposed method for fuel consumption reduction in vehicles. A hybrid vehicle contains two power converters instead of one.

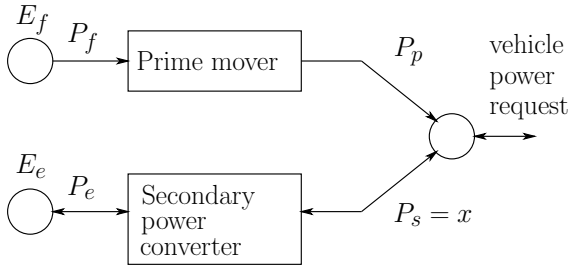

Main advantage of hybrid vehicles is that kinetic energy can be recovered and stored, such that it can be used at a later, more convenient, time to propel the vehicle. The use of the stored energy is governed by the energy management strategy (EMS), see, e.g., [3] for an overview on current EMS.

2 Problem Definition

Typically the energy management problem of a hybrid vehicle is formulated as a minimal fuel consumption problem, where the optimal power split between the prime mover and the secondary power converter is calculated off line based on a given driving cycle and solved numerically with dynamic programming techniques. An important constraint in these calculations is that the energy level of the secondary power source at the end is the same as in the beginning.

$$\min_x J(x,t) = \min_x \left(\int_0^{t_f} P_f(x,t)dt + \int_0^{t_f} P_e(x,t)dt \right) \quad (1)$$

$$\text{sub}\left(\int_0^{t_f} P_e(x,t)dt = 0 \right) \quad (2)$$

Here t_f is the total drive cycle time. To minimize $J(x,t)$ subject to the end-point constraint, the method of Lagrange multipliers can be applied.

$$\min_{x,\lambda} \bar{J}(x,t) = \min_{x,\lambda} \left(\int_0^{t_f} P_f(x,t)dt + \lambda \cdot \int_0^{t_f} P_e(x,t)dt \right) \quad (3)$$

The Lagrange multiplier λ has a physical interpretation, it represents the relative incremental cost of the prime mover and secondary power converter.

3 Online Strategy

In real live the future driving cycle is not known a priori, making it difficult to calculate the exact optimal power split beforehand. To arrive at a practical real time control algorithm, a sub-optimal control law can be applied, where the end-point constraint is replaced by a term in the cost function that accounts for the change in energy; in case of a hybrid electric vehicle it represents the fuel equivalence of the stored reversible energy. One way to deal with this is to replace λ by a term in the cost function that expresses the stored energy in a fuel equivalence value $s(t)$, that is controlled by the EMS. This will simplify the optimization problem to an optimization only depending on the vehicular parameters at the current time. In [2] the equivalence factor is chosen to be an affine function of the current state of energy $E_e(t)$, with proportional feedback gain K. In [1] it is reasoned that the reversible energy contains also kinetic and potential energy of the vehicle as well as energy stored in the secondary power source. The kinetic and potential energy $\hat{E}_r(t)$ can be estimated online, and used as

$$s(t) = s_0 + K\left[\left(E_{e0} - \hat{E}_r(t)\right) - E_e(t)\right] \quad (4)$$

Here E_{e0} is the battery reference state of energy. By stabilizing feedback control law (4), the amount of stored energy is such that the total amount of reversible energy tends to remain constant. Kinetic and potential energy is proportional with vehicle mass, therefore this control law adapts to vehicle loading. Simulations show that the new control law obtains a performance, even at different vehicle masses, close to the optimum obtained with DP.

References

[1] T.A.C. van Keulen, B. de Jager, M. Steinbuch. An Adaptive Sub-Optimal Energy Management Strategy for Hybrid Drivetrains. *IFAC world congress*(accepted), 2008.

[2] M. Koot, J. Kessels, B. de Jager, W. Heemels, P. van den Bosch, M. Steinbuch. Energy Management Strategies for Vehicular Electric Power Systems. *IEEE Transactions on Vehicular Technology*, Vol. 54, No. 3, pages 771-782, May 2005.

[3] A. Sciarretta, L. Guzzella. Control of Hybrid Electric Vehicles. *IEEE Control Systems Magazine*, April 2007.

Acceleration Constraints of Moving-Magnet Planar Actuators with Integrated Magnetic Bearing

C.M.M. van Lierop J.W. Jansen A.A.H. Damen P.P.J. van den Bosch
Eindhoven University of Technology
Department of Electrical Engineering
Control Systems Group
P.O.Box 513
5600 MB Eindhoven
The Netherlands
Email: c.m.m.v.lierop@tue.nl

1 Introduction

Magnetically levitated planar actuators are developed as alternatives to xy-drives constructed of stacked linear motors. Although the translator of these ironless planar actuators can move over relatively large distances in the xy-plane only, it has to be controlled in six degrees-of-freedom (DOF) because of the active magnetic bearing. The advantage of magnetically levitated planar actuators is that they can operate in vacuum, for example in extreme-UV lithography equipment. Planar actuators can be constructed in two ways. The actuator has either moving coils and stationary magnets or moving magnets and stationary coils [1]. The last type of planar actuator does not require a cable to the moving part. However, only the coils underneath the translator significantly contribute to its levitation and propulsion. Therefore, the set of active coils needs to change with the position of the translator during movements in the xy-plane. A special commutation strategy called direct wrench-current decoupling has been derived which allows for switching between different active sets of coils without influencing the decoupling of the force and torque components [2]. Due to the switching and the need to compensate the complex torque, the resulting current waveforms are non-sinusoidal and each stator coil needs to be controlled individually using a single phase amplifier. This paper discusses a novel method to find the worst-case acceleration specification as a function of the current amplifier constraints.

2 research

Traditionally, the $dq0$ transformation is used which results in relatively simple bounds on the maximum force or acceleration. However, due to the non-sinusoidal waveforms and the switching of active coil sets, the calculation of the maximum acceleration as a function of the current amplifier constraints demands for a highly non-convex minimization problem. Using the direct wrench-current decoupling [2] a vector containing the coil currents can be determined for a given wrench and position setpoint. The resulting current vector is optimal with respect to the dissipated energy because its 2-norm is minimized. The bounds on the acceleration in the xy-plane of the planar actuator can be determined for each xy-position by finding the smallest force-vector in the xy-plane which causes the infinity-norm of the current vector to equal the maximum current bound of the current amplifiers.

3 results

The novel method is successfully applied to a moving-magnet planar actuator called the Herringbone Pattern Planar Actuator (HPPA) [1]. The resulting worst-case acceleration constraints in the xy-plane can be explained by the physics of the HPPA planar actuator and have been verified on the actuator.

4 Conclusion

In this paper a novel method is presented to derive the worst-case acceleration specification in the xy-plane of a moving-magnet planar actuator topology with integrated magnetic bearing, as a function of the current amplifier constraints, using a special commutation algorithm which allows for coil switching. The novel method is successfully applied to a moving-magnet planar actuator called the Herringbone Pattern Planar Actuator (HPPA) [1].

References

[1] J. W. Jansen, C. M. M. van Lierop, E. A. Lomonova, and A. J. A. Vandenput, "Magnetically levitated planar actuator with moving magnets," in *IEEE Int. Electric Machines and Drives Conference (IEMDC'07)*, Antalya, Turkey, May 2007, pp. 272–278.

[2] C. M. M. van Lierop, J. W. Jansen, E. A. Lomonova, A. A. H. Damen, A. J. A. Vandenput, and P. P. J. van den Bosch, "Commutation of a magnetically levitated planar actuator with moving-magnets," in *Proc. of the 6^{th} international symposium on linear drives for industrial applications*, Lille, France, Sep. 2007.

Control of induction motors with voltage saturation

Christian Bastin, Rodolphe Sepulchre
Systems and Modeling Research Unit
University of Liège
B-4000 Liège, Belgium.
Ch.Bastin@ulg.ac.be,
R.Sepulchre@ulg.ac.be

Fabrice Jadot, François Malrait
Schneider Toshiba Inverter Europe
Rue A. Blanchet
F-27120 Pacy sur Eure, France.
Fabrice.Jadot@schneider-electric.com,
Francois.Malrait@schneider-electric.com

Abstract

The paper analyzes the speed and flux regulation of induction motors under saturation of the input voltage. Starting from a control law that achieves regulation in the absence of saturation, we propose a design that guarantees convergence to an admissible operating point, in the presence of input saturation.

1 Introduction

Control of induction motors is a challenging non-linear control problem of industrial importance. Industrial inverters must achieve regulation over a broad range od speed and torque conditions. At high speed, field weakening is necessary to prevent voltage saturation.

Many control algorithms have been proposed in the recent years, but the issue of voltage saturation is rarely addressed in the literature in spite of its importance for industrial applications.

We propose a control design method that achieves automatic field weakening where it is necessary, together with a complete convergence analysis and encouraging simulation results.

2 Motor model

The induction motor model is written in a rotating frame to permit field oriented control (see [2]) :

$$\begin{aligned}
\frac{J}{n_p}\frac{d}{dt}\omega_r &= \frac{3n_p}{2} < i_s, j\varphi_r > -\tau_l, \\
\frac{d}{dt}\varphi_r &= -\left[T_r^{-1} + j(\omega_s - \omega_r)\right]\varphi_r + R_{req} i_s, \\
L_f \frac{d}{dt} i_s &= -(R_s + R_{req} + jL_f\omega_s) i_s \\
&\quad + (T_r^{-1} - j\omega_r)\varphi_r + u_s
\end{aligned}$$

with the state variables ω_r (rotation speed), φ_r (rotor flux), i_s (stator current), the input voltage u_s, the load torque τ_l, the electrical parameters T_r^{-1}, R_{req}, R_s and L_f, the stator electrical frequency ω_s, the motor shaft inertia J and the number of pole pairs n_p.

The input voltage u_s is saturated :

$$u_s = sat(\bar{u}_s) = \kappa \bar{u}_s, \quad \kappa = \min(1, u_M/\bar{u}_s)$$

where u_M is the maximal admissible input voltage and $\bar{u}_s$ the output of the controller.

3 Control design

We assume perfect knowledge of the parameters and measurement of current and velocity variables. The control is based upon reference trajectories for current and fluxes obtained in [3], where the authors prove globally asymptotical convergence of the flux and the mechanical speed for any constant speed reference and load torque.

In order to take input constraints into account, we augment the controller with additional state variables that mimic the behavior of the controller in the absence of saturation, allowing for a scaling of the operating point that can be interpreted as automatic field weakening. The design principle is reminiscent of the anti-windup methodology proposed in [1].

4 Future work

In the future, we plan to address the issues of voltage and current saturation simultaneously, and to adapt these results in the case of parameters uncertainty or sensorless control.

References

[1] F. Morabito, A. Teel, and L. Zaccarian, "Nonlinear Antiwindup Applied to Euler-Lagrange Systems", *IEEE Transaction on robotics and automation*, vol. 20, pp 526-537, 2004.

[2] W. Leonhard, *Control of Electrical Drives*, Springer-Verlag, 1985.

[3] F. Jadot, F. Malrait, J. Moreno, and R. Sepulchre, "Adaptive Regulation of Induction Motors", *IEEE Transactions on Control Systems Technology*, to appear.

Acknowledgements

This paper presents research results of the Belgian Network DYSCO (Dynamical Systems, Control, and Optimization), funded by the Interuniversity Attraction Poles Programme, initiated by the Belgian State, Science Policy Office. The scientific responsibility rests with its authors.

Energy-based modeling and control of longitudinal tyre forces

Johan Koopman
Delft Center for Systems and Control
Delft University of Technology
Mekelweg 2, 2628 CD Delft
Email: j.j.koopman@tudelft.nl

Dimitri Jeltsema
Delft Institute of Applied Mathematics
Delft University of Technology
Mekelweg 4, 2628 CD Delft
Email: d.jeltsema@tudelft.nl

Michel Verhaegen
Delft Center for Systems and Control
Delft University of Technology
Mekelweg 2, 2628 CD Delft
Email: m.verhaegen@moesp.org

1 Introduction

With the introduction of driver-assisting control systems and X-by-wire technology, the automotive industry is now able to redesign the interface between the driver and the vehicle dynamical behaviour. The control systems help to make the car more consistent, predictable and therefore more safe to operate. Additionally, the car can easily be designed to have a specific 'driving feel'. Since vehicle dynamics control is strongly centered around tyre force control, the problem of longitudinal tyre force control is chosen as a first step towards a global chassis control system design. This constitutes a challenging nonlinear modeling and control problem.

2 Approach

The starting point for modeling the tyre force is the LuGre friction model that is presented in the work of Canudas-de-Wit et al. [1], and the related tyre model presented in [2]. The LuGre friction model is a dynamic, bristle-based friction model that contains all the relevant friction effects such as Coulomb friction, stiction, viscous friction and the Stribeck effect. However, a severe difficulty of the LuGre friction model in its present form is that it is only piecewise continuous. This can be problematic when designing high-performance model-based continuous controllers. To avoid this problem, alternative parameterizations are proposed to render the LuGre-based tyre model continuously differentiable. First, a different parametrization of the static friction curve that is presented in the work of Makkar et al. [3], is used to create a continuously differentiable LuGre-type dynamic friction model. A further re-parametrization is used to deal with a specific signum term in the original LuGre-based tyre model.

The next step is to embed the friction model, together with the quarter-vehicle dynamics, into a port-Hamiltonian structure [4] of the form

$$\dot{x} = [J(x) - R(x)]\frac{\partial^T H}{\partial x}(x) + G(x)u, \qquad (1)$$

with state vector x, interconnection structure $J(x)$, dissipation structure $R(x)$, and Hamiltonian $H(x)$ expressing total stored energy. The input to the system is the braking torque u. In this way, the physical properties of the system are underscored and can advantageously be exploited at the feedback controller design stage. Furthermore, the port-Hamiltonian form makes the system suitable for applying Interconnection- and Damping Assignment Passivity-Based Control. This control design method is extremely useful for assigning a specific 'braking feel' to the closed loop. Another central issue in the control design is the stabilization of unstable regions that are originally present in the tyre force characteristics.

References

[1] C. Canudas-de-Wit, H. Olsson, K.J. Åström, and P. Lischinsky. "A new model for control of systems with friction", *IEEE Trans. Aut. Cont.*, 40(3):419-425, March 1995.

[2] C. Canudas-de-Wit, P. Tsiotras, E. Velenis, M. Basset, and G. Gissinger. "Dynamic friction models for road/tire longitudinal interaction", *Vehicle System Dynamics*, 39(3):189-226, 2003.

[3] C. Makkar, W. Dixon, W. Saywer and G. Hu, "A new coninuously differentiable friction model for control systems design", in *Proc. IEEE/ASME Int. Conf. on Advanced Intelligent Mechatronics*, pp. 600-605, Montery, California, USA, July 2005.

[4] A.J. van der Schaft, "$\mathscr{L}_2$-gain and passivity techniques in nonlinear control", Berlin: Springer-Verlag 1999.

LQG control of a doubly-fed induction machine for wind turbine applications

Manuel Gálvez-Carrillo and Michel Kinnaert
Control Engineering Department
Université Libre de Bruxelles
Av. F.D. Roosevelt 50 - CP 165/55, B-1050 Brussels, Belgium.
mgalvezc@ulb.ac.be, Michel.Kinnaert@ulb.ac.be

1 Introduction

Among the renewable energies, wind energy presents the highest growth in installed capacity and penetration in modern power systems. Different kinds of technologies are used for wind turbine applications, but the variable-speed, variable-pitch wind turbine is the state-of-the-art technology for wind farms because of its high efficiency and control performance characteristics. In the present work, a doubly-fed induction generator with back-to-back converter is simulated for wind generation purposes and controlled using the LQG approach.

2 System description

In a doubly-fed induction generator (DFIG), the stator windings are connected to the electrical grid while the rotor windings are connected to a back-to-back converter via slip-rings [1]. The converter rating will be only a fraction of the total power of the system, reducing the cost of the power electronics and the losses compared with other technologies as synchronous generator for example. The back-to-back converter consists of a rectifier connected to the rotor windings: the rotor side converter or RSC; and an inverter connected to the power grid: the grid side converter or GSC. A DC-link is placed between them for energy storage in order to reduce the DC ripple. Finally, a line filter (here, a L filter) is connected between the GSC and the grid in order to reduce the harmonics injected by the GSC (see figure 1).

3 Control strategy

The electrical system is controlled by varying the a.c. voltage at the terminals of both RSC and GSC. The RSC control is responsible for both the active and reactive power delivered to the power grid. The GSC control is responsible for both the DC-link voltage and the power factor (normally equal to one). A stator-flux oriented reference frame is used to perform a vector control.

A state-space representation of the system, linearized around a given operating point, is used in combination with a Linear Quadratic Gaussian (LQG) approach. A feedback controller that includes an integrating action is combined with a state estimator (the Kalman filter) in order to produce two MIMO controllers for the RSC and the GSC respectivelly, as presented in figure 1. Feedforward control is added, taking into account the rotor speed for the RSC control, and the DC power from the RSC for the GSC control. The alternative consisting in a single MIMO controller for both RSC and GSC is also considered. These control schemes are tested and compared via simulations.

The future work is designing a fault diagnosis and isolation system regarding grid faults and sensor faults, and finally studying and implementing fault tolerant control approach.

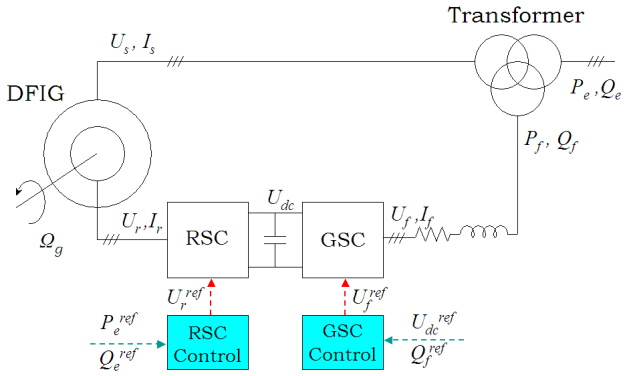

Figure 1: Schematic of DFIG, converters and controllers.

Acknowledgments

The work of Manuel Gálvez-Carrillo is supported by the ARC project "Advanced supervision and dependability of complex processes: application to power systems". This paper presents research results of the Belgian Network DYSCO (Dynamic Systems, Control and Optimization), funded by the Interuniversitary Attraction Poles Programme, initiated by the Belgian State, Science Policy Office. The scientific responsibility rests with its authors.

References

[1] W. Leonhard, *Control of Electrical Drives*, 2nd Ed., Springer-Verlag, 1996.

State-of-charge observers for lead-acid storage unit in photovoltaic installations

A. Skrylnyk, R. Lepore*, C. Renotte**, M. Remy**
Faculté Polytechnique de Mons
Boulevard Dolez 31, B - 7000 Mons
alexandre.skrylnik@student.fpms.ac.be,
*http://poleenergie.fpms.ac.be, **http://www.autom.fpms.ac.be

Introduction

Lead-acid accumulators can be used in autonomous photovoltaic (PV) systems. However the storage units are used irregularly in terms of charge/discharge and quick ageing results. Thus, many battery managing systems have been developed to extend batteries life time. The managing systems rely on the state-of-charge (SOC) of a single accumulator or strings of storage units. In such systems the correct SOC determination is very important in order to control all charging and discharging currents. We define the SOC as an energy available for the user in given charge/discharge conditions.

SOC observers design

Since the plant is time-varying, nonlinear and with parameter uncertainties it appears interesting to study and compare two approaches of SOC estimation:

- black-box modeling with fuzzy logic observer;
- robust state estimation based on the sliding mode technique.

Numerous papers describe fuzzy logic observers which use the impedance knowledge database to determine SOC [2]. However, the implementation of such observers is rather complicated because of the impedance measuring scheme. In practice only two measurements are available - voltage and current. Since the SOC can be described with a linear model [3] it is suggested to use Takagi-Sugeno architecture where the output represents a combination of piece wise linear functions of current integral and voltage. The training datasets for fuzzy logic model were collected from 12 V lead-acid battery of 125 Ah of nominal capacity during charging/discharging tests with constant current. The clustering algorithm has been used to obtain fuzzy rules. Then the input/output parameters have been adapted with evolutionary technique. However, the fuzzy-logic observer does not reflect physical properties and is sensitive to errors.
The novel researches in sliding mode state estimation result in robust SOC determination [1]. This method is highly effective to observe plants with varying parameters and unpredictable external disturbances. Thus, an observer for a battery (12 V, 125 Ah) based on the equivalent electric circuit has been designed. In practice this representation is generally implemented to model lead-acid accumulators. The suggested physical model takes into account SOC as a nonlinear function of battery open-circuit voltage. The physical parameters have been extracted from step function accumulator's response. The nonlinear open circuit voltage function has been derived from short discharge tests with a 10 A current value. The sliding mode observer takes into account dynamic properties of the plant and is more robust.
The validating experiment based on STECA TAROM charge controller's indications (fig.1) exhibits high estimating performances for the both designed observers.

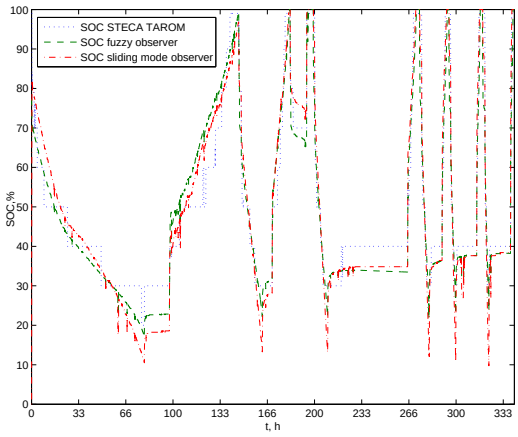

Figure 1: Comparison between measured, fuzzy-logic observed and sliding mode SOC estimation

References

[1] Il-Song Kim. The novel state of charge estimation method for lithium battery using sliding mode observer. *Journal Of Power Sources*, 163:584–590, 2006.

[2] David Raisner, Pritpal Singh, Craig Fennie. Fuzzy logic modeling of state-of-charge and available capacity of nickel/metal hybride batteries. *Journal Of Power Sources*, 136:322–333, 2004.

[3] Andreas Jossen, Sabine Piller, Marion Perrin. Methods for state-of-charge determination and their application. *Journal Of Power Sources*, 96:113–120, 2001.

Observer Design and Output Feedback Stabilization for a Class of Underactuated Mechanical Systems

A. Venkatraman, A. J. van der Schaft
Institute for Mathematics and Computing Science
University of Groningen
P.O.Box 407, 9700 AK Groningen
The Netherlands
aneesh@math.rug.nl

R. Ortega, I. Sarras
Laboratoire de Signaux et Systemes (LSS)
Supelec - 3, rue Joliot-Curie
91192 Gif-sur-Yvette cedex (France)

1 Introduction

The problem of constructing globally convergent observers for nonlinear systems has attracted much attention over the years. Unlike the linear case where a complete observer design framework has been developed, the nonlinear case has not been tackled in the general sense. Special classes of nonlinear systems have been considered and full/reduced order observer designs have been proposed for them. Our work is focussed mainly on port-hamiltonian systems, which arise from port-based network modeling of lumped-parameter physical systems with independent storage elements and thereby represent an important class of nonlinear systems. We consider problems of observer design and output feedback stabilization for these systems.

2 I & I Observers for a class of Underactuated Mechanical Systems

We are interested in the problems of observation and output feedback control of general n degree of freedom underactuated mechanical systems, modeled in port-hamiltonian form with the generalized position q and the generalized momentum p as the system states. We assume q to be measurable and p to be unmeasurable and thus aim to construct a reduced order observer that asymptotically estimates p. We adopt the observer design framework proposed in [1], which follows the Immersion and Invariance (I&I) principles introduced in [2]. We also refer the reader to [3] for a tutorial account of this method and its applications. In the context of observer design the objective of I&I is to render a manifold defined in the extended state space of the plant and observer, positively invariant and globally attractive. We show that by following this approach, we obtain a reduced order observer for p with exponentially converging error dynamics. We then consider some well known underactuated mechanical systems and construct observers for them.

3 Separation Principle

A major factor that stymies the observer design for a nonlinear system is the absence of the so called "Separation Principle" which holds otherwise when the system is linear. Due to this, even when a globally convergent observer is available, the certainty-equivalence implementation of a control law may lead to severe forms of instability, including finite escape time. Therefore, establishing the stability of such certainty-equivalence designs is equally important from the control design viewpoint. We therefore also show a separation principle for the proposed observer when used in conjunction with a full state feedback control law which is designed following the Interconnection and Damping Assignment Passivity–Based Control (IDA–PBC) [4, 5].

References

[1] D. Carnevale, D. Karagiannis, A. Astolfi, "Reduced-order observer design for nonlinear systems," *Proc. European Contr. Conf.*, Kos, Greece, pp. 559-564, July 2007.

[2] A. Astolfi, R. Ortega, "Immersion and Invariance: A new tool for Stabilization and Adaptive Control of Nonlinear Systems," , Vol. 48, No. 4, pp. 590-606, April 2003.

[3] A. Astolfi, D. Karagiannis, R. Ortega, *Nonlinear and Adaptive Control with Applications*, Springer-Verlag, Berlin, Communications and Control Engineering, 2007.

[4] R. Ortega, M. Spong, F. Gomez and G. Blankenstein, "Stabilization of underactuated mechanical systems via interconnection and damping assignment," , Vol. 47, No. 8, August 2002, pp. 1218–1233.

[5] J. Acosta, R. Ortega, A. Astolfi and A. Mahindrakar, "Interconnection and damping assignment passivity–based control of mechanical systems with underactuation degree one," , Vol 50, No. 12, pp. 1936-1955, December 2005.

HYBRID STATE OBSERVER FOR A LOCALLY LIPSCHITZ SYSTEM

Denis V. Efimov
Montefiore Institute
the University of Liege
B-4000 Liege, Belgium
e-mail: efimov@montefiore.ulg.ac.be

1. INTRODUCTION

The state observers design problem for nonlinear systems has been an area of intensive research during the last two decades. There exists a lot of solutions in the area dealing with diverse forms of systems models: high gain techniques, nonlinear coordinate changes, approaches dealing with smooth and nonsmooth output functions. Observers design procedures find their applications not only in areas of control under partial measurements, but also for fault detection, systems synchronization and secured data transmission and encoding.

The class of *Lipschitz* nonlinear systems has seen much attention:

$$\dot{\mathbf{x}} = \mathbf{A}\,\mathbf{x} + \boldsymbol{\varphi}(\mathbf{y}) + \mathbf{f}(\mathbf{x},\mathbf{d})\,,\ \mathbf{y} = \mathbf{C}\,\mathbf{x}\,, \qquad (1)$$

where $\mathbf{x} \in R^n$ is the state vector; $\mathbf{d} \in R^m$ is the disturbing input; $\mathbf{y} \in R^p$ is the available for measurements output; the functions $\boldsymbol{\varphi} : R^p \to R^n$ and $\mathbf{f} : R^{n+m} \to R^n$ are Lipschitz continuous (function $\mathbf{f}$ *globally*).

Under assumption on the *globality* of Lipschitz property for function $\mathbf{f}$, applying sufficiently high observer feedback gain it is possible to cancel an influence of nonlinearity on observation error dynamics and the problem is solvable via linear systems approach.

If system is *locally* Lipschitz, only local solution is possible applying conventional approaches. In this work a solution of the problem is proposed for perturbed system (1), where growing observer gains are calculated as solutions of a Riccati equation off-line. After that they are substituting in the observer using logic-based scheme if the previous observer gains fail.

2. MAIN RESULT

For locally Lipschitz function $\mathbf{f}$ the inequality

$$|\mathbf{f}(\mathbf{x},\mathbf{d}) - \mathbf{f}(\mathbf{z},0)| \le \alpha_1(1+|(\mathbf{x},\mathbf{d})|)\alpha_2(1+|\mathbf{z}|)|(\mathbf{x},\mathbf{d}) - (\mathbf{z},0)|$$

holds for any $\mathbf{x} \in R^n$, $\mathbf{z} \in R^n$ for some $\alpha_1, \alpha_2 \in \mathcal{K}$.

Consider the hybrid state observer for system (1):

$$X_i = h_x(i, X_{i-1})\,,\ D_i = h_d(i, D_{i-1})\,,\ X_0 > 0\,,\ D_0 > 0\,,$$
$$Z_i = h_z(i, Z_{i-1})\,,\ Z_0 > |\mathbf{z}(0)|\,,\ i = 1,2,3,\ldots N \le +\infty\,; \qquad (2)$$

$$\nu_i = 4D_i^2\varepsilon^{-2}\lambda_{\min}^{-1}(\mathbf{P})\,,\ \varepsilon > 0\,; \qquad (3)$$

$$\kappa_i = 2\alpha_1(1 + X_i + D_i)^2\,\alpha_2(1 + Z_i)^2\,, \qquad (4)$$

$$(\mathbf{A} - \mathbf{L}_i\,\mathbf{C})^T\mathbf{P} + \mathbf{P}(\mathbf{A} - \mathbf{L}_i\,\mathbf{C}) + [\,\nu_i + \kappa_i\,\mathbf{P}\,]\mathbf{P} + (1+\mu)\mathbf{I}_n = 0\,, \mu > 0\,; \qquad (5)$$

$$\dot{\mathbf{z}}(t) = \mathrm{Proj}[\,\mathbf{z}, \mathbf{A}\,\mathbf{z}(t) + \boldsymbol{\varphi}(\mathbf{y}(t)) + \mathbf{f}(\mathbf{z}(t),0) + \mathbf{L}_i\,(\mathbf{y}(t) - \mathbf{C}\,\mathbf{z}(t))\,]\,,\ t \in [t_i, t_{i+1})\,, \qquad (6)$$

$$\mathrm{Proj}(\mathbf{z},\zeta) = \begin{cases} \zeta, & if\ |\mathbf{z}| < Z_i \vee \mathbf{n}(\mathbf{z})^T\zeta \le 0\,; \\ \left(\mathbf{I}_n - \boldsymbol{\Gamma}\dfrac{\mathbf{n}(\mathbf{z})\,\mathbf{n}(\mathbf{z})^T}{\mathbf{n}(\mathbf{z})^T\boldsymbol{\Gamma}\,\mathbf{n}(\mathbf{z})}\right)\zeta, \boldsymbol{\Gamma} > 0, & \\ if\ |\mathbf{z}| = Z_i \wedge \mathbf{n}(\mathbf{z})^T\zeta > 0\,, & \end{cases} \qquad (7)$$

$$t_{i+1} = \arg\sup_{t \ge T_i}\{|\mathbf{y}(t) - \mathbf{C}\,\mathbf{z}(t)| > |\mathbf{C}|\,\varepsilon\}\,,\ t_0 = 0\,, \qquad (8)$$

$$T_i = \max\{t_i + \tau_D,\ t_i - \frac{2}{\nu_i}\ln\left(\sqrt{\frac{\lambda_{\min}(\mathbf{P})}{8\lambda_{\max}(\mathbf{P})}}\frac{\varepsilon}{|\mathbf{z}(t_i)| + X_i}\right)\}\,,\ \tau_D > 0\,, \qquad (9)$$

where $\mathbf{z} \in R^n$ serves as vector $\mathbf{x}$ estimate; $\mathbf{L}_i$ is the observer feedback matrix gain with dimension $n \times p$, which value is calculated from Riccati equation (5) with positive definite and symmetric matrix $\mathbf{P}$; t_i is the time instant of gain $\mathbf{L}_i$ calculation, this gain is applied in (6) on interval $[t_i, t_{i+1})$; X_i, D_i, Z_i, are estimates on maximum amplitudes of vectors $\mathbf{x}$, $\mathbf{d}$ and $\mathbf{z}$ correspondingly, discrete systems (2) have well defined strictly increasing solutions for any $X_0 > 0$, $D_0 > 0$, $Z_0 > 0$ for all $i \ge 0$; constants μ, τ_D, ε and matrix $\boldsymbol{\Gamma}$ can be taken arbitrary; $\mathbf{n}(\mathbf{z})$ is the unit outward normal vector for $|\mathbf{z}| = Z_i$ (projection algorithm (7) ensure existence and boundedness of system (6) solutions for the cases of wrong choices of values X_i, D_i, Z_i). The dwell-time constant τ_D ensures finiteness number of steps of algorithm (2)–(9) on any finite time interval.

Non-linear observers (estimators) and symmetries : theory and examples

S. Bonnabel
Systems and Modeling Department of Electrical Engineering
and Computer Science, B28 Universit de Liege B-4000 Liege Sart-Tilman, Belgium.
bonnabel@montefiore.ulg.ac.be

P. Rouchon
CAS
Ecole des Mines de Paris

1 Abstract

One way to build non-linear estimators in control theory is to make observers. They use a model of the system and noisy measurements to provide a real-time estimation of its internal state. When the system admits symmetries, the usual observers (Luenberger observer, extended Kalman filter) break these symmetries. We developed a method which provides a way to modify the usual observers equations so that they respect the symmetries of the system. Once this is done, one can define a new estimation error (which is the difference between the estimated state and the true state of the system) which relies on symmetries. The whole analysis of the convergence of the observer (i.e how to make the estimation error tend to zero) is then based on the symmetries. We will not spend much time on the theoretical developments and we will rather focus on some examples. The first example is tutorial. We consider a non-holonomic car equipped with a GPS (position measurement) and we want to find its orientation. The symmetries are associated to the invariance of the equations under the action of the SE(2) group : translations and rotations in the plane. The second example deals with the estimation of a 2-level quantum system. Its state is a superposition of two states. The state space is a two dimensional space which has an underlying geometry of the surface of a sphere (Bloch sphere). The Schrodinger equation is invariant under the action of SU(2) - or in the Bloch sphere representation the dynamics is invariant under the action of the rotation group SO(3) acting on the sphere. Finally we will present a preliminary work on data assimilation in oceanography (nudging) where the model is invariant under the action of SE(2).

References

[1] S. Bonnabel, Ph. Martin, and P. Rouchon. A non-linear symmetry-preserving observer for velocity-aided inertial navigation. In *American Control Conference (ACC06)*, pages 2910–2914, June 2006.

[2] S. Bonnabel, M. Mirrahimi, and P. Rouchon. Qubit Hamiltonian identification : a symmetry-preserving observer based approach. In *IFAC08*

[3] S. Bonnabel, M. Martin, and P. Rouchon. Symmetry-preserving observers. In *To appear in IEEE AC*

[4] P. J. Olver. *Equivalence, Invariants and Symmetry*. Cambridge University Press, 1995.

Boundary observer synthesis: static and dynamic structure design

D. Vries, K.J. Keesman
Bornsesteeg 59, 6708 PD Wageningen
{dirk.vries, karel.keesman}@wur.nl

H. Zwart
P.O. Box 217, 7500 AE Enschede
h.j.zwart@math.utwente.nl

Abstract

We design and analyze a static boundary and a dynamic boundary observer for a typical Convection–Diffusion–Reaction system. The system is a model of a UV disinfection process, which is used in water treatment and food industry.

1 Introduction

In many (control) applications where (bio)chemical reactions and transport phenomena occur, measurement and control actions take place at the boundaries. While a theoretical framework already exist ([1] and references therein), there is little attention to apply this theory in practice, as far as we know.

In [2], the analysis and design of a static Luenberger observer for a UV disinfection example is explored. In this work, we take a glance at some of these design results; we will refer to this as case A. We will also analyze the synthesis of a (robust) dynamic observer and evaluate its performance for the same system with boundary inputs and boundary outputs[1]; this will be referred to as case B.

The system is described by,

$$\Sigma := \left\{ \begin{array}{rcll} \dot{z}(t) & = & \mathfrak{A}z(t) - b_1 u_1(t) z(t); & z(\eta,0) = z_0 \\ \mathfrak{B}z(t) & = & u_2(t) & \\ \mathfrak{C}z(t) & = & y(t). & \end{array} \right. \tag{1}$$

And, the observer system A and B is written as:

$$\Sigma^{\text{obs}} := \left\{ \begin{array}{rcll} \dot{\hat{z}}(t) & = & \mathfrak{A}\hat{z}(t) - b_1 u_1(t) \hat{z}(t); & \hat{z}(\eta,0) = \hat{z}_0 \\ \mathfrak{B}\hat{z}(t) & = & u_2(t) + L(t)\mathfrak{C} * (\hat{z}(t) - z(t)) & \\ \mathfrak{C}\hat{z}(t) & = & \hat{y}(t) & \end{array} \right. \tag{2}$$

with $z, \hat{z} \in Z$, $Z = L_2(\eta_1, \eta_2)$ a Hilbert space. Furthermore, $\mathfrak{A} : D(\mathfrak{A}) \subset Z \mapsto Z$ with domain $D(A) = D(\mathfrak{A}) \cap \ker(\mathfrak{B})$ and $Az = \mathfrak{A}z$, for $z \in D(A)$. We consider a scalar positive control $u_1 \in U_1 \subset \mathbb{R}_+$ and the vector $u_2 = \begin{pmatrix} \tilde{u}_2 & 0 \end{pmatrix}^\top \in U_2 \subset \mathbb{R}^2_+$, since we have two boundaries. The vector Robin-type boundary control operator $\mathfrak{B}$ and observation operator $\mathfrak{C}$ should be interpreted in the sense of definition 3.3.2 in [1], where $\mathfrak{B} : D(\mathfrak{B}) \subset Z \mapsto U$ satisfies $D(\mathfrak{A}) \subset D(\mathfrak{B})$ and point observation operator $\mathfrak{C} : D(\mathfrak{C}) \subset Y \mapsto \mathbb{R}^q$, $q \geq 1$. The matrix $L \in \mathbb{R}^{q \times m}$ comprises of observer gains.

In the following, we consider:

case A: $L(t) \equiv L$ is constant;

case B: $\tilde{u}_2$ is disturbed with signal v_1 and y is disturbed with v_2, both disturbances are L_2–bounded.

2 Results

During the presentation, we will further elucidate on (2), design and synthesis conditions on L and the performance evaluation for both cases. In addition, the suitability of both approaches will be discussed.

[1] see [2] for physical background of the model and [3] for more details about the observer synthesis.

References

[1] R.F. Curtain and H. Zwart. *An Introduction to Infinite Dimensional Linear Systems Theory*. Springer-Verlag, New York, 1995.

[2] D. Vries, K.J. Keesman, and H. Zwart. A Luenberger observer for an infinite dimensional bilinear system: a UV disinfection example. *In: Proceedings of the 3rd IFAC Symposium on System, Structure and Control.* Foz de Iguassu, Brazil. October 17–19, 2007.

[3] D. Vries, K.J. Keesman, and H. Zwart. An H_∞–observer at the boundary of an infinite dimensional system. *In: 5th IFAC Workshop on Distributed Parameter Systems.* (Book of Abstracts), Namur, Belgium. July 23–27, 2007.

Initial Estimates for Wiener-Hammerstein Models using the Best Linear Approximation

Lieve Lauwers, Johan Schoukens and Rik Pintelon
Vrije Universiteit Brussel, dep. ELEC, Pleinlaan 2, 1050 Brussels, BELGIUM
e-mail: lieve.lauwers@vub.ac.be

Abstract - *We present a method to initialize the linear dynamic blocks of a Wiener-Hammerstein model. The idea is to build these blocks from the poles and zeros of the Best Linear Approximation of the system under test. This approach results in an easy to solve problem from which initial estimates for the linear dynamics can be obtained. The proposed method is applied to measurements from an electronic Wiener-Hammerstein circuit.*

I. INTRODUCTION

A Wiener-Hammerstein model is a block-oriented structure that consists of two linear dynamic systems G_1 and G_2 with a static nonlinearity $f(\,.\,)$ in between (see Fig. 1).

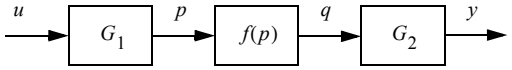

Fig. 1. Wiener-Hammerstein system.

The most difficult step in the identification of such models is to generate starting values for the linear dynamic blocks. We will present an initialization procedure which makes use of the Best Linear Approximation G_{BLA} [1]-[3].

II. APPROACH

The idea is to split the system in two subsystems (see Fig. 2), and to write the linear dynamic blocks as a linear combination of basis functions, W_i and H_i, which contain the poles and zeros of G_{BLA}, respectively:

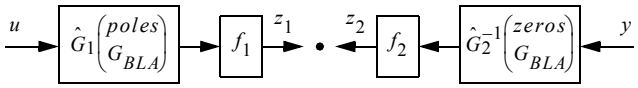

Fig. 2. Decomposed Wiener-Hammerstein system.

$$\begin{cases} \hat{G}_1 = \sum_{i=1}^{r} \hat{\theta}_1^L(i) W_i \\ \hat{G}_2^{-1} = \sum_{i=1}^{s} \hat{\theta}_2^L(i) H_i \end{cases} \quad (1)$$

The goal is then to find the proper coefficients $\hat{\theta}^L$ of these basis functions.

III. INITIALIZATION PROCEDURE

In the following, we will briefly discuss the different steps of the initialization procedure.

A. Determine G_{BLA} parametrically

After the Best Linear Approximation is obtained nonparametrically, a parametric model needs to be estimated for G_{BLA}.

B. Construct basis functions for $\hat{G}_1$ and $\hat{G}_2^{-1}$

In order to obtain the poles and zeros, we decompose G_{BLA} and G_{BLA}^{-1}, respectively, into partial fractions. From this expansion, we then deduce basis functions for $\hat{G}_1$ and $\hat{G}_2^{-1}$: W_i and H_i, respectively.

C. Use a general model structure

To circumvent a problem that is nonlinear in the parameters, we consider the general model structure depicted in Fig. 3. Note that the nonlinearities consist of a linear and a nonlinear part. As such, a problem that is linear-in-the-parameters (θ^L, θ^{NL}) needs to be solved to find the coefficients of the basis functions. The price to be paid is the increased number of parameters in the multiple input, single output nonlinearities.

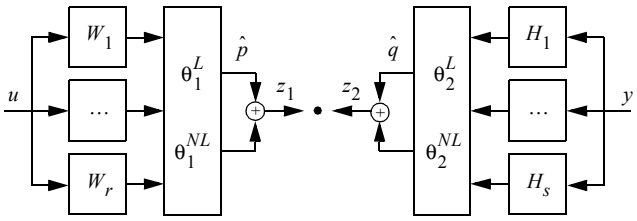

Fig. 3. Generalized model structure.

D. Estimate θ

The structure in Fig. 3 contains the Wiener-Hammerstein structure (Fig. 1) if the output of both subsystems are equal: $z_1 = z_2$. By satisfying this continuity requirement, we obtain a Total Least Squares problem [4] from which θ^L and θ^{NL} can easily be estimated.

E. Initial estimates

It is easy to see that the estimated linear parameters $\hat{\theta}^L$ determine the coefficients of the basis functions. $\hat{G}_1$ and $\hat{G}_2^{-1}$ are then composed parametrically by making the linear combination in (1). Furthermore, the linear output of the nonlinearity in each subsystem (see Fig. 3) is an initial (nonparametric) estimate for the corresponding intermediate signal p or q.

IV. CONCLUSION

We have presented a non-iterative method to generate starting values for the different blocks of Wiener-Hammerstein models. The proposed intialization procedure was successfully applied to measurement data.

REFERENCES

[1] J. Schoukens, R. Pintelon, T. Dobrowiecki, Y. Rolain. Identification of linear systems with nonlinear distortions. *Automatica*, Vol. 41, No. 3, pp. 491-504, 2005.

[2] R. Pintelon, J. Schoukens (2001). *System Identification. A Frequency domain approach*. IEEE Press, New Jersey.

[3] J.S. Bendat, A.G. Piersol (1980). *Engineering Applications of Correlations and Spectral Analysis*. Wiley, New York.

[4] S. Van Huffel, J. Vandewalle (1991). *The Total Least Squares Problem: Computational Aspects and Analysis*. Frontiers in Applied Mathematics. SIAM, Philadelphia.

Parameter-varying decoupling for 3-DOF platform with manipulator on top of it

Michal GAJDUŠEK, Ad DAMEN and Paul van den BOSCH
Department of Electrical Engineering,
Eindhoven University of Technology
P.O. Box 513, 5600 MB Eindhoven, The Netherlands
Email: m.gajdusek@tue.nl, a.a.h.damen@tue.nl, p.p.j.v.d.bosch@tue.nl

1 Abstract

The goal of this article is to describe parameter-varying decoupling method. The method is based on modification of Dyadic Transformation Matrices (DTM) method described in [1]. The improved decoupling method is tested on a 3-DOF magnetically levitated platform which has 2-DOF manipulator on top of the platform [2].

The proposed decoupling method is based on computation of DTM ($\mathbf{T}_u$, $\mathbf{T}_y$). As the result, independent SISO controller k_n can be designed for each DOF. If the system is not exactly dyadic, there are still off-diagonal terms after transformation, but nthe transformation matrices significantly reduce influence of the cross terms. The improvement has been made for a system with varying parameters p. Instead of having constant DTM as proposed in [1], parameter-varying DTM can improve decoupling of such a system.

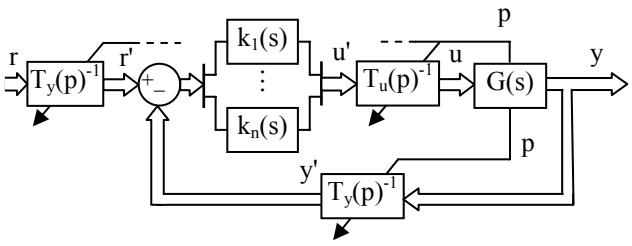

Fig. 1: Parameter-varying decoupling

The experimental setup consists of two main parts: a 3-DOF platform, actuated by 9 voice coils underneath, and 2-DOF manipulator on top of it. The platform is suspended such that it can only move in 3 DOFs: vertically and two tilting angles. The manipulator on top of the platform is essentially an H-bridge with a rotary motor on the beam, which provides linear and rotary movement of an end tip of the manipulator.

The setup was used to test independent controllers for each DOF of the platform. Position of the beam of the manipulator is the varying parameter of the system which significantly influences dynamics of the platform. Constant and variable decouplings were compared using Relative Gain Array (RGA) measure. Variable DTM can clearly decouple the system much better in various positions of the beam than constant DTM.

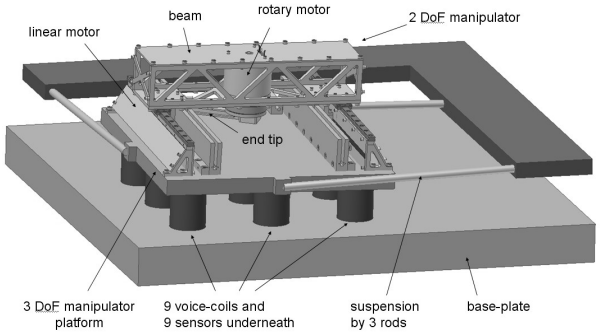

Fig. 2: The experimental setup

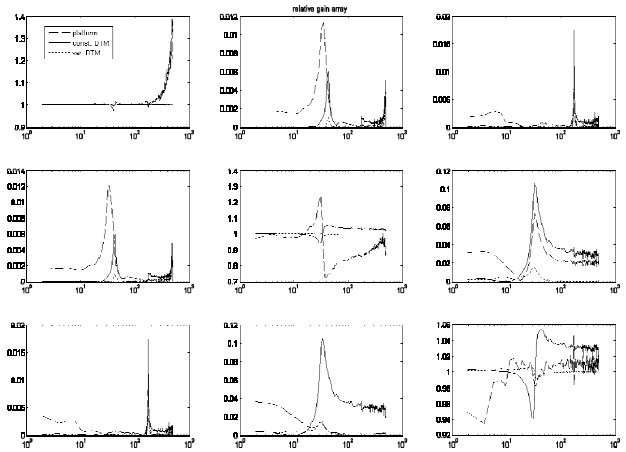

Fig. 3: RGA graphs of the original system, system decoupled by constant DTM (got at different pos. of the beam) and position dependent DTM, respectively.

References

[1] D. Vaes, W. Souverijns, J. De Cuyper, J. Swevers, P. Sas, "Decoupling feedback control for improved multivariable vibration test rig tracking", In: *Proc. ISMA 2002*, pp. 525-534, 2002.

[2] M. Gajdusek, A. A. H. Damen, P. P. J. van den Bosch, "Contactless planar actuator with manipulator - Experimental setup for control", In: Proc. LDIA2007, Lille, France, 2007.

Identification of a harmonic signal in the presence of additive noise, an unknown time base distortion, and an averaging effect

Veerle Beelaerts, Fjo De Ridder, Maite Bauwens and Rik Pintelon
Vrije Universiteit Brussel, Dept. ELEC, Pleinlaan 2, 1050 Brussel
vbeelaer@vub.ac.be

Introduction

Natural archives are recorders of global climate changes. Data acquisition from natural archives mostly involves sampling solid substrates. This imposes two problems:
Problem 1: The signals are sampled at a non-equidistant time grid.
Problem 2: When solid substrates are sampled, these samples are taken over a volume in distance. As a consequence, when the continuous signal is sampled, it will be averaged over the volume of the sample.
Existing methods [1] do not take into account problem 2 and, henceunderestimate the amplitudes of the harmonics.
The aim of this work is to provide an efficient identification algorithm to identify the non-linearities in the distance-time relationship, called time base distortions, and to correct for the averaging effects.

Approach

A parametric model is proposed which estimates a harmonic signal in the presence of additive noise, a time base distortion and an averaging effect. In a first approach the averaging effects are assumed to be in one direction only, i.e. the direction of the axis on which the measurements were performed.

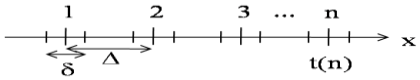

Figure 1.: Convention. δ:distance over which is averaged; Δ: distance between two samples; n: sample position, n $\in \{1, \ldots, N\}$; x: distance, x(n)=Δn; t(n): unknown time variable.

The following signal model for the averaged signal is proposed:

$$\bar{y}(n,\theta) = \frac{\Delta}{\delta}\int_{n-\frac{1\Delta}{2\delta}}^{n+\frac{1\Delta}{2\delta}} y(m,\theta)\, dm \qquad (1)$$

where m is the position, $x(m)=\Delta m$; θ are the unknown parameters and $y(m,\theta)$ is the continuous signal we want to identify.
The time base is modelled as follows [1].

$$t(m) = mT_s + g(m)T_s \qquad (2)$$

Here $T_s = {}^{1}/_{f_s}$ is the sampling period, f_s the sampling frequency, and $g(m)$ the unknown time base distortion (TBD). In this work a splines approximation of the TBD is chosen:

$$g(m) = \sum_{l=1}^{b} b_l \emptyset_l(m) \qquad (3)$$

where, b is a vector of unknown time base distortion parameters, and $\emptyset$ is a set of splines.

The estimates of the unknown parameters were obtained with a nonlinear least squares algorithm

Results

The vessel density measured in the mangrove tree *R mucronata* is used to illustrate the method. The samples were collected and prepared according to [2]. The vessel density is a proxy for the rain fall in tropical regions. The data record is 23 samples long and covers 3.3 years.
A signal model consisting of 2 harmonics A; and a time base distortion model with 4 time base distortion parameters b are used. The constructed time base can be seen in Figure 1. As expected, a yearly periodicity is visible in Figure 1b.
The correction for the averaging effect is shown in figure 1c. The amplitude increased with 11.18%.

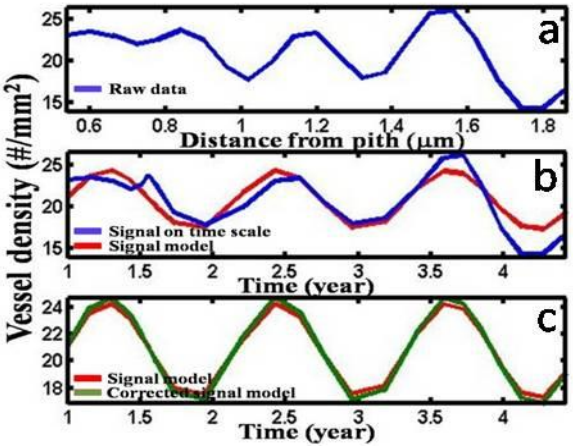

Figure 1.: Vessel density in mangrove trees.

Conclusion

The method discussed in this work is a valuable tool for the construction of a time base and the correction for averaging, as the conclusion hold for other environmental archives and averaging in more than one direction.

References

[1] F. De Ridder, R. Pintelon, J. Schoukens, and A. Verheyden, "Reduction of the Gibbsz phenomenon applied on non-harmonic time base distortions," *IEEE Trans. Instrum. Meas.* vol. 54, pp 1118-1125, 2005.
[2] A. Verheyden, F. De Ridder, N. Schmitz, H. Beeckman, and N. Koedam, "High-resolution time series of vessel density in Kenian mangrove trees reveal a link with climate," *New Phytologist*, vol. 167, pp. 425-435, 2005.

Comparison of friction compensation methods in bilateral teleoperation

T. Delwiche, L. Catoire and M. Kinnaert
Control Engineering Department
Université Libre de Bruxelles
Thomas.Delwiche@ulb.ac.be

J. Lataire, L. Vanbeylen and J. Schoukens
Department ELEC
Vrije Universiteit Brussel
jlataire@vub.ac.be

1 Introduction

Teleoperation consists in performing a remote task with an electromechanical master-slave device. When force feedback is present at the master side to make the user feel the interaction forces between the slave and its environment, one refers to bilateral teleoperation.
Most of the controller design techniques proposed in the teleoperation literature require linear models. However, in most cases, friction makes the linearity assumption invalid. Improving linearity is therefore one of the main reasons why friction compensation systems (FCS) are used in teleoperation. However, a performance index, i.e. a tool characterizing the ability of a FCS to linearize the system in the frequency band of interest, seems to be still lacking in the teleoperation literature.

2 Frequency domain performance index

In this paper, we propose to use the tools developed in [2] to build a performance index. These tools allow at the same time the characterization of the nonlinear behavior of a dynamical system and the measurement of the non-parametric frequency response function, using different realizations of multisine signals.

3 Experiments

A FCS can be based either on a friction model or not. Both types have been applied to teleoperation. The performance index proposed in this work will be illustrated for three configurations :

1. No compensation
2. FCS based on a friction model (MBFC)
3. FCS based on a friction observer (OBFC)

In the second case, a smoothed Coulomb model is used (friction estimated based on speed measurements) and in the third case, the observer described in [1] is used. This observer uses a linear model of the mechanism together with speed and force measurements to evaluate the friction. The absence of friction model allows the latter FCS to cope with time-varying friction properties.
For each configuration, the performance index clearly shows the frequency dependency of the performance of the FCS (see figure 1 below). The OBFC shows better performance at lower frequencies while the other FCS performs better at higher frequencies. As voluntary motions occur at low frequencies in teleoperation, we conclude that the OBFC is better suited to our application.

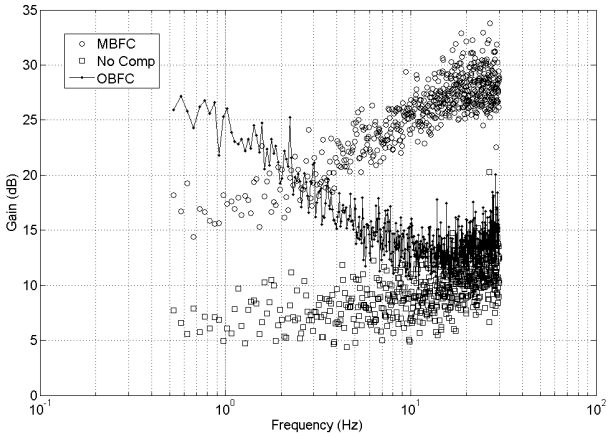

FIG. 1: Performance index for the three configurations. Higher values of the index corresponds to a better ability to linearize the system.

Acknowledgments

The work of Thomas Delwiche is supported by a FRIA grant. The teleoperation setup is financed by the FNRS. This paper presents research results of the Belgian Network DYSCO (Dynamical Systems, Control, and Optimization), funded by the Interuniversity Attraction Poles Programme, initiated by the Belgian State, Science Policy Office. The scientific responsibility rests with its authors.

References

[1] A. Albu-Schäffer, C. Ott, and A. De Luca. Disturbance observer. *Lecture Notes, Workshop on Nonlinear control of flexible joint robots, IEEE ICRA'07, april 10-14, Rome, Italy*, 2007.

[2] J. Schoukens, R. Pintelon, T. Dobrowiecki, and Y. Rolain. Identification of linear systems with nonlinear distorsions. *Automatica*, 41 :491–504, 2005.

Experimental investigation of the stability of nonlinear systems

L. Vanbeylen, J. Schoukens

Vrije Universiteit Brussel, dept. ELEC, Pleinlaan 2, B1050 Brussels, BELGIUM
e-mail: laurent.vanbeylen@vub.ac.be

1 Introduction

Since all real-life plants are nonlinear to some extent, control loops may have unexpected stability problems. Indeed, usually, one checks (theoretically) the stability of the controller-plant feedback combination, e.g. by means of standard Lyapunov based methods [1]. Besides the conversativity of these methods, there is another serious drawback: even if stability can be proven, there is still a risk of unstable operation, because of the discrepancy between the plant model and its actual behaviour. Due to these model errors, the stability of the actual controlled plant is not guaranteed anymore. The goal of this research is to make statements about the stability of the feedback system, based on experimental data rather than on models.

2 Problem statement

Consider the feedback system shown in Fig. 1, driven by a stationary random input $u(t)$ with bounded variance.

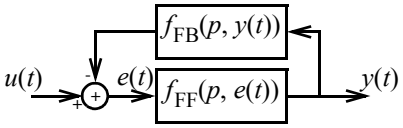

Fig. 1. Block schematic representation of a nonlinear feedback system.

Herein, the subblocks $f_{FF}(p, e(t))$ and $f_{FB}(p, y(t))$ are dynamic nonlinear systems, and p is the differentiation operator $px(t) = \frac{d}{dt}x(t)$, that introduces the dynamics.
Since the system is nonlinear, in terms of state space, the state trajectories may end in stable equilibria, in limit cycles or drift away to infinity. Due to the random input, there is a risk of jumping to such away-drifting trajectories. Hence, instability becomes a random event. And this random event depends on both the statistical properties of the input and on the nature of the nonlinear system. The ultimate goal of this research is, based on a set of input-output measurements, to make two statistical statements about the instability:

- can the system become unstable ?
- what is the risk of instability ?

Some elements of an answer were already given in the discrete time case [2], [3]. The former relies on the framework of the best linear approximations, and on the small gain theorem [1]. The latter is based on extreme value statistics, allowing to make a statistical postulation on the boundedness of the output power (i.e. stability in the bounded input power - bounded output power sense).

This work was supported by the FWO-Vlaanderen, the Flemish community (Concerted action ILiNoS), and the Belgian government (IAP-VI/4 - Dysco).

3 Alternative interpretation of instability

Several different alternative interpretations of the instability phenomenon occuring in continuous time nonlinear systems are the following:

- for a given (bounded) input power, the resulting output signal does not have a bounded output power;
- there is a non-zero probability that the output signal either starts to oscillate or starts to grow without limits;
- the pdf of the residual signal (between a stable model and the exact output of the feedback loop) has so heavy tails that its variance is not bounded;
- there is also a clear link to the state space representation of the unforced system (i.e. with $u(t) = 0$); spikes in the (non-zero) random perturbation $u(t)$ will cause more risky jumps in the state space.

3.1 Example

Consider e.g. the case:

$$f_{FF}(p, e(t)) = \frac{1}{p^2 + p + 1}e(t)\,;\, f_{FB}(p, y) = y - 10^{-3}y^3 \quad (1)$$

From the corresponding phase portrait shown in Fig. 2, it is seen that there is a risk of unstable operation due to the fact that some state trajectories are escaping from the attractor.

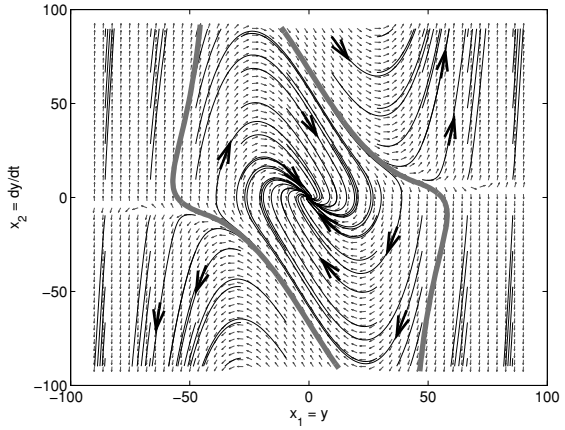

Fig. 2. Phase portrait of the unperturbed second order nonlinear system. The border of the attractor is depicted in grey.

References

[1] Khalil H. L. (1996), *Nonlinear systems* (2nd ed.). Englewood Cliffs, NJ: Prentice-Hall.

[2] Schoukens J., Dobrowiecki T., Pintelon R. (2004), Estimation of the risk for an unstable behaviour of feedback systems in the presence of nonlinear distortions. *Automatica* 40 (7), 1275-1279.

[3] Vanbeylen L., Schoukens J. (2007), Experimental stability analysis of nonlinear feedback systems, *26th Benelux meeting on systems and control*, p. 123.

PWA identification of nonlinear interconnected systems

Eleni Pepona
Dep. of Mathematics, SISCM
Brunel University
John Crank Building
Uxbridge, UB8 3PH
United Kingdom
eleni.pepona@brunel.ac.uk

Paresh Date
CARISMA, SISCM
Brunel University
John Crank Building
Uxbridge, UB8 3PH
United Kingdom
paresh.date@brunel.ac.uk

1 Introduction

The problem of identifying a discrete-time nonlinear system composed by interconnected linear and nonlinear subsystems is addressed in this work. Such systems will be represented under the Linear Fractional Transformation (LFT) modeling formalism [2]. An iterative procedure is developed that interchanges between identification of the linear and the nonlinear part. Standard techniques are used for the identification of the linear subsystem whereas the bounded-error identification technique for Piece-Wise Affine (PWA) identification proposed in [1] is used for the identification of the nonlinear subsystem.

Numerical examples show that the proposed iterative scheme is able to exploit the knowledge of the system interconnection structure, thus providing simpler models compared to those obtained when applying black-box PWA identification techniques to the overall system.

2 Problem Formulation

A discrete-time networked dynamical system composed by interconnected linear and nonlinear subsystems will be represented by an LFT as in Figure 1. The blocks $\mathscr{L}$ and $\mathscr{N}$ describe the overall linear and nonlinear dynamics of the system, respectively. Signals u_k, y_k and e_k are the system input, output and noise at time $k \in \mathbb{Z}$, while z_k and w_k are internal signals representing the input and the output of the nonlinear part. We consider only the case where $z_k \in \mathbb{R}^{n_z}$ is a vector consisting of n_y past values of the output, and the current and n_u past values of the input, i.e. $z_k = [\, y_{k-1} \ \dots \ y_{k-n_y} \ u_k \ u_{k-1} \ \dots \ u_{k-n_u}]^T$, $n_z = n_y + n_u + 1$. Further, we assume that $\mathscr{N}$ is a static mapping, i.e. $w_k = \mathscr{N}(z_k)$ with $\mathscr{N} : \mathbb{R}^{n_z} \to \mathbb{R}$.

The following model class is considered :

$$A(q)y_k = B(q)u_k + G(q)w_k + \varepsilon_k \tag{1a}$$
$$w_k = f(z_k). \tag{1b}$$

The linear part $\mathscr{L}$ is described by the ARX model (1a), where $\varepsilon_k \in \mathbb{R}$ is the error term, and $A(q), B(q), G(q)$ are finite polynomials of orders n_a, n_b and n_g, respectively, in the delay operator q^{-1}. The nonlinear part $\mathscr{N}$ is described by the static relation (1b), where $f(\cdot)$ is a PWA map of the form

$$f(z) = \begin{cases} \theta_1^T \phi & \text{if } z \in \mathscr{Z}_1 \\ \quad \vdots & \\ \theta_s^T \phi & \text{if } z \in \mathscr{Z}_s. \end{cases} \tag{2}$$

In (2), $\phi = [\, z^T \ 1 \,]^T$, s is the number of modes, $\theta_i \in \mathbb{R}^{n_z+1}$, $i = 1, ..., s$, are the parameters of each mode, and $\{\mathscr{Z}_i\}_{i=1}^s$ is a complete partition of the domain $\mathscr{Z} \subseteq \mathbb{R}^{n_z}$ where $f(\cdot)$ is defined. Each set $\mathscr{Z}_i$, $i = 1, ..., s$, is a convex polyhedron described by $\mathscr{Z}_i = \{z \in \mathbb{R}^{n_z} : \ H_i\phi \preceq_{[i]} 0\}$, where $H_i \in \mathbb{R}^{\mu_i \times (n_z+1)}$, $i = 1, \dots, s$, μ_i is the number of linear inequalities defining the ith polyhedral region $\mathscr{Z}_i$.

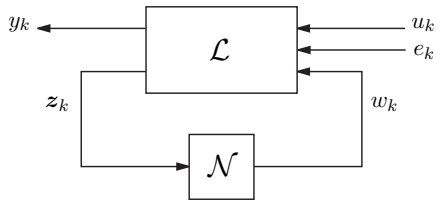

Figure 1: The considered LFT model structure.

Given N pairs of input-output data $\{u_k, y_k\}_{k=1}^N$ we develop an iterative algorithm that interchanges the identification of the above linear and nonlinear subsystems. We demonstrate that exploiting the information of the interconnection structure yields simpler and more parsimonious models in comparison with modeling the interconnected system as a single nonlinear one.

References

[1] A. Bemporad, A. Garulli, S. Paoletti and A. Vicino, "A bounded-error approach to PWA system identification", IEEE Transactions on Automatic Control, vol.50, no.10, pp. 1567-1580, 2005.

[2] M.S. Claassen, *System Identification for structured nonlinear systems*. PhD Thesis, Department of Mechanical Engineering, University of California at Berkeley, USA, 2001.

RF pulse train generator for a dense frequency grid phase calibration

Liesbeth Gommé and Yves Rolain

Vrije Universiteit Brussel (Dept. ELEC/IW); Pleinlaan 2; B-1050 Brussels (Belgium)
Phone: +32.2.629.28.68; Fax: +32.2.629.28.50; Email: lgomme@vub.ac.be

***Abstract* - The aim of this work is to introduce an RF pulse train generator to provide a reference signal for the phase calibration of the Large Signal Network Analyser (LSNA) under modulated excitation.**

I. Introduction

One of the challenges in modulated measurements of nonlinear devices resides in the calibration of the measurement instrument's phase distortion for narrow band (a few % of the carrier frequency) signals with a large number of tones. Since many telecom applications rely on the use of narrow band modulated signals, it is mandatory to calibrate the phase distortion of the LSNA operating under narrow band modulated excitation. The current state-of-the-art for the calibration of waves composed of a carrier and its harmonics relies on the well-established step recovery diode (SRD [1]) as a reference element that produces a repeatable periodic reference pulse train. The problem is that this method cannot be used for spectra containing lines that do not lie on the harmonic grid (f_0, $2f_0$...) with f_0 the repetition frequency of the pulse train. As a consequence, we are not able to calibrate the spectral lines of a narrow band modulated signal with this method. In this paper, the calibration is achieved by measuring a characterised signal, in analogy to the SRD method. However, the signal is now constructed such that a dense frequency grid is obtained.

II. A Pulse Train as Calibration Signal

In order to perform a signal based phase calibration for a modulated signal we need to construct a test signal that contains a large number of spectral components in a frequency band with a high spectral resolution. We will use a pulse position modulated signal as a broadband periodic signal containing a high density of spectral lines. This signal is composed of a sequence of broadband pulses and is designed to exhibit a very flat amplitude spectrum. The proposed generator combines two distinct technologies: an ultra wide band 50 GHz digital logic gate, [2], and a pseudo-random-bit-sequence (PRBS) generator with a high periodicity and a clock frequency of 100 MHz. This generator is designed in differential Emitter-Coupled-Logic (ECL,[3]), to maximise the analog signal quality. (Jitter<5ps)

The principle of the generator is shown in figure 1. The transitions of the PRBS-signal are used as a trigger signal for generating the pulse. A PRBS-signal is generated by means of a shift register and a XOR-gate in ECL[4]. This sequence is applied to input 1 of the AND gate while input 2 is excited by an inverted and delayed copy of the PRBS-signal. The AND gate detects a high level for a very short duration at both inputs and generates a fast pulse.

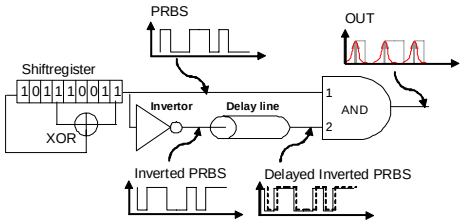

Figure 1 : Fine frequency phase calibration setup

III. Simulation and Initial Measurements

By means of simulations in which the pulse train is constructed starting from a clock signal and a PRBS, we confirm that the generator scheme is able to provide the desired reference signal.

Measurements of the pulse train generated by means of the 50 GHz logic gate when triggered by a square wave instead of the PRBS sequence confirm the simulations and encourage to proceed with incorporating the ECL generator.

IV. Conclusion

This work presents a new calibration signal generator, built using 50 GHz Digital Logic and Emitter Coupled Logic. The theoretical background for the application of the generator scheme is explained and simulations demonstrate the potential of the method. Initial measurements of the digital gate confirm the simulations.

The author is indebted to the Research Foundation Flanders for her research fellowship (FWO-aspirant) and financial support.

References

[1] W. Van Moer, Y. Rolain, A Large-Signal Network Analyzer: Why is it needed? IEEE Microwave Mag.,Vol.7, No.6, pp.46-62, 2006.
[2] Inphi Corporation, http://www.inphi-corp.com
[3] ON Semiconductor, http://www.onsemi.com
[4] J. K. Holmes, Coherent spread spectrum system, John Wiley & Sons, Inc., 1982

Dynamic optimization for minimizing the fuel consumption of a gasoline engine

Bart Saerens, Jeroen Vandersteen, Jan Swevers and Eric Van den Bulck
Katholieke Universiteit Leuven, Mechanical engineering department
Celestijnenlaan 300b, 3001 Heverlee, Belgium
bart.saerens@mech.kuleuven.be

Moritz Diehl
Katholieke Universiteit Leuven, Optimization in engineering center
Kasteelpark Arenberg 10, 3001 Heverlee, Belgium

1 Introduction

Environmental issues, stringent emission norms and rising fuel prices have triggered car manufacturers to develop vehicles that consume less fuel. Several new systems and technologies have been introduced in power trains that have greatly improved the fuel economy. The problem is that the room for technology improvements is constantly shrinking and it is believed that cost-effective solutions will come to an end in a foreseeable future. Apart from technical measures, a high potential to reduce fuel consumption lies in the adaptation of the driving style, especially in speed transients. These accelerations and decelerations frequently occur in city traffic and significantly increase the fuel consumption. Dynamic optimization can be used to calculate optimal control inputs, using a system model, to drive speed transients with minimum fuel consumption.

2 Dynamic system model

The model used for optimization is a mean value phenomenological dynamic model [1]. This model has three subsystems: the gasoline engine, the transmission (gearbox and differential) and the vehicle (longitudinal dynamics). The considered engine is a Toyota 1.6l 3ZZ-FE gasoline engine, which is mounted on a fully equipped test bench. Certain model parameters are determined from a set of steady-state experiments at various engine speeds and throttle valve positions. The transmission and vehicle model parameters are taken from a Toyota Corolla. The complete model has two state variables: the engine speed and the intake manifold pressure, and two control inputs: the throttle valve position and the gearbox ratio.

3 Dynamic optimization

Dynamic optimization uses dynamic system models to minimize an objective function, with multiple constraints taken into account. It is used for several tasks such as parameter estimation, model development, optimal control and trajectory optimization. Stoicescu [2] used dynamic optimization for fuel consumption minimization during vehicle speed transients. The used method, based on Pontriagin's maximum principle, seems to be more of theoretical rather than practical use. The presented paper uses a direct multiple shooting method [3]. This method is easy to use in practical applications and can easily handle constraints.

4 Case study

A case study is presented where the vehicle accelerates from 1100 rpm to 3700 rpm in 30 s in 4th gear. The optimal throttle valve trajectory and according state trajectories are calculated with direct multiple shooting. Both simulations and experimental tests on the test bench show that the optimized trajectories yield minimal fuel consumption. The experiments show that a linear engine speed trajectory yields an extra fuel consumption of 13% when compared to the optimal trajectory. It is shown that, with a simple model, a significant amount of fuel can be saved without loss of drivability and fun to drive.

References

[1] Moskwa J J, Hedrick J K. Modeling and Validation of Automotive Engines for Control Algorithm Development. Transactions of the ASME, Journal of Dynamic Systems, Measurement and Control 1992;114:278-285.

[2] Stoicescu A P. On fuel-optimal velocity control of a motor vehicle. Int. J. of Vehicle Design 1995;16(2/3):229-256.

[3] Leineweber D B, Bauer I, Bock H G, Schlöder J P. An Efficient Multiple Shooting Based Reduced SQP Strategy for Large-Scale Dynamic Process Optimization. Part II: Software Aspects and Application. Computers and Chemical Engineering 2003;27:157-166.

Formulation and Solution of Economic Dynamic Process Optimization

A.E.M. Huesman, O.H. Bosgra and P.M.J. Van den Hof
Delft Center for Systems and Control,
Delft University of Technology,
Mekelweg 2, 2628 CD, Delft, The Netherlands
Email: a.e.m.huesman@tudelft.nl

1 Introduction

In the beginnings of the 1970's the process industry became more interested in economic operation when due to the oil crises energy prices increased drastically overnight. This interest received another incentive in the latter half of the 1990's when competition increased considerably because of globalization. Based on past experience (CO_2-tax, NO_X and SO_X quota etc.) it can be expected that in the future the authorities will promote sustainbility further by economic measures. In more or less the same time frame the process industry has implemented Scheduling & Planning (S&P), Model Predictive Control (MPC) and Real Time Optimization (RTO). These three systems work in a cascaded structure and are considered state-of-the-art for industrial process operation. However as explained by Huesman e.a. [1] this structure does not achieve the best economic operation for two reasons:

1. The presence of restrictions (constraints) that are not strictly necessary. For example the models used in S&P and RTO limit operational improvement to steady state only.
2. The absence of a real economic objective. A good example is MPC that uses a tracking control cost function[1] which implies that economic improvement is achieved in an indirect and therefore incomplete way.

The same paper also points out that the two shortcomings mentioned above have received little attention from the academic community. This research aims to improve the economic performance of processes by *economic dynamic optimization*. The research is limited to a plantwide scope (no site optimization) in an off-line setting (no feedback).

2 Approach and results

The first step is to arrive at *a general formulation* of economic dynamic process optimization. The formulation was tested in two numerical experiments. The first system consists of a Stirred Tank Reactor (STR) and a tank, the second system of a Distillation Column (DC) and a tank. These systems are described in detail in Huesman e.a. [2]. The optimization results can be given a process interpretation; the STR experiment prefers batch operation while the DC experiment shows preference for constant reflux/feed and vapor/feed ratios. Both experiments also show the existence of *multiple solutions*[2]. Multiple solutions are caused by *linearity and/or sparsity* of the economic objective. Multiple solutions imply that there are still degrees of freedom left to optimize process operation further. The best way to deal with multiple solutions is to select a solution from the multiple solution space in a consistent and meaningful way, for example by hierarchical optimization. Hierarchical optimization was applied successfully to the two numerical experiments. It not only resulted in unique solutions but the remaining degrees of freedom were used to optimize other criteria like minimize conversion time and maximize operational smoothness.

3 Outlook

Future research will focus on:

1. Obtaining still a better, read more fundamental, understanding of multiple solutions.
2. Extension of the general framework to account for the existence of multiple solutions.
3. Alternatives for hierarchical optimization to select a solution from the multiple solution space.

References

[1] A.E.M. Huesman, O.H. Bosgra and P.M.J. Van den Hof. Multiple Solutions in Economic Dynamic Process Optimization.17th International Federation on Automatic Control (IFAC) world congress, Korea, 2008 (submitted).

[2] A.E.M. Huesman, O.H. Bosgra and P.M.J. Van den Hof. Degrees of Freedom Analysis of Economic Dynamic Optimal Plantwide Operation. 8th International Symposium on Dynamics and Control of Process Systems (DYCOPS), Mexico, 2007.

[1] $(y-y_r)^T Q(y-y_r)+\Delta u^T R\Delta u$, with y being the outputs, y_r the references, Δu the moves and Q and R weighing matrices.

[2] Also known as non-unique solutions. Multiple solutions *should not be confused* with isolated local optima!

Efficient solution of multiple objective optimal control problems

Peter M.M. Van Erdeghem, Filip Logist, Ilse Y. Smets and Jan F. Van Impe
BioTeC, Department of Chemical Engineering
Katholieke Universiteit Leuven
W. de Croylaan 46, B-3001 Leuven, Belgium
Email: {peter.vanerdeghem, filip.logist, ilse.smets, jan.vanimpe}@cit.kuleuven.be

1 Introduction

In practical optimisation problems often several and conflicting objectives are simultaneously present, e.g., maximising the strength of a construction, while minimising its weight. These *multiple objective optimisation* problems produce most often a set of optimal solutions (or the *Pareto set*) instead of one sole. While research on scalar multiple objective optimisation problems has attracted much attention over the years (see, e.g., [3] for an overview), much less effort is spent on *multiple objective optimal control* problems (i.e., when an infinite dimensional optimal control profile has to be found).

2 Procedure

Recently, [2] have proposed a procedure which allows to derive analytical optimal profiles for an exothermic tubular reactor under steady-state with conflicting conversion and energy objectives. The rationale behind this procedure is to combine (*i*) a *weighted sum* approach (which converts the multiple objective problem into a single objective problem) with (*ii*) an *analytical control parameterisation*. By varying the weights, a representation of the Pareto frontier is obtained.

The procedure involves four steps. First, the set of all possible optimal arcs is derived analytically. Second, approximate piecewise constant optimal controls are computed numerically for a coarse grid of weights. From these approximate solutions the optimal arc sequences are each time identified. Based on the analytical control expressions and the optimal sequences an analytical control parameterisation is built each time. Finally, the switching positions between the different intervals are optimised over a refined weight grid.

However, several points for further improvement have been noticed. First, a uniform distribution of the weights, does not necessarily yield an equal distribution on the Pareto front, and second, the analytical derivations involved, become intractable for large-scale systems. Therefore, (*i*) the weighted sum can be replaced as approach to tackle the multiple objective aspect by, e.g., normal boundary intersection [1], and (*ii*) low-order polynomials can be employed to approximate the analytical relations.

3 Results

To illustrate the general applicability and enhanced efficiency of the modified procedure two cases are studied. The first case involves transferring a car from an initial position to a specified target in minimum time, and with a minimum control effort, while the second case investigates the design of a jacketed tubular plug flow reactor with a fixed length, which operates under steady-state conditions. Inside the reactor an exothermic irreversible first-order reaction takes place. Based on these cases, it has been observed that the adaptations result in an increased efficiency. First due to an equal distribution along the Pareto set an accurate description of the Pareto front is obtained with less points. Second, the use of low-dimensional polynomials instead of the analytical arcs renders the (tedious) analytical relations obsolete, while only inducing a minor increase in cost. Hence, this feature paves the way to addressing larger (and large-scale) systems.

4 Acknowledgements

Work supported in part by Projects OT/03/30 and EF/05/006 (Center-of-Excellence Optimization in Engineering) of the Research Council of the Katholieke Universiteit Leuven, and by the Belgian Program on Interuniversity Poles of Attraction, initiated by the Belgian Federal Science Policy Office. The scientific responsibility is assumed by its authors.

References

[1] I. Das and J.E. Dennis. Normal-Boundary Intersection: A new method for generating the Pareto surface in nonlinear multicriteria optimization problems. *SIAM Journal on Optimization*, 8:631–657, 1998.

[2] F. Logist, P. Van Erdeghem, I.Y. Smets, and J.F. Van Impe. Multiple-objective optimisation of a jacketed tubular reactor. In *Proceedings of the European Control Conference*, pages 963–970, 2007.

[3] R.T. Marler and J.S. Arora. Survey of multi-objective optimization methods for engineering. *Structural and Multidisciplinary Optimization*, 26:369–395, 2004.

Convexity-base homotopy method for the initialization of optimal control problems

Julian Bonilla[1,2], Moritz Diehl[2], Jan Van Impe[1] and Bart De Moor[2]

[1]Department of Chemical Engineering
CIT/BioTec-Katholieke Universiteit Leuven
W. de Croylaan 46,
Leuven-Belgium
Email: julian.bonilla@cit.kuleuven.be

[2]Department of Electrical Engineering
ESAT/SCD-Katholieke Universiteit Leuven
Kasteelpark Arenberg 10, bus 2446,
Leuven-Belgium
Email: moritz.diehl@esat.kuleuven.be

1 Introduction

Methods to solve nonconvex *Optimal Control Problems* (OCP) are of particular interest in the control community since convexity disappears in all nonlinear optimal control application. One of the issues in solving these kind of problems is that they exhibit local minima and derivative based optimization techniques can easily lock on to a local solution depending on the initialization of the optimization problem. The classical global optimization approaches to deal with non-convex OCPs are based on techniques which relax the problem [1]. However, mathematicians and practitioners have recently realized that some of these problems can be reformulated such that the new formulation exhibits convexity [2]. The advantages of using convex formulations lie not only in the fact that local solutions are global, but in that they present polynomial-time convergence, and efficient and reliable methods, such as *Interior Points* are well developed for such convex problems.

This work addresses the task of solving non-convex OCPs employing the model structure. We have noticed that for problems involving input-affine models, it is possible to improve the convergence to global optima by solving first a related convex OCP connected by a homotopy path with the original non-convex OCP.

2 Convexity-based Homotopy Method

Consider finite-time non-convex OCP with optimization variables $x(t)$ and $u(t)$ corresponding to the states and inputs respectively

$$\min_{x(.),u(.)} \int_0^T \left(\|x(t)-x^{\text{ref}}(t)\|_Q^2 + \|u(t)-u^{\text{ref}}(t)\|_R^2 \right) dt \quad (1)$$

subject to

$$\begin{aligned} \dot{x}(t) &= f(x,t)+g(x,t)u(t), \quad t\in[0,T], && (2)\\ x(0) &= x_0, && (3)\\ x(t) &\in \mathbb{X}(t), \quad t\in[0,T], && (4)\\ u(t) &\in \mathbb{U}(x(t),t), \quad t\in[0,T]. && (5) \end{aligned}$$

Let us now introduce a pseudo control $v(t)$ and a scalar parameter $\lambda \in (0,1)$ that interpolates between the original problem ($\lambda \to 1$) and one of its possible homotopies ($\lambda \to 0$), as follows:

$$\begin{aligned} P(\lambda): \min_{v_0,v(\cdot),x(\cdot),u(\cdot)} & \frac{1}{\lambda}\int_0^T \| x(t)-x^{\text{ref}}(t) \|_Q^2 \; dt \\ & + \int_0^T \|u(t)-u^{\text{ref}}(t)\|_R^2 dt \\ & + \frac{1}{(1-\lambda)}\left(\int_0^T \| v(t) \| \; dt + \| v_0 \| \right) \end{aligned} \quad (6)$$

subject to

$$\begin{aligned} \dot{x}(t) &= f(x,t)+g(x,t)u(t)+v(t),\ t\in[0,T], && (7)\\ x(0) &= x_0+v_0, && (8)\\ x(t) &\in \mathbb{X}(t), \quad t\in[0,T], && (9)\\ u(t) &\in \mathbb{U}(x(t),t), \quad t\in[0,T]. && (10) \end{aligned}$$

Lemma 1. Assuming $x^{\text{ref}}(t)\in\mathbb{X}(t)$, $\mathbb{U}(x^{\text{ref}}(t),t)$ convex for all $t\in[0,T]$ and Q positive definite, if $\lambda\to 0$, the above parametric optimization problem $P(\lambda)$, (6)-(10), is equivalent to a convex optimization problem. If $\lambda\to 1$ its solution approaches the solution of the original problem (1)-(5).

In this context, it is possible to solve a non-convex OCP with the given structure by convexifying it through the formulation in (6)-(10) with $\lambda\to 0$. The solution of the convex problem used to initialize successive OCPs on the homotopy path by moving λ towards 1 in order to recover the original OCP.

References

[1] McCormick G. Computability of global solutions to factorable nonconvex programs: part I - convex underestimating problems. *Mathematical Programming* 1976; **10**(1976):147-175.

[2] Boyd S, Crusius C, and Hansson A. Control applications of nonlinear convex programming. *Journal of Process Control* 1998; **8**(5-6):313-324.

The smoothed spectral abscissa for robust controller design

Joris Vanbiervliet, Bart Vandereycken, Wim Michiels, Stefan Vandewalle and Moritz Diehl
Katholieke Universiteit Leuven,
Department of Computer Science,
Celestijnenlaan 200A, 3001 Leuven, Belgium.
{firstname.lastname}@cs.kuleuven.be

1 Introduction

Stability optimization of linear and nonlinear continuous-time dynamic systems is both a highly relevant and a difficult task. The optimization parameters often stem from a feedback controller, which can be used to optimize either a performance criterion or the asymptotic stability around a certain steady state. When also robustness against perturbations of the system must be taken into account, the resulting optimization problem becomes even more challenging.

Assuming an adequate parameterization of the desired feedback controller is available, the problem of finding a suitable steady state along with a stabilizing feedback controller can essentially be transformed into a nonlinear programming problem. By collecting all optimization variables in a vector x, we can summarize the described stability optimization problem as

$$\min_x \ \Phi_{\textbf{stab}}(A(x)), \quad \text{s.t.} \quad g(x) = 0,\, h(x) \leq 0,$$

where $A(x)$ is the system matrix depending smoothly on x and the function $\Phi_{\textbf{stab}}(\cdot)$ shall express our desire to optimize stability, under the given constraints. In the field of linear output feedback control, the closed-loop system matrix $A(x)$ will typically be of the form $A+BKC$, with A the open-loop system matrix, B and C the input and output matrices, and K containing the controller parameters x to be optimized.

2 Spectral abscissa minimisation

The most straightforward choice for the objective function $\Phi_{\textbf{stab}}$ is related to the eigenvalues of A, namely the spectral abscissa $\alpha(A)$. This value is defined as the real part of the rightmost eigenvalue of the spectrum $\Lambda(A) = \{z \in \mathbb{C} \,|\, \det(zI-A) = 0\}$, that is, $\alpha(A) := \sup\{\Re(z) \,|\, z \in \Lambda(A)\}$. However, it is well known that the minimization of the spectral abscissa function $\alpha(A)$ gives rise to very difficult optimization problems, since $\alpha(A)$ is not everywhere differentiable, and even not everywhere Lipschitz. Moreover, the spectral abscissa is also known to perform quite poorly in terms of robustness against parameter uncertainties. A tiny perturbation or disturbance to a parameter of a system that was optimized in the spectral abscissa can possibly lead to instability.

3 The smoothed spectral abscissa

We therefore propose a new stability measure, namely the *smoothed spectral abscissa* $\alpha_\varepsilon(A)$, which is based on the inversion of a relaxed H_2-type cost function. It alleviates the problem of nonsmoothness, and has at the same time certain beneficial robustness properties. A regularization parameter ε allows to tune the degree of smoothness. For ε approaching zero, the smoothed spectral abscissa $\alpha_\varepsilon(A)$ converges towards the nonsmooth spectral abscissa from above, so that $\alpha_\varepsilon(A) \leq 0$ guarantees asymptotic stability. Evaluation of the smoothed spectral abscissa and its derivatives w.r.t. the matrix parameters can be performed – by using an adjoint differentiation technique – at the cost of solving only a single primal-dual Lyapunov equation pair

$$\begin{aligned} 0 &= (A-sI)P + P(A-sI)^{\mathrm{T}} + UU^{\mathrm{T}}, \\ 0 &= (A-sI)^{\mathrm{T}}Q + Q(A-sI) + V^{\mathrm{T}}V. \end{aligned}$$

for s. This allows for an efficient integration into a derivative based optimization framework.

4 Optimization formulations

Two optimization problems are considered. A first variant is to simply choose a fixed $\varepsilon > 0$ and then solve

$$\min_x \ \alpha_\varepsilon(A(x)), \quad \text{s.t.} \quad g(x) = 0,\, h(x) \leq 0.$$

Should this problem not result in a negative optimum for the chosen ε, then one can try again with a smaller ε.

As the choice for ε of α_ε is somewhat arbitrary, we might alternatively search for the largest ε so that the stability certificate $\alpha_\varepsilon(A) \leq 0$ still holds. Because $\alpha_\varepsilon(A)$ becomes smoother with increasing values for $\varepsilon > 0$, we can expect a larger ε to yield a more robust optimal controller. This translates into the following optimization problem

$$\max_{x,\varepsilon} \ \varepsilon \quad \text{s.t.} \quad \alpha_\varepsilon(A(x)) \leq 0 \ \text{ and } \ g(x) = 0,\, h(x) \leq 0.$$

Note that this second problem can be shown to be equivalent to minimizing the H_2-norm of the systems transfer function over all feasible parameters x.

In both cases additional equality and inequality constraints on the variables can be naturally taken into account in the optimization problem.

Non-parametric Optimal Control Synthesis

Arjen den Hamer[1] a.j.d.hamer@tue.nl
Siep Weiland[1] s.weiland@tue.nl
Maarten Steinbuch[1] m.steinbuch@tue.nl
Georgo Angelis[2] georgo.angelis@philips.com

[1] Technische Universiteit Eindhoven
[2] Philips Applied Technologies

1 Introduction

Identification of plant behavior is crucial in control synthesis for practical systems. Non-parametric frequency response identification offers a relative easy and accurate identification method for LTI systems. However, optimal control synthesis requires an additional parametrization step to be performed. For high order systems, this parametrization imposes a trade-off between fit-error and closed-loop performance which is not straightforward to make since this relation is not directly visible during parametrization and therefore requires an iterative approach.

In this work, it is investigated if controller synthesis can be performed directly on experimental data. As a result, parametrization is applied on the controller instead of plant with full knowledge of the closed-loop behavior such that iterative approaches can be omitted.

2 Objective

The SISO mixed sensitivity problem is chosen to explore and develop a framework for non-parametric optimal control synthesis. The objective can be states as: develop a non-parametric approach, e.g. FRF based, to solve the standard mixed-sensitivity problem:

$$\min_{\mathcal{C}} | \, [W_1 S, \, W_2 R]^T \, |_{2/\infty} \qquad (1)$$

where $\mathcal{C}$ represents the set of stabilizing (non-parametric) controllers.

Non-parametric stability

The Youla-Kucera parametrization [1] is introduced to on the one hand map $\mathcal{C}$ onto $\mathcal{RH}_\infty$ to enable a stability constraint of the closed-loop system. One the other, this parametrization convexifies the optimization problem. The resulting matching problem equals:

$$\min_{Q \in \mathcal{RH}_\infty} |T_1 - T_2 Q|_{2/\infty}$$

To enable synthesis, a non-parametric sufficient condition for $Q \in \mathcal{RH}_\infty$ is derived from [2]:

$$\oint_\gamma Q(s) \, ds = 2\pi j \sum_{a \in \mathcal{A}} Res_{z=a_i}(Q(s))$$

where γ represents the contour that encloses the right-half s-plane and $\mathcal{A}$ contains the poles in γ. For the continuous time case, this results in the following condition for stability:

$$Im(H(j\omega_0)) = \frac{1}{2\pi} \int_{-\infty}^{\infty} \frac{Re(H(j\omega))}{(\omega - \omega_0)} d\omega \qquad (2)$$

Synthesis

A discrete approximation of (2) is used to enable non-parametric control synthesis. The resulting approximation of problem (1) is given by:

$$\begin{aligned} &\min_{Q(\omega_i) \in \mathbb{C}} |T_1(\omega_i) - T_2(\omega_i) Q(\omega_i)|_2 \\ &s.t. : \quad |T_1(\omega_i) - T_2(\omega_i) Q(\omega_i)|_\infty \leq \gamma \\ &\qquad Im(Q(\omega_i)) = \frac{1}{2\pi} \sum_{j=1}^{n} \frac{Re(Q(\omega_j))}{(\omega_j - \omega_i)} (\omega_{j+1} - \omega_j) \end{aligned}$$

Results

A comparison with a solution based on a parametric model is given below.

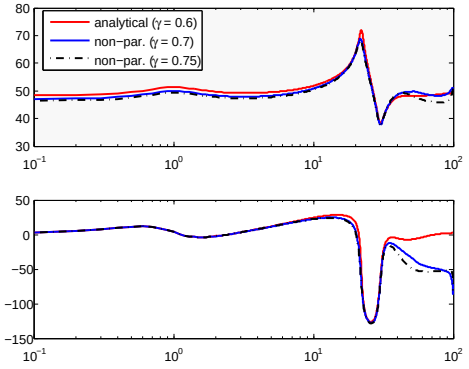

Deviations in the high-frequent region are mainly caused by truncation errors of the integral in (2). It is expected that synthesis in the discrete domain will eliminate this effect.

References

[1] B.A. Francis. *A course in H_∞ Control Theory.* Springer-Verlag, 1987.

[2] T.W. Gamelin. *Complex Analysis.* Springer, 2001.

Fault Tolerant Control: A Data-Driven Approach

Jianfei Dong
Delft Center for Systems and Control
Delft University of Technology
2628 CD Delft
The Netherlands
Email: j.dong@tudelft.nl

Michel Verhaegen
Delft Center for Systems and Control
Delft University of Technology
2628 CD Delft
The Netherlands
Email: m.verhaegen@moesp.org

1 Introduction

Faults cause not only production downtime, but also risk human life in a safety-critical system, such as an automobile and an aeroplane. Fault detection and controller reconfiguration, known as fault tolerant control (FTC), are therefore important to improve safety in such systems. The objective of our research is to develop an active FTC scheme, which adapts to changing conditions by recursively identifying the Markov parameters of a system and tuning the optimal $\mathscr{H}_2$ control gain. In this abstract, we review our current work on linking closed-loop subspace identification and the $\mathscr{H}_2$ optimal control and its recursive solution, which leads to a data-driven FTC approach.

2 Problem Statement

Conventional model-based $\mathscr{H}_2$ control relies on system models either built from physical principles or identified. The subspace predictive control (SPC) approaches as recently seen in [2, 4, 5, 7], circumvents the modeling step, and directly seeks the predictors of future outputs from data. [4] and [7] focuses on open-loop data; while [2] and [5] extend the applicability of the SPC to closed loops. The closed-loop SPC algorithm in [2] is constructed upon the VARX (vector autoregressive with exogenous inputs) algorithm, [1]. The advantage of the VARX-based approach over that proposed in [5] is shown in the sense that the new approach excludes the need of any information about the controller in the loop; while [5], based on the closed-loop identification algorithm of [6], leads to a biased predictor when the controller is not LTI.

The VARX algorithm results in unbiased estimates when infinite number of I/O samples are available, [1]. However, when only finite data length is allowed in online application, this is not true any more. The estimates are then subject to a norm-bounded bias due to the ignorance of the initial states, and a stochastic noise due to the noisy I/O samples. A cautious design of $\mathscr{H}_2$ optimal control is proposed in [3] against these deterministic and stochastic model uncertainties.

The recursive solution to the closed-loop SPC is proposed in [2], which provides an adaptive way to control a time varying system or a system subject to faults. The application of this approach to a steer-by-wire actuator has demonstrated its effectiveness.

3 Future Work

The future research shall be focused on the stability guarantee of the closed-loop SPC algorithms and handling constraints. Fast online algorithms shall be developed for both the unconstrained and constrained formulations.

Acknowledgement

The authors would like to thank the research grant of the AI4IA project (Contract No. 514510) of the European Marie Curie FP6 Research Training Programme and *SKF ERC* in the Netherlands.

References

[1] A. Chiuso. “The role of Vector AutoRegressive modeling in Predictor Based Subspace Identification”. Automatica, 118, 57 - 291, 2007.

[2] J. Dong, M. Verhaegen, and Edward Holweg. “Closed-loop Subspace Predictive Control for Fault Tolerant MPC Design”. Accepted for publication in 17th IFAC World Congress. 2007.

[3] J. Dong and M. Verhaegen. “Cautious H2 optimal control using uncertain markov parameters identified in closed loop”. Submitted for publication, Jan. 2008.

[4] W. Favoreel, B. de Moor, M. Gevers, and P. van Overschee (1998). “Model-free subspace-based LQG-design”. Tech. Rep. ESAT-SISTA/TR 1998-34, KU Leuven, Leuven, Belgium.

[5] W. Favoreel, B. de Moor, M. Gevers, and P. van Overschee (1999). “Closed-loop model-free subspace-based LQG-design”. in the Proceedings of the 7th Mediterranean Conference on Control and Automation, Haifa, Israel, 1999.

[6] P. van Overschee and B. de Moor. “Closed-loop subspace identification”. Tech. Rep. ESAT-SISTA/TR 1996-52I, KU Leuven, Leuven, Belgium, 1996.

[7] B.R. Woodley. “Model free subspace based $\mathscr{H}_\infty$ control”. PhD Dissertation, Stanford University, 2001.

The use of inverse modelling in ILC methods

Anne Van Mulders, Jan Swevers and Johan Schoukens
Vrije Universiteit Brussel, dep. ELEC, Pleinlaan 2, 1050 Brussel, BELGIUM
email: anne.van.mulders@vub.ac.be

I. Iterative Learning Control

Iterative Learning Control (ILC) is a control method that iteratively improves the performance of a system. It can be used for systems that execute the same task several times (under the same operating conditions and with the same initial conditions), such as a robot arm that performs the same part of a fabrication process over and over again. By using information from previous iterations, the control input is modified in order to get a better approximation of the desired trajectory.

A widely used ILC learning algorithm [1] is

$$u_{j+1}(k) = Q(q)\big(u_j(k) + L(q)e_j(k+1)\big)$$

where $u_j(k)$ denotes the control input with time index k and iteration index j.

$e_j(k) = y_d(k) - y_j(k)$ is the performance or error signal, which describes the difference between the desired and the measured output. $Q(q)$ and $L(q)$ are the Q-filter and learning function, respectively. Both are a function of the forward time-shift operator q: $qx(k) \equiv x(k+1)$.

Basic idea

Using this iterative method, the input that corresponds to a desired output can be determined if the method converges.

Consider a linear system $y(k) = P\,u(k)$.

If $Q(q)$ is an identity matrix and $L(q) = q^{-1}P^{-1}(q)$, then

$$u_{j+1}(k) = u_j(k) + L(q)e_j(k+1)$$

can be transformed

$$\begin{aligned} u_{j+1}(k) &= u_j(k) + L(q)\big(y_d(k+1) - y_j(k+1)\big) \\ &= \big(I - L(q)P(q)q\big)u_j(k) + L(q)y_d(k+1) \end{aligned}$$

and becomes $u_{j+1}(k) = u_d(k)$.

This is the ideal case, where convergence is reached in one step.

Application to nonlinear systems

If the inverse model of a nonlinear system would be available, the method could also be successfully applied to the nonlinear system. That's why identification of the inverse model should be given due attention. That is the aim of this work.

II. Calculating the inverse model

Classic approach: A nonlinear model $y = \hat{P}(u)$ is used to calculate $\hat{u}_d$ from a measured y_d by solving $y_d = \hat{P}(u_d)$.

One possibility is to use $\hat{P}$ to iteratively determine $\hat{u}_d$ by minimizing $y_d - \hat{P}(u)$. Another option is to identify directly the inverse model $u = \hat{P}_{inv}(y)$. Although this looks simple and attractive, some problems should be studied in more detail, such as bias and stability.

1) Bias errors can occur when noise is present on the input of the inverse system (i.e. the output of the system). On the other hand, this noise is also present when a new input is calculated from a measured output. A first study of this problem will be made.

2) Another difficulty is the possible **instability** of the inverse model (and/or system) in the case of non-minimum phase systems.

We will try to work in the frequency domain, because there, the calculation of the inverse of an unstable linear system can be done without any problems: the dynamic relations are reduced to algebraic relations between the spectra of the input and output. This approach should be extended to nonlinear systems. An alternative is to split up the transfer function into a minimum phase and a maximum phase part and to apply causal filtering and anti-causal filtering on resp. the minimum phase and maximum phase part.

3) Nonlinear modelling is difficult. Therefore, we will only apply it where it's necessary. The idea is to identify a global linear model and to use local nonlinear models where the linear model is insufficient.

III. PNLSS Models

In this work we will use Polynomial Nonlinear State Space Models to describe (approximately) the nonlinear systems. The expressions of the PNLSS models are simply an extension of the linear state- and output equations, as can be seen below [2]:

$$\begin{aligned} \bar{x}(k+1) &= A\bar{x}(k) + B\bar{u}(k) + E\bar{\zeta}(k) \\ \bar{y}(k) &= C\bar{x}(k) + D\bar{u}(k) + F\bar{\eta}(k) \end{aligned}$$

$\bar{\eta}(k)$ and $\bar{\zeta}(k)$ contain monomials in $\bar{x}(k)$ and $\bar{u}(k)$. The matrices E and F contain the coefficients associated with these monomials.

The previously discussed methods should be generalised to be applicable on this nonlinear structure.

IV. References

[1] D. A. Bristow, M. Tharayil, A. G. Alleyne. *A Survey of Iterative Learning Control A learning-based method for high-performance tracking control*. IEEE control systems magazine, vol. 26, pp. 96-114, June 2006.

[2] J. Paduart. *Identification of Nonlinear Systems using Nonlinear Polynomial State Space Models*. PhD Thesis, Vrije Universiteit Brussel, 2007.

[3] O. Markusson. *Model and System Inversion with Applications in Nonlinear System Identification and Control.* PhD Thesis, Royal Institute of Technology, Stockholm, Sweden, 2002

A Hybrid Steepest Descent Method for Constrained Convex Optimization

Mathieu Gerard*, Michel Verhaegen, Bart De Schutter
Delft Center for Systems and Control
Mekelweg, 2 2628 CD Delft The Netherlands
*Email: m.p.gerard@tudelft.nl

1 Introduction

Optimization problems play a role of increasing importance in many engineering domains, and especially in control theory. One specific type of problem is when a vector variable x should be adapted on-line to decrease over time a desired cost function. Moreover, it would be desirable in many applications to constrain x at all time in a given set called feasible set. This research focuses on the development of a new technique applicable to such problems featuring any convex cost function and convex feasible set.

2 The hybrid steepest descent solution

The idea is to construct a dynamical system of the form

$$\dot{x}(t) = f(x(t)) \tag{1}$$

such that its asymptotically stable equilibrium points are the optimal points of the convex optimization problem

$$\begin{aligned} \min_{x} \quad & q(x) \\ \text{subject to} \quad & g(x) \leq 0 \end{aligned} \tag{2}$$

In case the optimization problem (2) changes over time, the dynamical system (1) will also end up being time-varying and the trajectory will then track the optimal points.

The proposed feedback law satisfying the objectives is:

$$f(x) = \begin{cases} -\nabla q(x) & \text{if } g_j(x) \leq 0 \ \ \forall j \\ -\sum_{i \in L(x)} \nabla g_i(x) & \text{if } \exists j : \ g_j(x) > 0 \end{cases} \tag{3}$$

with $L(x) = \{l : g_l(x) \geq 0\}$. The interpretation is that the system follows the steepest descent direction for the objective function in the feasible set and for the constraints in the infeasible set.

Since the dynamical equation (1) has a discontinuous right-hand side, the Filippov solution concept [4] is used to analyze the trajectory and identify possible sliding modes along the boundary of the feasible set. Further the Karush-Kuhn-Tucker conditions [3] are used to prove the optimality of the stationary points of (1). Finally the non-smooth Lyapunov function

$$V(x) = \max(q(x), q^*) - q^* + \beta \sum_{i=1}^{m} \max(g_i(x), 0) \tag{4}$$

is used to show the asymptotic stability [5].

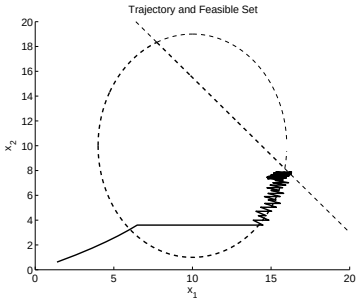

Figure 1: The plain line is the trajectory of the dynamical system constructed for the cost function $q = -x_1$ and the dashed-bold feasible set.

3 Discretization, simulation example and application

Discretization for simulation is done using Euler's method. Then a sliding mode with infinitely fast switching becomes impossible and the trajectory meanders around the sliding surface before oscillating around the equilibrium. However, the global behaviour is maintained.

In the simulation example shown in Figure 1, the trajectory starts near the origin and first converges to the feasible set. Then it moves along the opposite gradient of the cost function before "sliding" along the quadratic constraint toward the optimal point.

This method is suitable for example for control allocation and model predictive control [2] with implementation on embedded hardware. This is thanks to its simplicity, its low computational cost and its simple steps for which most of the computations can be done in parallel.

References

[1] M. Gerard, M. Verhaegen, B. De Schutter. A Hybrid Steepest Descent Method for Constrained Convex Optimization. Submitted for publication. 2008.

[2] M. Gerard, M. Verhaegen. Model Predictive Control using Hybrid Feedback. Proceedings of IFAC World Congress, Seoul, Korea. 2008.

[3] S. Boyd, L. Vandenberghe. Convex Optimization. Cambridge University Press. 2004.

[4] A.F. Filippov. Differential Equations with Discontinuous Right-hand Side. Kluwer Academic Publishers, The Netherlands. 1988.

[5] D. Shevitz, B. Paden. Lyapunov Stability of Nonsmooth Systems. IEEE Transactions on Automatic Control, Vol 39, No 9, pg 1910-1914. September 1994.

Identification of Wiener-Hammerstein systems by means of Support Vector Machines for Regression

A. Marconato(*), D. Petri(*), J. Schoukens(**)
(*)DISI - University of Trento, Italy - anna.marconato@disi.unitn.it
(**)ELEC - Vrije Universiteit Brussel, Belgium

1 Abstract

In this work we propose the use of Support Vector Machines for Regression for the identification of Wiener-Hammerstein systems. The proposed methodology not only leads to the definition of an alternative tool for system identification, but gives also a better insight on the behaviour of the Support Vector Machines approach.

2 Introduction

A Wiener-Hammerstein system can be described, in general terms, as the cascade of a first linear dynamic system, a static nonlinear block, and a second linear dynamic system, as depicted in Fig.1.

Figure 1: General scheme of a Wiener-Hammerstein system.

Examples of standard approaches for the identification of Wiener-Hammerstein systems can be found in [1]. Here we address the problem of identifying such systems by employing a well-known learning–from–examples algorithm, namely the Support Vector Machines for Regression (SVR) [2]. A nice property of this approach is given by the fact that no *a priori* knowledge on the system is required, instead a general rule which models the system is inferred by using only a set of Input/Output measures. As a preliminary step, we simulate the output signal as a function of the input values only, while in the final version of the work we will also estimate y by taking into account both input and previously simulated output values. The obtained results will be compared with the ones given by the Best Linear Approximation (BLA) [3], and nonlinear polynomial state space models [1].

3 Methodology and preliminary results

Methodology: The idea of an SVR-based identification approach is to build an estimating function $\hat{y}$ of the output signal, on the basis of a set of Input/Output data

$$Z = \{(\boldsymbol{u}_i, y_i)\}_{i=1}^{M}$$

Here y_i is the current output value, and $\boldsymbol{u}_i$ is a vector of length d that contains the current input value $u(n)$ and previous input samples $u(n-1), \cdots, u(n-d+1)$, the number of which can be chosen by looking at the impulse response of the system. Then, by solving a constrained quadratic optimization problem, the following estimation function is obtained:

$$\hat{y} = \hat{f}\left(\boldsymbol{u}, \boldsymbol{a}, b\right) = \sum_{i \in SV} a_i \cdot k\left(\boldsymbol{u}_i, \boldsymbol{u}\right) + b$$

where $k\left(\cdot,\cdot\right)$ represents a suitable kernel function, and SV is the set of indices of the only contributing samples, the Support Vectors (see [2] for the details).

Preliminary results: We have applied this methodology to several examples of Wiener-Hammerstein systems, considering both a Random Phase Multisine and Gaussian noise as excitations signals [3]. A first comment that can be made about the obtained results is the fact that the SVR behaviour seems to be quite sensitive to the nature of the input signal. The SVR fails completely to reproduce the linear dynamics G_1, G_2 in those frequency bands that were not excited during the training. So the excitation used during the model selection phase needs to be designed carefully. However, in all the considered examples, we noticed that the SVR approach outperformed, in terms of simulation error, the BLA estimate.

4 Conclusions

We have shown that SVR can be employed as an interesting tool for the identification of Wiener-Hammerstein systems, although care should be taken in the choice of the excitation signals, in order to fully exploit the potential of the approach. In the final presentation the results will also be compared with those of [1].

References

[1] J. Paduart, Identification of nonlinear systems using nonlinear polynomial state space models, PhD Thesis (submitted in December 2007).

[2] V. Vapnik, Statistical Learning Theory, Wiley, 1998.

[3] R. Pintelon and J. Schoukens, System Identification: a Frequency Domain Approach, IEEE Press, 2001.

Neural network global optimization using interval analysis

E. de Weerdt, Q.P. Chu, J.A. Mulder
Kluyverweg 1, 2629 HS Delft
E.deWeerdt@TUDelft.nl, Q.P.Chu@TUDelft.nl, J.A.Mulder@TUDelft.nl

1 Abstract

Currently there is only one method available which can guarantee to find the global optimal structure and weight of a network for a input-output data set: Interval Analysis. Interval analysis is a truly global optimization method which uses interval arithmetic instead of crisp arithmetic. There have been several succesful attempts to optimize feedforward neural networks. The only drawback however is that the computational load can be significant for large network sizes. We propose to use spline type activation function to reduce the computational load.

2 Neural network optimizaton

When using neural networks one typically encounters difficulties in the field of weight optimization and structure optimization. How does one determine which structure is the optimal one in the sense of minimizing the number of neurons while keeping the approximation errors below a certain desired value? And, once the optimial structure is determined, how do you obtain the optimal values for the weights? The optimal structure is most commonly defined by Monte Carlo simulations or is simply fixed before learning. There is therefore no absolute guarantee that the defined structure is the optimal one. Once the structure of a network is designed one typically uses a gradient based learning algorithm which is easy to implement and fast. It does however not give a guarantee that the optimial values are obtained, i.e. the learning algorithm could get stuck in a local minimum. A few researcher have used interval analysis [1, 2] to solve both problems simultaneously [3]. Due to the nature of interval analysis one can present theoretical proof which states that the described methods are guaranteed to find the global optimal structure and weights. The only drawback, however, is that the computational load can be significant for larger networks. This fact is due to the nature of interval analysis in combination with the choice of activation functions. The commonly used tangent sigmoidal function and radial basis function are highly bounded nonlinear function which makes them so perfect for neural networks. However, taking the derivatives with respect to the adaptable parameters leads to more occurences of the adaptable parameters which significantly increases the so-called dependency effect which is inherently coupled to interval analysis. We propose to use spline like activation function for which we encounter less problems. The optimization of the network with these activation function therefore requires less computational load and makes the algorithm more applicable in real life.

3 Interval analysis

Interval Analysis uses interval arithmetic to obtain guaranteed bounds on the function output of any function, i.e. $f(x) \in F(X) \forall x \in X$ where $f(x)$ is the function output $F(X)$ is the function output interval obtained by evaluating the function with the interval X instead of the crisp values x. An interval parameter X is defined as the set of number between a lower bound a and an upper bound b: $x \in X = [a,b] \rightarrow a \leq x \leq b$. By using simple rules such as:

Addition

$$X + Y = [a+c, b+d] \tag{1}$$

Substraction

$$X - Y = [a-d, b-c] \tag{2}$$

Multiplication

$$X \times Y = [\min(ac,ad,bc,bd), \max(ac,ad,bc,bd)] \tag{3}$$

Division

Excluding division by an interval Y containing 0

$$\frac{X}{Y} = X \times \left(\frac{1}{Y}\right) \text{ with } \frac{1}{Y} = \left[\frac{1}{d}, \frac{1}{c}\right] \tag{4}$$

one can easily obtain guaranteed upper and lower bounds on any function $f(x)$.

References

[1] R.E. Moore *Interval Analysis*, vol. 1, Prentice-Hall, Inc., 1988.

[2] E. Hanson AND G.W. Walster *Global Optimixation Using Interval Analysis*, Marcel Dekker, Inc. and Sun Microsystems, Inc., 2nd Edition, 2004.

[3] M. Jamett AND G. Acua "An Interval Approach for Weights Initialization of Feedforward Neural Networks" in *MICAI 2006: Advances in Artificial Intelligence*, pp. 400–402. Springer Berlin / Heidelberg, ISSN 302-9743 (Print) 1611-3349 (Online), Volume 4293/2006

Part 3

Plenary Lectures

Self-optimizing control: Simple implementation of optimal operation

Sigurd Skogestad

Department of Chemical Engineering
Norwegian University of Science and Tecnology (NTNU)
Trondheim, Norway

Benelux control meeting, March 2008

PART 1

1

Outline

- Control structure design
  - Hierarchical time-scale decomposition
  - Procedure control structure design
- Implementation of optimal operation
  - Centralized or hierarchical?
- **What should we control?**
  - Control of active constraints. Back-off
  - Control of unconstrained variables
    - **Looking for magic "self-optimizing" variables**
    - Maximum gain rule
- Examples

2

How we design a control system for a complex plant?

- How do we deal with complexity?
- Where do we start?
- What should we control? and why?
- etc.
- etc.

5

Control structure design

- *Not* the tuning and behavior of each control loop,
- But rather the *control philosophy* of the overall plant with emphasis on the ***structural decisions***:
  - *Selection of controlled variables ("outputs")*
  - *Selection of manipulated variables ("inputs")*
  - *Selection of (extra) measurements*
  - *Selection of control* ***configuration*** (structure of overall controller that interconnects the controlled, manipulated and measured variables)
  - *Selection of controller type* (LQG, H-infinity, PID, decoupler, MPC etc.).

7

S. Skogestad, ``Control structure design for complete chemical plants'', Computers and Chemical Engineering, Vol. 28, 219-234 (2004)

Main objectives control system

1. Stabilization
2. Implementation of acceptable (near-optimal) operation

ARE THESE OBJECTIVES CONFLICTING?

- Usually NOT
  - Different time scales
    - Stabilization fast time scale
  - Stabilization doesn't "use up" any degrees of freedom
    - Reference value (setpoint) available for layer above
    - But it "uses up" part of the time window (frequency range)

11

Dealing with complexity

Main simplification: Hierarchical decomposition

Process control

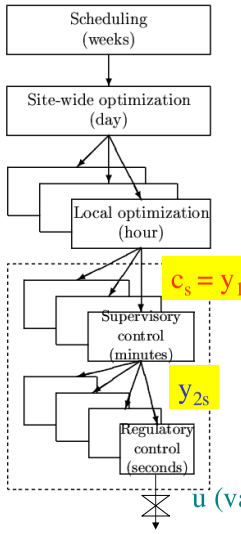

RTO

MPC

PID

The controlled variables (CVs) interconnect the layers

OBJECTIVE

Min J (economics); MV=y_{1s}

$c_s = y_{1s}$

Follow path CV=y_1; MV=y_{2s}

y_{2s}

Stabilize + avoid drift CV=y_2; MV=u

u (valves)

12

Hierarchical decomposition

Example: Bicycle riding

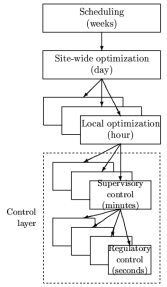

Note: design starts from the bottom

- *Regulatory control*:
  - First need to learn to stabilize the bicycle
    - CV = y_2 = tilt of bike
    - MV = body position

- *Supervisory control*:
  - Then need to follow the road.
    - CV = y_1 = distance from right hand side
    - MV=y_{2s}
  - Usually a constant setpoint policy is OK, e.g. y_{1s}=0.5 m

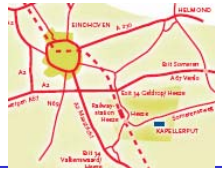

- *Optimization*:
  - Which road should you follow?
  - Temporary (discrete) changes in y_{1s}

13

Stepwise procedure control structure design

I. TOP-DOWN

Step 1. DEGREES OF FREEDOM
Step 2. OPERATIONAL OBJECTIVES (ECONOMICS)
Step 3. OPTIMAL OPERATION (optimal path)
Step 4. IMPLEMENTATION OF OPTIMAL OPERATION (Stay on optimal path):
- What to control ? (primary CV's c=y_1)

II. BOTTOM-UP (structure control system):

Step 5. REGULATORY CONTROL LAYER (PID)
- "Stabilization"
- *What more to control*? (secondary CV's y_2)

Step 6. SUPERVISORY CONTROL LAYER (MPC)
- *Decentralization?*

Step 7. OPTIMIZATION LAYER (RTO)
- *Can we do without it?*

S. Skogestad, ``Control structure design for complete chemical plants'', Computers and Chemical Engineering, Vol. 28, 219-234 (2004)

17

Step 4. Implementation of optimal operation

OUTLINE

- Centralized or hierarchical?
- **What should we control** (c)?
  1. Control active constraints
     - Possible back-off
  2. Remaining unconstrained: Self-optimizing control
     - Maximum gain rule
     - Examples

18

Implementation of optimal operation

- Consider static optimization problem.

$$\min_u \; J(u,x,d)$$

subject to:

Model equations: $f(u,x,d) = 0$

Operational constraints: $g(u,x,d) < 0$

$\rightarrow u_{opt}(d^*)$

Problem:

Usually cannot use open-loop policy (u_{opt} constant or on given trajectory) because *disturbances d* change

How should we adjust the degrees of freedom (u)?

19

Implementation of optimal operation (Cannot keep u_{0opt} constant)

"Obvious" solution: Centralized optimizing control

Estimate d from measurements and recompute $u_{opt}(d)$

Problem: Too complicated (requires detailed model *and* description of uncertainty)

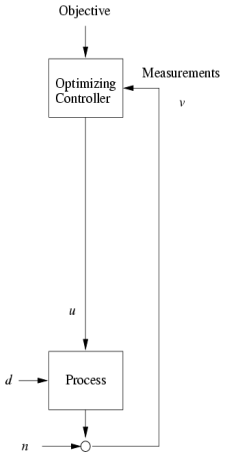

20

In practice: Hierarchical decomposition with separate layers

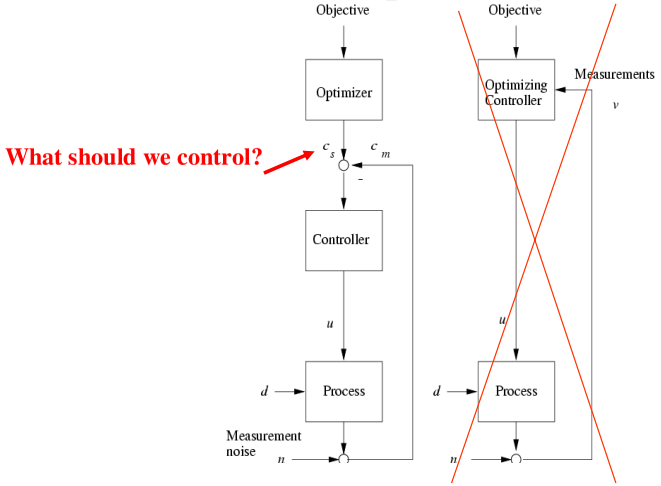

21

Self-optimizing control: When constant setpoints is OK

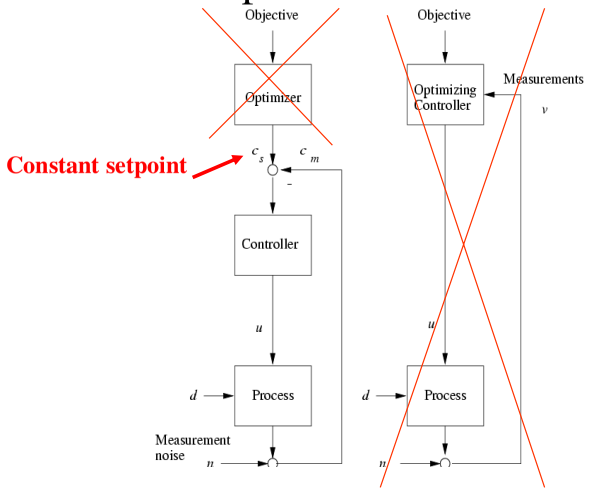

22

What c's should we control?

- Optimal solution is usually at constraints, that is, most of the degrees of freedom are used to satisfy "active constraints", g(u,d) = 0

1. CONTROL ACTIVE CONSTRAINTS!
   - c_s = value of active constraint
   - Implementation of active constraints is usually "obvious"
     - May need "back-off" (safety limit)

2. WHAT MORE SHOULD WE CONTROL?
   - Remaining unconstrained degrees of freedom u
     (Sometimes none left, e.g. LP-problem)
   - Find associated "self-optimizing" variables c

23

Optimal operation runner

Minimize J = T
u = power

Two main cases (modes):

1. Short race (100 m, 200m)
   "Run as fast as you can"
   Optimal operation is *constrained by max. power*

   Control: **Active constraint control!**
   Operate at max. power ("obvious")

2. Long race (800m – marathon)
   "Must be smarter".
   Optimal operation is *unconstrained.*

   Control: Operate at optimal trade-off between "fast and slow"
   (**not obvious what to control**)

25

What should we control? – Marathon

- Optimal operation of Marathon runner, J=T
  - No active constraints
  - Any "self-optimizing" variable c (to control at constant setpoint)?
    - c_1 = distance to leader of race
    - c_2 = speed
    - c_3 = heart rate
    - c_4 = level of lactate in muscles

27

The difficult *unconstrained* variables

Rule. Control variables that give "self-optimizing control"

- *Self-optimizing control:* Constant setpoints c_s give "near-optimal operation" (= acceptable loss L for expected disturbances d and implementation errors n)

$$L(d) = J(c_s + n, d) - J_{opt}(d)$$

Old idea. Morari et al. (1980):
""We want to find a function c of the process variables which when held constant, leads automatically to the optimal adjustments of the manipulated variables, and with it, the optimal operating conditions"

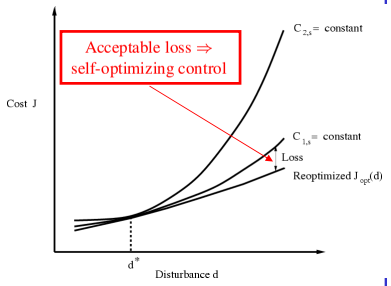

S. Skogestad, ``Plantwide control: The search for the self-optimizing control structure", J. Proc. Control, 10, 487-507 (2000).

28

Further examples self-optimizing control

- Marathon runner
- Central bank
- Cake baking
- Business systems (KPIs)
- Investment portifolio
- Biology
- Chemical process plants: Optimal blending of gasoline

Define optimal operation (J) and look for "magic" variable (c) which when kept constant gives acceptable loss (self-optimizing control)

S. Skogestad, ``Near-optimal operation by self-optimizing control: From process control to marathon running and business systems", Computers and Chemical Engineering, 29 (1), 127-137 (2004).

29

More on further examples

- Central bank. J = welfare. u = interest rate. c=inflation rate (2.5%)
- Cake baking. J = nice taste, u = heat input. c = Temperature (200C)
- Business, J = profit. c = "Key performance indicator (KPI), e.g.
  - Response time to order
  - Energy consumption pr. kg or unit
  - Number of employees
  - Research spending

  Optimal values obtained by "benchmarking"
- Investment (portofolio management). J = profit. c = Fraction of investment in shares (50%)
- Biological systems:
  - "Self-optimizing" controlled variables c have been found by natural selection
  - Need to do "reverse engineering" :
    - Find the controlled variables used in nature
    - From this possibly identify what overall objective J the biological system has been attempting to optimize

30

What should we control (c)? - More details

1. Control active constraints
   - Need Back-off
2. Remaining *unconstrained* DOFs (if any): Control "self-optimizing" variables
   - How do we find them?
   - Maximum gain rule

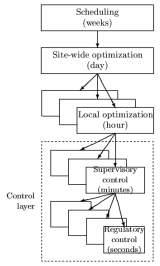

37

1. The "easy" *active constraints*

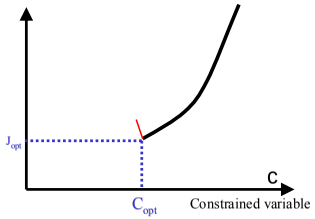

"Obvious" : Want to keep (control) c at $c_{opt} = c_{constraint}$

1) If c = u = manipulated input (MV):
- Implementation trivial: Keep u at constraint (u_{min} or u_{max})

2) If c = y = output variable (CV):
- Use u to control y at constraint
- BUT: Need to introduce backoff (safety margin)

39

Back-off for output constraints

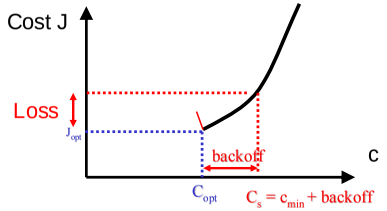

a) If constraint on c can be violated dynamically (so only average matters)
Required Backoff = "bias" (steady-state meas. error for c)
b) If constraint on c can be not be violated dynamically ("hard constraint")
Required Backoff = "bias" + max. dynamic control error
= Variance
Can be reduced by improved control!

Rule for control of hard output constraints: "Squeeze and shift"!
Reduce variance ("Squeeze") and "shift" setpoint c_s to reduce backoff

40

Hard active constraints

« SQUEEZE AND SHIFT »

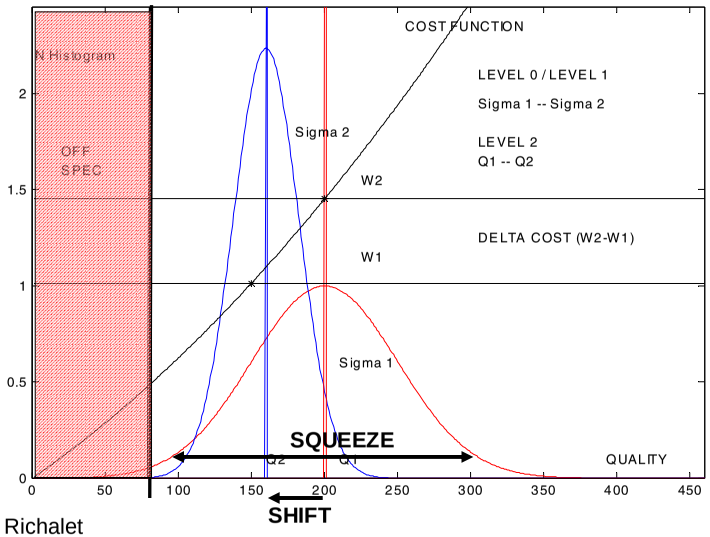

© Richalet

41

2. The difficult *unconstrained* variables

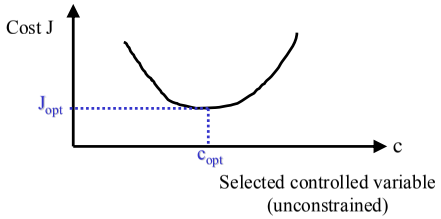

How do we find them (CVs) ?

- **Intuition:** "*Dominant variables*" (Shinnar)
- Rijnsdorp (1990): ``*…requires good process insight and control structure know-how. "*
- **Any systematic procedure?**

42

Unconstrained degrees of freedom:

Optimal operation

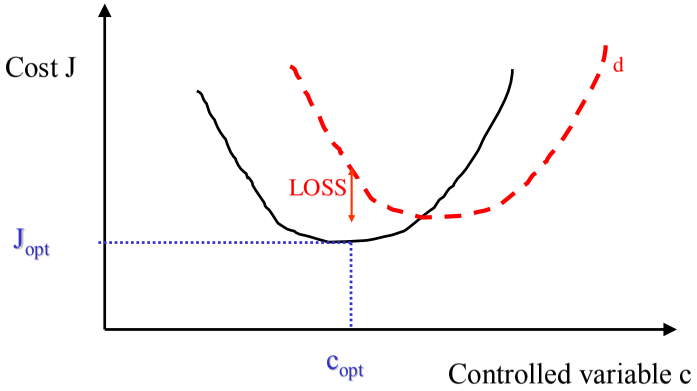

Two problems:

- **1. Optimum moves because of disturbances d: $c_{opt}(d)$**

43

Unconstrained degrees of freedom:

Optimal operation

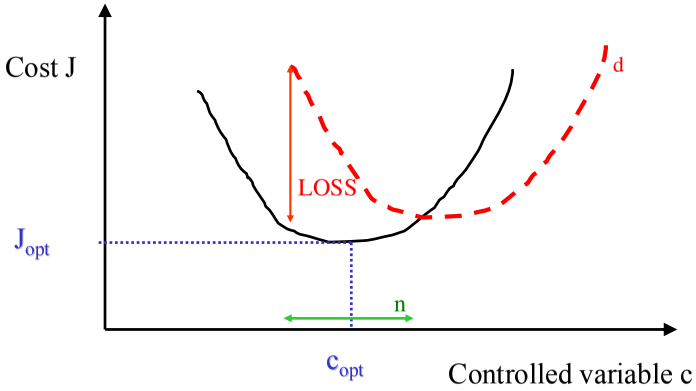

Two problems:

- 1. Optimum moves because of disturbances d: $c_{opt}(d)$
- **2. Implementation error, $c = c_{opt} + n$**

44

Unconstrained degrees of freedom:

Effect of implementation error on cost ("problem 2")

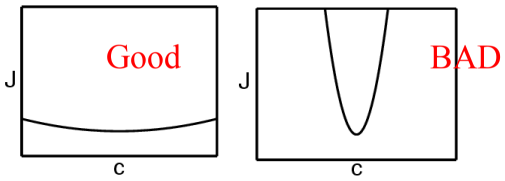

(b) Flat optimum: Implementation easy

(c) Sharp optimum: Sensitive to implementation erros

45

Unconstrained degrees of freedom:

Candidate controlled variables

- **We are looking for some "magic" variables c to control..... What properties do they have?'**
- Intuitively 1: Should have small optimal variation $\Delta c_{opt}(d)$
  - since we are going to keep them constant!
- Intuitively 2: Should have small "implementation error" n

} span(c)

- "Intuitively" 3: Should be sensitive to inputs u (remaining unconstrained degrees of freedom), that is, the gain G_0 from u to c should be large
  - Large gain gives flat optimum in c
- Can combine everything into the "maximum gain rule":
  - Maximize scaled gain $G = G_o / \text{span}(c)$

46

Unconstrained degrees of freedom:

Justification for why large gain is good

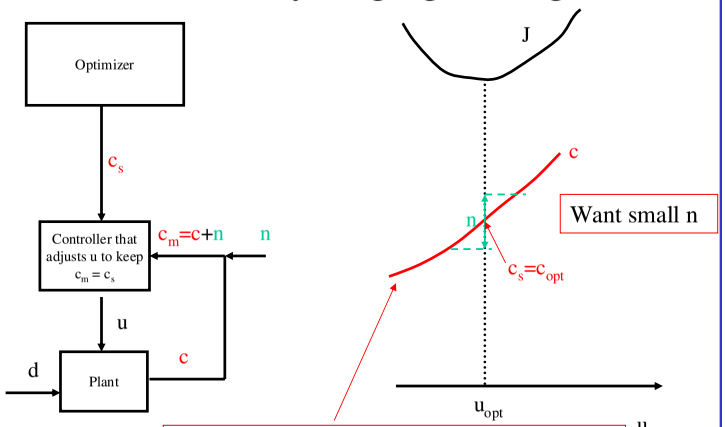

Want the slope (= gain G_0 from u to c) large – corresponds to flat optimum in c

47

Unconstrained degrees of freedom:

Maximum gain (MSV) rule

Maximum gain rule *(Skogestad and Postlethwaite, 1996): Control variables c with a large scaled gain $\underline{\sigma}(G)$*

"Gain"= $\underline{\sigma}$(G) : Minimum singular value (MSV) of the appropriately scaled steady-state gain matrix G from u to c

$$\text{Loss} \le \tfrac{1}{2}\bar{\sigma}(G^{-1})^2 = \tfrac{1}{2}\tfrac{1}{\underline{\sigma}(G)^2}; \quad G = S_1 G_0 S_2$$
$$\text{Output scaling: } S_1 = diag\{1/\text{span}(c_i)\}$$
$$\text{Input scaling: } S_2 = J_{uu}^{-1/2}$$

$\underline{\sigma}$(G) is called the "Morari Resiliency index" (MRI) by Luyben

48

Unconstrained degrees of freedom:

Proof of "maximum gain rule" (local analysis)

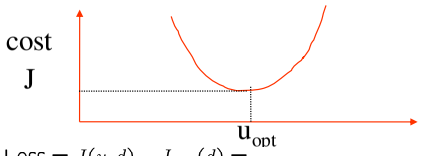

$$\text{Loss} = J(u,d) - J_{opt}(d) =$$
$$\underbrace{\left(\frac{\partial J}{\partial u}\right)_{opt}^{T}}_{=0}(u - u_{opt}(d)) \quad + \tfrac{1}{2}(u - u_{opt}(d))^T \underbrace{\left(\frac{\partial^2 J}{\partial u^2}\right)_{opt}}_{=J_{uu}} (u - u_{opt(d)}) + \cdots$$
$$\approx \tfrac{1}{2}\left(c - c_{opt}(d)\right)^T G_0^{-T} J_{uu} G_0^{-1} \left(c - c_{opt}(d)\right)$$
$$\le \tfrac{1}{2} span(c)^T G_0^{-T} J_{uu} G_0^{-1} span(c) = \tfrac{1}{2}\underline{1}^T G^{-T} G^{-1} \underline{1}$$

where

G_0 = unscaled gain ($\Delta c = G_0 \Delta u$)

G = scaled gain= $S_1 G_0 S_2$;

$S_1 = diag(\frac{1}{span(c_i)})$; $S_2 = J_{uu}^{-1/2}$;

span (c) = max. expected $c - c_{opt}(d)$

Detailed proof: I.J. Halvorsen, et al. ``Optimal selection of controlled variables", *Ind. Eng. Chem. Res.*, **42** (14), 3273-3284 (2003).

49

Unconstrained degrees of freedom:

Maximum gain rule for scalar system

Scaled steady-state gain from u to c:

$$|G| = \frac{|G_0|}{|c_{opt}| + |n|} = \frac{|G_0|}{\text{optimal span } c}$$

$$\text{Loss} \approx \frac{|J_{uu}|}{2} \cdot \frac{1}{|G|^2}$$

J_{uu}: Hessian for effect of u's on cost

Scalar system: J_{uu} does not matter

50

Unconstrained degrees of freedom:

Maximum gain rule in words

Select controlled variables c for which
the gain G_0 (="controllable range") is large compared to
its span (=sum of optimal variation and control error)

51

Toy Example

$J = (u-d)^2$
$n_u = 1$ unconstrained degrees of freedom
$u_{opt} = d$

Alternative measurements:
- $y_1 = 0.1(u-d)$
- $y_2 = 20u$
- $y_3 = 10u - 5d$
- $y_4 = u$

Scaled such that:
- $|d| \le 1$, $|n_i| \le 1|$, i.e. all y_i's are ± 1

Nominal operating point:
- $d = 0 \Rightarrow u_{opt} = 0, y_{opt} = 0$

What variable c should we control?

52

Toy Example: Single measurements

A. Maximize minimum singular value, $|G_s|$

c	G	Expected variation in y $y_{span} = \|y_{opt}\| + \|n\|$	$\|G_s\| = \|G\|/y_{span}$	Rank
y_1	0.1	$0+1=1$	$0.1/1 = 0.1$	4
y_2	20	$20+1=21$	$20/21 = 0.95$	2
y_3	10	$5+1=6$	$10/6 = 1.67$	1
y_4	1	$1+1=2$	$1/2 = 0.5$	3

Loss = constant / $|G_s^2|$

C. Exact evaluation of loss: Same order

- $L_{wc,1} = 100$
- $L_{wc,2} = 1.0025$
- $L_{wc,3} = 0.26$
- $L_{wc,4} = 2$

Constant input, $c = y_4 = u$

Want loss < 0.1: Consider variable combinations

53

Unconstrained degrees of freedom:

Use of maximum gain rule

- Want to find good *candidate* controlled variables c
  - *Simplest:* Control individual "measurements" y (also include inputs u):

$$c = Hy; \quad \text{Example: } c = \begin{pmatrix} y_2 \\ u \end{pmatrix} = \underbrace{\begin{pmatrix} 0 & 1 & 0 & 0 \\ 0 & 0 & 0 & 1 \end{pmatrix}}_{\text{selection matrix H}} \begin{pmatrix} y_1 \\ y_2 \\ y_3 \\ u \end{pmatrix}$$

- **A. Maximum gain rule.** Linearized models:
  - All measurements: $y = G^y u$
  - Selected controlled variables (n_c=n_u): $c = G_o u = H G^y u$
  - Want $\underline{\sigma}(G)$ large, $G = S_1 H G^y J_{uu}^{-1/2}$
- Many candidate combinations:

$$\binom{n_y}{n_c} = \frac{n_y!}{n_c!(n_y-n_c)!}, \quad \text{Examples: } \binom{4}{2} = 6; \quad \binom{30}{5} = 142506$$

  - Exist efficient branch-and-bound methods for maximixing $\underline{\sigma}(G)$ (Cao and Kariwala, 2008)
- **B.** If no single-measurement combination acceptable:
  - Consider variable combinations, c = H y, where H is a "full" combination matrix
- **C.** Final choice between good candidates:
  - Nonlinear "brute force" evaluation of loss and feasibility + controllability considerations

Y. Cao, V. Kariwala, "Bidirectional branch and bound for controlled variable selection. Part I. Principles and minimum singular value criterion", Comp. Chem. Engng., In press (2008)

54

EXAMPLE: Recycle plant (Luyben, Yu, etc.)

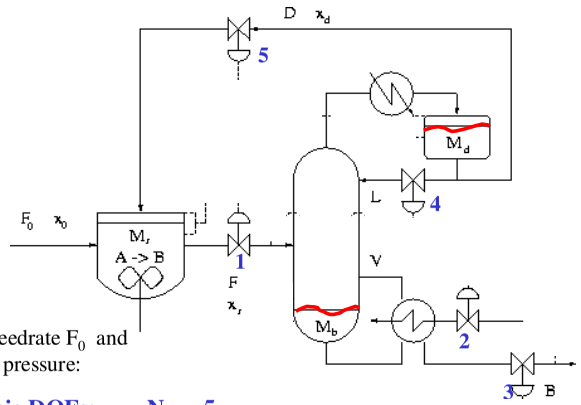

Given feedrate F_0 and column pressure:

Dynamic DOFs: $N_m = 5$
Column levels: $N_{0y} = 2$
Steady-state DOFs: $N_0 = 5 - 2 = 3$

Recycle plant: Optimal operation

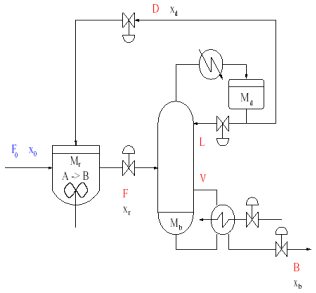

Manipulated variables:

$$\mathbf{m}^T = [V\ L\ B\ D\ F]$$

Steady-state degrees of freedom: 3

Minimize costs

$$J = V$$

Constraints:

x_b	$\leq 0.015\ \frac{\text{molA}}{\text{mol}}$	active
M_r	≤ 2800 kmol	active
V	≤ 5000 kmol/h	
Flows	≥ 0 kmol/h	

Disturbances:

$$d^T = [F_0\ x_0] = [460 \pm 92\ \frac{\text{kmol}}{\text{h}}\ \ 0.90 \pm 0.05]$$

1 remaining unconstrained degree of freedom

A. Maximum gain rule: Steady-state gain

Rank	c	$\lvert G(0)\rvert \cdot 10^3$
1	x_D	13.1
2	L/F	8.9
3	D/L	7.7
4	D/V	5.8
5	V/L	4.5
6	B/L	4.1
7	V/F	4.0
8	B/D	3.3
9	L	3.0
10	B/F	2.6
11	D	2.6
12	F/F_0	2.5
13	D/F	2.5
14	F	1.9
15	B/V	0
15	V	0
15	x_r	0
15	B	0

Conventional: Looks good

Luyben rule: Not promising economically

Gain from $u = L$ to c with active constraints (M_r and x_B) constant.
Scaling: $\Delta c_i = \max_d |c_{opt,i}(d) - c_{opt,i}(d^*)|$ + implementation error.
$d = F_0, z_F$.

How did we find the gains in the Table?

1. Find nominal optimum
2. Find (unscaled) gain G_0 from input to candidate outputs: $\Delta c = G_0 \Delta u$.
   - In this case only a single unconstrained input (DOF). Choose at u=L
   - Obtain gain G_0 numerically by making a small perturbation in u=L while adjusting the other inputs such that the active constraints are constant (bottom composition fixed in this case)

     IMPORTANT!
3. Find the span for each candidate variable
   - For each disturbance d_i make a typical change and reoptimize to obtain the optimal ranges $\Delta c_{opt}(d_i)$
   - For each candidate output obtain (estimate) the control error (noise) n
   - The expected variation for c is then: span(c) = $\Sigma_i\ |\Delta c_{opt}(d_i)|\ + |n|$
4. Obtain the scaled gain, $G = |G_0| / \text{span}(c)$
5. Note: The absolute value (the vector 1-norm) is used here to "sum up" and get the overall span. Alternatively, the 2-norm could be used, which could be viewed as putting less emphasis on the worst case. As an example, assume that the only contribution to the span is the implementation/measurement error, and that the variable we are controlling (c) is the average of 5 measurements of the same y, i.e. c=sum yi/5, and that each yi has a measurement error of 1, i.e. nyi=1. Then with the absolute value (1-norm), the contribution to the span from the implementation (meas.) error is span=sum abs(nyi)/5 = 5*1/5=1, whereas with the two-norm, span = sqrt(5*(1/5^2) = 0.447. The latter is more reasonable since we expect that the overall measurement error is reduced when taking the average of many measurements. In any case, the choice of norm is an engineering decision so there is not really one that is "right" and one that is "wrong". We often use the 2-norm for mathematical convenience, but there are also physical justifications (as just given!).

C. Check: "Brute force" loss evaluation: Disturbance in F_0

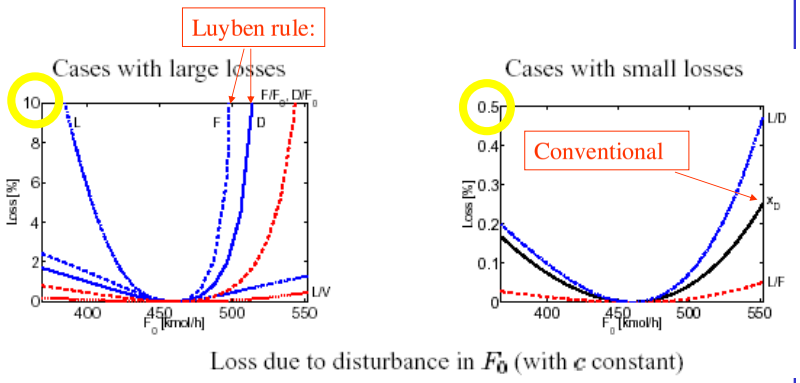

Loss due to disturbance in F_0 (with c constant)

Loss with nominally optimal setpoints for M_r, x_B and c

61

C. Check: "Brute force" loss evaluation: Implementation error

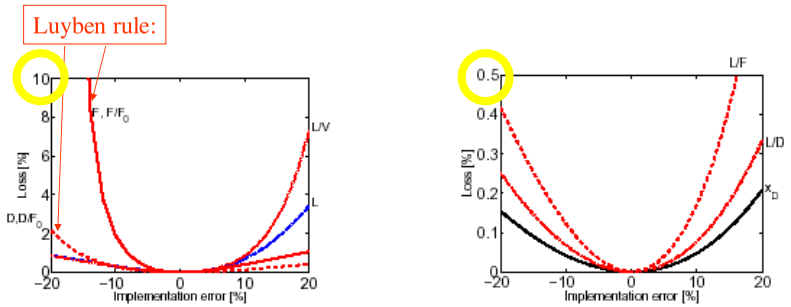

Loss due to implementation error in c

Loss with nominally optimal setpoints for M_r, x_B and c

62

Conclusion: Control of recycle plant

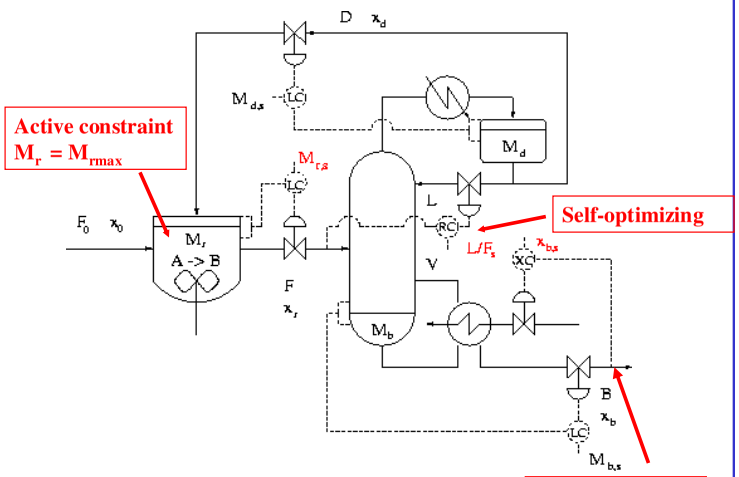

L/F constant: Easier than "two-point" control

Assumption: Minimize energy (V)

64

Summary unconstrained degrees of freedom:

Looking for "magic" variables to keep at constant setpoints.

How can we find them systematically?

Candidates

$c = y_i$: Single measurements, e.g. pressure, temperature, composition

$c = \frac{y_i}{y_j}$: Combinations of measurements (e.g flow ratios)

A. Start with: Maximum gain (minimum singular value) rule:

(Scaled) gain $\underline{\sigma}(G)$ from u to y should be large

B. If no good single candidates: Consider linear combinations (matrix H):

$$c = h_1 y_1 + h_2 y_2 + \ldots + h_n y_n = Hy$$

C. Finally: "Brute force evaluation" of most promising alternatives.

- Evaluate loss when the candidate variables c are kept constant
- In particular, may be problem with **feasibility**
- **Also: Consider controllability**

65

Conclusion
Control the right variable!
Important irrespective of what control strategy you use
Decentralized control
LQG
MPC
H-infinty
....
Look for "self-optimizing" variables with large scaled gain
• Self-optimizing control is when acceptable operation can be achieved using constant set points (c_s) for the controlled variables c (without the need to re-optimize when disturbances occur).
Tomorrow (part 2):
• Effective Implementation of optimal operation using off-line computations
• Dynamic and other generalizations
• Links to optimal control and MPC
Scheduling (weeks)
Site-wide optimization (day)
Local optimization (hour)
Supervisory control (minutes)
Regulatory control (seconds)
Control layer
c=c_s
NTNU
66

Self-optimizing control: Simple implementation of optimal operation

Sigurd Skogestad

Department of Chemical Engineering
Norwegian University of Science and Tecnology (NTNU)
Trondheim, Norway

Benelux Control Meeting, March 2008

PART 2: **Effective Implementation of optimal operation using Off-Line Computations**

1

Outline

- Implementation of optimal operation
- Paradigm 1: On-line optimizing control
- Paradigm 2: "Self-optimizing" control schemes
  - Precomputed (off-line) solution
- Control of optimal measurement combinations
  - Nullspace method
  - Exact local method
- Link to optimal control / Explicit MPC
- Current research issues

2

Optimal operation

- A typical dynamic optimization problem

$$\begin{aligned} \min_u \; & J(x,u,d) \\ \text{s.t. } & \dot{x} = f(x,u,d), \\ & h(x,u,d) = 0, \\ & g(x,u,d) \le 0. \end{aligned}$$

- **Implementation:** "Open-loop" solutions not robust to disturbances or model errors
- Want to introduce feedback

3

Implementation of optimal operation

- **Paradigm 1: On-line optimizing control** where measurements are used to update model and states
- **Paradigm 2: "Self-optimizing" control scheme** found by exploiting properties of the solution in control structure design
  - Usually feedback solutions
  - Use **off-line** analysis/optimization to find "properties of the solution"
  - "self-optimizing " = "inherent optimal operation"

4

Implementation: Paradigm 1

- Paradigm 1: **Online** optimizing control
- Measurements are primarily used to update the model
- The optimization problem is resolved online to compute new inputs.
- Example: Conventional MPC
- This is the "obvious" approach (for someone who does not know control)

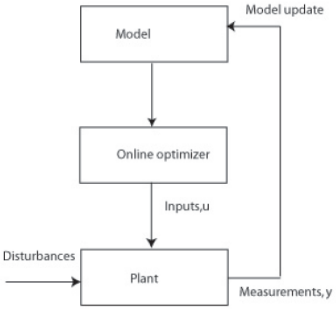

5

Example paradigm 1: Marathon runner

- Even getting a reasonable model requires > 10 PhD's ☺ … and the model has to be fitted to each individual….
- Clearly impractical!

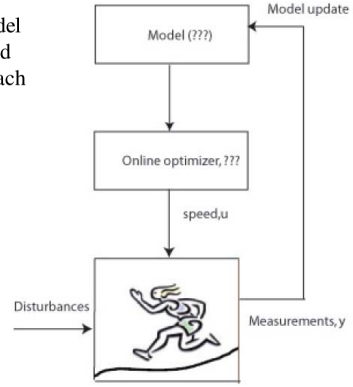

6

Implementation: Paradigm 2

- **Paradigm 2:** Precomputed solutions based on **off-line** optimization
- Find properties of the solution suited for simple and robust on-line implementation
- Examples
  - Marathon runner
  - Hierarchical decomposition
  - Optimal control
  - Explicit MPC

7

Example paradigm 2: Marathon runner

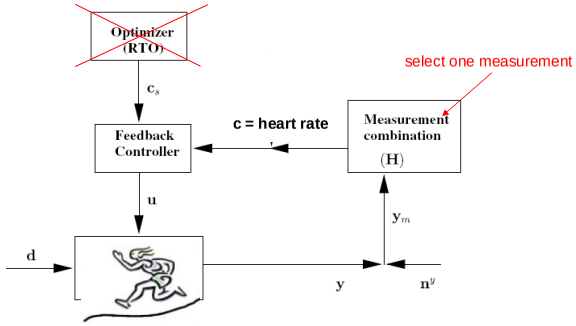

- Simple and robust implementation
- Disturbances are indirectly handled by keeping a constant heart rate
- May have infrequent adjustment of setpoint (heart rate)

8

Example paradigm 2: Optimal operation of chemical plant

- Hierarchial decomposition based on time scale separation

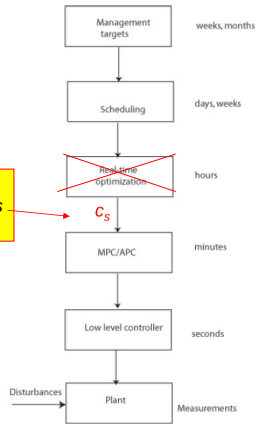

Self-optimizing control: *Acceptable operation (=acceptable loss) achieved using constant set points (c_s) for the controlled variables c*

- No or infrequent online optimization.
- Controlled variables c are found based on **off-line** analysis.

9

Example paradigm 2: Feedback implementation of optimal control (LQ)

- Optimal solution to infinite time dynamic optimization problem
- Originally formulated as a "open-loop" optimization problem (no feedback)
- "By chance" the optimal u can be generated by simple state feedback
  $u = K_{LQ}\, x$
- K_{LQ} is obtained **off-line** by solving Riccatti equations

- Explicit MPC: Extension using different K_{LQ} in each constraint region

- **Summary: Two paradigms MPC**
  1. Conventional MPC: On-line optimization
  2. Explicit MPC: Off-line calculation of K_{LQ} for each region (must determine regions online)

10

Example paradigm 2: Explicit MPC

The optimal solution $U^*(x)$ is a Piece-Wise Affine function of the current state x_t: (Bemporad et al., 2002)

$$U^*(x) = \begin{cases} K_1 x + g_1, & \text{if } x \in X_1 \\ K_2 x + g_2, & \text{if } x \in X_2 \\ \vdots & \\ K_n x + g_n, & \text{if } x \in X_n \end{cases}$$

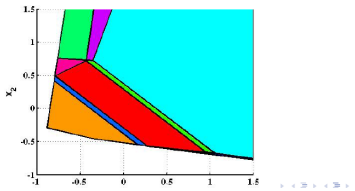

MPC: Model predictive control
Note: Many regions because of future constraints

A. Bemporad, M. Morari, V. Dua, E.N. Pistikopoulos, "The Explicit Linear Quadratic Regulator for Constrained Systems", Automatica, vol. 38, no. 1, pp. 3-20 (2002).

11

Issues Paradigm 2: Precomputed on-line solutions based on **off-line** optimization

Issues (expected research results for specific application):

1. Find structure of optimal solution for specific problems
   - Typically, identify **regions** where different set of constraints are active
2. Find optimal values (or trajectories) for unconstrained variables
3. Find analytical or precomputed solutions suitable for on-line implementation
4. Find good "self-optimizing" variables c to control in each **region**
   - Find good variable *combinations* to control
5. Determine a switching policy between different **regions**

12

Unconstrained degrees of freedom:

How find "self-optimizing" variable *combinations* in a systematic manner?

- The ideal "self-optimizing" variable is the gradient (first-order optimality condition (ref: Bonvin and coworkers)):

$$c = \alpha J_u; \qquad J_u = \frac{\partial J}{\partial u}$$

  - Optimal setpoint = 0
- BUT: Gradient can not be measured in practice
- Possible approach: Estimate gradient J_u based on measurements y

- Here alternative approach: Find **optimal linear measurement combination**

$$c = Hy$$

  which when kept constant (± n) minimize the effect of d on loss.
  Loss = J(u,d) – J(u_{opt},d); where u is input for c = constant ± n

- Candidate measurements (y): Include also inputs u

13

Unconstrained degrees of freedom:

B. Optimal measurement combination

$$\Delta c = h_1 \Delta y_1 + h_2 \Delta y_2 + \cdots = H \Delta y$$

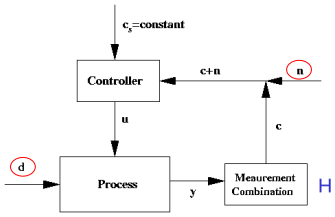

14

Unconstrained degrees of freedom:

B. Optimal measurement combination

$$\Delta c = h_1 \Delta y_1 + h_2 \Delta y_2 + \cdots = H \Delta y$$

B1. Nullspace method for n = 0 *(Alstad and Skogestad, 2007)*

Basis: Want optimal value of c to be independent of disturbances

$$\Rightarrow \quad \Delta c_{opt} = 0 \cdot \Delta d$$

- Find optimal solution as a function of d: $u_{opt}(d)$, $y_{opt}(d)$
- Linearize this relationship: $\Delta y_{opt} = F\, \Delta d$
- Want: $\Delta c_{opt} = H \Delta y_{opt} = HF \Delta d = 0$
- To achieve this for all values of Δ d:

$$HF = 0 \;\Rightarrow\; H \in \mathcal{N}(F^T)$$

- To find a F that satisfies HF=0 we must require

$$n_y \geq n_u + n_d$$

- *Optimal* when we disregard implementation error (n)

Amazingly simple!

Sigurd is told how easy it is to find H

15

V. Alstad and S. Skogestad, ``Null Space Method for Selecting Optimal Measurement Combinations as Controlled Variables", Ind.Eng.Chem.Res, 46 (3), 846-853 (2007).

Unconstrained degrees of freedom:

Nullspace method continued

- To handle implementation error: Use "sensitive" measurements, with information about all independent variables (u and d)

$$y = Gu + G_d d = \begin{pmatrix} G & G_d \end{pmatrix} \begin{pmatrix} u \\ d \end{pmatrix}$$

Maximize minimum singular value of $[G \quad G_d]$

16

Unconstrained degrees of freedom:

B. Optimal measurement combination

$$\Delta c = h_1 \Delta y_1 + h_2 \Delta y_2 + \cdots = H \Delta y$$

B2. Combined disturbances and implementation errors *("exact local method")*

Loss L = J(u,d) – $J_{opt}(d)$. Keep c = Hy constant , where y = $G^y u + G^y_d d + n^y$

Theorem 1. Worst-case loss for given H (Halvorsen et al, 2003):

$$L_{wc} = \max_{\left\| \begin{bmatrix} \mathbf{d}' \\ \mathbf{n}^y \end{bmatrix} \right\|_2 \le 1} L = \frac{1}{2}(\bar{\sigma}[\mathbf{M}])^2 \qquad \mathbf{M} \triangleq [\mathbf{M_d} \quad \mathbf{M_{n^y}}]$$

$$\mathbf{M}_d = -\mathbf{J}_{uu}^{1/2}(\mathbf{HG}^y)^{-1}\mathbf{HW}_d$$

$$\mathbf{M}_{n^y} = -\mathbf{J}_{uu}^{1/2}(\mathbf{HG}^y)^{-1}\mathbf{HW}_{n^y}$$

$$\Delta \mathbf{y}^{opt} = \underbrace{-(\mathbf{G}^y \mathbf{J}_{uu}^{-1} \mathbf{J}_{ud} - \mathbf{G}_d^y)}_{\mathbf{F}} \Delta \mathbf{d}$$

Applies to any H (selection/combination)

Optimization problem for optimal combination: $\mathbf{H}_{opt} = \arg\min_{\mathbf{H}} \bar{\sigma}(\mathbf{M})$

• I.J. Halvorsen, S. Skogestad, J.C. Morud and V. Alstad, ``Optimal selection of controlled variables", Ind. Eng. Chem. Res., 42 (14), 3273-3284 (2003).

Unconstrained degrees of freedom:

B. Optimal measurement combination

$$\Delta c = h_1 \Delta y_1 + h_2 \Delta y_2 + \cdots = H \Delta y$$

B2. Exact local method *for combined disturbances and implementation errors.*

Theorem 2. Explicit formula for optimal H. (Alstad et al, 2008):

Define $\tilde{F} = [F W_d \; W_{n^y}]$. Then

$$H_{opt}^T = (\tilde{F}\tilde{F}^T)^{-1} G^y \left(G^{yT} (\tilde{F}\tilde{F}^T)^{-1} G^y \right)^{-1} J_{uu}^{1/2}$$

F – optimal sensitivity matrix = dy_{opt}/dd

Theorem 3. (Kariwala et al, 2008).

The solution in Theorem 2 minimizes both $\|M\|_F$ and $\bar{\sigma}(M)$, that is, minimizes both the "average" and worst-case loss.

V. Alstad, S. Skogestad and E.S. Hori, ``Optimal measurement combinations as controlled variables", Journal of Process Control, 18, in press (2008).
V. Kariwala, Y. Cao, S. jarardhanan, "Local self-optimizing control with average loss minimization", Ind.Eng.Chem.Res., in press (2008)

Toy Example

$J = (u - d)^2$

$n_u = 1$ unconstrained degrees of freedom

$u_{opt} = d$

Alternative measurements:

$y_1 = 0.1(u - d)$

$y_2 = 20u$

$y_3 = 10u - 5d$

$y_4 = u$

Scaled such that:

$|d| \le 1$, $|n_i| \le 1|$, i.e. all y_i's are ± 1

Nominal operating point:

$d = 0 \Rightarrow u_{opt} = 0, y_{opt} = 0$

What variable c should we control?

Toy Example: Single measurements

A. Maximize minimum singular value, $|G_s|$

c	G	Expected variation in y $y_{span} = \lvert y_{opt}\rvert + \lvert n\rvert$	$\lvert G_s\rvert = \lvert G\rvert / y_{span}$	Rank
y_1	0.1	$0 + 1 = 1$	$0.1/1 = 0.1$	4
y_2	20	$20 + 1 = 21$	$20/21 = 0.95$	2
y_3	10	$5 + 1 = 6$	$10/6 = 1.67$	1
y_4	1	$1 + 1 = 2$	$1/2 = 0.5$	3

Loss = constant / $|G_s^2|$

C. Exact evaluation of loss: Same order

$L_{wc,1} = 100$

$L_{wc,2} = 1.0025$

$L_{wc,3} = 0.26$

$L_{wc,4} = 2$ ← Constant input, c = y_4 = u

Want loss < 0.1: Consider variable combinations

NTNU

Toy Example: Measurement combinations

$$c = Hy = \begin{pmatrix} h_1 & h_2 & h_3 & h_4 \end{pmatrix} \begin{pmatrix} y_1 \\ y_2 \\ y_3 \\ y_4 \end{pmatrix} = h_1 y_1 + h_2 y_2 + h_3 y_3 + h_4 y_4$$

B1. Nullspace method

Neglect measurement error ($n = 0$):

$HF = 0$

Sensitivity matrix

$\Delta y_{\text{opt}} = F \Delta d; F = \begin{pmatrix} 0 & 20 & 5 & 1 \end{pmatrix}^T$

To find H that satisfies $HF = 0$ must combine at least two measurements:

$n_y \geq n_u + n_d = 1 + 1 = 2$

21

NTNU

B1. Nullspace method (no noise)

Table 2
Combinations of two measurements, $c = h_1 y_i + h_2 y_j$, with zero disturbance loss ($\mathbf{M}_d = 0$) and resulting loss L_{wc} caused by measurement error

y_i	y_j	$HF = 0 \Rightarrow H \in \mathcal{N}(F^T)$			$\underline{\sigma}(\tilde{\mathbf{G}}^y)$
		h_1	h_2	L_{wc}	
2	3	−0.2425	0.9701	0.0425	4.449
3	4	−0.1961	0.9806	1.04	0.446
1	2	−1	0	100	0.1
1	4	−1	0	100	0.0995
1	3	−1	0	100	0.0447
2	4	−0.0499	0.988	∞	0

- Loss caused by measurement error only
- Recall rank single measurements: 3 > 2 > 4 > 1

22

NTNU

B2. Exact local method (with noise)

Minimum loss for combined disturbances and measurement errors:

$$H^T = (\tilde{F}\tilde{F}^T)^{-1} G^y \left(G^{yT} (\tilde{F}\tilde{F}^T)^{-1} G^y \right)^{-1} J_{uu}^{1/2}$$

where $\tilde{F} = [F W_d \; W_{n^y}]$.

For toy example:

$G^y = \begin{pmatrix} 0.1 & 20 & 10 & 1 \end{pmatrix}^T$

$F = \begin{pmatrix} 0 & 20 & 5 & 1 \end{pmatrix}^T, \; J_{uu} = 2$

$W_d = 1, W_{n^y} = I$

23

NTNU

B2. Exact local method, 2 measurements

Table 3
Combinations of two measurements, $c = h_1 y_i + h_2 y_j$, with minimum loss L_{wc} for combined disturbances and measurement error

y_i	y_j	$H_{\text{opt}}^T = (\tilde{F}\tilde{F}^T)^{-1} G^y \left(G^{yT} (\tilde{F}\tilde{F}^T)^{-1} G^y \right)^{-1} J_{uu}^{1/2}$		
		h_1	h_2	L_{wc}
2	3	−0.2312	0.9729	0.0406
3	4	−0.8296	0.5584	0.198
1	3	0.2293	0.9733	0.2351
1	2	0.8753	0.4836	0.8969
2	4	0.0499	0.9988	0.9050
1	4	0.1869	0.9824	1.8670

Combined loss for disturbances and measurement errors

24

B2. Exact local method, all 4 measurements

$H_{\text{opt}} = (\,0.0208 \quad -0.2317 \quad 0.9725 \quad -0.0116\,)$

Resulting loss

$L_{wc} = 0.0405$

Almost no improvement in this case compared to 2 measurements (2 and 3)

25

Example: CO2 refrigeration cycle

Unconstrained DOF (u)
Control what?
c=?

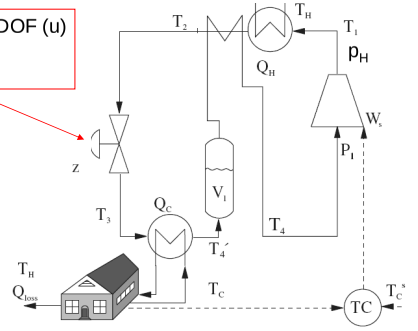

26

CO2 refrigeration cycle

Step 1. One (remaining) degree of freedom (u=z)

Step 2. Objective function. J = W_s (compressor work)

Step 3. Optimize operation for disturbances (d_1=T_C, d_2=T_H, d_3=UA)

- Optimum always unconstrained

Step 4. Implementation of optimal operation

- No good single measurements (all give large losses):
  - p_h, T_h, z, …
- Nullspace method: Need to combine n_u+n_d=1+3=4 measurements to have zero disturbance loss
- Simpler: Try combining two measurements. Exact local method:
  - $c = h_1 p_h + h_2 T_h = p_h + k T_h$; k = -8.53 bar/K
- Nonlinear evaluation of loss: OK!

27

Refrigeration cycle: Proposed control structure

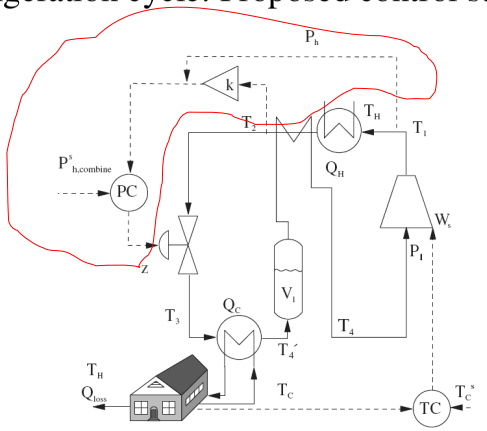

Control c= “temperature-corrected high pressure”

28

Summary: Procedure selection controlled variables

1. Define economics and operational constraints
2. Identify degrees of freedom and important disturbances
3. Optimize for various disturbances
4. Identify active constraints regions (off-line calculations)

For each active constraint region do step 5-6:

5. Identify "self-optimizing" controlled variables for remaining degrees of freedom
6. Identify switching policies between regions

29

Example switching policies – 10 km

1. *"Startup":* Given speed or follow "hare"
2. *When heart beat > max or pain > max:* Switch to slower speed
3. *When close to finish*: Switch to max. power

30

Current research 1 (Sridharakumar Narasimhan and Henrik Manum):

Conditions for switching between regions of active constraints

Idea:

- Within each region it is optimal to
  1. Control active constraints at $c_a = c_{,a,\ constraint}$
  2. Control self-optimizing variables at $c_{so} = c_{,so,\ optimal}$
- Define in each region i:

$$c_i = \begin{pmatrix} c_a - c_{a,constraint} \\ c_{so} - c_{so,optimal} \end{pmatrix}$$

- Keep track of c_i (active constraints and "self-optimizing" variables) in all regions i
- Switch to region i when element in c_i changes sign
- Research issue: can we get lost?

31

Current research 2 (Håkon Dahl-Olsen):

Extension to dynamic systems

- Basis. From dynamic optimization:
  - Hamiltonian should be minimized along the trajectory
- Generalize steady-state local methods:
  - Generalize maximum gain rule
  - Generalize nullspace method (n=0)
  - Generalize "exact local method"

32

Current research 3 (Sridharakumar Narasimhan and Johannes Jäschke):

Extension of noise-free case (nullspace method) to nonlinear systems

- Idea: The ideal self-optimizing variable is the gradient

$$c = \alpha J_u; \qquad J_u = \frac{\partial J}{\partial u}$$

  - Optimal setpoint = 0
- Certain problems (e.g. polynomial)
  - Find analytic expression for J_u in terms of u and d
  - Derive J_u as a function of measurements y (eliminate disturbances d)

33

Current research 4 (Henrik Manum and Sridharakumar Narasimhan):

Self-optimizing control and Explicit MPC

- Our results on optimal measurement combination (keep c = Hy constant)
  - Nullspace method for n=0 (Alstad and Skogestad, 2007)

$$HF = 0 \;\Rightarrow\; H \in \mathcal{N}(F^T)$$

  - Explicit expression ("exact local method") for n≠0 (Alstad et al., 2008)

$$H_{\text{opt}}^T = (\tilde{F}\tilde{F}^T)^{-1}G^y\left(G^{yT}(\tilde{F}\tilde{F}^T)^{-1}G^y\right)^{-1}J_{uu}^{1/2}$$

- Observation 1: Both result are exact for quadratic optimization problems

$$\min_{\mathbf{u}} \mathbf{J}(\mathbf{u},\mathbf{d}) = \begin{bmatrix}\mathbf{u} & \mathbf{d}\end{bmatrix}\begin{bmatrix}\mathbf{J}_{uu} & \mathbf{J}_{ud}\\ \mathbf{J}_{ud}^{\mathrm{T}} & \mathbf{J}_{dd}\end{bmatrix}\begin{bmatrix}\mathbf{u}\\ \mathbf{d}\end{bmatrix}$$

- Observation 2: MPC can be written as a quadratic optimization problem and optimal solution is to keep c = u – Kx constant.
- Must be some link!

34

Quadratic optimization problems

- Noise-free case (n=0)
- Reformulation of nullspace method of Alstad and Skogestad (2007)
  - **Can add linear constraints (c=Hy) to quadratic problem with no loss**
  - **Need $n_y \geq n_u + n_d$. H is unique if $n_y = n_u + n_d$ ($n_{ym} = n_d$)**
  - **H may be computed from nullspace method,** $H \in \mathcal{N}(F^T)$

Theorem 3 (Linear invariants for quadratic optimization problem). *Consider an unconstrained quadratic optimization problem in the variables* **u** *(input vector of length n_u) and* **d** *(disturbance vector of length n_d)*

$$\min_{\mathbf{u}} \mathbf{J}(\mathbf{u},\mathbf{d}) = \begin{bmatrix}\mathbf{u} & \mathbf{d}\end{bmatrix}\begin{bmatrix}\mathbf{J}_{uu} & \mathbf{J}_{ud}\\ \mathbf{J}_{ud}^{\mathrm{T}} & \mathbf{J}_{dd}\end{bmatrix}\begin{bmatrix}\mathbf{u}\\ \mathbf{d}\end{bmatrix} \qquad (55)$$

In addition, there are "measurement" variables $\mathbf{y} = \mathbf{G}^y\mathbf{u} + \mathbf{G}_d^y\mathbf{d}$. *If there exists $n_y \geqslant n_u + n_d$ independent measurements (where "independent" means that the matrix* $\bar{\mathbf{G}}^y = [\mathbf{G}^y \quad \mathbf{G}_d^y]$ *has full rank), then the optimal solution to (55) has the property that there exists $n_c = n_u$ linear variable combinations (constraints)* $\mathbf{c} = \mathbf{H}\mathbf{y}$ *that are invariant to the disturbances d. Here,* **H** *may be obtained from the nullspace method using*

•V. Alstad and S. Skogestad, ``Null Space Method for Selecting Optimal Measurement Combinations as Controlled Variables", Ind. Eng. Chem. Res, 46 (3), 846-853 (2007).

35

Quadratic optimization problems

- With noise / implementation error (n ≠ 0)
- Reformulation of exact local method of Alstad et al. (2008)
  - **Can add linear constraints (c=Hy) with minimum loss.**
  - **Have explicit expression for H from "exact local method"**

$$\mathbf{H}^{\mathrm{T}} = (\tilde{\mathbf{F}}\tilde{\mathbf{F}}^{\mathrm{T}})^{-1}\mathbf{G}^{y}(\mathbf{G}^{y\mathrm{T}}(\tilde{\mathbf{F}}\tilde{\mathbf{F}}^{\mathrm{T}})^{-1}\mathbf{G}^{y})^{-1}\mathbf{J}_{uu}^{1/2} \qquad (31)$$

Theorem 4. (Loss by introducing linear constraint for noisy quadratic optimization problem). *Consider the unconstrained quadratic optimization problem in Theorem 3,*

$$\min_{\mathbf{u}} \mathbf{J}(\mathbf{u},\mathbf{d}) = \begin{bmatrix}\mathbf{u} & \mathbf{d}\end{bmatrix}\begin{bmatrix}\mathbf{J}_{uu} & \mathbf{J}_{ud}\\ \mathbf{J}_{ud}^{\mathrm{T}} & \mathbf{J}_{dd}\end{bmatrix}\begin{bmatrix}\mathbf{u}\\ \mathbf{d}\end{bmatrix}$$

and a set of noisy measurements $\mathbf{y}_m = \mathbf{y} + \mathbf{n}^y$, *where* $\mathbf{Y} = \mathbf{G}^y\mathbf{u} + \mathbf{G}_d^y\mathbf{d}$. *Assume that $n_c = n_u$ constraints* $\mathbf{c} = \mathbf{H}\mathbf{y}_m = \mathbf{c}_s$ *are added to the problem, which will result in a non-optimal solution with a loss $L = J(u,d) - J_{\text{opt}}(d)$. Consider disturbances* **d** *and noise* $\mathbf{n}^y$ *with magnitudes*

$$\mathbf{d} = \mathbf{W}_d\mathbf{d}'; \quad \mathbf{n}^y = \mathbf{W}_{n^y}\mathbf{n}^{y\prime}; \quad \left\|\begin{bmatrix}\mathbf{d}'\\ \mathbf{n}^{y\prime}\end{bmatrix}\right\|_2 \leqslant 1$$

Then for a given **H**, *the worst-case loss is* $L_{\text{wc}} = \bar{\sigma}(\mathbf{M})^2/2$, *where* **M** *is given in (20)–(22), and the optimal* **H** *that minimizes $\bar{\sigma}(\mathbf{M})$ is given by (31) in Theorem 1. This optimal* **H** *also minimizes* $\|\mathbf{M}\|_{\mathrm{F}}$.

•V. Alstad, S. Skogestad and E.S. Hori, ``Optimal measurement combinations as controlled variables", Journal of Process Control, 18, in press (2008).

36

Optimal control / Explicit MPC

- Treat initial state x_0 as disturbance d. Discrete time constrained MPC problem:

$$\min_U \frac{1}{2}\begin{bmatrix} U^T & d^T \end{bmatrix}\begin{bmatrix} H & F \\ F & Y \end{bmatrix}\begin{bmatrix} U \\ d \end{bmatrix}$$
$$\text{s.t. } GU \leq W + Ed,$$

- In each active constraint region this becomes an unconstrained quadratic optimization problem ⇒ *Can use above results to find linear constraints*

1. State feedback with no noise (LQ problem)

Measurements: y = [u x]

Linear constraints: c = H y = u – K x

- $n_x = n_d$: No loss (solution unchanged) by keeping c = 0, so $u = Kx$ *optimal*!
- Can find optimal feedback K from "nullspace method", $H \in \mathcal{N}(F^T)$
  - Same result as solving Riccatti equations
- *NEW INSIGHT EXPLICIT MPC: Use change in sign of c for neighboring regions to decide when to switch regions*

•H. Manum, S. Narasimhan and S. Skogestad, ``A new approach to explicit MPC using self-optimizing control", ACC, Seattle, June 2008.

37

Explicit MPC. State feedback.

Second-order system

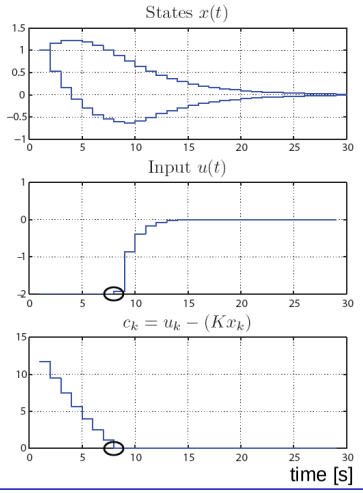

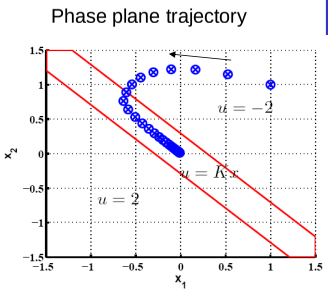

38

Optimal control / Explicit MPC

2. Output feedback (All states <u>not</u> measured). No noise

- Option 1: State estimator
- Option 2: Direct use of measurements for feedback

"Measurements": y = [u y_m]

Linear constraints: c = H y = u – K y_m

- No loss (solution unchanged) by keeping c = 0 (constant), so $u = Ky_m$ *is optimal,* <u>provided</u> we have enough independent measurements:

$n_y \geq n_u + n_d \quad \Rightarrow \quad n_{ym} \geq n_d$

- Can find optimal feedback K from "self-optimizing nullspace method"
- *Can also add previous measurements, but get some loss due to causality (cannot affect past outputs)*

H. Manum, S. Narasimhan and S. Skogestad, ``Explicit MPC with output feedback using self-optimizing control", IFAC World Congress, Seoul, July 2008.

39

Explicit MPC. Output feedback

Second-order system

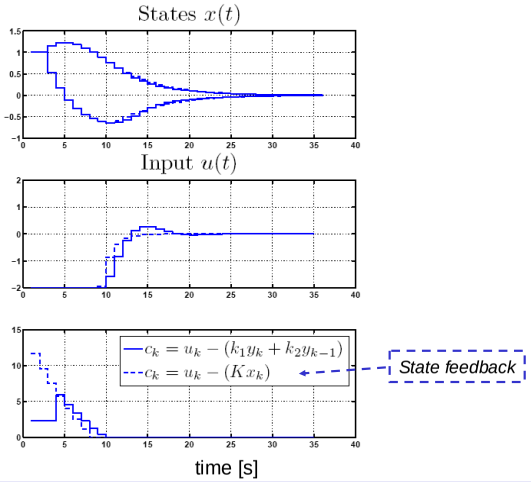

40

Optimal control / Explicit MPC

2. Output feedback – Further extensions

- Explicit expressions for certain fix-order optimal controllers
- Example: Can find optimal multivariable PID controller by using as "measurements"
  - Current output (P)
  - Sum of outputs (I)
  - Change in output (D)

41

Optimal control / Explicit MPC

3. Further extension: Output feedback with noise

- Option 1: State estimator
- Option 2: Direct use of measurements for feedback

  "Measurements": $y = [u \;\; y_m]$

  Linear constraints: $c = H y = u - K y_m$
- Loss by using this feedback law (adding these constraints) is minimized by computing feedback K using "exact local method"

$$\mathbf{H}^{\mathrm{T}} = (\widetilde{\mathbf{F}}\widetilde{\mathbf{F}}^{\mathrm{T}})^{-1}\mathbf{G}^{y}(\mathbf{G}^{y\mathrm{T}}(\widetilde{\mathbf{F}}\widetilde{\mathbf{F}}^{\mathrm{T}})^{-1}\mathbf{G}^{y})^{-1}\mathbf{J}_{uu}^{1/2}$$

42

H. Manum, S. Narasimhan and S. Skogestad, ``Explicit MPC with output feedback using self-optimizing control", IFAC World Congress, Seoul, July 2008.

Conclusion

- Simple control policies are always preferred in practice (if they exist and can be found)
- **Paradigm 2**: Use off-line optimization and analysis to find simple near-optimal control policies suitable for on-line implementation
- Current research: Several interesting extensions
  - Optimal region switching
  - Dynamic optimization
  - Explicit MPC

- *Acknowledgements*
  - *Sridharakumar Narasimhan*
  - *Henrik Manum*
  - *Håkon Dahl-Olsen*
  - *Vinay Kariwala*

43

Noncooperative Cooperation

Jeff Shamma
Electrical and Computer Engineering
Georgia Institute of Technology

Joint work with J. Marden & G. Arslan

Benelux Meeting 2008
March 19 & 20, 2008

Game theory: Descriptive agenda

- Descriptive agenda = modeling
- Noncooperative game setting:
  - Set of players & actions
  - Repeated interactions guided by:
    - Player preferences
    - Available information
- Metrics:
  - Reasonable description of sociocultural phenomena?
  - Matches available experimental/observational data?

3

Multiagent scenarios

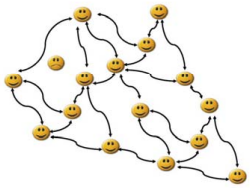

- Distributed routing
- Evolution of convention
- Social network formation

2

More multiagent scenarios

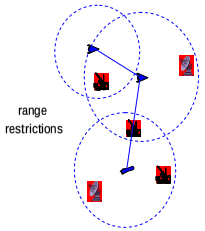

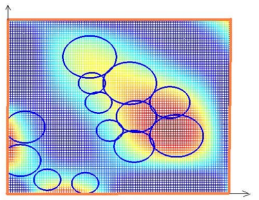

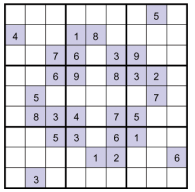

- Weapon target assignment
- Mobile sensor allocation
- Sudoku?

4

Multiagent sudoku

- Global objective: Solve puzzle
- Model cells as "agents"
  - Set of actions
  - Payoff functions
- Appeal:
  - Local processing
  - Fault tolerance
  - Adversarial robustness
  - Rich starting point

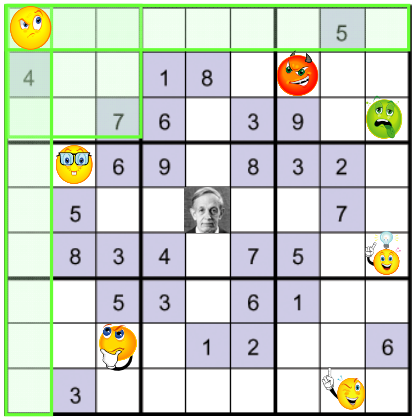

5

Game theory: Prescriptive agenda

- Prescriptive agenda = distributed robust optimization
- *Choose* to address cooperation as noncooperative game
- Must *specify*
  - Elements of game (players, actions, payoffs)
  - Adaptation algorithm
- Metrics:
  - Information available to agent?
  - Communications/stage?
  - Processing/stage?
  - Asymptotic behavior?
  - Global objective performance?
  - Convergence rates?

6

Outline

- Learning in games framework
- Potential games
- Survey of algorithms
- Methods of proofs
- Illustrations

7

Learning in games

- Setup:
  - Players: $\{1, 2, \ldots, P\}$
  - Actions: $a_i \in \mathcal{A}_i$
    $(a_1, a_2, \ldots, a_P) \in \mathcal{A} = \mathcal{A}_1 \times \mathcal{A}_2 \times \ldots \times \mathcal{A}_P$
  - Payoffs: $U_i : (a_1, a_2, \ldots, a_P) = (a_i, a_{-i}) \mapsto \mathbf{R}$
  - Global objective: $G : \mathcal{A} \to \mathbf{R}$
- Iterations:
  - $t = 0, 1, 2, \ldots$
  - $a_i(t) = \texttt{rand}(s_i(t)), \quad s_i(t) \in \Delta(\mathcal{A}_i)$
  - $s_i(t) = \mathcal{F}_i(\text{available info at time } t)$

8

Nash equilibrium

- Action profile $a^* \in \mathcal{A}$ is a ***Nash equilibrium*** (NE) if for all players:

$$U_i(a_1^*, a_2^*, \ldots, a_P^*) = U_i(a_i^*, a_{-i}^*) \geq U_i(a_i', a_{-i}^*)$$

  i.e., no ***unilateral*** incentive to change actions.

- Note: No mention of global objective
  - Is the global objective maximized at a NE?
  - Are NE efficient?

9

(Ordinal) Potential games

- For some $\phi : \mathcal{A} \to \mathbf{R}$

$$\phi(a_i, a_{-i}) - \phi(a_i', a_{-i}) > 0$$
$$\Leftrightarrow$$
$$U_i(a_i, a_{-i}) - U_i(a_i', a_{-i}) > 0$$

i.e., potential function increases iff unilateral improvement

- Features:
  - Typical of "coordination games"
  - Desirable convergence properties under various algorithms
  - Need not imply "cooperation" or $\phi = G$

10

Illustration: Distributed routing

- Payoff = negative congestion

$$c_r(N_r)$$

- Potential function:

$$\phi = \sum_r \sum_{n=1}^{N_r} c_r(n)$$

- Overall congestion:

$$G = \sum_r N_r c_r(N_r)$$

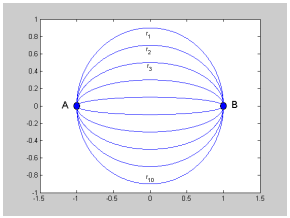

11

Learning algorithms

- Starting point: Potential games
- Algorithms:
  - Fictitious play
  - Regret monitoring
  - Spatial adaptive play
- Focus:
  - Asymptotic behavior
  - Processing per stage
  - Communications per stage

12

Fictitious play (FP)

- Each player:
  - Maintains empirical frequencies (histograms) of other player actions
  - Assumes (incorrectly) that others are playing randomly and independently according to empirical frequencies
  - Selects an action that maximizes expected payoff
- Bookkeeping is "action based"
- Monderer & Shapley (1996): FP converges to a NE in potential games.

13

FP bookkeeping

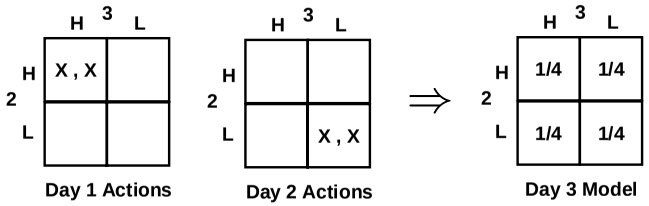

- Viewpoint of driver 1 for 3 drivers & 2 roads (High & Low)
- Prohibitive-per-stage for large numbers of players with large action sets:
  - Monitor all other players with IDs (cf., distributed routing)
  - Takes expectation over large joint action space (cf., Sudoku)
- Possible to exploit sparse payoff interconnection

14

Virtual payoffs

- Define virtual payoff vector (player dependence suppressed):

$$V_j(t+1) = V_j(t) + \rho\Big(U_i(j, a_{-i}(t)) - V_j(t)\Big)$$

- Interpretation: Payoff that *would have* been obtain had agent *i* used action *j*
- Stepsize: Either constant (fading memory) or $\rho = \frac{1}{t+1}$ (averaging)
- Bookkeeping is "oracle based" (cf., traffic reports)

15

Joint strategy fictitious play (JSFP) with inertia

- Each player:
  - Maintains virtual payoff vectors
  - Selects an action that maximizes virtual payoff
  - *OR* repeats previous stage action with some probability (i.e., inertia)
- Marden, Arslan, & JSS (2005): JSFP with inertia converges to a NE in potential games.

16

JSFP bookkeeping

- Equivalent to best response to *joint actions* of other players

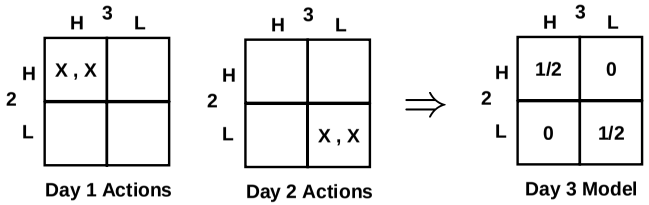

- Related to "no regret" algorithms (cf. Arslan, Marden & JSS (2007))

17

Equilibrium selection & Gibbs distribution

- Alternative algorithms offer more quantitative characterization of asymptotic behavior.
- Preliminary: Gibbs distribution (cf., softmax, logit response)

$$\sigma(v_1,\ldots,v_n;T)=\begin{pmatrix}\frac{e^{v_1/T}}{e^{v_1/T}+\cdots+e^{v_n/T}}\\ \vdots\\ \frac{e^{v_n/T}}{e^{v_1/T}+\cdots+e^{v_n/T}}\end{pmatrix}\subset\Delta$$

- As $T\downarrow 0$ assigns all probability to $\arg\max\{v_1,\ldots,v_n\}$

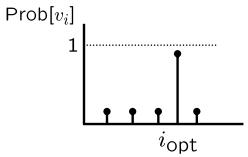

18

Spatial adaptive play (SAP)

- At stage *t*: Player *i* is selected at random
  - Chosen player sets next action according to distribution
    $$\sigma\big(U_i(1,a_{-i}(t-1)),\ldots,U_i(n,a_{-i}(t-1));T\big)$$
  - Interpretation: Softmax best reply to previous joint actions
- Fact: SAP results in Markov chain on *joint action space* $\mathcal{A}$ with unique stationary distribution π(a).
- Young (1998): In (cardinal) potential games:
  $$\pi(a)=\sigma(\phi(a);T)=e^{\phi(a)/T}/\textstyle\sum_{a'\in\mathcal{A}}e^{\phi(a')/T}$$
- As $T\downarrow 0$ assigns all probability to potential maximizer

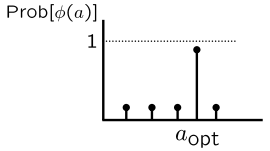

19

Binary SAP

- Motivation:
  - Reduced processing per stage
  - First step towards constrained actions
- At stage *t*:
  - Player *i* is selected at random
  - Chosen player sets next action according to distribution
    $$(a_i(t-1),a_i')\sim\sigma(U_i(a_i(t-1),a_{-i}(t-1)),U_i(a_i',a_{-i}(t-1));T)$$
    where a_i' is a randomly selected alternative
- Arslan, Marden, & JSS (2007): *Same* stationary distribution as SAP.
- Consequence: Arbitrarily high steady state probability on potential function maximizer.

20

Payoff based algorithms

- Action & oracle based algorithms require:
  - Explicit communications
  - Explicit representations of payoff functions
- Payoff based algorithms:
  - No (explicit) communication among agents
  - Only requires ability to *measure* payoff upon deployment

21

Experimentation dynamics

- Initialization of *baseline Action* and *baseline utility*:

$$a_i^b(1) = a_i(0)$$
$$u_i^b(1) = U_i(a(0))$$

- Action selection:

$a_i(t) = a_i^b(t)$ with probability $(1-\epsilon)$

$a_i(t)$ is chosen randomly (uniformly) over $\mathcal{A}_i$ with prob ϵ

- Baseline action and baseline utility update:

Successful Experimentation	*Unsuccessful Experimentation*	*No Experimentation*
$a_i(t) \neq a_i^b(t)$	$a_i(t) \neq a_i^b(t)$	$a_i(t) = a_i^b(t)$
$U_i(a(t)) > u_i^b(t)$	$U_i(a(t)) \leq u_i^b(t)$	
$a_i^b(t+1) = a_i(t)$	$a_i^b(t+1) = a_i^b(t)$	$a_i^b(t+1) = a_i^b(t)$
$u_i^b(t+1) = U_i(a(t))$	$u_i^b(t+1) = u_i^b(t)$	$u_i^b(t+1) = U_i(a(t))$

22

Experimentation dynamics, cont

- Marden, Young, Arslan & JSS (2007): For potential games,

$$\liminf_{t\to\infty} \text{Prob}[a(t) \text{ is a NE}] > p$$

for any $p < 1$ provided sufficiently small exploration rate ε.

- Suitably modified algorithm admits *noisy utility measurements*.

23

Payoff assignment

- How to assign individual payoff functions?
- Desirable features:
  - Induce "localization"
  - Have desirable NE
  - Produce potential game
- Obvious possibility: Global utility, i.e., $U_i(a) = G(a)$
- Disadvantages:
  - Is not localized
  - Low signal/noise ratio in case of noisy payoff based algorithms

24

Illustration: Sensor placement

- Sensors (players):
  - g: Prob(detect) = 0.9
  - b: Prob(detect) = 0.1
- Search space rewards (L,H): (2,3)
- Optimal: g = H & b = L

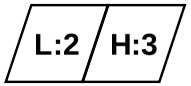

g \ b	L	H
L	0.91, 0.91	1.8, 0.3
H	2.7, 0.2	1.37, 1.37

Equally Shared Incentives

(No Pure NE)

g \ b	L	H
L	1.8, 0.2	1.8, 0.3
H	2.7, 0.2	2.7, 0.3

Selfish Incentives

(Global optimum not NE)

25

Marginal contribution payoff

- Introduce “null” action, 0
- Interpretation: Context dependent
- Define:

$$U_i(a_i, a_{-i}) = G(a_i, a_{-i}) - G(\mathbf{0}, a_{-i})$$

  i.e., unilateral marginal contribution (also called “wonderful life utility”)
- Advantages:
  - Results in a potential game…with $\phi = G$
  - Can induce “localization” effect in presence of spatial separation
  - For sensor placement: Marginal contribution in selected cell

26

Proofs: Better reply graph

- Better reply graph
  - Nodes: Joint actions
  - Directed edges: Better reply for *unilaterally* deviating player
- Illustration: 3 players, 2 moves
- Features:
  - Potential increases along edges
  - NE iff no outgoing edges

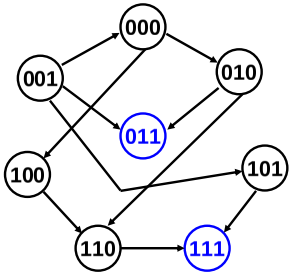

27

Proofs: Sticky NE

- Recall JSFP with inertia:
  - Players monitor virtual payoff vector & choose maximizing action
  - OR repeat previous action with some probability
  - Virtual payoff maximizer is *not* best reply to previous stage
- A path to NE that occurs with $\varepsilon > 0$ probability:
  - Players linger (inertia)…
  - Eventually, maximizer of virtual payoff = best reply to joint action
  - Single player deviates if not NE
  - Repeat
- NE + lingering implies permanent NE
- Cannot avoid NE path indefinitely…

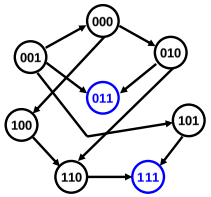

28

Proofs: Steady state Gibbs distribution

- Recall (binary) SAP
  - Single agent, randomly selected
  - Uses Gibbs distribution to select next action
- Features:
  - Node hops not limited to better replies (softmax)
  - Better replies have higher probabilities
- Detailed balance equation:

$$\text{Prob}[a \to a']\pi(a) = \text{Prob}[a' \to a]\pi(a')$$

(stronger condition than stationary distribution)

- Proof: Transition probabilities under SAP satisfy detailed balance equation with Gibbs distribution.

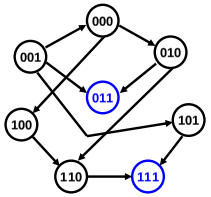

29

Restricted SAP

- Restricted action set:

$$a_i(t) \in \mathcal{R}(a_i(t-i))$$

- Consequence: Some better replies eliminated
- Potential function *still* increases in remaining graph
- Marden, Arslan & JSS (2007): Under assumptions of:
  - Reachability
  - Reversability

suitably modified binary SAP still results in Gibbs distribution of potential function

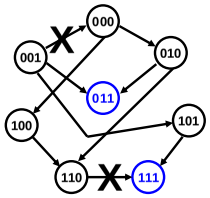

30

Proofs: Stochastic stability

- Coarsening of Gibbs distribution conclusion
- Stochastic stability:
  - Let $\pi(\varepsilon)$ denote the stationary distribution of an ε-dependent Markov chain
  - Let $\pi(0) = \lim_{\varepsilon \downarrow 0} \pi(\varepsilon)$
  - Stochastically stable states are those in the support of $\pi(0)$
- Implication: Increasing probability of being in stochastically stable state with decreasing ε.

31

Proofs: Stochastic stability, cont

- Proof of experimentation dynamics: *Establish NE are stochastically stable*
- Young (1993): To determine stochastic stability:
  - View learning dynamics as ε-perturbation of reference ($\varepsilon = 0$) Markov chain
  - Divide reference Markov chain into recurrence classes
  - Define "resistance" to transition recurrence classes

$$0 < \lim_{\varepsilon \downarrow 0} \frac{P_{ij}^{\varepsilon}}{\varepsilon^{r(i \to j)}} < \infty$$

  - Form stochastic potential for each recurrence class
  - Minimal stochastic potential implies stochastic stability

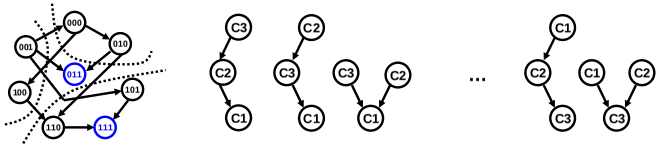

32

Illustration: Rendezvous with obstacles

- Assume undirected connected constant graph (can be generalized)
- Global objective:

$$\phi(a_i, a_{-i}) = -\frac{1}{2} \sum_{\mathcal{P}_k \in \mathcal{P}} \sum_{\mathcal{P}_j \in N_k} \|a_k - a_j\|$$

- Global objective without agent *i*

$$\phi(a_i^0, a_{-i}) = -\frac{1}{2} \sum_{\mathcal{P}_k \neq \mathcal{P}_i} \sum_{\mathcal{P}_j \in N_k \setminus \mathcal{P}_i} \|a_k - a_j\|$$

- Marginal contribution utility

$$\begin{aligned} U_i(a_i, a_{-i}) &= \phi(a_i, a_{-i}) - \phi(a_i^0, a_{-i}) \\ &= -\sum_{\mathcal{P}_j \subset N_i} \|a_i - a_j\| \end{aligned}$$

- Apply (restricted) binary SAP…

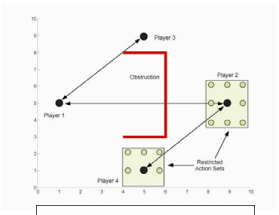

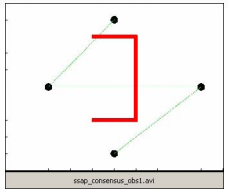

33

Illustration: Sensor allocation

- Objective: Maximize (sensor location dependent) expected reward

$$\phi(a) = \sum_{x \in X} R(x) P(x, a)$$

$$P(x, a) = 1 - \prod_{i=1}^{n} (1 - p_i(x, a_i))$$

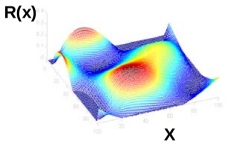

- Implementation:
  - Define marginal contribution utility
  - Apply (restricted) binary SAP…
- Can incorporate joint detection probabilities

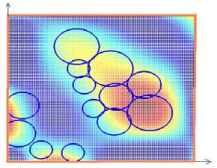

35

Illustration: Distributed routing

- Setup: 10 roads, 100 vehicles
- Marginal contribution utility using overall congestion induces "tolls"

$$\tau_r(k) = (k-1) \cdot (c_r(k) - c_r(k-1))$$

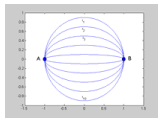

- Apply JSFP with inertia…

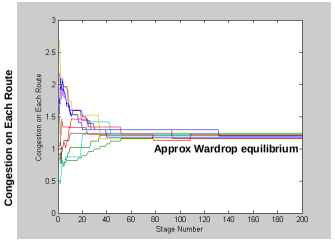

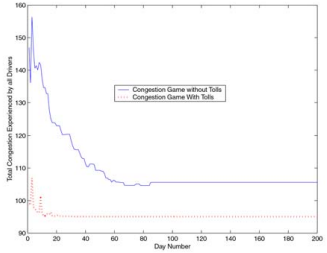

34

Illustration: Sudoku

- Cell utility penalizes repetition in row, column, and sector (with repetition)

$$U_i(a) = n_i(a, N_i^R) + n_i(a, N_i^C) + n_i(a, N_i^B)$$

- Resulting potential is sum of individual potentials: $\phi(a) = \sum_{\mathcal{P}_i} U_i(a)$

	1		5		7		6	
		6	9		2	7		
7								9
		4		7		9		
2								3
		8		1		6		
6								4
		7	3		1	5		
	3		8		6		1	

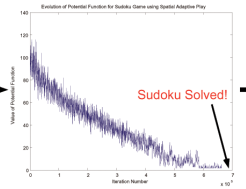

9	1	3	5	8	7	4	6	2
5	4	6	9	3	2	7	8	1
7	8	2	1	6	4	3	5	9
1	5	4	6	7	3	9	2	8
2	6	9	4	5	8	1	7	3
3	7	8	2	1	9	6	4	5
6	9	1	7	2	5	8	3	4
8	2	7	3	4	1	5	9	6
4	3	5	8	9	6	2	1	7

36

Final Remarks

- Recap:
  - Action/Oracle/Payoff based algorithms
  - NE or potential function maximization
  - Potential games & payoff design
  - Multiple illustrations under common framework
- Future work:
  - Convergence rates
  - State dependencies
  - *Systems, controls, and the descriptive agenda*

37

Learning in Games under Dynamic Reinforcement

Jeff Shamma
Electrical and Computer Engineering
Georgia Institute of Technology

Joint work with G. Arslan & G. Chasparis

Benelux Meeting 2008
March 19 & 20, 2008

Outline

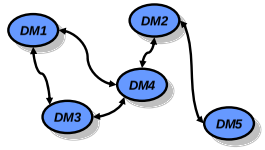

- Simple learning models & Nash equilibrium
- Feedback control & "dynamic reinforcement"
- Implications in various settings

3

Noncooperative ~~cooperation~~ learning

- Setup: Multiple decision makers
  - Private preferences
  - Graphical dependencies
  - *Absence of cooperative structure*

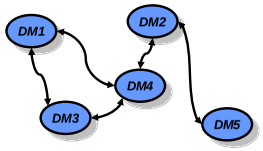

- Background:
  - Biological models (*Evolution and the Theory of Games*, J. Maynard Smith, 1982)
  - Sociocultural models (*Individual Strategy & Social Structure*, H. Peyton Young, 2001)
  - Many monographs…
- Learning challenge:
  - Single agent: Stationary environment
  - Multiagent: *Reactive & equally capable* environment
- Motivation: Explore role of Nash equilibrium in "descriptive" agenda
  - Dynamics away from equilibrium
  - Bounded rationality

2

Shapley "fashion" game

- 2 players, each with 3 moves: {*Red*, *Green*, *Blue*}
- *Private roles:*
  - Player1: Fashion leader wants to differ from Player2
  - Player2: Fashion follower wants to copy Player1
- Daily routine:
  - Play game
  - Observe actions
  - Update strategies
  - "Strategies" are probabilities of move

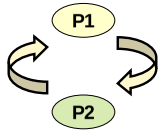

4

Jordan "anti-coordination" game

- 3 players, each with 2 moves: {*Left*, *Right*}
- Private roles:
  - Player1 wants to differ from Player2
  - Player2 wants to differ from Player3
  - Player3 wants to differ from Player1
- Daily routine:
  - Play game
  - Observe actions
  - Update strategies

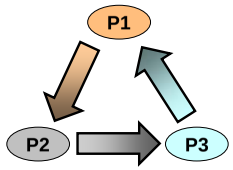

5

Recurring question

- Nash Equilibrium: No *unilateral* incentive to alter strategy.

  How can simple rules lead players to a Nash equilibrium?

- "Mixed strategy" NE problematic
- Separate issues:
  - Will they?
  - Should they?
  - How to compute NE?

6

Nonconvergence

- Shapley game (1964) introduced as *counterexample* to show Nash convergence might not occur in "fictitious play"
- Fudenberg & Tirole (1991), "Game Theory", MIT Press: "*Game theory lacks a general and convincing argument that a Nash outcome will occur*"
- Crawford (1985), "Learning behavior and mixed strategy in Nash equilibria": *specific class of learning algorithms unstable.*
- Krishna and Sjostrom (1998), "On the convergence of fictitious play": *almost all multiagent multimove (>2) games cannot converge to mixed equilibrium.*
- Hofbauer and Hopkins (2005), "Learning in perturbed asymmetric games": "*A mixed equilibrium is asymptotically stable under all such dynamics [FP] if and only if the game is linearly equivalent to a zero sum game.*"
- Sato et al (2002), "Chaos in learning a simple two-person game", PNAS: *"Many economists have noted the lack of any compelling account of how agents might learn to play a Nash equilibrium. Our results strongly reinforce this concern, in a game simple enough for children to play."*

7

Categorical nonconvergence

Uncoupled Dynamics Do Not Lead to Nash Equilibrium

Sergiu Hart & Andreu Mas-Colell

Abstract

We call a dynamical system *uncoupled* if the dynamic for each player does *not* depend on the payoff functions of the other players. We show that there are no uncoupled dynamics that are guaranteed to converge to Nash equilibrium, even when the Nash equilibrium is unique.

American Economic Review 2003

- Continuous time Jordan game is universal counterexample.
- Work around: Discrete time, stochastic, approximate NE.

8

Learning in games

- Setup:
  - Players: $\{1, 2, \ldots, P\}$
  - Actions:

    $a_i \in \mathcal{A}_i = \text{vert}[\Delta]$, e.g., $a_i \in \left\{ \begin{pmatrix} 1 \\ 0 \\ 0 \end{pmatrix}, \begin{pmatrix} 0 \\ 1 \\ 0 \end{pmatrix}, \begin{pmatrix} 0 \\ 0 \\ 1 \end{pmatrix} \right\}$

    $(a_1, a_2, \ldots, a_P) \in \mathcal{A} = \mathcal{A}_1 \times \mathcal{A}_2 \times \ldots \times \mathcal{A}_P$
  - Payoffs: $U_i : (a_1, a_2, \ldots, a_P) = (a_i, a_{-i}) \mapsto \mathbf{R}$
- Iterations:
  - $t = 0, 1, 2, \ldots$
  - $a_i(t) = \texttt{rand}(p_i(t)), \quad s_i(t) \in \Delta(\mathcal{A}_i)$
  - $p_i(t) = \mathcal{F}_i(\text{available info at time } t)$

9

Repeated games in continuous time

- Empirical frequencies:

$$q_i(k+1) = q_i(k) + \frac{1}{k+1}(\texttt{rand}(p_i(k)) - q_i(k))$$
$$\Downarrow$$
$$\dot{q}_i(t) = -q_i(t) + p_i(t)$$

- ODE method of stochastic approximation:

Deterministic continuous time analysis

$\Downarrow$

Probabilistic discrete time conclusions

10

Smooth fictitious play (FP)

- Define smoothed best response:

$$\beta(v) = \arg\max_{s \in \Delta} s^T M v + \tau \mathcal{H}(s)$$
$$= \text{softmax}(Mv; \tau)$$

- Today's strategy is *best response* to empirical frequencies:

$$\dot{q}_1(t) = -q_1(t) + \beta_1(q_2(t))$$
$$\dot{q}_2(t) = -q_2(t) + \beta_2(q_1(t))$$

11

Convergence properties for FP

- Convergent cases:
  - zero-sum games (1951)
  - 2x2 games (1961)
  - potential games (1996)
  - 2xN games (2003)
- Counterexamples:
  - Shapley fashion game (1964)
  - Jordan anticoordination game (1993)
  - Foster/Young merry-go-round game (1998)

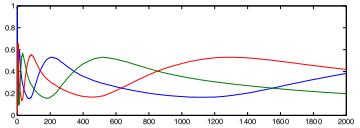

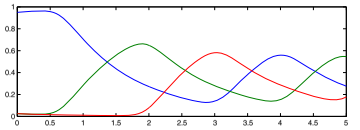

12

Dynamic reinforcement

- Negative results only apply to "static" (i.e., memoryless) strategies:

$$p_i(t) \sim F_i(q_i(t), q_{-i}(t)) \quad \text{e.g.} \quad F_i(q_i(t), q_{-i}(t)) = \beta_i(q_{-i}(t))$$

- Well known: *Static* compensation cannot stabilize all plants

- What if we allow *dynamic* update mechanisms?

$$p_i(t) \sim F_i(q(\cdot))(t)$$

13

Anticipatory/derivative action FP (daFP)

- FP:

$$p_i(t) = \beta_i(q_{-i}(t))$$

- Derivative action FP:

$$p_i(t) = \beta_i(q_{-i}(t) \underbrace{+\gamma \frac{dq_{-i}}{dt}(t)}_{\text{new term}})$$

- "First order" model of adversary: Moving target.
  - Myopic prediction: $q_i(t) + \gamma \dot{q}_i(t) \approx q(t+\gamma)$
  - Approximate inversion ($\gamma = 1$): $q_i(t) + \dot{q}_i(t) \approx p_i(t)$

14

Approximate differentiator implementation

- Ideal ⇒ Implicit Equations

$$\dot{q}_1 = -q_1 + \beta_1(q_2 + \gamma \dot{q}_2)$$
$$\dot{q}_2 = -q_2 + \beta_2(q_1 + \gamma \dot{q}_1)$$

- Approximate (*-i* = other player)

$$\dot{q}_i = \beta_i(q_{-i} + \gamma \dot{r}_{-i}) - q_i$$
$$\dot{r}_i = \lambda(q_i - r_i)$$

- Asymptotically:

$$\left| \frac{dq}{dt} - \frac{dr}{dt} \right| \leq \frac{1}{\lambda} \left| \frac{d^2 q}{dt^2} \right|_{\max}$$

15

Local stability with approximate differentiators

- JSS & Arslan 2005:

  Consider a two-player game with a NE q^*.

  1) FP stable at q^* ⇒ DAFP stable at q^* for *all* $0 \leq \gamma < 1$

  2) FP unstable at q^* with evals $a_i + j\, b_i$ and

$$\max_i \frac{a_i}{a_i^2 + b_i^2} < \frac{1}{\max_i a_i}$$

  ⇒ DAFP stable at q^* for *some* $0 < \gamma < 1$

- Proof: Express evals of DAFP in terms of FP evals

16

Shapley counterexample revisited

- Unique mixed NE is unstable under FP
- $\max_i \frac{a_i}{a_i^2+b_i^2} < \frac{1}{\max_i a_i}$, hence stabilizable by daFP

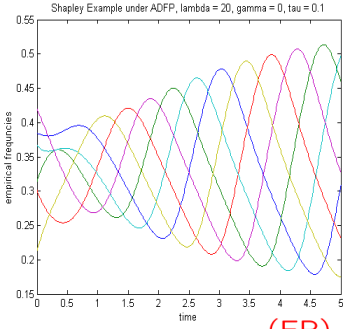

(FP)

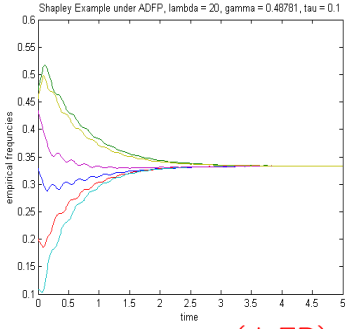

(daFP)

17

Jordan counterexample revisited

- Unique mixed NE is unstable under FP
- $\max_i \frac{a_i}{a_i^2+b_i^2} < \frac{1}{\max_i a_i}$, hence stabilizable by daFP

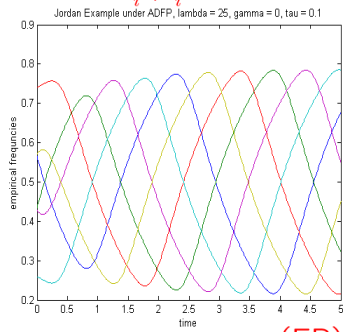

(FP)

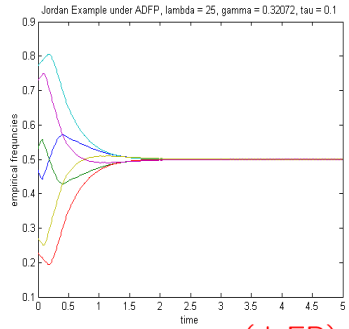

(daFP)

18

Beyond FP

- Similar methods & analysis for broad class of dynamics:
  - Gradient play (better response vs best response)
  - Replicator dynamics
  - X-dynamics
  - Property: Mixed strategy equilibrium *never* stable w/o modification.
- RPS chaos revisited:

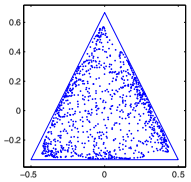

(RD)

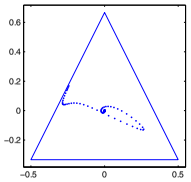

(daRD)

19

Discrete time, payoff based, multiplayer, etc

- Discrete-time implementation:
  - Local attractor in continuous time ⇒ Positive probability of convergence to NE in discrete-time.
  - …as opposed to *Zero* probability.
- Payoff-based implementation:
  - Only measure day-by-day rewards.
  - Similar convergence properties.

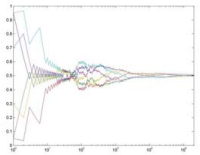

- Multiplayer games: Depends on utility structure.
- Strategic advantage & Unilateral motivation
- References: Arslan & JSS (2004), Mannor, Arslan & JSS (2007)

20

Exchange economy (preliminary)

- **Set of agents:** $i = 1, 2, ..., n$
- **Set of goods:** $j = 1, 2, ..., m+1$
- **Initial endowments:** $w_i \in \mathbb{R}_+^{m+1}, i = 1, 2, ..., n$
- **Utilities:** $U_i : \mathbb{R}_+^{m+1} \to \mathbb{R}, i = 1, 2, ..., n$
- **Prices:** $p \in \mathbb{R}_+^{m+1}$
- **Optimized demand:**

$$d_i^*(p) = \arg\max_d U_i(d)$$
$$p^\top d \leq p^\top w_i$$

- **Excess demand function:** $\xi : p \to \mathbb{R}^{m+1}$

$$\zeta(p) = \sum_{i=1}^{n} d_i^*(p) - w_i$$

21

Exchange economy, cont

- Equilibrium prices: "Supply = Demand"

$$\zeta(p^*) = 0 \iff \sum_{i=1}^{m+1} w_i = \sum_{i=1}^{m+1} d_i^*(p^*)$$

- Homogeneity condition: $\zeta(\alpha p) = \zeta(p)$

- Normalized excess demand: Set $p_{m+1} = 1$

$$F(p_1, ..., p_m) = \zeta(p_1, ..., p_m, 1)$$

(will still use notation "p")

22

Tatonnement

- Tatonnement price mechanism:

$$\frac{dp}{dt} = \zeta(p) \text{ or } \frac{dp}{dt} = F(p)$$

- Interpretation:
  - Price adjuster interacts with agents via excess demands
  - Positive excess demand $\Leftrightarrow$ price increase
  - Admits localized adjustment

23

Scarf's example (1960)

- Three agents and three goods:

$$U_1(q^1, q^2, q^3) = \min(q_1, q_2); w_1 = (1, 0, 0)$$
$$U_2(q^1, q^2, q^3) = \min(q^2, q^3); w_2 = (0, 1, 0)$$
$$U_3(q^1, q^2, q^3) = \min(q^1, q^3); w_3 = (0, 0, 1)$$

- Tatonnement process:

$$\dot{p}_1 = \frac{p_1(1 - p_2)}{(1 + p_1)(p_1 + p_2)}$$
$$\dot{p}_2 = \frac{p_2(p_1 - 1)}{(1 + p_2)(p_1 + p_2)}$$

24

Scarf's example, cont

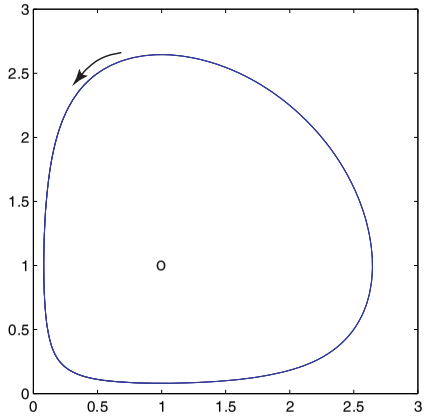

25

Global stability & information requirements

- Newton method: $\frac{dp}{dt} = -(\nabla F(p))^{-1} F(p)$
- Price adjuster requires:
  - Excess demand functions
  - Excess demand sensitivities
  - Global access (via inverse)
- Compare to: $\frac{dp}{dt} = F(p)$

26

Saari & Simon (1978) setup

- Generalized price mechanism, *M*:

$$\frac{dp}{dt} = M(F(p); \nabla F(p))$$
$$M : \mathbb{R}^m \times \mathbb{R}^{m^2} \to \mathbb{R}^m$$

- *Local effective price mechanism:*

  For any smooth excess demand function, *F*, and for any equilibrium, p^*, the point p^* is a local attractor for *M*.

- Example: Newton method

27

Saari & Simon impossibility result

- *Ignorable coordinate:*

  For some y_{ij}

$$\frac{\partial M}{\partial y_{ij}}(x; y) = 0, \quad \forall x, y$$

- Interpretation: *M* never uses specific ∇F component.
- Saari & Simon (1978): For $m \geq 2$, if *M* has an ignorable coordinate, then *M* cannot be a local effective price mechanism.
- Compare to Hart & Mas-Colell, "Uncoupled dynamics"

28

Anticipatory tatonnement

$$\frac{dp}{dt} = F(p) + \gamma \dot{r}$$
$$\dot{r} = \lambda(F(p) - r)$$

- Interpretation: Price increase proportional to *anticipated* excess demand.
- Maintains localized adjustment structure.
- Corollary: Let $a_i + jb_i$ denote evals of ∇F at p^*. Anticipatory tatonnement locally stable for

$$\max_i \frac{a_i}{a_i^2 + b_i^2} < \gamma < \frac{1}{\max_i a_i}$$

- Q: Are there "dynamic" local effective price mechanisms?

29

Scarf's example, revisited

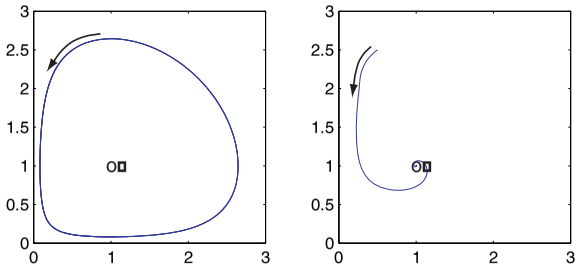

30

Equilibrium selection (preliminary)

- Thus far: Enable stability of mixed strategy NE
- New issue: Equilibrium selection

	A	B
A	4, 4	0, 0
B	0, 0	3, 3

Typewriter Game

	S	H
S	3, 3	0, 1
H	1, 0	1, 1

Stag Hunt

- What equilibrium "should" emerge?
- Alternatives:
  - Payoff dominance (game based)
  - Risk dominance (game based)
  - *Stochastic stability (dynamics based)*

31

Reinforcement learning

- Standard:

$$\Pr[a_i = a_i^*] = \frac{\text{cumulative payoff using action } a_i^*}{\text{total cumulative payoff}}$$

- Recursive form (with ε experimentation):

$$U_i(t+1) = U_i(t) + u_i(a(t))a_i(t)$$
$$x_i(t+1) = x_i(t) + \delta(t)\big(a_i(t) - x_i(t)\big)$$
$$\delta(t) = \frac{u_i(a(t))}{\mathbf{1}^\top U_i(t) + u_i(a(t))}$$
$$p_i(t) = (1 - \varepsilon)x_i(t) + \frac{\varepsilon}{N}\mathbf{1}$$

32

Alternative step size

$$x_i(t+1) = x_i(t) + \delta(t)\big(a_i(t) - x_i(t)\big)$$

$$\delta_{\text{old}}(t) = \frac{u_i(a(t))}{1^\top U_i(t) + u_i(a(t))} \longrightarrow \delta_{\text{new}}(t) = \frac{u_i(a(t))}{t+1}$$

$$p_i(t) = (1-\varepsilon)x_i(t) + \frac{\varepsilon}{N}1$$

- Preserves
  - Payoff based
  - All actions reinforced with familiarity incentive
  - Progressively sluggish

33

Dynamic reinforcement

$$x_i(t+1) = x_i(t) + \frac{u_i(t)}{t+1}\big(a_i(t) - x_i(t)\big)$$

$$y_i(t+1) = y_i(t) + \frac{1}{t+1}\big(x_i(t) - y_i(t)\big)$$

$$p_i(t) = (1-\varepsilon)\Pi_\Delta\left[(x_i(t) + \underbrace{\gamma(x_i(t) - y_i(t))}_{\text{new term}})\right] + \frac{\varepsilon}{N}1$$

- y_i is running average of x_i
- New term reinforces deviations from long run

34

Equilibrium selection & stability

- Chaparis & JSS (2007): A pure NE a^* is locally stable iff

$$0 < \gamma_i < \frac{u_i(a_i^*, a_{-i}^*) - u_i(a_i', a_{-i}^*) + 1}{u_i(a_i', a_{-i}^*)}, \quad \forall a_i' \neq a_i^*$$

- Discrete time implications:
  - Positive probability of convergence if continuous time is locally *stable*
  - Zero probability of convergence if continuous time is locally *unstable*
- Learning implications:
  - Some NE destabilized before others
  - *Single agent* can influence collective (agent based fragility?)

35

Illustration: Coordination game

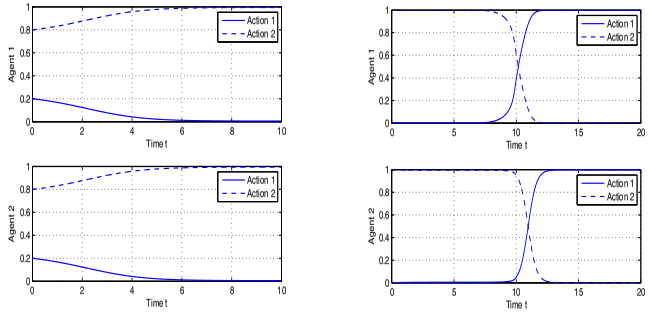

- Two equilibria: "All A" or "All B"
- Both are stable attractors for RL
- Only "All A" stable if *single agent* uses dynamic RL

Dynamic reinforcement reinforcement induces qualitative change

36

Illustration: Network formation

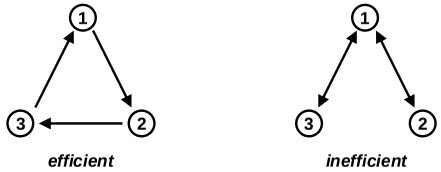

- Setup:
  - Agents form links
  - Benefit from derived number of connections
  - Penalized by number of links
- Both above networks are NE
- Dynamic RL induces efficiency

37

Final Remarks

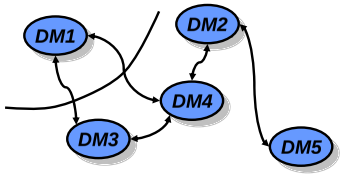

- Game theory for controls:
  - Zero-sum games vs all-knowing nature
  - "Team theory" popular in 70's
  - Networked controls systems ripe with opportunities

    (Correlated equilibrium, Folk theorems, Mechanism design, Coalitions, Bargaining, etc)
- Controls for game theory:
  - Our domain: Sequential decision making under dynamic & uncertain environments
  - DM_i is in *feedback* with other DM's
  - Strategic adjustment = Feedback control

38

The port-Hamiltonian approach to physical system modeling and control

Arjan van der Schaft, University of Groningen

Hans Zwart, University of Twente

In collaboration with Bernhard Maschke, Romeo Ortega, Stefano Stramigioli, Alessandro Macchelli, Peter Breedveld, Dimitri Jeltsema, Jacquelien Scherpen, Morten Dalsmo, Guido Blankenstein, Damien Eberard, Goran Golo, Ram Pasumarthy, Javier Villegas, Gerardo Escobar, Guido Blankenstein ..

Part I : Network Modeling and Analysis
Part II : Control of Port-Hamiltonian Systems
Part III : Distributed-Parameter Systems (Hans Zwart)

Part I : Network Modeling and Analysis

1. Motivation and context
2. From passive systems to port-Hamiltonian systems
3. Some properties of port-Hamiltonian systems
4. Intro to distributed-parameter port-Hamiltonian systems
5. Mixed lumped- and distributed-parameter port-Hamiltonian systems
6. Conclusions of Part I

From passive systems to port-Hamiltonian systems

A square nonlinear system

$$\Sigma: \quad \begin{aligned} \dot{x} &= f(x) + g(x)u, \quad u \in \mathbb{R}^m \\ y &= h(x), \qquad\qquad y \in \mathbb{R}^m \end{aligned}$$

where $x \in \mathbb{R}^n$ are coordinates for an n-dimensional state space $\mathcal{X}$, is **passive** if there exists a **storage function** $H : \mathcal{X} \to \mathbb{R}$ with $H(x) \geq 0$ for every x, such that

$$H(x(t_2)) - H(x(t_1)) \leq \int_{t_1}^{t_2} u^T(t) y(t) dt$$

for all solutions $(u(\cdot), x(\cdot), y(\cdot))$ and times $t_1 \leq t_2$.
The system is **lossless** if $\leq$ is replaced by $=$.

If H is *differentiable* then 'passive' is equivalent to (Willems, Hill-Moylan)

$$\begin{aligned} \frac{\partial^T H}{\partial x}(x) f(x) &\leq 0 \\ h(x) &= g^T(x) \frac{\partial H}{\partial x}(x) \end{aligned}$$

while in the lossless case $\leq$ is replaced by $=$. In the *linear* case

$$\begin{aligned} \dot{x} &= Ax + Bu \\ y &= Cx \end{aligned}$$

is passive if there exists a *quadratic* storage function $H(x) = \frac{1}{2} x^T Q x$, with $Q = Q^T \geq 0$ satisfying the LMIs

$$A^T Q + QA \leq 0, \quad C = B^T Q$$

Every *linear* passive system with storage function $H(x) = \frac{1}{2}x^T Q x$, satisfying

$$\ker Q \subset \ker A$$

can be rewritten as a linear **port-Hamiltonian system**

$$\begin{aligned} \dot{x} &= (J-R)Qx + Bu, \quad J = -J^T, \quad R = R^T \geq 0 \\ y &= B^T Q x, \end{aligned}$$

in which case the storage function $H(x) = \frac{1}{2}x^T Q x$ is called the **Hamiltonian**.

- **Passive linear systems are thus port-Hamiltonian with non-negative Hamiltonian.**
- *Conversely* **every port-Hamiltonian system with non-negative Hamiltonian is passive.**

Mutatis mutandis 'most' nonlinear lossless systems can be written as a port-Hamiltonian system

$$\begin{aligned} \dot{x} &= J(x)\frac{\partial H}{\partial x}(x) + g(x)u \\ y &= g^T(x)\frac{\partial H}{\partial x}(x) \end{aligned}$$

with $J(x) = -J^T(x)$ and $\frac{\partial H}{\partial x}(x)$ the *column vector* of partial derivatives. Note that

$$\dot{x} = J(x)\frac{\partial H}{\partial x}(x)$$

is the internal Hamiltonian dynamics known from physics, which in classical mechanics can be written as

$$\begin{aligned} \dot{q} &= \frac{\partial H}{\partial p}(q,p) \\ \dot{p} &= -\frac{\partial H}{\partial q}(q,p) \end{aligned}$$

with the Hamiltonian H the total (kinetic + potential) energy.

Similarly, most nonlinear passive systems can be written as a port-Hamiltonian system (with dissipation)

$$\begin{aligned} \dot{x} &= [J(x) - R(x)]\frac{\partial H}{\partial x}(x) + g(x)u \\ y &= g^T(x)\frac{\partial H}{\partial x}(x) \end{aligned}$$

with $R(x) = R^T(x) \geq 0$ specifying the energy dissipation

$$\frac{d}{dt}H = -\frac{\partial^T H}{\partial x}(x)R(x)\frac{\partial H}{\partial x}(x) + u^T y$$

However, in *network modeling* it is the **other way around**: one derives the system in port-Hamiltonian form (and if the Hamiltonian $H \geq 0$ then it is the storage function of a passive system).

The matrix $J(x)$ corresponds to the internal **power-conserving interconnection** structure of physical systems due to:

- Basic conservation laws such as Kirchhoff's laws.
- Powerless constraints; kinematic constraints.
- Transformers, gyrators, exchange between different types of energy.

The matrix $R(x)$ corresponds to the **internal energy dissipation** in the system (due to resistors, damping, viscosity, etc.)
Main message: **start with port-Hamiltonian models instead of passive models**. Closer to physical modeling, and capturing more information than just the energy-balance of passivity.

A bit of port-based network modeling

The **passivity** framework considers a system component, and its power-exchange with other system components:

$$\frac{d}{dt}H \leq u^T y$$

The feedback interconnection of two passive systems

$$\tfrac{d}{dt}H_1 \leq u_1^T y_1, \quad \tfrac{d}{dt}H_2 \leq u_2^T y_2$$

$$u_1 = -y_2 + v_1, \quad u_2 = y_1 + v_2$$

leads to an interconnected system that is **again passive**, since

$$\frac{d}{dt}(H_1 + H_2) \leq v_1^T y_1 + v_2^T y_2$$

The feedback interconnection is a typical example of a *power-conserving interconnection* (total power is zero):

$$u_1^T y_1 + u_2^T y_2 + v_1^T y_1 + v_2^T y_2 = 0$$

In port-based modeling, e.g. bond graphs, one looks at the system as the general power-conserving interconnection of ideal basic system components: (energy-) storage elements, resistive elements, transformers, gyrators, constraints, etc.

- The total energy of the resulting port-Hamiltonian system is the sum of the energies of the storage elements.
- The J- and B-matrix is determined by the transformers, gyrators, constraints, and the power-conserving interconnection.
- The R-matrix is determined by the resistive elements, and the way they are connected.

An k dimensional storage element is determined by a k-dimensional state vector $x = (x_1, \cdots, x_k)$ and a Hamiltonian $H(x_1, \cdots, x_k)$ (energy storage), defining the lossless system

$$\begin{aligned} \dot{x}_i &= f_i, \qquad i = 1, \cdots, k \\ e_i &= \tfrac{\partial H}{\partial x_i}(x_1, \cdots, x_k) \\ \tfrac{d}{dt}H &= \textstyle\sum_{i=1}^k f_i e_i \end{aligned}$$

Such a k- dimensional storage component is written in vector notation as a port-Hamiltonian system with $J = 0$, $R = 0$, and $B = I$:

$$\begin{aligned} \dot{x} &= f \\ e &= \tfrac{\partial H}{\partial x}(x) \end{aligned}$$

The elements of x are called **energy variables**, those of $\frac{\partial H}{\partial x}(x)$ **co-energy variables**. Furthermore the elements of f are **flow variables**, and of e **effort variables**.
Note that $e^T f$ is power.

Example: The ubiquitous mass-spring-damper system:

Two storage elements:

- **Spring** Hamiltonian $H_s(q) = \frac{1}{2}kq^2$ (potential energy)

$$\begin{aligned} \dot{q} &= f_s &&= \text{velocity} \\ e_s &= \tfrac{dH_s}{dq}(q) = kq &&= \text{force} \end{aligned}$$

- **Mass** Hamiltonian $H_m(p) = \frac{1}{2m}p^2$ (kinetic energy)

$$\begin{aligned} \dot{p} &= f_m &&= \text{force} \\ e_m &= \tfrac{dH_m}{dp}(p) = \tfrac{p}{m} &&= \text{velocity} \end{aligned}$$

interconnected by

$$f_s = e_m = y, \quad f_m = -e_s + u$$

(power-conserving since $f_s e_s + f_m e_m = uy$) yields the port-Hamiltonian system

$$\begin{bmatrix} \dot{q} \\ \dot{p} \end{bmatrix} = \begin{bmatrix} 0 & 1 \\ -1 & 0 \end{bmatrix} \begin{bmatrix} \frac{\partial H}{\partial q}(q,p) \\ \frac{\partial H}{\partial p}(q,p) \end{bmatrix} (q,p) + \begin{bmatrix} 0 \\ 1 \end{bmatrix} u$$

$$y = \begin{bmatrix} 0 & 1 \end{bmatrix} \begin{bmatrix} \frac{\partial H}{\partial q}(q,p) \\ \frac{\partial H}{\partial p}(q,p) \end{bmatrix}$$

with

$$H(q,p) = H_s(q) + H_m(p)$$

Addition of the damper

$$e_d = \frac{dR}{df_d} = cf_d, \quad R(f_d) = \frac{1}{2}cf_d^2 \quad \text{(Rayleigh function)}$$

via the extended interconnection

$$f_s = e_m = f_d = y, \quad f_m = e_s - e_d + u$$

leads to the **mass-damper-spring system** in port-Hamiltonian form

$$\begin{bmatrix} \dot{q} \\ \dot{p} \end{bmatrix} = \left(\begin{bmatrix} 0 & 1 \\ -1 & 0 \end{bmatrix} - \begin{bmatrix} 0 & 0 \\ 0 & c \end{bmatrix} \right) \begin{bmatrix} \frac{\partial H}{\partial q}(q,p) \\ \frac{\partial H}{\partial p}(q,p) \end{bmatrix} + \begin{bmatrix} 0 \\ 1 \end{bmatrix} u$$

$$y = \begin{bmatrix} 0 & 1 \end{bmatrix} \begin{bmatrix} \frac{\partial H}{\partial q}(q,p) \\ \frac{\partial H}{\partial p}(q,p) \end{bmatrix}$$

Example: Electro-mechanical systems

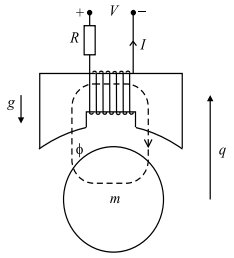

$$\begin{bmatrix} \dot{q} \\ \dot{p} \\ \dot{\varphi} \end{bmatrix} = \begin{bmatrix} 0 & 1 & 0 \\ -1 & 0 & 0 \\ 0 & 0 & -\frac{1}{R} \end{bmatrix} \begin{bmatrix} \frac{\partial H}{\partial q}(q,p,\phi) \\ \frac{\partial H}{\partial p}(q,p,\phi) \\ \frac{\partial H}{\partial \varphi}(q,p,\phi) \end{bmatrix} + \begin{bmatrix} 0 \\ 0 \\ 1 \end{bmatrix} V, \quad I = \frac{\partial H}{\partial \varphi}(q,p,\phi)$$

Coupling electrical/mechanical domain via Hamiltonian $H(q,p,\phi)$.

Example: LC circuits. Two inductors with magnetic energies $H_1(\varphi_1), H_2(\varphi_2)$ (φ_1 and φ_2 magnetic flux linkages), and capacitor with electric energy $H_3(Q)$ (Q charge). V denotes the voltage of the source.

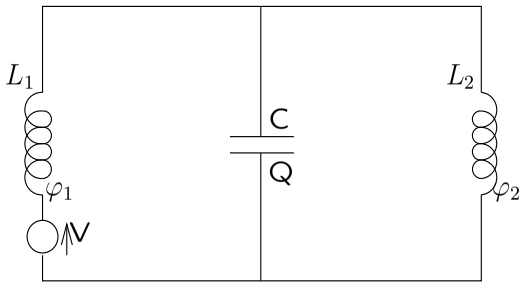

Question: *How to write this circuit as a port-Hamiltonian system in a modular way?*

Hamiltonian equations for the components of the LC-circuit:

$$\begin{array}{lllll} \textit{Inductor } 1 & & \dot{\varphi}_1 & = & f_1 \quad \text{(voltage)} \\ & \text{(current)} & e_1 & = & \frac{\partial H_1}{\partial \varphi_1} \\ \textit{Inductor } 2 & & \dot{\varphi}_2 & = & f_2 \quad \text{(voltage)} \\ & \text{(current)} & e_2 & = & \frac{\partial H_2}{\partial \varphi_2} \\ \textit{Capacitor} & & \dot{Q} & = & f_3 \quad \text{(current)} \\ & \text{(voltage)} & e_3 & = & \frac{\partial H_3}{\partial Q} \end{array}$$

All are port-Hamiltonian systems with $J = 0$ and $g = 1$.

If the elements are *linear* then the Hamiltonians are *quadratic*, e.g. $H_1(\varphi_1) = \frac{1}{2L_1}\varphi_1^2$, and $\frac{\partial H_1}{\partial \varphi_1} = \frac{\varphi_1}{L_1} =$ current , etc.

Kirchhoff's interconnection laws in $f_1, f_2, f_3, e_1, e_2, e_3, f = V, e = I$ are

$$\begin{bmatrix} -f_1 \\ -f_2 \\ -f_3 \\ e \end{bmatrix} = \begin{bmatrix} 0 & 0 & 1 & -1 \\ 0 & 0 & -1 & 0 \\ -1 & 1 & 0 & 0 \\ 1 & 0 & 0 & 0 \end{bmatrix} \begin{bmatrix} e_1 \\ e_2 \\ e_3 \\ f \end{bmatrix}$$

Substitution of eqns. of components yields port-Hamiltonian system

$$\begin{bmatrix} \dot{\varphi}_1 \\ \dot{\varphi}_2 \\ \dot{Q} \end{bmatrix} = \begin{bmatrix} 0 & 0 & -1 \\ 0 & 0 & 1 \\ 1 & -1 & 0 \end{bmatrix} \begin{bmatrix} \frac{\partial H}{\partial \varphi_1} \\ \frac{\partial H}{\partial \varphi_2} \\ \frac{\partial H}{\partial Q} \end{bmatrix} + \begin{bmatrix} 1 \\ 0 \\ 0 \end{bmatrix} f$$

$$e = \frac{\partial H}{\partial \varphi_1}$$

with $H(\varphi_1, \varphi_2, Q) := H_1(\varphi_1) + H_2(\varphi_2) + H_3(Q)$ total energy.

However, this class of port-Hamiltonian systems is **not closed under interconnection**:

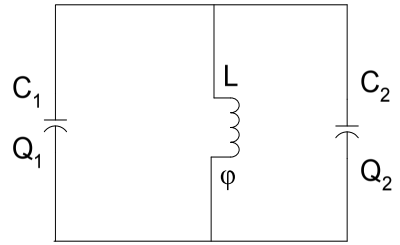

Figure 1: Capacitors and inductors swapped

Interconnection leads to **algebraic constraints** between the state variables Q_1 and Q_2.

How to model DAEs as port-Hamiltonian systems ?

Intermezzo: what is the appropriate generalization of the skew-symmetric mapping J ? Answer: **Dirac structures**. ('From skew-symmetric *mappings* to skew-symmetric *relations*')

Power is defined by

$$P = e(f) =: < e \mid f >= e^T f, \quad (f, e) \in \mathcal{V} \times \mathcal{V}^*.$$

where the linear space $\mathcal{V}$ is called the space of *flows* f (e.g. currents), and $\mathcal{V}^*$ the space of *efforts* e (e.g. voltages). Symmetrized form of power is the indefinite *bilinear form* $\ll, \gg$ on $\mathcal{V} \times \mathcal{V}^*$:

$$\ll (f^a, e^a), (f^b, e^b) \gg \quad := \quad < e^a \mid f^b > + < e^b \mid f^a >,$$

$$(f^a, e^a), (f^b, e^b) \in \mathcal{V} \times \mathcal{V}^*.$$

Definition 1 (Weinstein, Courant, Dorfman) *A (constant) Dirac structure is a subspace*

$$\mathcal{D} \subset \mathcal{V} \times \mathcal{V}^*$$

such that

$$\mathcal{D} = \mathcal{D}^\perp,$$

where $\perp$ denotes orthogonal complement with respect to the bilinear form $\ll, \gg$.

For a *finite-dimensional* space $\mathcal{V}$ this is equivalent to

(i) $< e \mid f >= 0$ for all $(f, e) \in \mathcal{D}$,

(ii) $\dim \mathcal{D} = \dim \mathcal{V}$.

For any skew-symmetric map $J : \mathcal{V}^* \to \mathcal{V}$ its **graph**

$$\{(f, e) \in \mathcal{V} \times \mathcal{V}^* \mid f = Je\}$$

is a Dirac structure !

For many systems, especially those with 3-D mechanical components, the interconnection structure will be *modulated* by the energy or geometric variables.

This leads to the notion of *non-constant* Dirac structures on *manifolds*.

Definition 2 *Consider a smooth manifold M. A Dirac structure on M is a vector subbundle $\mathcal{D} \subset TM \oplus T^*M$ such that for every $x \in M$ the vector space*

$$\mathcal{D}(x) \subset T_xM \times T_x^*M$$

is a Dirac structure as before.

Geometric definition of a port-Hamiltonian system

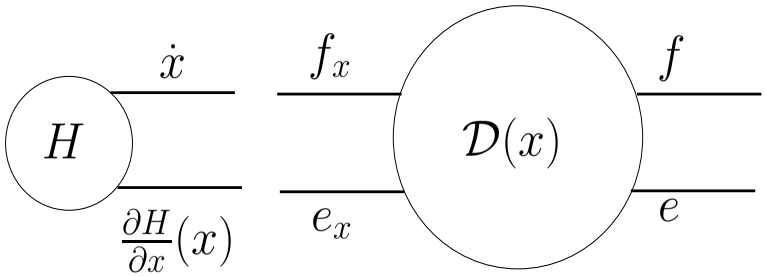

Figure 2: Port-Hamiltonian system

The dynamical system defined by the DAEs

$$(-\dot{x}(t) = f_x(t), \frac{\partial H}{\partial x}(x(t)) = e_x(t), f(t), e(t)) \in \mathcal{D}(x(t)), \quad t \in \mathbb{R}$$

is called a **port-Hamiltonian system**.

Particular case is a Dirac structure $\mathcal{D}(x) \subset T_x\mathcal{X} \times T_x^*\mathcal{X} \times \mathcal{F} \times \mathcal{F}^*$ given as the graph of the skew-symmetric map

$$\begin{bmatrix} f_x \\ e \end{bmatrix} = \begin{bmatrix} -J(x) & -g(x) \\ g^T(x) & 0 \end{bmatrix} \begin{bmatrix} e_x \\ f \end{bmatrix},$$

leading ($f_x = -\dot{x}, e_x = \frac{\partial H}{\partial x}(x)$) to a Hamiltonian open system as before

$$\dot{x} = J(x)\frac{\partial H}{\partial x}(x) + g(x)f, \quad x \in \mathcal{X}, f \in \mathbb{R}^m$$

$$e = g^T(x)\frac{\partial H}{\partial x}(x), \qquad e \in \mathbb{R}^m$$

Energy-dissipation is included by terminating some of the ports by static resistive elements

$$f_R = -F(e_R), \qquad \text{where } e_R^T F(e_R) \geq 0, \quad \text{for all } e_R.$$

If $H \geq 0$ then the system stays passive with respect to the remaining flows and efforts f and e:

$$\frac{d}{dt}H \leq e^T f$$

This leads, e.g. for linear damping, to input-state-output port-Hamiltonian systems in the form

$$\begin{cases} \dot{x} &= [J(x) - R(x)]\frac{\partial H}{\partial x}(x) + g(x)f \\ e &= g^T(x)\frac{\partial H}{\partial x}(x) \end{cases}$$

where $J(x) = -J^T(x)$, $R(x) = R^T(x) \geq 0$ are the interconnection and damping matrices, respectively.

Example: Mechanical systems with kinematic constraints

Constraints on the generalized velocities $\dot{q}$:

$$A^T(q)\dot{q} = 0.$$

This leads to **constrained** Hamiltonian equations

$$\begin{aligned} \dot{q} &= \tfrac{\partial H}{\partial p}(q,p) \\ \dot{p} &= -\tfrac{\partial H}{\partial q}(q,p) + A(q)\lambda + B(q)u \\ 0 &= A^T(q)\tfrac{\partial H}{\partial p}(q,p) \\ y &= B^T(q)\tfrac{\partial H}{\partial p}(q,p) \end{aligned}$$

with $H(q,p)$ total energy, and λ the **constraint forces**.
By elimination of the constraints and constraint forces one derives a port-Hamiltonian model *without constraints*.

Can be extended to general *multi-body systems*.

Intermezzo: Relation with classical Hamiltonian equations

$$\dot{x} = J\frac{\partial H}{\partial x}(x)$$

with constant or ' integrable' J- matrix admits coordinates $x = (q,p,r)$ in which

$$J = \begin{bmatrix} 0 & I & 0 \\ -I & 0 & 0 \\ 0 & 0 & 0 \end{bmatrix}, \qquad \begin{aligned} \dot{q} &= \tfrac{\partial H}{\partial p}(q,p,r) \\ \dot{p} &= -\tfrac{\partial H}{\partial q}(q,p,r) \\ \dot{r} &= 0 \end{aligned}$$

For constant or integrable Dirac structure one gets Hamiltonian DAEs

$$\begin{aligned} \dot{q} &= \tfrac{\partial H}{\partial p}(q,p,r,s) \\ \dot{p} &= -\tfrac{\partial H}{\partial q}(q,p,r,s) \\ \dot{r} &= 0 \\ 0 &= \tfrac{\partial H}{\partial s}(q,p,r,s) \end{aligned}$$

Some properties of port-Hamiltonian systems

Port-Hamiltonian systems modeling encodes more information than energy-balance.

The Dirac structure determines all the *Casimir functions* (conserved quantities which are independent of H).
Example: In the first LC circuit the total flux $\phi_1 + \phi_2$ is a conserved quantity that is solely determined by the circuit topology. (In Part II this will be used for *set-point control*.)
Furthermore, the Dirac structure directly determines the *algebraic constraints*.
Example: In the second LC-circuit the state variables Q_1 and Q_2 are related by

$$\frac{Q_1}{C_1} = \frac{Q_2}{C_2}$$

Any power-conserving interconnection of port-Hamiltonian systems is again port-Hamiltonian

- The resulting Hamiltonian is the sum of the Hamiltonians of the individual systems.
- The Dirac structure is determined by the Dirac structures of the individual systems, and the way they are interconnected.
- The resistive structure is determined by the resistive structures of the individual systems.

Conclusion: **port-Hamiltonian systems theory provides a modular framework for modeling and analysis of complex multi-physics lumped-parameter systems.**

Network modeling is prevailing in modeling and simulation of lumped-parameter physical systems (multi-body systems, electrical circuits, electro-mechanical systems, hydraulic systems, robotic systems, etc.), with many advantages:

- Modularity and flexibility. Re-usability ('libraries').
- Multi-physics approach.
- Suited to design/control.

Disadvantage of network modeling: it generally leads to a large set of DAEs, *seemingly without any structure*.
Port-based modeling and port-Hamiltonian system theory identifies the underlying structure of network models of physical systems, to be used for analysis, simulation and control.

Distributed-parameter port-Hamiltonian systems

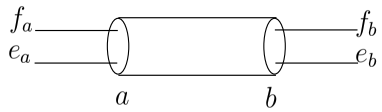

Figure 3: **Simplest example: Transmission line**

Telegrapher's equations define the boundary control system

$$\begin{array}{rclcrcl}
\frac{\partial Q}{\partial t}(z,t) & = & -\frac{\partial}{\partial z} I(z,t) & = & -\frac{\partial}{\partial z}\frac{\phi(z,t)}{L(z)} \\
\frac{\partial \phi}{\partial t}(z,t) & = & -\frac{\partial}{\partial z} V(z,t) & = & -\frac{\partial}{\partial z}\frac{Q(z,t)}{C(z)} \\
f_a(t) & = & V(a,t), \quad e_1(t) & = & I(a,t) \\
f_b(t) & = & V(b,t), \quad e_2(t) & = & I(b,t)
\end{array}$$

Transmission line as port-Hamiltonian system
Define *internal* flows $f_x = (f_E, f_M)$ and efforts $e_x = (e_E, e_M)$:

electric flow	$f_E : [a,b] \to \mathbb{R}$
magnetic flow	$f_M : [a,b] \to \mathbb{R}$
electric effort	$e_E : [a,b] \to \mathbb{R}$
magnetic effort	$e_M : [a,b] \to \mathbb{R}$

together with *external* boundary flows $f = (f_a, f_b)$ and boundary efforts $e = (e_a, e_b)$. Define the *infinite-dimensional Dirac structure*

$$\begin{bmatrix} f_E \\ f_M \end{bmatrix} = \begin{bmatrix} 0 & \frac{\partial}{\partial z} \\ \frac{\partial}{\partial z} & 0 \end{bmatrix} \begin{bmatrix} e_E \\ e_M \end{bmatrix}$$

$$\begin{bmatrix} f_{a,b} \\ e_{a,b} \end{bmatrix} = \begin{bmatrix} e_{E|a,b} \\ e_{M|a,b} \end{bmatrix}$$

This defines a Dirac structure on the space of *internal* flows and efforts and *boundary* flows and efforts.

Substituting (as in the lumped-parameter case)

$$\left.\begin{array}{rcl} f_E &=& -\frac{\partial Q}{\partial t} \\ f_M &=& -\frac{\partial \varphi}{\partial t} \end{array}\right\} f_x = -\dot{x}$$

$$\left.\begin{array}{rcl} e_E &=& \frac{Q}{C} = \frac{\partial \mathcal{H}}{\partial Q} \\ e_M &=& \frac{\varphi}{L} = \frac{\partial \mathcal{H}}{\partial \varphi} \end{array}\right\} e_x = \frac{\partial H}{\partial x}$$

with, for example, quadratic energy density

$$\mathcal{H}(Q,\varphi) = \frac{1}{2}\frac{Q^2}{C} + \frac{1}{2}\frac{\varphi^2}{L}$$

we recover the telegrapher's equations.

Of course, the telegrapher's equations can be rewritten as the linear **wave equation**

$$\frac{\partial^2 Q}{\partial t^2} = -\frac{\partial}{\partial z}\frac{\partial I}{\partial t} = -\frac{\partial}{\partial z}\frac{\partial}{\partial t}\frac{\phi}{L} =$$

$$-\frac{\partial}{\partial z}\frac{1}{L}\frac{\partial \phi}{\partial t} = \frac{\partial}{\partial z}\frac{1}{L}\frac{\partial}{\partial z}\frac{Q}{C} = \frac{1}{LC}\frac{\partial^2 Q}{\partial z^2}$$

(if $L(z), C(z)$ do not depend on z), or similar expressions in ϕ, I or V.

The same equations hold for a *vibrating string*, or for a *compressible gas/fluid* in a one-dimensional pipe (see Part III).

Basic question:

Which of the boundary variables f_a, f_b, e_a, e_b can be considered to be inputs, and which outputs ? **See Part III**.

Example 2: Shallow water equations; distributed-parameter port-Hamiltonian system with non-quadratic Hamiltonian

The dynamics of the water in an open-channel canal can be described by

$$\partial_t \begin{bmatrix} h \\ v \end{bmatrix} + \begin{bmatrix} v & h \\ g & v \end{bmatrix} \partial_z \begin{bmatrix} h \\ v \end{bmatrix} = 0$$

with $h(z,t)$ the height of the water at position z, and $v(z,t)$ the velocity (and g gravitational constant).

This can be written as a port-Hamiltonian system by recognizing the total energy

$$H(h,v) = \frac{1}{2}\int_a^b [hv^2 + gh^2] dz$$

yielding the co-energy functions[a]

$$\begin{array}{rcll} e_h &=& \frac{\partial \mathcal{H}}{\partial h} = hv & \text{mass flow} \\ e_v &=& \frac{\partial \mathcal{H}}{\partial v} = \frac{1}{2}v^2 + gh & \text{Bernoulli function} \end{array}$$

It follows that the shallow water equations can be written, similarly to the telegraphers equations, as

$$\frac{\partial h}{\partial t}(z,t) = -\frac{\partial}{\partial z}\frac{\partial \mathcal{H}}{\partial v}$$

$$\frac{\partial v}{\partial t}(z,t) = -\frac{\partial}{\partial z}\frac{\partial \mathcal{H}}{\partial h}$$

with boundary variables $-hv_{|a,b}$ and $(\frac{1}{2}v^2 + gh)_{|a,b}$.

[a] Daniel Bernoulli, born in 1700 in Groningen as son of Johann Bernoulli, professor in mathematics at the University of Groningen and founder of the Calculus of Variations.

Figure 4: Johann Bernoulli, professor in Groningen 1695-1705.

Figure 5: Daniel Bernoulli, born in Groningen in 1700.

We obtain the energy balance

$$\frac{d}{dt}\int_a^b [hv^2 + gh^2]dz = -(hv)(\frac{1}{2}v^2 + gh)|_a^b$$

which can be rewritten as

$$-v(\tfrac{1}{2}gh^2)|_a^b - v(\tfrac{1}{2}hv^2 + \tfrac{1}{2}gh^2))|_a^b =$$

velocity $\times$ pressure $+$ energy flux through the boundary

Conservation laws

All examples sofar have the same structure

$$\frac{\partial \alpha_1}{\partial t}(z,t) = -\frac{\partial}{\partial z}\frac{\partial \mathcal{H}}{\partial \alpha_2} = -\frac{\partial}{\partial z}\beta_2$$

$$\frac{\partial \alpha_2}{\partial t}(z,t) = -\frac{\partial}{\partial z}\frac{\partial \mathcal{H}}{\partial \alpha_1} = -\frac{\partial}{\partial z}\beta_1$$

with boundary variables $\beta_1|_{\{a,b\}}, \beta_2|_{\{a,b\}}$, corresponding to two coupled **conservation laws**:

$$\frac{d}{dt}\int_a^b \alpha_1 = -\int_a^b \frac{\partial}{\partial z}\beta_2 = \beta_2(a) - \beta_2(b)$$

$$\frac{d}{dt}\int_a^b \alpha_2 = -\int_a^b \frac{\partial}{\partial z}\beta_1 = \beta_1(a) - \beta_1(b)$$

(In the transmission line, α_1 and α_2 is charge- and flux-density, and β_1, β_2 voltage V and current I, respectively.)

For some purposes it is illuminating to rewrite the equations in terms of the co-energy variables β_1, β_2:

$$\begin{bmatrix} \frac{\partial \beta_1}{\partial t} \\ \frac{\partial \beta_2}{\partial t} \end{bmatrix} = \begin{bmatrix} \frac{\partial^2 H}{\partial \alpha_1^2} & \frac{\partial^2 H}{\partial \alpha_1 \alpha_2} \\ \frac{\partial^2 H}{\partial \alpha_2 \alpha_1} & \frac{\partial^2 H}{\partial \alpha_2^2} \end{bmatrix} \begin{bmatrix} \frac{\partial \alpha_1}{\partial t} \\ \frac{\partial \alpha_2}{\partial t} \end{bmatrix} = - \begin{bmatrix} \frac{\partial^2 H}{\partial \alpha_1^2} & \frac{\partial^2 H}{\partial \alpha_1 \alpha_2} \\ \frac{\partial^2 H}{\partial \alpha_2 \alpha_1} & \frac{\partial^2 H}{\partial \alpha_2^2} \end{bmatrix} \begin{bmatrix} \frac{\partial \beta_2}{\partial z} \\ \frac{\partial \beta_1}{\partial z} \end{bmatrix}$$

For the transmission line this yields

$$\begin{bmatrix} \frac{\partial V}{\partial t} \\ \frac{\partial I}{\partial t} \end{bmatrix} = - \begin{bmatrix} 0 & \frac{1}{C} \\ \frac{1}{L} & 0 \end{bmatrix} \begin{bmatrix} \frac{\partial V}{\partial z} \\ \frac{\partial I}{\partial z} \end{bmatrix}$$

The matrix is called the **characteristic matrix**, whose eigenvalues are the characteristic velocities $\frac{1}{\sqrt{LC}}$ and $-\frac{1}{\sqrt{LC}}$ corresponding to the characteristic eigenvectors (and curves).

For the shallow water equations this yields

$$\begin{bmatrix} \frac{\partial \beta_1}{\partial t} \\ \frac{\partial \beta_2}{\partial t} \end{bmatrix} = - \begin{bmatrix} v & g \\ h & v \end{bmatrix} \begin{bmatrix} \frac{\partial \beta_1}{\partial z} \\ \frac{\partial \beta_2}{\partial z} \end{bmatrix}$$

with

$$\beta_1 = \frac{1}{2}v^2 + gh, \quad \beta_2 = hv$$

being mass flow and Bernoulli function, respectively.

This corresponds to two characteristic velocities $v \pm \sqrt{gh}$ of opposite signs (subcritical or fluvial flow) if

$$v^2 \leq gh$$

In this nonlinear case, the characteristic curves *may* intersect, corresponding to shock waves

Power converter connected to the load via transmission line

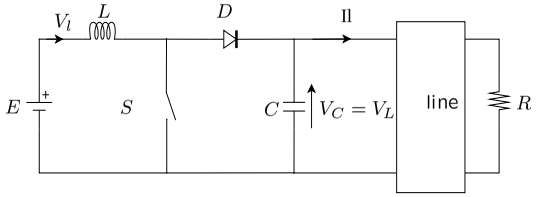

Figure 6: The Boost converter with a transmission line

Mixed lumped- and distributed-parameter port-Hamiltonian systems

Typical example: power-converter connected via a transmission line to a resistive load or an induction motor:

- The power-converter is a port-Hamiltonian system (with switching Dirac structure).
- Transmission line is distributed-parameter port-Hamiltonian system.
- Induction motor is a port-Hamiltonian system, with Hamiltonian being the electro-mechanical energy.

Boost power converter

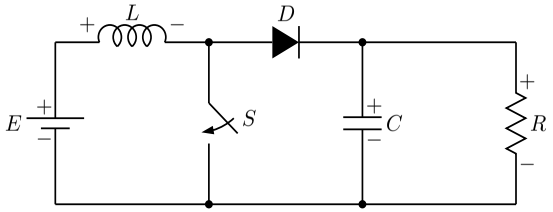

Figure 7: Boost circuit with clamping diode

The circuit consists of a capacitor C with electric charge q_C, an inductor L with magnetic flux linkage ϕ_L, and a resistive load R, together with an ideal diode and an ideal switch S, with switch positions $s = 1$ (switch closed) and $s = 0$ (switch open).

The voltage-current characteristics of the ideal diode and switch are depicted in Figure 8.

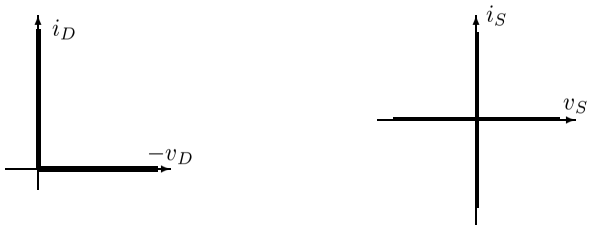

Figure 8: Voltage-current characteristic of an ideal diode and ideal switch

The ideal diode thus satisfies the complementarity conditions:

$$v_D i_D = 0, \quad v_D \leq 0, \quad i_D \geq 0.$$

This yields the port-Hamiltonian model
(with $H(q_C, \phi_L) = \frac{1}{2C} q_C^2 + \frac{1}{2L} \phi_L^2$):

$$\begin{bmatrix} \dot{q}_C \\ \dot{\phi}_L \end{bmatrix} = \begin{bmatrix} -\frac{1}{R} & 1-s \\ s-1 & 0 \end{bmatrix} \begin{bmatrix} \frac{\partial H}{\partial q_C} = \frac{q_C}{C} \\ \frac{\partial H}{\partial \phi_L} = \frac{\phi_L}{L} \end{bmatrix} + \begin{bmatrix} 0 \\ 1 \end{bmatrix} E + \begin{bmatrix} s i_D \\ (s-1) v_D \end{bmatrix}$$

$$I = \frac{\phi_L}{L}$$

Assume that the switch and the diode are **coupled** in the following sense: if the switch is closed ($s = 1$) then the diode is open ($i_D = 0$), while if the switch is open ($s = 0$), then the diode is closed ($v_D = 0$). (This means that we disregard the so-called *discontinuous* modes.)

In this case we obtain the *switching port-Hamiltonian system*

$$\begin{bmatrix} \dot{q}_C \\ \dot{\phi}_L \end{bmatrix} = \begin{bmatrix} -\frac{1}{R} & 1-s \\ s-1 & 0 \end{bmatrix} \begin{bmatrix} \frac{\partial H}{\partial q_C} = \frac{q_C}{C} \\ \frac{\partial H}{\partial \phi_L} = \frac{\phi_L}{L} \end{bmatrix} + \begin{bmatrix} 0 \\ 1 \end{bmatrix} E$$

$$I = \begin{bmatrix} 0 & 1 \end{bmatrix} \begin{bmatrix} \frac{\partial H}{\partial q_C} = \frac{q_C}{C} \\ \frac{\partial H}{\partial \phi_L} = \frac{\phi_L}{L} \end{bmatrix} = \frac{\phi_L}{L}$$

A port-Hamiltonian system where the J-matrix depends on the switch position.

In general, a switching port-Hamiltonian system (without algebraic equality and inequality constraints) is defined as

$$\dot{x} = F(\rho) z + g(\rho) u, \quad z = \frac{\partial H}{\partial x}(x)$$

$$y = g^T(\rho) z$$

with $\rho \in \{0, 1\}^p$, and

$$F(\rho) = J(\rho) - R(\rho), \quad J(\rho) = -J^T(\rho), \quad R(\rho) = R^T(\rho) \geq 0$$

Note that the system is passive for every switching sequence:

$$\frac{d}{dt} H = -\frac{\partial^T H}{\partial x}(x) R(\rho) \frac{\partial H}{\partial x}(x) + u^T y \leq u^T y$$

Conclusions of Part I

- Port-Hamiltonian systems provide a unified framework for *modeling, analysis, and simulation* of complex lumped-parameter multi-physics systems.
- Inclusion of distributed-parameter components.
- Spatial discretization of distributed-parameter port-Hamiltonian systems to finite-dimensional port-Hamiltonian systems.
  - Extensions to thermodynamic systems and chemical reaction networks.
  - Further exploration of the network (graph) information.

See the forthcoming book on port-Hamiltonian systems produced by the EU-IST GeoPleX consortium,
or the website www.math.rug.nl/~arjan, for further info.

The port-Hamiltonian approach to physical system modeling and control

Part II: Control of Port-Hamiltonian systems

Contents

- Use of passivity for control
- Control by interconnection: set-point stabilization
- The dissipation obstacle
- A state feedback perspective; shaping the Hamiltonian
- New control paradigms
- Model reduction of port-Hamiltonian systems

Use of passivity for control and beyond

- The storage function of a passive system can be used as a Lyapunov function, implying some sort of stability for the uncontrolled system.
- The standard feedback interconnection of two passive systems is again passive, with storage function being the **sum** of the individual storage functions.
- Passive systems can be asymptotically stabilized by adding artificial **damping**. In fact,

  $$\frac{d}{dt}H \leq u^T y$$

  together with the additional damping $u = -y$ leads to

  $$\frac{d}{dt}H \leq - \parallel y \parallel^2$$

  provided an **observability condition** is met.

Example The Euler equations for the motion of a rigid body revolving about its center of gravity with one input are

$$\begin{aligned} I_1\dot{\omega}_1 &= [I_2 - I_3]\omega_2\omega_3 + g_1 u \\ I_2\dot{\omega}_2 &= [I_3 - I_1]\omega_1\omega_3 + g_2 u \\ I_3\dot{\omega}_3 &= [I_1 - I_2]\omega_1\omega_2 + g_3 u, \end{aligned}$$

Here $\omega := (\omega_1, \omega_2, \omega_3)^T$ are the angular velocities around the principal axes of the rigid body, and $I_1, I_2, I_3 > 0$ are the principal moments of inertia. The system for $u = 0$ has the origin as an equilibrium point. Linearization yields the linear system

$$A = \begin{pmatrix} 0 & 0 & 0 \\ 0 & 0 & 0 \\ 0 & 0 & 0 \end{pmatrix} \qquad B = \begin{pmatrix} I_1^{-1} g_1 \\ I_2^{-1} g_2 \\ I_3^{-1} g_3 \end{pmatrix}.$$

Hence the linearization does not say anything about stabilizability.

Stabilization method by damping injection

Rewrite the system in Hamiltonian form by defining the angular momenta

$$p_1 = I_1\dot{\omega}_1,\ p_2 = I_2\dot{\omega}_2,\ p_3 = I_3\dot{\omega}_3$$

and defining the Hamiltonian $H(p)$ as the total energy

$$H(p) = \frac{1}{2}(\frac{p_1^2}{I_1} + \frac{p_2^2}{I_2} + \frac{p_3^2}{I_3})$$

Then the system can be rewritten as

$$\begin{bmatrix}\dot{p}_1\\ \dot{p}_2\\ \dot{p}_3\end{bmatrix} = \begin{bmatrix}0 & -p_3 & p_2\\ p_3 & 0 & -p_1\\ -p_2 & p_1 & 0\end{bmatrix}\begin{bmatrix}\frac{\partial H}{\partial p_1}\\ \frac{\partial H}{\partial p_2}\\ \frac{\partial H}{\partial p_3}\end{bmatrix} + \begin{bmatrix}g_1\\ g_2\\ g_3\end{bmatrix}u$$

Since $\dot{H} = 0$ and H has a minimum at $p = 0$ the origin is stable.

The damping injection amounts to

$$u = -g_1\frac{p_1}{I_1} - g_2\frac{p_2}{I_2} - g_3\frac{p_3}{I_3} = -g_1\omega_1 - g_2\omega_2 - g_3\omega_3,$$

yielding convergence to the largest invariant set contained in

$$\mathcal{S} := \{p \in \mathbb{R}^3 \mid \dot{H}(p) = 0\} = \{p \in \mathbb{R}^3 \mid g_1\frac{p_1}{I_1} + g_2\frac{p_2}{I_2} + g_3\frac{p_3}{I_3} = 0\}$$

It can be shown that the largest invariant set contained in $\mathcal{S}$ is the origin $p = 0$ if and only if

$$g_1 \neq 0, g_2 \neq 0, g_3 \neq 0,$$

in which case the origin is rendered asymptotically (even, globally) stable.

Beyond control via passivity: What can we do if the desired set-point is **not** a minimum of the storage function ??

Recall the proof of stability of an equilibrium $(\omega_1^*, 0, 0) \neq (0, 0, 0)$ of the Euler equations The total energy $H = \frac{2I_1}{p_1^2} + \frac{2I_2}{p_2^2} + \frac{2I_3}{p_3^2} = \frac{1}{2}I_1\omega_1^2 + \frac{1}{2}I_2\omega_2^2 + \frac{1}{2}I_3\omega_3^2$ has a minimum at $(0, 0, 0)$. Stability of $(\omega_1^*, 0, 0)$ is shown by taking as Lyapunov function a suitable combination of the total energy K and another **conserved quantity**, namely the total angular momentum

$$C = p_1^2 + p_2^2 + p_3^2 = I_1^2\omega_1^2 + I_2^2\omega_2^2 + I_3^2\omega_3^2$$

This follows from

$$\begin{bmatrix}p_1 & p_2 & p_3\end{bmatrix}\begin{bmatrix}0 & -p_3 & p_2\\ p_3 & 0 & -p_1\\ -p_2 & p_1 & 0\end{bmatrix} = 0$$

In general, for any Hamiltonian dynamics

$$\dot{x} = J(x)\frac{\partial H}{\partial x}(x)$$

one may search for conserved quantities C, called **Casimirs**, as being solutions of

$$\frac{\partial^T C}{\partial x}(x)J(x) = 0$$

Then $\frac{d}{dt}C = 0$ for *every* H, and thus $H + C$ is a **candidate Lyapunov function**. Note that the minimum of $H + C$ may be **different** from the minimum of H.

Control by interconnection: set-point stabilization:

Consider first a lossless Hamiltonian plant system P

$$\begin{aligned} \dot{x} &= J(x)\frac{\partial H}{\partial x}(x) + g(x)u \\ y &= g^T(x)\frac{\partial H}{\partial x}(x) \end{aligned}$$

where the desired set-point x^* is **not** a minimum of the Hamiltonian H, while the Hamiltonian dynamics $\dot{x} = J(x)\frac{\partial H}{\partial x}(x)$ does not possess useful Casimirs.

How to (asymptotically) stabilize x^* ?

Control by interconnection:

Consider a *controller* port-Hamiltonian system

$$C: \quad \begin{aligned} \dot{\xi} &= J_c(\xi)\frac{\partial H_c}{\partial \xi}(\xi) + g_c(\xi)u_c, \quad \xi \in \mathcal{X}_c \\ y_c &= g^T(\xi)\frac{\partial H_c}{\partial \xi}(\xi) \end{aligned}$$

via the standard feedback interconnection

$$u = -y_c, \quad u_c = y$$

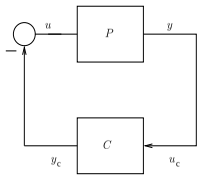

Then the closed-loop system is the port-Hamiltonian system

$$\begin{bmatrix} \dot{x} \\ \dot{\xi} \end{bmatrix} = \begin{bmatrix} J(x) & -g(x)g_c^T(\xi) \\ g_c(\xi)g^T(x) & J_c(\xi) \end{bmatrix} \begin{bmatrix} \frac{\partial H}{\partial x}(x) \\ \frac{\partial H_c}{\partial \xi}(\xi) \end{bmatrix}$$

with state space $\mathcal{X} \times \mathcal{X}_c$, and total Hamiltonian $H(x) + H_c(\xi)$.

Main idea: design the controller system in such a manner that the closed-loop system has useful Casimirs $C(x,\xi)$!. This may lead to a suitable candidate Lyapunov function

$$V(x,\xi) := H(x) + H_c(\xi) + C(x,\xi)$$

with H_c to-be-determined.

Thus we look for functions $C(x,\xi)$ satisfying

$$\left[\frac{\partial^T C}{\partial x}(x,\xi) \quad \frac{\partial^T C}{\partial \xi}(x,\xi)\right] \begin{bmatrix} J(x) & -g(x)g_c^T(\xi) \\ g_c(\xi)g^T(x) & J_c(\xi) \end{bmatrix} = 0$$

such that the candidate Lya[unov function

$$V(x,\xi) := H(x) + H_c(\xi) + C(x,\xi)$$

has a minimum at (x^*,ξ^*) for some (or a set of) $\xi^* \Rightarrow$ **stability**.

Remark: The set of such *achievable* closed-loop Casimirs $C(x,\xi)$ can be fully characterized.

Subsequently, one may add extra damping (directly or in the dynamics of the controller) to achieve **asymptotic** stability.

Example: the ubiquitous pendulum

Consider the mathematical pendulum with Hamiltonian

$$H(q,p) = \frac{1}{2}p^2 + (1 - \cos q)$$

actuated by a torque u, with output $y = p$ (angular velocity).
Suppose we wish to stabilize the pendulum at a **non-zero angle** q^* and $p^* = 0$.

Apply the nonlinear integral control

$$\begin{aligned} \dot{\xi} &= u_c = y \\ -u = y_c &= \tfrac{\partial H_c}{\partial \xi}(\xi) \end{aligned}$$

which is a port-Hamiltonian controller system with $J_c = 0$.

Casimirs $C(q,p,\xi)$ are found by solving

$$\begin{bmatrix} \frac{\partial C}{\partial q} & \frac{\partial C}{\partial p} & \frac{\partial C}{\partial \xi} \end{bmatrix} \begin{bmatrix} 0 & 1 & 0 \\ -1 & 0 & -1 \\ 0 & 1 & 0 \end{bmatrix} = 0$$

leading to Casimirs $C(q,p,\xi) = K(q - \xi)$, and candidate Lyapunov functions

$$V(q,p,\xi) = \frac{1}{2}p^2 + (1 - \cos q) + H_c(\xi) + K(q - \xi)$$

with the functions H_c and K to be determined.

For a local minimum, determine K and H_c such that

Equilibrium assignment

$$\begin{aligned} &\sin q^* + \tfrac{\partial K}{\partial z}(q^* - \xi^*) = 0 \\ &-\tfrac{\partial K}{\partial z}(q^* - \xi^*) + \tfrac{\partial H_c}{\partial \xi}(\xi^*) = 0 \end{aligned}$$

Minimum condition

$$\begin{bmatrix} \cos q^* + \frac{\partial^2 K}{\partial z^2}(q^* - \xi^*) & 0 & -\frac{\partial^2 K}{\partial z^2}(q^* - \xi^*) \\ 0 & 1 & 0 \\ -\frac{\partial^2 K}{\partial z^2}(q^* - \xi^*) & 0 & \frac{\partial^2 K}{\partial z^2}(q^* - \xi^*) + \frac{\partial^2 H_c}{\partial \xi^2}(\xi^*) \end{bmatrix} > 0$$

Many possible solutions.

Example: stabilization of the shallow water equations

The dynamics of the water in a canal can be described by

$$\partial_t \begin{bmatrix} h \\ v \end{bmatrix} + \begin{bmatrix} v & h \\ g & v \end{bmatrix} \partial_z \begin{bmatrix} h \\ v \end{bmatrix} = 0$$

with $h(z,t)$ the height of the water at position z, and $v(z,t)$ its velocity (and g the gravitational constant).

Recall that by recognizing the total energy

$$H(h,v) = \int_a^b \mathcal{H} dz = \int_a^b \frac{1}{2}[hv^2 + gh^2] dz$$

this can be written (similarly to the telegrapher's equations) as the port-Hamiltonian system

$$\frac{\partial h}{\partial t}(z,t) = -\frac{\partial}{\partial z}\frac{\partial \mathcal{H}}{\partial v}(h,v)$$

$$\frac{\partial v}{\partial t}(z,t) = -\frac{\partial}{\partial z}\frac{\partial \mathcal{H}}{\partial h}(h,v)$$

with the 4 boundary variables

$$hv_{|a,b}$$
$$-(\tfrac{1}{2}v^2+gh)_{|a,b}$$

denoting respectively the **mass flow** and the **Bernoulli function** at the boundary points a, b.

(Note that the product $hv \cdot (\frac{1}{2}v^2+gh)$ equals *power*.)

Suppose we want to control the water level h to a desired height h^*.

An obvious 'physical' controller is to add to one side of the canal, say the right-end b, an infinite water reservoir of height h^*, corresponding to the port-Hamiltonian 'source' system

$$\dot{\xi} = u_c$$
$$y_c = \frac{\partial H_c}{\partial \xi}(= gh^*)$$

with Hamiltonian $H_c(\xi) = gh^*\xi$, by the feedback interconnection

$$u_c = y = h(b)v(b), \quad y_c = -u = \frac{1}{2}v^2(b) + gh(b)$$

This yields a closed-loop port-Hamiltonian system with total Hamiltonian

$$\int_0^l \frac{1}{2}[hv^2+gh^2]dz + gh^*\xi$$

By mass balance,

$$\int_a^b h(z,t)dz + \xi + c$$

is a Casimir for the closed-loop system. Thus we may take as Lyapunov function

$$V(h,v,\xi) := \tfrac{1}{2}\textstyle\int_a^b [hv^2+gh^2]dz + gh^*\xi - gh^*[\int_a^b h(z,t)dz + \xi] + \frac{1}{2}g(b-a)h^{*2}$$

$$= \tfrac{1}{2}\textstyle\int_a^b [hv^2+g(h-h^*)^2]dz$$

which has a minimum at the desired set-point $(h^*, v^*=0, \xi^*)$ (with ξ^* arbitrary).

Remark Note that the source port-Hamiltonian system is **not** passive, since the Hamiltonian $H_c(\xi) = gh^*\xi$ is not bounded from below.

An alternative, passive, choice of the Hamiltonian controller system is to take e.g.

$$H_c(\xi) = \frac{1}{2}gh^*\xi^2$$

leading to the Lyapunov function

$$V(h,v,\xi) = \frac{1}{2}\int_a^b [hv^2+g(h-h^*)^2]dz + \frac{1}{2}gh^*(\xi-1)^2$$

Asymptotic stability of the equilibrium $(h^*, v^*=0, \xi^*=1)$ can be obtained by adding 'damping', that is, replacing $u_c = y = h(b)v(b)$ by

$$u_c := y - \frac{\partial V}{\partial \xi} = h(b)v(b) - gh^*(\xi-1)$$

leading to (if there is no power flow through the left-end a)

$$\frac{d}{dt}V = -gh^*(\xi-1)^2$$

See the work of Bastin & co-workers for related and more refined results.

The dissipation obstacle

Surprisingly, the presence of dissipation $R \neq 0$ may pose a problem !

$C(x)$ is a Casimir for the Hamiltonian dynamics with dissipation

$$\dot{x} = [J(x) - R(x)]\frac{\partial H}{\partial x}(x), \quad J = J^T, R = R^T \geq 0$$

iff

$$\frac{\partial^T C}{\partial x}[J-R] = 0 \Rightarrow \frac{\partial^T C}{\partial x}[J-R]\frac{\partial C}{\partial x} = 0 \Rightarrow \frac{\partial^T C}{\partial x}R\frac{\partial C}{\partial x} = 0 \Rightarrow \frac{\partial^T C}{\partial x}R = 0$$

and thus C is a Casimir iff

$$\frac{\partial^T C}{\partial x}(x)J(x) = 0, \quad \frac{\partial^T C}{\partial x}(x)R(x) = 0$$

The physical reason for the dissipation obstacle is that by using a passive controller only equilibria where **no** energy-dissipation takes place may be stabilized.

Similarly, if $C(x,\xi)$ is a Casimir for the closed-loop port-Hamiltonian system then it must satisfy

$$\begin{bmatrix}\frac{\partial^T C}{\partial x}(x,\xi) & \frac{\partial^T C}{\partial \xi}(x,\xi)\end{bmatrix}\begin{bmatrix}R(x) & 0\\ 0 & R_c(\xi)\end{bmatrix} = 0$$

implying by semi-positivity of $R(x)$ and $R_c(x)$

$$\frac{\partial^T C}{\partial x}(x,\xi)R(x) = 0$$
$$\frac{\partial^T C}{\partial \xi}(x,\xi)R_c(\xi) = 0$$

This is the **dissipation obstacle**, which implies that one cannot shape the Lyapunov function in the coordinates that are directly affected by energy dissipation.

Remark: For shaping the potential energy in mechanical systems this is **not** a problem since dissipation enters in the differential equations for the momenta.

To overcome the dissipation obstacle

Suppose one can find a mapping $C : \mathcal{X} \to \mathbb{R}^m$, with its (transposed) Jacobian matrix $K^T(x) := \frac{\partial C}{\partial x}(x)$ satisfying

$$[J(x) - R(x)]K(x) + g(x) = 0$$

Construct now the interconnection and dissipation matrix of an *augmented system* as

$$J_{aug} := \begin{bmatrix}J & JK\\ K^T J & K^T JK\end{bmatrix}, \quad R_{aug} := \begin{bmatrix}R & RK\\ K^T R & K^T RK\end{bmatrix}$$

By construction

$$[K^T(x) \mid -I]J_{aug} = [K^T(x) \mid -I]R_{aug} = 0$$

implying that the components of C are Casimirs for the Hamiltonian dynamics

$$\begin{bmatrix}\dot{x}\\ \dot{\xi}\end{bmatrix} = [J_{aug} - R_{aug}]\begin{bmatrix}\frac{\partial H}{\partial x}(x)\\ \frac{\partial H_c}{\partial \xi}(\xi)\end{bmatrix}$$

Furthermore, since $[J(x) - R(x)]K(x) + g(x) = 0$

$$J_{aug} - R_{aug} = \begin{bmatrix}J-R & [J-R]K\\ K^T[J-R] & K^T JK - K^T RK\end{bmatrix}$$

$$= \begin{bmatrix}J-R & -g\\ [g-2RK]^T & K^T JK - K^T RK\end{bmatrix}$$

Thus the augmented system is a closed-loop system for a **different output** !

Port-Hamiltonian systems with **feedthrough term** take the form

$$\begin{aligned} \dot{x} &= [J(x) - R(x)]\frac{\partial H}{\partial x}(x) + g(x)u \\ y &= (g(x) + 2P(x))^T \frac{\partial H}{\partial x}(x) + [M(x) + S(x)]u, \end{aligned}$$

with M skew-symmetric and S symmetric, while

$$\begin{bmatrix} R(x) & P(x) \\ P^T(x) & S(x) \end{bmatrix} \geq 0$$

The augmented system is thus the feedback interconnection of the nonlinear integral controller

$$\begin{aligned} \dot{\xi} &= u_c \\ y_c &= \frac{\partial H_c}{\partial \xi}(\xi) \end{aligned}$$

with the plant port-Hamiltonian system with **modified** output with feedthrough term

$$\begin{aligned} \dot{x} &= [J(x) - R(x)]\frac{\partial H}{\partial x}(x) + g(x)u \\ y_{mod} &= [g(x) - 2R(x)K(x)]^T \frac{\partial H}{\partial x}(x) + [-K^T(x)J(x)K(x) + K^T(x)R(x)K(x)]u \end{aligned}$$

Remark: See Jeltsema, Ortega and Scherpen for further explorations.

Generalization to feedback interconnection with state-modulation.

Recall that $K^T(x) := \frac{\partial C}{\partial x}(x)$ is a solution to $[J(x) - R(x)]K(x) + g(x) = 0$. This can be generalized to

$$[J(x) - R(x)]K(x) + g(x)\beta(x) = 0$$

with $\beta(x)$ an $m \times m$ design matrix.

The same scheme as above works if we extend the standard feedback interconnection $u = -y_c, u_c = y$ to the state-modulated feedback

$$u = -\beta(x)y_c, \quad u_c = \beta^T(x)y$$

Note that $K(x)$ is a solution for some $\beta(x)$ iff

$$g^\perp(x)[J(x) - R(x)]K(x) = 0$$

(In fact, $\beta(x) := -(g^T(x)g(x))^{-1}g^T(x)[J(x) - R(x)]K(x)$ does the job.)

A state feedback perspective: shaping the Hamiltonian

Restrict (without much loss of generality) to Casimirs of the form

$$C(x, \xi) = \xi_j - G_j(x)$$

It follows that for all time instants

$$\xi_j = G_j(x) + c_j, \quad c_j \in \mathbb{R}$$

Suppose that in this way all control state components ξ_i can be expressed as function

$$\xi = G(x)$$

of the plant state x. Then the dynamic feedback reduces to a **state feedback**, and the Lyapunov function $H(x) + H_c(\xi) + C(x, \xi)$ reduces to the **shaped** Hamiltonian

$$H(x) + H_c(G(x))$$

A direct state feedback perspective:
Interconnection-Damping Assignment (IDA)-PBC control

A direct way to generate candidate Lyapunov functions H_d is to look for state feedbacks $u = \hat{u}_{IDA}(x)$ such that

$$[J(x) - R(x)]\frac{\partial H}{\partial x}(x) + g(x)\hat{u}_{IDA}(x) = [J_d(x) - R_d(x)]\frac{\partial H_d}{\partial x}(x)$$

where J_d and R_d are newly assigned interconnection and damping structures.

Remark: For mechanical systems IDA-PBC control is equivalent to the theory of Controlled Lagrangians (Bloch, Leonard, Marsden, .).

For $J_d = J$ and $R_d = R$ (*Basic IDA-PBC*) this reduces to

$$[J(x) - R(x)]\frac{\partial (H_d - H)}{\partial x}(x) = g(x)\hat{u}_{BIDA}(x)$$

and thus in this case, there exists an $\hat{u}_{BIDA}(x)$ if and only if

$$g^{\perp}(x)[J(x) - R(x)]\frac{\partial (H_d - H)}{\partial x}(x) = 0$$

which is the same equation as obtained for stabilization by Casimir generation with a state-modulated nonlinear integral controller !

Conclusion: Basic IDA-PBC $\Leftrightarrow$ State-modulated Control by Interconnection.

Shifted passivity w.r.t. a controlled equilibrium
(see Jayawardhana, Ortega). Consider a port-Hamiltonian system

$$\begin{aligned} \dot{x} &= Fz + gu, \quad z = \tfrac{\partial H}{\partial x}(x) \\ y &= g^T z \end{aligned}$$

where $F = J - R, g$ are constant, and a controlled equilibrium x_0:

$$Fz_0 + gu_0 = 0, \quad z_0 = \frac{\partial H}{\partial x}(x_0)$$

Define the shifted storage function

$$V(x) := H_p(x) - (x - x_0)^T \frac{\partial H_p}{\partial x}(x_0) - H_p(x_0)$$

Note that $\frac{\partial V}{\partial x} = z - z_0$. It follows that

$\frac{d}{dt}V = (z - z_0)^T \dot{x} = (z - z_0)^T (Fz + gu) =$
$(z - z_0)^T F(z - z_0) + (z - z_0)^T g(u - u_0) + (z - z_0)^T (Fz_0 + gu_0) \leq (y - y_0)^T (u - u_0)$

implying passivity w.r.t. the shifted inputs $u - u_0$ and outputs $y - y_0$.

Application to switching control
Consider the port-Hamiltonian model of a power-converter

$$\dot{x} = F(\rho)z + g(\rho)E + g_l u, \quad z = \frac{\partial H_p}{\partial x}(x),\ F(\rho) := J(\rho) - R(\rho)$$

with vector of Boolean variables $\rho \in \{0,1\}^k$, $H_p(x)$ the total stored electromagnetic energy, and output vector $y = g_l^T z$.
Let x_0 be an equilibrium of the *averaged* model, that is

$$F(\rho_0)z_0 + g(\rho_0)E + g_l u_0 = 0, \quad z_0 = \frac{\partial H}{\partial x}(x_0)$$

for some $\rho_0 \in [0,1]^k$ and u_0. Then

$$\begin{aligned} \dot{x} &= F(\rho)(z - z_0) + F(\rho)z_0 + g(\rho)E + g_l u \\ &= F(\rho)(z - z_0) + [F(\rho) - F(\rho_0)]z_0 + [g(\rho) - g(\rho_0)]E + g_l(u - u_0) \\ &\quad + F(\rho_0)z_0 + g(\rho_0)E + g_l u_0 \\ &= F(\rho)(z - z_0) + [F(\rho) - F(\rho_0)]z_0 + [g(\rho) - g(\rho_0)]E + g_l(u - u_0) \end{aligned}$$

For many power converters we know that

$$\begin{aligned} F(\rho) - F(\rho_0) &= \sum_{i=1}^{p} F_i(\rho_i - \rho_{0i}) \\ g(\rho) - g(\rho_0) &= \sum_{i=1}^{p} g_i(\rho_i - \rho_{0i}) \end{aligned}$$

and thus

$$\dot{x} = F(\rho)(z - z_0) + \sum_{i=1}^{p} [F_i z_0 + g_i E](\rho_i - \rho_{0i}) + g_l(u - u_0)$$

Take as Lyapunov/storage function

$$V(x) := H_p(x) - (x - x_0)^T \frac{\partial H_p}{\partial x}(x_0) - H_p(x_0)$$

Then

$\frac{d}{dt}V(x) = [\frac{\partial H_p}{\partial x}(x) - \frac{\partial H_p}{\partial x}(x_0)]^T \dot{x} = (z - z_0)^T \dot{x} =$
$(z - z_0)^T F(\rho)(z - z_0) + \sum_{i=1}^{p} (z - z_0)^T [F_i z_0 + g_i E](\rho_i - \rho_{0i}) + (z - z_0)^T g_l(u - u_0)$

with $(z - z_0)^T F(\rho)(z - z_0) \leq 0$.

Thus at any time we can choose $\rho_i \in \{0, 1\}$ such that

$$\frac{d}{dt}V(x) \leq (z - z_0)^T g_l(u - u_0)$$

implying passivity of the switched system with respect to the input vector $u - u_0$ and output vector $y - y_0 = g_l^T(z - z_0)$. As a consequence, if the converter is terminated on a static resistive load then the switched converter is (asymptotically) stable around x_0. Thus the voltage over the resistive load can be stabilized around any set-point.
This can be immediately generalized to converters **connected to a load via a transmission line** (see Part I).

Note that for linear capacitors and inductors we have

$$H_p(x) = \frac{1}{2}x^T Q x, \quad V(x) = \frac{1}{2}(x - x_0)^T Q (x - x_0)$$

(cf. Buisson & co-workers)

New control paradigms

Example: Energy transfer control

Consider two port-Hamiltonian systems Σ_i

$$\begin{aligned} \dot{x}_i &= J_i(x_i)\frac{\partial H_i}{\partial x_i}(x_i) + g_i(x_i)u_i \\ y_i &= g_i^T(x_i)\frac{\partial H_i}{\partial x_i}(x_i), \qquad i = 1, 2 \end{aligned}$$

Suppose we want to transfer the energy from the port-Hamiltonian system Σ_1 to the port-Hamiltonian system Σ_2, while keeping the total energy $H_1 + H_2$ constant.

This can be done by using the output feedback

$$\begin{bmatrix} u_1 \\ u_2 \end{bmatrix} = \begin{bmatrix} 0 & -y_1 y_2^T \\ y_2 y_1^T & 0 \end{bmatrix} \begin{bmatrix} y_1 \\ y_2 \end{bmatrix}$$

It follows that the closed-loop system is energy-preserving. However, for the individual energies

$$\frac{d}{dt}H_1 = -y_1^T y_1 y_2^T y_2 = -||y_1||^2 ||y_2||^2 \leq 0$$

implying that H_1 is decreasing as long as $||y_1||$ and $||y_2||$ are different from 0. On the other hand,

$$\frac{d}{dt}H_2 = y_2^T y_2 y_1^T y_1 = ||y_2||^2 ||y_1||^2 \geq 0$$

implying that H_2 is increasing at the same rate. Has been successfully applied to energy-efficient *path-following control* of mechanical systems (Duindam & Stramigioli).

Impedance control

Consider a system with two (not necessarily distinct) ports

$$\begin{aligned} \dot{x} &= [J(x) - R(x)]\frac{\partial H}{\partial x}(x) + g(x)u + k(x)f, \quad x \in \mathcal{X},\, u \in \mathbb{R}^m \\ y &= g^T(x)\frac{\partial H}{\partial x}(x) \quad u, y \in \mathbb{R}^m \\ e &= k^T(x)\frac{\partial H}{\partial x}(x) \quad f, e \in \mathbb{R}^m \end{aligned} \tag{1}$$

The relation between the f and e variables is called the 'impedance' of the (f,e)-port. In **Impedance Control** (Hogan) one tries to *shape* this impedance by using the control port corresponding to u, y.
Typical application: the (f,e)-port corresponds to the end-point of a robotic manipulator, while the (u,y)-port corresponds to actuation.

Basic question: what are achievable impedances of the (f,e)-port ?

Model reduction of port-Hamiltonian systems

(Ongoing joint work with Polyuga, Scherpen.)

- Network modeling of complex lumped-parameter systems (circuits, multi-body systems) often leads to high-dimensional models.
- Structure-preserving spatial discretization of distributed-parameter port-Hamiltonian systems yields high-dimensional port-Hamiltonian models.
- Lumped-parameter modeling of systems like MEMS gives high-dimensional port-Hamiltonian systems
- Controller systems may be in first instance *distributed-parameter*, and need to be discretized to low-order controllers.

In many cases we want the reduced-order system to be **again port-Hamiltonian**:

- Port-Hamiltonian model reduction preserves passivity.
- Port-Hamiltonian model reduction may (approximately) preserve other balance laws /conservation laws.
- Physical interpretation of reduced-order model.
- Reduced-order system can replace the high-order port-Hamiltonian system in a larger context.

Thus there is a need for **structure-preserving** *model reduction of high-dimensional port-Hamiltonian systems.*

Controllability analysis

Consider a linear port-Hamiltonian system, written as

$$\begin{aligned} \dot{x} &= FQx + Bu, \quad F := J - R, \quad J = -J^T,\ R = R^T \geq 0 \\ y &= B^T Q x, \quad Q = Q^T \geq 0 \end{aligned}$$

Take linear coordinates $x = (x_1, x_2)$ such that the upper part of

$$\begin{bmatrix} \dot{x}_1 \\ \dot{x}_2 \end{bmatrix} = \begin{bmatrix} F_{11} & F_{12} \\ F_{21} & F_{22} \end{bmatrix} \begin{bmatrix} Q_{11} & Q_{12} \\ Q_{21} & Q_{22} \end{bmatrix} \begin{bmatrix} x_1 \\ x_2 \end{bmatrix} + \begin{bmatrix} B_1 \\ B_2 \end{bmatrix} u$$

$$y = \begin{bmatrix} B_1^T & B_2^T \end{bmatrix} \begin{bmatrix} Q_{11} & Q_{12} \\ Q_{21} & Q_{22} \end{bmatrix} \begin{bmatrix} x_1 \\ x_2 \end{bmatrix}$$

is the reachability subspace R.

By invariance of R this implies

$$\begin{aligned} F_{21}Q_{11} + F_{22}Q_{21} &= 0 \\ B_2 &= 0 \end{aligned}$$

If follows that the dynamics restricted to R is given as

$$\begin{aligned} \dot{x}_1 &= (F_{11}Q_{11} + F_{12}Q_{21})x_1 + B_1 u \\ y &= B_1^T Q_{11} x_1 \end{aligned}$$

Now solve for Q_{21} as $Q_{21} = -F_{22}^{-1}F_{21}Q_{11}$. This yields

$$\begin{aligned} \dot{x}_1 &= (F_{11} - F_{12}F_{22}^{-1}F_{21})Q_{11}x_1 + B_1 u \\ y &= B_1^T Q_{11} x_1 \end{aligned}$$

which is **again a port-Hamiltonian system**.

Observability analysis

Suppose the system is not observable. Then there exist coordinates $x = (x_1, x_2)$ such that the *lower* part is the unobservability subspace N. By invariance of N it follows that

$$\begin{aligned} F_{11}Q_{12} + F_{12}Q_{22} &= 0 \\ B_1^T Q_{12} + B_2^T Q_{22} &= 0 \end{aligned}$$

Then the dynamics on the quotient space $\mathcal{X}/N$ is

$$\begin{aligned} \dot{x}_1 &= (F_{11}Q_{11} + F_{12}Q_{21})x_1 + B_1 u \\ y &= B_1^T Q_{11} x_1 + B_2^T Q_{21} x_1 \end{aligned}$$

It follow from that $F_{12} = -F_{11}Q_{12}Q_{22}^{-1}$ and $B_2^T = -B_1^T Q_{12}Q_{22}^{-1}$. Substitution yields

$$\begin{aligned} \dot{x}_1 &= F_{11}(Q_{11} - Q_{12}Q_{22}^{-1}Q_{21})x_1 + B_1 u \\ y &= B_1^T(Q_{11} - Q_{12}Q_{22}^{-1}Q_{21})x_1 \end{aligned}$$

which is again a port-Hamiltonian system with Hamiltonian $\bar{H} = \frac{1}{2}x_1^T(Q_{11} - Q_{12}Q_{22}^{-1}Q_{21})x_1$.

Remark Note that the Schur complement $(Q_{11} - Q_{12}Q_{22}^{-1}Q_{21}) \geq 0$ if $Q \geq 0$.

This suggests two canonical ways for structure-preserving model reduction.

Conclusions of Part II

- Beyond passivity by port-Hamiltonian systems theory.
- Control by interconnection and Casimir generation, IDA-PBC control.
- Allows for 'physical' interpretation of control strategies. Suggests new control paradigms for nonlinear systems.
  - Use of passivity generally yields good robustness, but performance theory is yet lacking.
  - Observer theory for port-Hamiltonian systems; see talk Venkatraman.
  - Structure-preserving model reduction of port-Hamiltonian systems, see talk Polyuga.

Some Selected References for Part I and Part II

1. A.J. van der Schaft, *L_2-Gain and Passivity Techniques in Nonlinear Control*, Lect. Notes in Control and Information Sciences, Vol. 218, Springer-Verlag, Berlin, 1996, p. 168, 2nd revised and enlarged edition, Springer-Verlag, London, 2000, p. xvi+249.

2. B.M. Maschke, A.J. van der Schaft, P.C. Breedveld, "An intrinsic Hamiltonian formulation of network dynamics: Non-standard Poisson structures and gyrators", *Journal of the Franklin Institute, 329*, pp. 923–966, 1992.

3. A.J. van der Schaft, B.M. Maschke, "On the Hamiltonian formulation of nonholonomic mechanical systems", *Rep. Mathematical Physics, 34*, pp. 225–233, 1994.

4. A.J. van der Schaft, B.M. Maschke, "The Hamiltonian formulation of energy conserving physical systems with external ports", *Archiv für Elektronik und Übertragungstechnik, 49*, pp. 362–371, 1995.

5. M. Dalsmo, A.J. van der Schaft, "On representations and integrability of mathematical structures in energy-conserving physical systems", *SIAM J. Control and Optimization, vol.37*, pp. 54–91, 1999.

6. G. Escobar, A.J. van der Schaft, R. Ortega, "A Hamiltonian viewpoint in the modelling of switching power converters", *Automatica, vol.35*, pp.445–452, 1999.

7. R. Ortega, A.J. van der Schaft, I. Mareels, & B.M. Maschke, "Putting energy back in control", *Control Systems Magazine, vol. 21*, pp. 18–33, 2001.

8. G. Blankenstein, R. Ortega, A.J. van der Schaft, "The matching conditions of controlled Lagrangians and interconnection assignment passivity based control", *Int. Journal Robust and Nonlinear Control, vol. 75*, pp. 645–665, 2002.

9. R. Ortega, A.J. van der Schaft, B. Maschke, G. Escobar, "Interconnection and damping assignment passivity-based control of port-controlled Hamiltonian systems", *Automatica, vol. 38*, pp. 585–596, 2002.

10. A.J. van der Schaft, B.M. Maschke, "Hamiltonian formulation of distributed-parameter systems with boundary energy flow", *Journal of Geometry and Physics, vol. 42*, pp.166-194, 2002.

11. G. Golo, V. Talasila, A.J. van der Schaft, B.M. Maschke, "Hamiltonian discretization of boundary control systems", *Automatica, vol. 40/5*, pp. 757–711, 2004.

12. J. Cervera, A.J. van der Schaft, A. Banos, "Interconnection of port-Hamiltonian systems and composition of Dirac structures" *Automatica, vol. 43*, pp. 212–225, 2007.

13. R. Pasumarthy, A.J. van der Schaft, "Achievable Casimirs and its Implications on Control of port-Hamiltonian systems", *Int. J. Control, vol. 80* Issue 9, pp. 1421-1438, 2007.

14. D. Eberard, B. Maschke, A.J. van der Schaft, "An extension of pseudo-Hamiltonian systems to the thermodynamic space: towards a geometry of non-equilibrium thermodynamics", *Reports on Mathematical Physics, Vol. 60, No. 2*, pp. 175–198, 2007.

Part III: Distributed Parameter Systems

Hans Zwart, University of Twente
Arjan van der Schaft, University of Groningen

Contents

1 A simple example

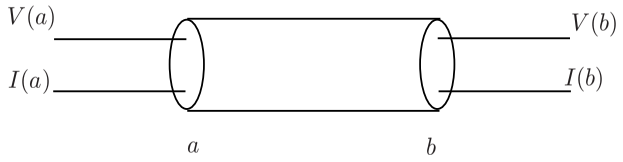

Consider the transmission line on the spatial interval $[a,b]$

$$\begin{aligned}\frac{\partial Q}{\partial t}(z,t) &= -\frac{\partial}{\partial z}\frac{\phi(z,t)}{L(z)} \\ \frac{\partial \phi}{\partial t}(z,t) &= -\frac{\partial}{\partial z}\frac{Q(z,t)}{C(z)}.\end{aligned} \tag{1}$$

We write $x_1 = Q$ (charge) and $x_2 = \phi$ (flux), and we find that

$$\begin{aligned}\frac{\partial}{\partial t}\begin{pmatrix} x_1 \\ x_2 \end{pmatrix}(z,t) &= \begin{pmatrix} 0 & -1 \\ -1 & 0 \end{pmatrix}\frac{\partial}{\partial z}\begin{pmatrix} \frac{1}{C(z)}x_1(z,t) \\ \frac{1}{L(z)}x_2(z,t) \end{pmatrix} \\ &= \begin{pmatrix} 0 & -1 \\ -1 & 0 \end{pmatrix}\frac{\partial}{\partial z}\left[\begin{pmatrix} \frac{1}{C(z)} & 0 \\ 0 & \frac{1}{L(z)} \end{pmatrix}\begin{pmatrix} x_1(z,t) \\ x_2(z,t) \end{pmatrix}\right] \\ &= P_1\frac{\partial}{\partial z}(\mathcal{L}x)(z,t)\end{aligned} \tag{2}$$

So we have the format as seen before, $J = P_1\frac{\partial}{\partial z}$ and $\frac{\partial \mathcal{H}}{\partial x} = \mathcal{L}x$. Thus the Hamiltonian equals $H = \frac{1}{2}\int_a^b x^T\mathcal{L}x dz = \int_a^b \mathcal{H}dz$.

To recapitulate some work done before, we differentiate the Hamiltonian (energy) along trajectories.

$$\begin{aligned}\frac{dH}{dt}(t) &= \frac{1}{2}\int_a^b \frac{\partial x}{\partial t}(z,t)^T \mathcal{L}(z)x(z,t)dz + \frac{1}{2}\int_a^b x(z,t)^T\mathcal{L}(z)\frac{\partial x}{\partial t}(z,t)dz \\ &= \frac{1}{2}\int_a^b \left(P_1\frac{\partial}{\partial z}\left(\mathcal{L}x\right)(z,t)\right)^T \mathcal{L}(z)x(z,t)dz + \\ &\quad \frac{1}{2}\int_a^b x(z,t)^T\mathcal{L}(z,t)(P_1\frac{\partial}{\partial z}\left(\mathcal{L}x\right)(z,t)dz \\ &= \frac{1}{2}\int_a^b \frac{\partial}{\partial z}\left[\left(\mathcal{L}x\right)^T(z,t)P_1\left(\mathcal{L}x\right)(z,t)\right]dz \\ &= \frac{1}{2}\left[\left(\mathcal{L}x\right)^T(z,t)P_1\left(\mathcal{L}x\right)(z,t)\right]_a^b,\end{aligned}$$

where we have used the symmetry of P_1.

So we have that the time-change of Hamiltonian satisfies

$$\frac{dH}{dt}(t) = \frac{1}{2}\left[\left(\mathcal{L}x\right)^T(z,t)P_1\left(\mathcal{L}x\right)(z,t)\right]_a^b. \tag{3}$$

That is the change of internal energy goes via the boundary.

Note the we only used that P_1 was symmetric. We did not need the specific form of P_1 or $\mathcal{L}$.

The balance equation (3) also holds for the system

$$\frac{\partial x}{\partial t}(z,t) = P_1\frac{\partial \mathcal{L}x}{\partial z}(z,t) + P_0\left[\mathcal{L}x\right](z,t) \tag{4}$$

with P_0 anti-symmetric, i.e., $P_0^T = -P_0$.

Many systems can be written in this format.

2 More examples

Example

Wave equation for the vibrating string:

$$\frac{\partial^2 w}{\partial t^2}(z,t) = \frac{T}{\rho}\frac{\partial^2 w}{\partial z^2}(z,t),$$

where ρ is the mass density, and T is Young's modulus.

This is in our format with

$$P_1 = \begin{pmatrix} 0 & 1 \\ 1 & 0 \end{pmatrix}, \qquad \mathcal{L} = \begin{pmatrix} \frac{1}{\rho} & 0 \\ 0 & T \end{pmatrix}$$

The state variable are $x_1 = \rho\frac{\partial w}{\partial t}$ (the momentum) and $x_2 = \frac{\partial w}{\partial z}$ (the strain).

Example

The model of Timoshenko beam is given

$$\begin{aligned}\rho(z)\frac{\partial^2 w}{\partial t^2}(z,t) &= \frac{\partial}{\partial z}\left[K(z)\left[\frac{\partial w}{\partial z}(z,t) - \phi(z,t)\right]\right] \\ I_\rho(z)\frac{\partial^2 \phi}{\partial t^2} &= \frac{\partial}{\partial z}\left[EI(z)\frac{\partial \phi}{\partial z}\right] + K(z)\left[\frac{\partial w}{\partial z}(z,t) - \phi\right],\end{aligned}$$

where $w(z,t)$ is the transverse displacement of the beam and $\phi(z,t)$ is the rotation angle of a filament of the beam. The positive coefficients $\rho(z)$, $I_\rho(z)$, $E(z)$, $I(z)$, and $K(z)$ are the mass per unit length, the rotary moment of inertia of a cross section, Young's modulus of elasticity, the moment of inertia of a cross section, and the shear modulus respectively.

By introducing the state variables

$$\begin{aligned} x_1 &= \frac{\partial w}{\partial z} - \phi : && \text{shear displacement,} \\ x_2 &= \rho \frac{\partial w}{\partial t} : && \text{transverse momentum distribution,} \\ x_3 &= \frac{\partial \phi}{\partial z} : && \text{angular displacement,} \\ x_4 &= I_\rho \frac{\partial \phi}{\partial t} : && \text{angular momentum distribution,} \end{aligned}$$

we can write this in our standard format, with

$$P_1 = \begin{pmatrix} 0 & 1 & 0 & 0 \\ 1 & 0 & 0 & 0 \\ 0 & 0 & 0 & 1 \\ 0 & 0 & 1 & 0 \end{pmatrix} \quad P_0 = \begin{pmatrix} 0 & 0 & 0 & -1 \\ 0 & 0 & 0 & 0 \\ 0 & 0 & 0 & 0 \\ 1 & 0 & 0 & 0 \end{pmatrix}$$

and

$$\mathcal{L} = \operatorname{diag}\{K, \frac{1}{\rho}, EI, \frac{1}{I_\rho}\}.$$

Example

Consider transmission lines in a network

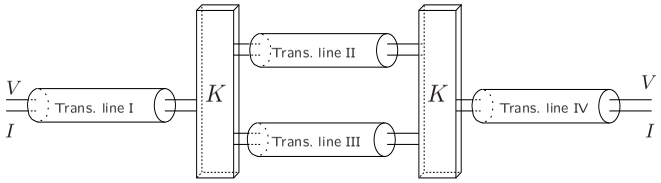

In the coupling parts K, we have that Kirchhoff laws holds. Hence charge flowing out of the transmission line I, enters II and III, etc.

The P_1 of the big system is the diagonal matrix, build from the uncoupled P_1's (which are all the same). The $\mathcal{L}$ of the coupled system is the diagonal matrix of the uncoupled $\mathcal{L}$.

The coupling is written down as boundary conditions of the p.d.e.

3 Choice of inputs and outputs

For our p.d.e.

$$\frac{\partial x}{\partial t}(z,t) = P_1 \frac{\partial \mathcal{L}x}{\partial z}(z,t) + P_0 \left[\mathcal{L}x\right](z,t)$$

we have

$$\frac{dH}{dt}(t) = \frac{1}{2}\left[(\mathcal{L}x)^T(z,t) P_1 (\mathcal{L}x)(z,t)\right]_a^b.$$

Hence one may influence the Hamiltonian via these boundary variables, and one may observe the system via the boundary. How to choose inputs and outputs?

Consider again the transmission line example, and assume that the C and L are constant.

$$\frac{\partial}{\partial t}\begin{pmatrix} x_1 \\ x_2 \end{pmatrix}(z,t) = \begin{pmatrix} 0 & -1 \\ -1 & 0 \end{pmatrix} \frac{\partial}{\partial z}\left[\begin{pmatrix} \frac{1}{C} & 0 \\ 0 & \frac{1}{L} \end{pmatrix}\begin{pmatrix} x_1(z,t) \\ x_2(z,t) \end{pmatrix}\right].$$

We diagonalize the matrix $P_1\mathcal{L} = \begin{pmatrix} 0 & \frac{-1}{C} \\ \frac{-1}{L} & 0 \end{pmatrix}$.

Hence

$$\begin{pmatrix} 0 & \frac{-1}{L} \\ \frac{-1}{C} & 0 \end{pmatrix} = \begin{pmatrix} 1 & 1 \\ -\sqrt{\frac{L}{C}} & \sqrt{\frac{L}{C}} \end{pmatrix}\begin{pmatrix} \sqrt{\frac{1}{LC}} & 0 \\ 0 & -\sqrt{\frac{1}{LC}} \end{pmatrix}\begin{pmatrix} 1 & -\sqrt{\frac{C}{L}} \\ 1 & \sqrt{\frac{C}{L}} \end{pmatrix}\frac{1}{2}.$$

In the new variables (characteristics)

$$\begin{pmatrix} \xi_1 \\ \xi_2 \end{pmatrix} = \begin{pmatrix} 1 & -\sqrt{\frac{C}{L}} \\ 1 & \sqrt{\frac{C}{L}} \end{pmatrix}\begin{pmatrix} x_1 \\ x_2 \end{pmatrix}$$

the transmission line becomes

$$\frac{\partial \xi_1}{\partial t} = \sqrt{\frac{1}{LC}}\frac{\partial \xi_1}{\partial z}, \qquad \frac{\partial \xi_2}{\partial t} = -\sqrt{\frac{1}{LC}}\frac{\partial \xi_2}{\partial z}.$$

Summarizing, we see that if we diagonalize $P_1\mathcal{L}$, then the p.d.e. becomes a set of p.d.e.'s in one variable.

Note that the coupling is now only via the boundary variables.

Assume that there is no coupling via the boundary, then we can study the choice of inputs and outputs for a scalar p.d.e.

Consider the shift on the interval $[0,1]$, described by the p.d.e.

$$\frac{\partial w}{\partial t}(z,t) = \frac{\partial w}{\partial z}(z,t), \qquad z \in (0,1). \tag{5}$$

with boundary condition

$$w(0,t) = 0.$$

The solution would be $w(z,t) = w_0(z+t)$. This is conflicting with the freedom of initial conditions, since
$w_0(1/2) = w_0(0+1/2) = w(0,1/2) = 0.$

The boundary condition

$$w(1,t) = 0.$$

is good.

A perfect choice for the input/output pair is

$$w(1,t) = u_s(t) \qquad w(0,t) = y_s(t). \tag{6}$$

We summarize the previous.

- The format

$$\frac{\partial x}{\partial t}(z,t) = P_1 \frac{\partial}{\partial z}\left(\mathcal{L}x\right)(z,t), \qquad z \in [a,b], \tag{7}$$

  with P_1 symmetric, $\det(P_1) \neq 0$, and $\mathcal{L} > 0$, is a very nice one, and general, see our examples.

  They are port-Hamiltonian systems with a positive (quadratic) Hamiltonian. Note that $J = P_1\frac{\partial}{\partial z}$, $\frac{\partial \mathcal{H}}{\partial x} = \mathcal{L}x$.

- If we diagonalize $P_1\mathcal{L}$, then we get a set of p.d.e.'s which are only coupled via the boundary. That is we write the system in its characteristics or Riemann coordinates.

- For a scalar p.d.e., we can easily find good inputs and outputs.

- How to find them general?

4 Well-posedness

For $t \geq 0$ and $z \in [a,b]$ we consider the system:

$$\frac{\partial x}{\partial t}(z,t) = P_1 \frac{\partial}{\partial z}\left(\mathcal{L}x\right)(z,t), \quad x(0,z) = x_0(z) \tag{8}$$

$$0 = M_{11}\left(\mathcal{L}x\right)(b,t) + M_{12}\left(\mathcal{L}x\right)(a,t) \tag{9}$$

$$u(t) = M_{21}\left(\mathcal{L}x\right)(b,t) + M_{22}\left(\mathcal{L}x\right)(a,t) \tag{10}$$

$$y(t) = C_1\left(\mathcal{L}x\right)(b,t) + C_2\left(\mathcal{L}x\right)(a,t). \tag{11}$$

We assume that x takes values in $\mathbb{R}^n$, $P_1^T = P_1$, $\det(P_1) \neq 0$, $\mathcal{L} > 0$, and that $\operatorname{rank}\begin{bmatrix} M_{11} & M_{12} \\ M_{21} & M_{22} \\ C_1 & C_2 \end{bmatrix} = n + \operatorname{rank}\begin{bmatrix} C_1 & C_2 \end{bmatrix}$.

Definition

Consider the system (8)–(11). This system is *well-posed* if there exists a $t_f > 0$ and m_f such that the following holds:

1. The homogeneous p.d.e., i.e., $u \equiv 0$ has for any initial condition, $x(0)$ a unique (weak) solution.
2. The following inequality holds for all smooth initial conditions, and all smooth inputs

$$H(t_f) + \int_0^{t_f} \|y(t)\|^2 dt \leq m_f \left[H(0) + \int_0^{t_f} \|u(t)\|^2 dt \right], \qquad (12)$$

where H is the Hamiltonian: $\frac{1}{2}\int_a^b x^T \mathcal{L} x dz$.

Theorem

Under the conditions we have imposed, the following holds:

- If condition 1 holds, then automatically condition 2 holds.
- That is: If the homogeneous p.d.e., i.e., $u \equiv 0$, has a weak solution, then the system (8)–(11) is well-posed.
- The transfer function $G(s)$ can also be obtained, and also $\lim_{s\to\infty} G(s)$.
- There is a matrix condition for checking condition 1.
- Same theorem holds for $\frac{\partial x}{\partial t}(z,t) = P_1 \frac{\partial}{\partial z}(\mathcal{L}x)(z,t) + P_0(\mathcal{L}x)(z,t)$.

Remark

- So well-posedness gives you that you have a unique solution for every square integrable input function and every initial condition. Furthermore, the output signal is always square integrable.
- Every well-posed system has a transfer function, bounded in some right-half plane.

We want to give an idea of the proof. Therefor we do it for our system with the following choice of boundary input and output

$$u(t) = \begin{pmatrix} V(a,t) \\ V(b,t) \end{pmatrix}, \qquad y(t) = \begin{pmatrix} I(a,t) \\ I(b,t) \end{pmatrix}. \qquad (13)$$

Now we preform the following steps:

1. Since $V = Q/C = x_1/C$ and $I = \phi/L = x_2/L$, we have that

$$[M_{21}, M_{22}] = \left(\begin{array}{cc|cc} 0 & 0 & \frac{1}{C} & 0 \\ \frac{1}{C} & 0 & 0 & 0 \end{array}\right), \quad [C_1, C_2] = \left(\begin{array}{cc|cc} 0 & 0 & 0 & \frac{1}{L} \\ 0 & \frac{1}{L} & 0 & 0 \end{array}\right).$$

2. Write the system in the "characteristic", $\xi_1 = x_1 - \sqrt{\frac{C}{L}} x_2$, $\xi_2 = x_2 + \sqrt{\frac{C}{L}} x_2$,
   The p.d.e. becomes

$$\frac{\partial \xi_1}{\partial t} = \sqrt{\frac{1}{LC}} \frac{\partial \xi_1}{\partial z}, \qquad \frac{\partial \xi_2}{\partial t} = -\sqrt{\frac{1}{LC}} \frac{\partial \xi_2}{\partial z}.$$

The "perfect" input and output for this system is

$$u_s(t) = \begin{pmatrix} \xi_1(b,t) \\ \xi_2(a,t) \end{pmatrix}, \qquad y_s(t) = \begin{pmatrix} \xi_1(a,t) \\ \xi_2(b,t) \end{pmatrix}. \tag{14}$$

3. Write our input-output pair in this input-output pair.

$$\begin{aligned} u(t) &= \begin{pmatrix} 0 & \frac{1}{2C} \\ \frac{1}{2C} & 0 \end{pmatrix} u_s(t) + \begin{pmatrix} \frac{1}{2C} & 0 \\ 0 & \frac{1}{2C} \end{pmatrix} y_s(t) \\ &= K u_s(t) + Q y_s(t) \end{aligned} \tag{15}$$

$$\begin{aligned} y(t) &= \begin{pmatrix} 0 & \frac{1}{2\sqrt{LC}} \\ \frac{-1}{2\sqrt{LC}} & 0 \end{pmatrix} u_s(t) + \begin{pmatrix} \frac{-1}{2\sqrt{LC}} & 0 \\ 0 & \frac{1}{2\sqrt{LC}} \end{pmatrix} y_s(t) \\ &= O_1 u_s(t) + O_2 y_s(t). \end{aligned} \tag{16}$$

Remark

- Since

$$G_s(s) = \begin{pmatrix} e^{-s\sqrt{LC}(b-a)} & 0 \\ 0 & e^{-s\sqrt{LC}(b-a)} \end{pmatrix}$$

one can calculate the transfer function from u to y.

- If we choose $u(t) = \begin{pmatrix} V(a,t) \\ I(a,t) \end{pmatrix}$, then not well-posed. The corresponding K is

$$K = \begin{pmatrix} 0 & \frac{1}{2C} \\ 0 & \frac{1}{2\sqrt{LC}} \end{pmatrix}.$$

We regard the system with input/output u, y as a feedback of the system with input/output u_s, y_s, i.e.,

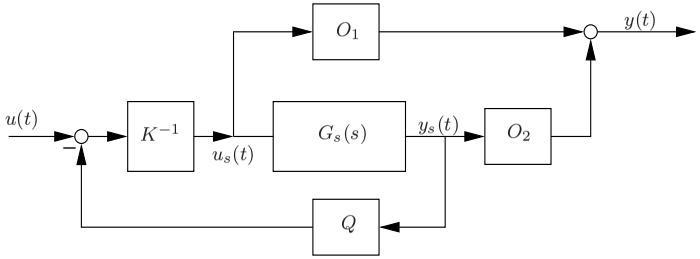

Now G_s has feed-through zero, and so any feedback is allowed.

Only condition: K^{-1} exists.

5 Stability

For our class of system, i.e., $\frac{\partial x}{\partial t} = P_1 \frac{\partial \mathcal{L} x}{\partial z}$, we have

$$\frac{dH}{dt}(t) = \frac{1}{2}\left[(\mathcal{L}x)^T(z,t) P_1 (\mathcal{L}x)(z,t) \right]_a^b.$$

Furthermore, we have written our boundary conditions, inputs, and outputs as linear combinations of these boundary variables. One would expect exponential stability of the uncontrolled system when $\frac{dH}{dt} < 0$ for zero inputs. This is the subject of the following theorem.

Theorem

Consider the p.d.e. $\frac{\partial x}{\partial t} = P_1 \frac{\partial \mathcal{L}x}{\partial z}$ with Hamiltonian $H = \frac{1}{2}\int_a^b x^T \mathcal{L}x dz$. If the homogeneous p.d.e., i.e., $u \equiv 0$ satisfies

- $\frac{dH}{dt} \leq -\kappa \|\mathcal{L}x(b)\|^2$, or
- $\frac{dH}{dt} \leq -\kappa \|\mathcal{L}x(a)\|^2$

for some $\kappa > 0$, then the (uncontrolled) system is exponentially stable.

$$\begin{aligned} \frac{\partial Q}{\partial t}(z,t) &= -\frac{\partial}{\partial z}\frac{\phi(z,t)}{L(z)} \\ \frac{\partial \phi}{\partial t}(z,t) &= -\frac{\partial}{\partial z}\frac{Q(z,t)}{C(z)}. \end{aligned} \tag{17}$$

For this system we have

$$P_1 = \begin{pmatrix} 0 & -1 \\ -1 & 0 \end{pmatrix} \qquad \text{and} \qquad \mathcal{L}(z) = \begin{pmatrix} \frac{1}{C(z)} & 0 \\ 0 & \frac{1}{L(z)} \end{pmatrix}.$$

Furthermore, $V = Q/C$, $I = \phi/L$. We choose the boundary input $V(a,t) = u(t)$, and we place a resistor at the other end, i.e., $V(b,t) = RI(b,t)$, $R > 0$.

Note that this is of the form (8)–(10), see slide 16.

Proof: We have that for τ_f large enough that (fact)

$$H(\tau_f) \leq c_f \int_0^{\tau_f} \|\mathcal{L}x(b,t)\|^2 dt.$$

Now from our assumption

$$\begin{aligned} H(\tau_f) - H(0) &= \int_0^{\tau_f} \frac{dH}{dt}(t)dt \\ &\leq -\kappa \int_0^{\tau_f} \|\mathcal{L}x(b,t)\|^2 dt \\ &\leq \frac{-\kappa}{c_f} H(\tau_f). \end{aligned}$$

Thus

$$H(\tau_f) \leq \frac{c_f}{c_f + \kappa} H(0) < H(0).$$

This proves exponential stability. □

We apply this theorem to our transmission line.

Since $\mathcal{L}x = \binom{V}{I}$, we find that

$$\begin{aligned} \frac{dH}{dt} &= \frac{1}{2}\left[(\mathcal{L}x)^T(z) P_1 (\mathcal{L}x)(z)\right]_a^b \\ &= \frac{1}{2}\left[\begin{pmatrix} V(z) & I(z) \end{pmatrix}\begin{pmatrix} 0 & -1 \\ -1 & 0 \end{pmatrix}\begin{pmatrix} V(z) \\ I(z) \end{pmatrix}\right]_a^b \\ &= -V(b)I(b) + V(a)I(a). \end{aligned}$$

Applying our conditions: $V(a) = 0$, and $V(b) = RI(b)$, we have

$$\frac{dH}{dt} = -RI(b)^2 = -\frac{R}{R^2+1}\left[V(b)^2 + I(b)^2\right].$$

Thus exponentially stable.

6 Diffusive systems

We have that the system $\frac{\partial x}{\partial t} = P_1 \frac{\partial \mathcal{L} x}{\partial z}$, satisfies
$\frac{dH}{dt} = \frac{1}{2}\left[(\mathcal{L}x)^T(z) P_1 (\mathcal{L}x)(z)\right]_a^b$.

As explained in Part I, there is an underlying structure.

If (f, e) are related like

$$f(z) = P_1 \frac{\partial e}{\partial z}(z) = J e(z), \tag{18}$$

then

$$\int_a^b f(z)^T e(z) dz = \frac{1}{2}\left[e^T(z) P_1 e(z)\right]_a^b. \tag{19}$$

Choosing now $f = \frac{\partial x}{\partial t}$, and $e = \frac{\partial \mathcal{H}}{\partial x} = \mathcal{L}x$, we recover our system and balance equation.

However, we can make other choices.

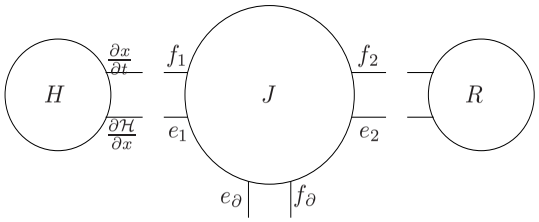

Figure 1: Port-Hamiltonian system with dissipation R

Example

Choose the P_1 from the transmission line, i.e.,

$$P_1 = \begin{pmatrix} 0 & -1 \\ -1 & 0 \end{pmatrix}$$

Now we choose

$$f = \begin{pmatrix} f_1 \\ f_2 \end{pmatrix} = \begin{pmatrix} \frac{\partial x}{\partial t} \\ f_2 \end{pmatrix}, \qquad e = \begin{pmatrix} e_1 \\ e_2 \end{pmatrix} = \begin{pmatrix} x \\ R f_2 \end{pmatrix}, \tag{20}$$

then we find the system ($f = P_1 \frac{\partial e}{\partial z}$)

$$\frac{\partial x}{\partial t} = -\frac{\partial}{\partial z}[R f_2] = -\frac{\partial}{\partial z}\left[-R\frac{\partial x}{\partial z}\right] = \frac{\partial}{\partial z}\left[R\frac{\partial x}{\partial z}\right]. \tag{21}$$

This is the p.d.e. which describes diffusion.

Theorem

Assume that the p.d.e.

$$\frac{\partial}{\partial t}\begin{pmatrix} x_1 \\ x_2 \end{pmatrix} = P_1 \frac{\partial}{\partial z}\begin{pmatrix} \mathcal{L}x_1 \\ x_2 \end{pmatrix} \tag{22}$$

with homogeneous boundary conditions has a (mild) solution for every initial condition, and that along these solutions

$$\frac{d}{dt}\left[\int_a^b x_1^T(z,t)\mathcal{L}x_1(z,t) + \|x_2(z,t)\|^2 dz\right] \leq 0. \tag{23}$$

Then the p.d.e.

$$\begin{pmatrix} \frac{\partial x}{\partial t} \\ f_2 \end{pmatrix} = P_1 \frac{\partial}{\partial z}\begin{pmatrix} \mathcal{L}x \\ R f_2 \end{pmatrix} \tag{24}$$

has a solution, provided $R > \varepsilon I$. Furthermore,
$\frac{d}{dt}\int_a^b x^T(z,t)\mathcal{L}x(z,t)dz \leq 0$.

References

1. Y. Le Gorrec, H. Zwart, and B. Maschke, "Dirac structures and boundary control systems associated with skew-symmetric differential operators," *SIAM J. Control and Optim.*, vol. 44, no. 2, pp. 1864–1892, 2005.

2. A.J. van der Schaft and B.M. Maschke, "Hamiltonian formulation of distributed-parameter systems with boundary energy flow," *J. of Geometry and Physics*, vol. 42, pp. 166–194, 2002.

3. J.A. Villegas, *A Port-Hamiltonian Approach to Distributed Parameter Systems*, Ph.D. thesis, Department of Applied Mathematics, University of Twente, Enschede, The Netherlands, May 2007, available at http://www.eng.ox.ac.uk/control/peopleAJV.shtml.

Part 4

List of Participants

Pierre-Antoine ABSIL
Dept. INMA
Université catholique de Louvain/UCL
Avenue Georges Lemaître, 4
1348 Louvain-la-Neuve
Belgium
absil@inma.ucl.ac.be

Ir. J. Albersmeyer
Dept. of Electrical Engineering
KU Leuven
Kasteelpark Arenberg 10
B-3001 Leuven
Belgium
jan.albersmeyer@esat.kuleuven.be

Alejandro Alvarez Aguirre
Dept. of Mechanical Engineering
Technische Universiteit Eindhoven
PO Box 513
5600 MB Eindhoven
The Netherlands
a.a.alvarez@tue.nl

J.M. Ast, van
Delft Center for Systems and Control
Delft University of Technology
Mekelweg 2
2628 CD Delft
The Netherlands
j.m.vanast@tudelft.nl

Kurt Barbé
Dept. ELEC
Vrije Universiteit Brussel
Pleinlaan 2
1050 Brussel
Belgium
Kurt.Barbe@vub.ac.be

Ir Ch. Bastin
Dept. of EECS
University of Liege
B28 Institut Montefiore, Grande Traverse, 10
4000 Liege
Belgium
ch.bastin@ulg.ac.be

Maite Bauwens
Dept. ELEC
Vrije Universiteit Brussel
Pleinlaan 2
1050 Brussels
Belgium
msbauwen@vub.ac.be

Charlotte Beauthier
Department of mathematics
University of Namur (FUNDP)
Rempart de la Vierge, 8
5000 Namur
Belgium
charlotte.beauthier@math.fundp.ac.be

Veerle Beelaerts
Dept. ELEC
Vrije Universiteit Brussel
Pleinlaan 2
1050 Brussels
Belgium
vbeelaer@vub.ac.be

Florence Belmudes
Dept. of Electrical Engineering and Computer Science
University of Liège
Bâtiment B28, Grande traverse 10
4000 Liège
Belgium
florence.belmudes@ulg.ac.be

Nadia BENIICH
Dept. INMA
Université catholique de Louvain/UCL
Avenue Georges Lemaître, 4
1348 Louvain-la-Neuve
Belgium
nadia.beniich@uclouvain.be

Ir N.C. Besseling
Department of Applied Mathematics
University of Twente
PO Box 217
7500 AE Enschede
The Netherlands
n.c.besseling@math.utwente.nl

IWM Bleylevens
Micc/Dept. of Mathematics
Maastricht University
P.O. Box 616
6200 MD Maastricht
The Netherlands
i.bleylevens@math.unimaas.nl

R.S. Blom
Delft Center for Systems and Control
Delft University of Technology
Mekelweg 2
2628 CD Delft
The Netherlands
r.s.blom@tudelft.nl

Julian Bonilla
Dept. of Chemical Engineering CIT/BioTec
Katholieke Universiteit Leuven
W. de Croyland 46
B-3001 Leuven
Belgium
julian.bonilla@cit.kuleuven.be

Silvere Bonnabel
Department of electrical engineering and computer science
Université de Liège
Université de Liège B28 Sart Tilman
B4000 Liège
Belgium
bonnabel@montefiore.ulg.ac.be

Dr J. Bontsema
Greenhouse Horticulture
Wageningen University and Research Centre
PO Box 16
6700 AA Wageningen
The Netherlands
jan.bontsema@wur.nl

Thomas CASON
Dept. INMA
Université catholique de Louvain/UCL
Avenue Georges Lemaître, 4
1348 Louvain-la-Neuve
Belgium
thomas.cason@uclouvain.be

Robert David
Service d'Automatique
Faculté Polytechnique de Mons
34 Boulevard Dolez
7000 Mons
Belgium
robert.david@fpms.ac.be

Jeroen de Best
Dept. of Mechanical Engineering
Technische Universiteit Eindhoven
PO Box 513
5600 MB Eindhoven
The Netherlands
j.j.t.h.d.best@tue.nl

Bram de Jager
Dept. of Mechanical Engineering
Technische Universiteit Eindhoven
PO Box 513
5600 MB Eindhoven
The Netherlands
A.G.de.Jager@tue.nl

Joris De Schutter
Dept. of Mechanical Engineering
K.U.Leuven
Celestijnenlaan 300 B
B 3001 Heverlee
Belgie
joris.deschutter@mech.kuleuven.be

Prof.dr.ir. B. De Schutter
Delft Center for Systems and Control
Delft University of Technology
Mekelweg 2
2628 CD Delft
The Netherlands
bart@deschutter.info

ir. C.C. de Visser
Aerospace Engineering
Delft University of Technology
Kluyverweg 1
2629 HS Delft
the Netherlands
c.c.devisser@tudelft.nl

ir E de Weerdt
Dept. of Aerospace Engineering, Control and Simulation Division
Technical University of Delft
PO Box 5058
2600GB Delft
The Netherlands
E.deWeerdt@TUDelft.nl

MSc. Ir. del Puerto Flores
Discrete Technologie en Productie Automatisering
Rijksuniversiteit Groningen
Nijenborgh 4
9747 AG Groningen
The Netherlands
d.del.puerto.flores@rug.nl

ir. C. Deliu
Dept. Mathematics and Computer Science
Technische Universiteit Eindhoven
PO Box 513
5600 MB Eindhoven
The Netherlands
c.deliu@tue.nl

Jean-Charles DELVENNE
Dept. INMA
Université catholique de Louvain/UCL
Avenue Georges Lemaître, 4
1348 Louvain-la-Neuve
Belgium
jean-charles.delvenne@uclouvain.be

Thomas Delwiche
Control Engineering department
Université Libre de Bruxelles
Av. F.D. Roosevelt, 50
1050 Brussels
Belgium
Thomas.Delwiche@ulb.ac.be

Arjen Den Hamer
Mechanical Engineering
Technische Universiteit Eindhoven
PO Box 513
5600 MB Eindhoven
The Netherlands
a.j.d.hamer@tue.nl

Ir L.D. Dewasme
Service d'automatique
Faculté polytechnique de Mons
Boulevard Dolez, 31
7000 Mons
Belgium
laurent.dewasme@fpms.ac.be

Prof. Dr. M. Diehl
Dept. of Electrical Engineering
KU Leuven
Kasteelpark Arenberg 10
B-3001 Leuven
Belgium
moritz.diehl@esat.kuleuven.be

C. M.Sc. Ding
Dept. of Electrical Engineering
Technische Universiteit Eindhoven
PO Box 513
5600 MB Eindhoven
The Netherlands
b.a.cornelissen@tue.nl

Ir. D.A. Dirksz
Discrete Technology
University of Groningen
Nijenborgh 4
9747 AG Groningen
The Netherlands
d.a.dirksz@rug.nl

S. Djordjevic
Delft Center for Systems and Control
Delft University of Technology
Mekelweg 2
2628 CD Delft
The Netherlands
s.djordjevic@tudelft.nl

Denis DOCHAIN
Dept. INMA
Université catholique de Louvain/UCL
Avenue Georges Lemaître, 4
1348 Louvain-la-Neuve
Belgium
denis.dochain@uclouvain.be

J.F. Dong
Delft Center for Systems and Control
Delft University of Technology
Mekelweg 2
2628 CD Delft
The Netherlands
j.dong@tudelft.nl

J.F.M. Doren
Delft Center for Systems and Control
Delft University of Technology
Mekelweg 2
2628 CD Delft
The Netherlands
j.f.m.vandoren@tudelft.nl

Prof. Dr. R. Eising
FCTW
Twente University
Postbus 217
7500 AE Enschede
The Netherlands
f.eising@ctw.utwente.nl

Dr. J.C. Engwerda
Dept. of Econometrics and O.R.
Tilburg University
P.O. Box 90153
5000 LE Tilburg
The Netherlands
engwerda1@hotmail.com

Dr. D. Ernst
Department of Electrical Engineering and Computer Science
University of Liège
Building B28, Parking P32
B-4020 Liège
Belgium
dernst@ulg.ac.be

Willem-Jan Evers
Dept. of Mechanical Engineering
Technische Universiteit Eindhoven
PO Box 513
5600 MB Eindhoven
The Netherlands
w.j.e.evers@tue.nl

Audrey FAVACHE
Unité IMAP
Université catholique de Louvain/UCL
Place Sainte Barbe, 2
1348 Louvain-la-Neuve
Belgium
audrey.favache@uclouvain.be

Ir. J. Ferreau
Dept. of Electrical Engineering
KU Leuven
Kasteelpark Arenberg 10
B-3001 Leuven
Belgium
jochaim.ferreau@esat.kuleuven.be

Raphael Fonteneau
Electrical Engineering and Computer Science
University of Liege
Grande Traverse, 10
4000 LIEGE
BELGIUM
raphael.fonteneau@ulg.ac.be

Wim Foubert
Dept. ELEC
Vrije Universiteit Brussel
Pleinlaan 2
1050 Brussel
Belgium
wfoubert@vub.ac.be

ir. (MSc) M.C.J. Franken
Dept. of Electrical Engineering
Universiteit Twente
PO box 217
7500 AE Enschede
The Netherlands
m.c.j.franken@utwente.nl

MSc. M. Gajdusek
Dept. of Electrical Engineering
Technische Universiteit Eindhoven
PO Box 513
5600 MB Eindhoven
The Netherlands
m.gajdusek@tue.nl

Manuel Gálvez-Carrillo
Control Engineering Department
Université Libre de Bruxelles
Av. F. D. Roosevelt 50 , CP 165/55
1050 Bruxelles
Belgium
mgalvezc@ulb.ac.be

Eloisa del Carmen Garcia Canseco
Faculty of Mathematics and Natural Sciences
University of Groningen
ITM, Nijenborgh 4
9747 AG Groningen
The Netherlands
e.garcia.canseco@rug.nl

M. Gerard
Delft Center for Systems and Control
Delft University of Technology
Mekelweg 2
2628 CD Delft
The Netherlands
M.P.Gerard@tudelft.nl

Michel GEVERS
Dept. INMA
Université catholique de Louvain/UCL
Avenue Georges Lemaître, 4
1348 Louvain-la-neuve
Belgium
michel.gevers@uclouvain.be

Geert Gins
BioTeC
Katholieke Universiteit Leuven
W. de Croylaan 46
3001 Heverlee
Belgium
geert.gins@cit.kuleuven,be

Guillaume Goffaux
Automatic Control Laboratory
Faculté Polytechnique de Mons
Boulevard Dolez 31
7000 Mons
Belgium
guillaume.goffaux@fpms.ac.be

Liesbeth Gommé
Dept. ELEC
Vrije Universiteit Brussel
Pleinlaan 2
1050 Brussels
Belgium
Liesbeth.Gomme@vub.ac.be

Niels Haverbeke
Elektrotechniek (ESAT)
Katholieke Universiteit Leuven
Kasteelpark Arenberg 10
B-3001 Leuven (Heverlee)
Belgium
niels.haverbeke@esat.kuleuven.be

Ir A.H. Haye
Unité de Bioinformatique génomique et structurale
Université Libre de Bruxelles
50, avenue Roosevelt CP 165/61
1050 Bruxelles
Belgium
ahaye@ulb.ac.be

MSc. J. Heijman
MICC / Mathematics
Maastricht University
PO Box 616
6200 MD Maastricht
The Netherlands
jordi.heijman@micc.unimaas.nl

Dr P.S.C. Heuberger
Delft Center for Systems and Control
Delft University of Technology
Mekelweg 2
2628 CD Delft
The Netherlands
p.s.c.heuberger@tudelft.nl

A.E.M. Huesman
Delft Center for Systems and Control
Delft University of Technology
Mekelweg 2
2628 CD Delft
The Netherlands
a.e.m.huesman@tudelft.nl

ing. B. Huyck
Dept. of Electrical Engineering
KU Leuven
Kasteelpark Arenberg 10
B-3001 Leuven
Belgium
bart.huyck@esat.kuleuven.be

Ir. Clara-Mihaela Ionescu
Electrical energy, Systems and Automation
Ghent University
Technologiepark 913
9000 Gent-Zwijnaarde
Belgium
clara@autoctrl.UGent.be

PhD Tzvetan IVANOV
Dept. INMA
Université catholique de Louvain/UCL
Avenue Georges Lemaître, 4
1348 Louvain-la-Neuve
Belgium
tzvetan.ivanov@uclouvain.be

Dr. B. Jayawardhana
Discrete Technologie en Productie Automatisering — Inst. voor Technologie, Engineering en Management
University of Groningen
Nijenborgh 4
9747 AG Groningen
The Netherlands
bayujw@ieee.org

D.A. Joosten
Delft Center for Systems and Control
Delft University of Technology
Mekelweg 2
2628 CD Delft
The Netherlands
d.a.joosten@tudelft.nl

Michel Journée
Dept. of Electrical Engineering and Computer Science
University of Liège
BAT. B28, Grande Traverse, 10
4000 Liège
Belgium
m.journee@ulg.ac.be

K.J. Keesman
Systems & Control Group
Wageningen University
P.O. Box 17
6700 AA Wageningen
The Netherlands
karel.keesman@wur.nl

F. J. Kerber
Insitituut voor Wiskunde en Informatica
University of Groningen
PO Box 407
9700 AK Groningen
The Netherlands
florian@math.rug.nl

T. Keviczky
Delft Center for Systems and Control
Delft University of Technology
Mekelweg 2
2628 CD Delft
The Netherlands
t.keviczky@tudelft.nl

Prof. M. Kinnaert
Dpt of Control Engineering and System Analysis
Université Libre de Bruxelles
CP 165/55, 50 Av. F.D. Roosevelt
B-1050 Brussels
Belgium
Michel.Kinnaert@ulb.ac.be

J.J. Koopman
Delft Center for Systems and Control
Delft University of Technology
Mekelweg 2
2628 CD Delft
The Netherlands
j.j.koopman@tudelft.nl

Gautier KRINGS
Dept. INMA
Université catholique de Louvain/UCL
Avenue Georges Lemaître, 4
B-1348 Louvain-la-Neuve
Belgium
gautier.krings@uclouvain.be

S. Kuiper
Delft Center for Systems and Control
Delft University of Technology
Mekelweg 2
2628 CD Delft
The Netherlands
Stefan.Kuiper@tudelft.nl

John Lataire
Dept. ELEC
Vrije Universiteit Brussel
Pleinlaan 2
1050 Brussel
Belgium
jlataire@vub.ac.be

Lieve Lauwers
Dept. ELEC
Vrije Universiteit Brussel
Pleinlaan 2
1050 Brussels
Belgium
Lieve.Lauwers@vub.ac.be

Dr Ir R. Lepore
Pôle Energie
Faculté Polytechnique de Mons
Boulevard Dolez 31
7000 Mons
Belgium
renato.lepore@fpms.ac.be

Dr Ir F. Logist
Dept. of Chemical Engineering / BioTeC
K.U.Leuven
W. de Croylaan 46
3001 Leuven
Belgium
filip.logist@cit.kuleuven.be

Thomas Lombaerts
Faculty of Aerospace Engineering
Technische Universiteit Delft
Kluyverweg 1
2629 HS Delft
The Netherlands
t.j.j.lombaerts@tudelft.nl

Johan Mailier
Service d'Automatique
Faculté Polytechnique de Mons
31 Boulevard Dolez
B-7000 Mons
Belgium
johan.mailier@fpms.ac.be

Anna Marconato
Dept. ELEC
Vrije Universiteit Brussel
Pleinlaan 2
1050 Brussels
Belgium
amarcon@disi.unitn.it

Jordi Martin Benet
Control Engineering Department
Université libre de Bruxelles
50 Av. F.D. Roosevelt, CP 165/55
1050 Bruxelles
Belgium
jmartinb@ulb.ac.be

A.M. Mauroy
Departement of Electrical Enginering and Computer Science
University of Liège
BAT. B28 Systèmes et modélisation; Grande Traverse, 10
4000 Liège
Belgium
Alexandre.Mauroy@ulg.ac.be

G Meinsma
Dept. of Applied Mathematics
University of Twente
PO Box 217
7500 AE Enschede
The Netherlands
g.meinsma@utwente.nl

Ir R.J.E. Merry
Dept. of Mechanical Engineering
Technische Universiteit Eindhoven
PO Box 513
5600 MB Eindhoven
The Netherlands
r.j.e.merry@tue.nl

A. Mesbah
Delft Center for Systems and Control
Delft University of Technology
Mekelweg 2
2628 CD Delft
The Netherlands
ali.mesbah@tudelft.nl

Ir Meyer
Dept. of Electical Engineering and Computer Science
University of Liège
Bat. B28, Montefiore Institute, Systems and Modeling, Grande Traverse, 10
4000 Liège
Belgium
G.Meyer@ulg.ac.be

O. Naeem
Delft Center for Systems and Control
Delft University of Technology
Mekelweg 2
2628 CD Delft
The Netherlands
o.naeem@tudelft.nl

Ir G.J.L. Naus
Mechanical Engineering
Eindhoven University
PO Box 513
5600 MB Eindhoven
The Netherlands
G.J.L.Naus@tue.nl

Carine Neus
Dept. ELEC
Vrije Universiteit Brussel
Pleinlaan 2
1050 Brussels
Belgium
cneus@vub.ac.be

Victor ONCLINX
Dept. INMA
Université catholique de Louvain/UCL
Avenue Georges Lemaître, 4
1348 Louvain-la-Neuve
Belgium
victor.onclinx@uclouvain.be

Ms Pepona
Dept. of Mathematics
Brunel University
John Crank Building
UB8 3PH Uxbridge, Middlesex
United Kingdom
eleni.pepona@brunel.ac.uk

Dr. Ir. Pinte
Group High-productivity machines
Flanders' Mechatronics Technology Centre
Celestijnenlaan 300 D
B-3001 Leuven
Belgium
gregory.pinte@fmtc.be

prof. Rik Pintelon
Dept. ELEC
Vrije Universiteit Brussel
Pleinlaan 2
1050 Brussel
Belgium
rpintel@vub.ac.be

Ir G. Pipeleers
Dept. of Mechanical Engineering
K.U.Leuven
Celestijnenlaan 300B
B-3001 Heverlee
Belgium
goele.pipeleers@mech.kuleuven.be

I. Polat
Delft Center for Systems and Control
Delft University of Technology
Mekelweg 2
2628 CD Delft
The Netherlands
I.Polat@tudelft.nl

R. Polyuga
Institute for Mathematics and Computing Science
University of Groningen
P.O.Box 407
9700 AK Groningen
The Netherlands
r.polyuga@math.rug.nl

Cristina Retamal
Service d'Automatique
Faculté Polytechnique de Mons
Boulevard Dolez 31
7000 Mons
Belgium
cristinaretamal@yahoo.es

Edwin Reynders
Dept. of Civil Engineering
K.U.Leuven
Kasteelpark Arenberg 40
3001 Leuven
Belgium
edwin.reynders@bwk.kuleuven.be

P.E. Rutten
Delft Center for Systems and Control
Delft University of Technology
Mekelweg 2
2628 CD Delft
The Netherlands
p.e.rutten@tudelft.nl

Ir. B. Saerens
Dept. of Mechanical Engineering
Katholieke Universiteit Leuven
Celectijnenlaan 300
3001 Heverlee
Belgium
bart.saerens@mech.kuleuven.be

Chafik SAMIR
Dept. INMA
Université catholique de Louvain/UCL
Avenue Georges Lemaître, 4
1348 Louvain-la-Neuve
Belgium
chafik.samir@uclouvain.be

Alain Sarlette
Electrical Engineering and Computer Science
University of Liege
Montefiore Institute (B28)
4000 Liege
Belgium
sarlette@montefiore.ulg.ac.be

Prof. dr. ir. J.M.A. Scherpen
faculty of Mathematics and Natural Sciences
University of Groningen
Nijenborgh 4
9747 AG Groningen
The Netherlands
j.m.a.scherpen@rug.nl

Johan Schoukens
ELEC
Vrije Universiteit Brussel
Pleinlaan 2
B1050 Brussel
Belgie
johan.schoukens@vub.ac.be

Jeff Shamma
Electrical and Computer Engineering
Georgia Institute of Technology
TSRB 455
30332 Atlanta, GA
United States
shamma@gatech.edu

Prof. S. Skogestad
Dept. of Chemical Engineering
Norwegian Un. of Sci.&Tech. (NTNU)
Sem Saelandsa vei 4
N7491 Trondheim
Norway
skoge@ntnu.no

Dr Ir A. Skrylnyk
Laboratoire d'Automatique
Faculté Polytechnique de Mons
Boulevard Dolez 31
7000 Mons
Belgium
alexandre.skrylnik@student.fpms.ac.be

Bert Stallaert
Dept. of Mechanical Engineering, division PMA
Katholieke Universiteit Leuven
Celestijnenlaan 300B
3001 Leuven
Belgium
Bert.stallaert@mech.kuleuven.be

Prof. Dr. Ir. M. Steinbuch
Mechanical Engineering
Eindhoven University
PO Box 513
5600 MB Eindhoven
The Netherlands
M.Steinbuch@tue.nl

Dr.Ir. J.D. Stigter
Systems and Control
Wageningen University
Bornsesteeg 59
6708 PD Wageningen
The Netherlands
hans.stigter@wur.nl

Ir. J. Stolte
Dept. of Electrical Engineering
Technische Universiteit Eindhoven
PO Box 513
5600 MB Eindhoven
The Netherlands
J.Stolte@tue.nl

Prof.dr.ir. Stramigioli
IMPACTInstitute
University of Twente
217
7500AE Enschede
The Netherlands
S.Stramigioli@utwente.nl

Jan Swevers
Dept. of Mechanical Engineering
K.U.Leuven
Celestijnenlaan 300B
B 3001 Heverlee
Belgium
jan.swevers@mech.kuleuven.be

dr. ir. W. Symens
High-Productivity Machinery
Flanders' Mechatronics Technology Centre (FMTC)
Celestijnenlaan 300D - bus 4027
3001 Heverlee
Belgium
wim.symens@fmtc.com

O.A. Tekin
Delft Center for Systems and Control
Delft University of Technology
Mekelweg 2
2628 CD Delft
The Netherlands
o.a.tekin@tudelft.nl

Ir I. Torres
MAC
LAAS-CNRS
7 avenue du Colonel Roche
31077 Toulouse
France
itorres@laas.fr

Ir. C. Trabuco Dorea
Dept. of Electrical Engineering
KU Leuven
Kasteelpark Arenberg 10
B-3001 Leuven
Belgium
CarlosEduardo.TrabucoDorea@esat.kuleuven.be

Ir F van Belzen
Dept. of Electrical Engineering
Technische Universiteit Eindhoven
PO Box 513
5600 MB Eindhoven
The Netherlands
f.v.belzen@tue.nl

Ir P.J. van Bree
Dept. of Electrical Engineering
Technische Universiteit Eindhoven
PO Box 513
5600 MB Eindhoven
The Netherlands
P.J.v.Bree@tue.nl

Mattijs Van de Walle
Dept. ELEC
Vrije Universiteit Brussel
Pleinlaan 2
1050 Brussel
Belgium
mattijs.van.de.walle@vub.ac.be

Ir. L. van den Broeck
Dept. of Mechanical Engineering, division PMA
Katholieke Universiteit Leuven
Celestijnenlaan 300B
3001 Heverlee (Leuven)
Belgium
lieboud.vandenbroeck@mech.kuleuven.be

Prof.dr.ir. P.M.J. Van den Hof
Delft Center for Systems and Control
Delft University of Technology
Mekelweg 2
2628 CD Delft
The Netherlands
p.m.j.vandenhof@tudelft.nl

Ben Van der Hasselt
Dept. ELEC
Vrije Universiteit Brussel
Pleinlaan 2
1050 Brussels
Belgium
Ben.Van.Der.Hasselt@vub.ac.be

ir. G.W. van der Poel
Dept. of Mechanical Engineering
University of Twente
PO Box 217
7500 AE Enschede
The Netherlands
g.w.vanderpoel@utwente.nl

prof. A.J. van der Schaft
Institute of Mathematics and Computing Science
University of Groningen
PO Box 407
9700 AK Groningen
The Netherlands
a.j.van.der.schaft@math.rug.nl

Eva Van Derlinden
Department of Chemical Engineering
Katholieke Universiteit Leuven
W. de Croylaan 46
3001 Leuven
Belgium
eva.vanderlinden@cit.kuleuven.be

Dr. ir. J. van Dijk
Dept. of Mechanical Engineering
Universiteit Twente Enschede
PO Box 217
7500 AE Enschede
The Neherlands
j.vandijk@ctw.utwente.nl

Ir P.M.M. Van Erdeghem
Dept. of Chemical Engineering / BioTeC
K.U.Leuven
W. de Croylaan 46
3001 Leuven
Belgium
peter.vanerdeghem@cit.kuleuven.be

Prof Jan F. M. Van Impe
Department of Chemical Engineering
Katholieke Universiteit Leuven
W. de Croylaan 46
3001 Leuven
Belgium
jan.vanimpe@cit.kuleuven.be

Ir. E. van Kampen
ASTI
Technische Universiteit Delft
Kluyverweg 1
2629 HS Delft
The Netherlands
E.vanKampen@TUDelft.nl

Ir. T.A.C. van Keulen
Control Systems Technology Group
Technische Universiteit Eindhoven
P.O. Box 513
5600 MB Eindhoven
The Netherlands
T.A.C.v.Keulen@tue.nl

Anne Van Mulders
Dept. ELEC
Vrije Universiteit Brussel
Pleinlaan 2
1050 Brussels
Belgium
Anne.Van.Mulders@vub.ac.be

Ir G. van Oort
IMPACT Institute / Control engineering
Universiteit Twente
PO Box 217
7500 AE Enschede
The Netherlands
g.vanoort@ewi.utwente.nl

Prof. Dr. Ir. G. van Straten
Dept. Agrotechnology and Food Sciences
Wageningen University
Bornsesteeg 59
6708 PD Wageningen
The Netherlands
gerrit.vanstraten@wur.nl

Dr. Ir. A. van Weeren
ICT Department
University of Antwerp
Universiteitsplein 1
B-2610 Wilrijk
Belgium
arie.weeren@ua.ac.be

Dr. L.G. Van Willigenburg
Systems and Control Group
Wageningen University
P.O. Box 17
6700 AA Wageningen
The Netherlands
gerard.vanwilligenburg@wur.nl

Laurent Vanbeylen
Dept. ELEC
Vrije Universiteit Brussel
Pleinlaan 2
1050 Brussel
Belgium
lvbeylen@vub.ac.be

Joris Vanbiervliet
Dept. of Computer Science
KULeuven
Celestijnenlaan 200A
3000 Leuven
Belgium
joris.vanbiervliet@cs.kuleuven.be

Pr. Dr. Ir. A. Vande Wouwer
Service d'Automatique
Faculte Polytechnique de Mons
31 Boulevard Dolez
7000 Mons
Belgium
Alain.VandeWouwer@fpms.ac.be

Koen Vandermot
Dept. ELEC
Vrije Universiteit Brussel
Pleinlaan 2
1050 Brussel
Belgium
koen.vandermot@vub.ac.be

Jef Vanlaer
BioTeC
K.U.Leuven
W. de Croylaan 46
3001 Leuven
Belgium
jef.vanlaer@cit.kuleuven.be

Vincent Vastemans
General Chemistry and Biosystems Department
Université Libre de Bruxelles
F.-D. Roosevelt 50 C.P. 165/61
B-1050 Brussels
Belgium
vincent.vastemans@ulb.ac.be

A Venkatraman
Institute of Mathematics and Computing Science
University of Groningen
P. O. Box 407
9700 AK Groningen
The Netherlands
aneesh@math.rug.nl

Ir C. Verhelst
Dept. of Mechanical Engineering
Katholieke Universiteit Leuven
Celestijnenlaan 300A
3001 Heverlee
Belgium
clara.verhelst@mech.kuleuven.be

Anke Verhulst
Dept. of Chemical Engineering
Katholieke Universiteit Leuven
W. de Croylaan 46
3001 Heverlee
Belgium
anke.verhulst@cit.kuleuven.be

Ir Verspecht
Control Engineering Department
Université Libre de Bruxelles
Av. F.D. Roosevelt, 50 CP 165/55
1050 Brussels
Belgium
jverspec@ulb.ac.be

Harsh Vinjamoor
Mathematics and Computing Science
University of Groningen
Postbus 407
9700 AK Groningen
The Netherlands
h.g.vinjamoor@rug.nl

Tri Vo Minh
Department of Biosystems (BIOSYST)
K.U. Leuven
Kasteelpark Arenberg 30, Heverlee
3001 Leuven
Belgium
tri.vominh@student.kuleuven.be

Ir M.L.J. Volckaert
Dept. of Mechanical Engineering
K.U.Leuven
Celestijnenlaan 300B
B-3001 Heverlee
Belgium
marnix.volckaert@mech.kuleuven.be

T. Voss
Faculty of Mathematics and Natural Sciences
University of Groningen
Nijenborgh 4
9747 AG Groningen
The Netherlands
t.voss@rug.nl

Dirk Vries
Dept. of Agrotechnology and Food Science
Wageningen Universiteit
Bornsesteeg 59
6708 PD Wageningen
The Netherlands
dirk.vries@wur.nl

S.K. Wattamwar
Control Systems
Technical University of Eindhoven
PO box 513
5600MB Eindhoven
The Netherlands
s.wattamwar@tue.nl

Prof. Dr. Winkin
Dept. of Mathematics
University of Namur (FUNDP)
Rempart de la Vierge, 8
5000 Namur
Belgium
joseph.winkin@fundp.ac.be

Ir M. Witters
Dept. of Mechanical Engineering
Katholieke Universiteit Leuven
Celestijnenlaan 300B
B-3001 Heverlee
Belgium
maarten.witters@mech.kuleuven.be

Ir G. Witvoet
Dept. of Mechanical Engineering
Technische Universiteit Eindhoven
PO Box 513
5600 MB Eindhoven
The Netherlands
g.witvoet@tue.nl

Francisca Zamorano
Service d'Automatique
Faculté Polytechnique de Mons
Boulevard Dolez 31
7000 Mons
Belgium
francisca.zamorano@fpms.ac.be

S.K. Zegeye
Delft Center for Systems and Control
Delft University of Technology
Mekelweg 2
2628 CD Delft
The Netherlands
S.K.Zegeye@tudelft.nl

Xiangping Zhang
Electrical Engineering
Eindhoven University of Technology
PO Box 513
5600 MB Eindhoven
The Netherlands
x.zhang1@tue.nl

Yucai Zhu
Electrical Engineering
Eindhoven University of Technology
PO Box 513
5600 MB Eindhoven
The Netherlands
y.zhu@tue.nl

Dr. H.J. Zwart
Afdeling Toegepaste Wiskunde
University of Twente
P.O. Box 217
7500 AE Enschede
The Netherlands
h.j.zwart@math.utwente.nl

Part 5

Organizational Comments

Welcome

The Organizing Committee has the pleasure of welcoming you to the *27th Benelux Meeting on Systems and Control*, at the "Kapellerput Conference Centre" in Heeze, The Netherlands.

Aim

The aim of the Benelux Meeting is to promote research activities and to enhance cooperation between researchers in Systems and Control. This is the twenty-seventh in a series of annual conferences that are held alternately in Belgium and The Netherlands.

Overview of the Scientific Program

1. Plenary lectures by invited speakers
   - *Sigurd Skogestad* (Norwegian University of Science and Technology (NTNU), Trondheim, Norway)
     - **Self-Optimizing Control: Simple Implementation of Optimal Operation**
     - **Effective Implementation of Optimal Operation Using Off-Line Computations**
   - *Jeff Shamma* (Georgia Institute of Technology, Atlanta, GA, USA)
     - **Noncooperative Cooperation**
     - **Learning in Games under Dynamic Reinforcement**
2. Mini course **The Port-Hamiltonian Approach to Physical System Modelling and Control** by *Arjan van der Schaft and Hans Zwart* (University of Groningen and Twente University, The Netherlands)
3. Contributed short lectures, see the list of sessions for the titles and authors of these lectures.

Directions for speakers

For a contributed lecture the available time is 25 minutes. Please leave a few minutes of this period for discussion and room changes and adhere to the indicated schedule. In each room overhead projectors and beamers will be available. Be careful with this equipment, because the beamers are supplied by some of the participating groups. *When using a beamer/projector, you have to provide a notebook yourself and you have to start your lecture with the notebook up and running and the external video port switched on.*

Registration

The Benelux Meeting registration desk, located in the foyer to the left of the entrance, will be open on Tuesday, March 18, from 10:00 to 14:00. Late registrations can be made at the Benelux Meeting registration desk, when space is still available. The on-site fee schedule is:

Arrangement	Price
single room	€480.–
twin-bedded room	€395.–
meals only (no dinner)	€280.–
one day (no dinner)	€140.–

The registration fee includes:

- Admission to all sessions.
- A copy of the Book of Abstracts.
- Coffee and tea during the breaks, and ice water and mints in the session rooms.
- In the case of an accommodation arrangement: lunch and dinner on Tuesday, breakfast, lunch, and dinner on Wednesday, and breakfast and lunch on Thursday.
- In the case of a "meals only" arrangement: lunch on Tuesday, Wednesday, and Thursday.
- In the case of a "one day" arrangement: lunch on Tuesday, or Wednesday, or Thursday.
- Free use of a wireless Internet connection (WiFi) at the conference location

The registration fee does *not* include:

- Cost of phone calls
- Special ordered drinks during lunch, dinner, in the evening, etc.

Organization

The Organizing Committee of the 27th Benelux Meeting consists of

O.H. Bosgra (Delft Univ. of Technology), M. Gevers (Univ. Catholique de Louvain), P.M.J. Van den Hof (Delft Univ. of Technology), G. Meinsma (Twente University), B.L.R. de Moor (Univ. of Leuven), H. Nijmeijer (Technische Univ. Eindhoven), A.J. van der Schaft (Rijksuniv. Groningen), J. Schoukens, (Free University, Belgium), J.M. Schumacher (Tilburg Univ.), M. Steinbuch (Technische Univ. Eindhoven), J.D. Stigter (Wageningen University),

A.A. Stoorvogel (Twente University), S. Stramigioli (Twente University), G. van Straten (Wageningen University), S. Weiland (Technische Univ. Eindhoven).

The meeting is sponsored or supported by the following organizations:

- Dutch Institute for Systems and Control (DISC),
- Nederlandse Organisatie voor Wetenschappelijk Onderzoek (NWO).

The meeting has been organized by Hans Stigter (Wageningen University) and Gjerrit Meinsma (University of Twente).

Conference location

The lecture rooms of "Kapellerput Conference Centre" are situated on the ground floor in the eastern part. Consult the map at the end of this book to locate rooms and to avoid getting lost. During the breaks, coffee and tea will be served in the foyer, while ice water and mints are available in the session rooms. Announcements and personal messages will be posted near the main conference room. Accommodation is provided in the conference center for most participants. Breakfast will be served between 7:30 and 8:30. Room keys can be picked up at lunch time on the first day and need to be returned before 10:00 on the day of departure. Luggage storage is provided in room "de Aa" (in the old chapel to the left of the entrance). Parking is free of charge. The address of "Kapellerput Conference Centre" is

Somerenseweg 100
5591 TN Heeze
The Netherlands
tel: +31 (0) 40 224 19 22
fax: +31 (0) 40 226 54 47

Facilities

The facilities at the center include a restaurant, bar, and recreation and sports facilities. We refer to the reception desk of the center for detailed information about the use of these facilities.

Best junior presentation award

Continuing a tradition that started in 1996, the Benelux meeting will close with the announcement of the winner of the Best Junior Presentation Award. This award is given for the best presentation at the meeting given by a junior researcher (*i.e.*, someone working towards a PhD degree). The award is specifically given for quality of presentation rather than quality of research, which is judged in a different way. At the meeting, the chairs of sessions will ask three volunteers in the audience to fill out an evaluation form. After the session, the evaluation forms will be collected by the Prize Commissioners who will then compute a ranking. The winner will be announced on Thursday March 20 in room **Samenspel**, immediately after the final lectures of the meeting and he or she will be presented with the award, which consists of a trophy that may be kept for one year and a certificate. The evaluation forms of each presentation will be returned to the junior researcher who gave the presentation. The Prize Commissioners are Dr. Jan Van Impe (Katholieke Universiteit Leuven), and Dr. Peter Heuberger (Delft University).

The organizing committee counts on the cooperation of the participants to make this contest a success.

Website

An *electronic version* of the Book of Abstracts can be downloaded from the Benelux Meeting web site.

Meetings

The following meetings are scheduled:

- Board DISC on Tuesday, March 18, Visie, 21:00–22:00.
- UNIT DISC on Wednesday, March 19, Hotelbar, 12:30–13:30.
- Management team DISC on Wednesday, March 19, Visie, 21:00–22:00.

Tuesday March 18

11:25 – 11:30	P0 Samenspel *Opening*				
11:30 – 12:30	P1 Samenspel *"Self-Optimizing Control: Simple Implementation of Optimal Operation"* Sigurd Skogestad				
12:30 – 14:00	Lunch				
Room	Samenspel	Samenkomst	Samenwerking	Visie	Uitdaging
TuM	TuM01 *Identification A*	TuM02 *System Theory A*	TuM03 *Modeling for Control*	TuM04 *Electro-Mech. Eng. A*	TuM05 *Games and Agent Based Models*
14:00 – 14:25	Huyck	Dirksz	Djordjevic	van Bree	Engwerda
14:25 – 14:50	Merry	Cason	Stolte	Symens	Trottemant
14:50 – 15:15	De Caigny	Besseling	Rutten	van der Poel	Weeren
15:15 – 15:40	Neus	Polyuga	Kuiper	Ding	Delvenne
15:40 – 16:05	Vandermot	Garcia-Cansco	Mesbah	Foubert	Keviczky
16:05 – 16:35	Break with snack				
TuP	TuP01 *Identification B*	TuP02 *Medical Applications*	TuP03 *Biochemical Eng. A*	TuP04 *Electro-Mech. Eng B*	TuP05 *Aerospace Eng.*
16:35 – 17:00	Lataire	Heijman	Vanlaer	Evers	de Visser
17:00 – 17:25	Klomp	Mauroy	Haye	Aydin Tekin	Van de Walle
17:25 – 17:50	Van der Hasselt	Tri Vo-Minh	Verhulst	van den Broeck	Lombaerts
17:50 – 18:15	Barbé	Fonteneau	Mailier	Damoiseaux	Joosten
18:15 – 18:40	Reynders	Ionescu	Vastemans	Belmudes	van Kampen
19:00 – 20:30	Dinner (for accommodation arrangement)				

Wednesday March 19

8:30 – 9:30	P2 Samenspel *"Noncooperative Cooperation"* Jeff Shamma				
9:30 – 10:00	Break				
10:00 – 11:00	P3 Samenspel *"The Port-Hamiltonian Approach to Physical System Modeling and Control (Part 1)"* Arjan van der Schaft				
11:00 – 11:30	Break				
11:30 – 12:30	P4 Samenspel *"Effective Implementation of Optimal Operation Using Off-Line Computations"* Sigurd Skogestad				
12:30 – 14:00	Lunch				
Room	Samenspel	Samenkomst	Samenwerking	Visie	Uitdaging
WeM	WeM01 *Identification C*	WeM02 *System Theory B*	WeM03 *Biochemical Eng. B*	WeM04 *Electro-Mechanical Eng. C*	WeM05 *Aerospace and Traffic*
14:00 – 14:25	Witters	Ivanov	Favache	van Hulzen	Voß
14:25 – 14:50	van Doren	Beauthier	Goffaux	Pinte	Naus
14:50 – 15:15	Bauwens	Kerber	Van Derlinden	Stallaert	Zegeye
15:15 – 15:40	Blom	van Willigenburg	Beniich	Pipeleers	van Oort
15:40 – 16:05	Merry	Ciprian Deliu	Drame	Witvoet	Sonneveldt
16:05 – 16:35	Break with snack				
WeP	WeP01 *Robotics*	WeP02 *Model Reduction*	WeP03 *Biochemical Eng. C*	WeP04 *Mechnical Eng.*	WeP05 *Observers*
16:35 – 17:00	van Oort	Bleylevens	David	van Keulen	Skrylnyk
17:00 – 17:25	van Ast	Meyer	Logist	van Lierop	Venkatraman
17:25 – 17:50	Sarlette	Journée	van Derlinden	Bastin	Efimov
17:50 – 18:15	de Best	Naeem	Gins	Koopman	Bonnabel
18:15 – 18:40	Benet	Wattamwar	Dewasme	Gálvez-Carrillo	Vries
18:40 – 19:05	Polat	van Belzen	Zamorano		
19:30 – 21:00	Dinner (for accommodation arrangement)				

Thursday March 20

8:30 – 9:30	P5 Samenspel *"The Port-Hamiltonian Approach to Physical System Modeling and Control (Part 2)"* Arjan van der Schaft				
9:30 – 10:00	Break				
10:00 – 11:00	P6 Samenspel *"Learning in Games under Dynamic Reinforcement"* Jeff Shamma				
11:00 – 11:30	Break				
11:30 – 12:30	P7 Samenspel *"The Port-Hamiltonian Approach to Physical System Modeling and Control (Part 3)"* Hans Zwart				
12:30 – 14:00	Lunch				
Room	Samenspel	Samenkomst	Samenwerking	Visie	Uitdaging
ThP	ThP01 *Identification D*	ThP02 *Optimization*	ThP03 *Dynamic Optimization*	ThP04 *Optimal Control*	ThP05 *Nonlinear systems*
14:00 – 14:25	Lauwers	Gerard	Saerems	Vanbiervliet	Delwiche
14:25 – 14:50	Gajdusek	Marconato	Huesman	den Hamer	Vanbeylen
14:50 – 15:15	Beelaerts	de Weerdt	Van Erdeghem	Dong	Pepona
15:15 – 15:40			Bonilla	van Mulders	Gommé
15:50 – 16:00	Best Junior Presentation Award				
16:00	Closure of 27th Benelux Meeting				

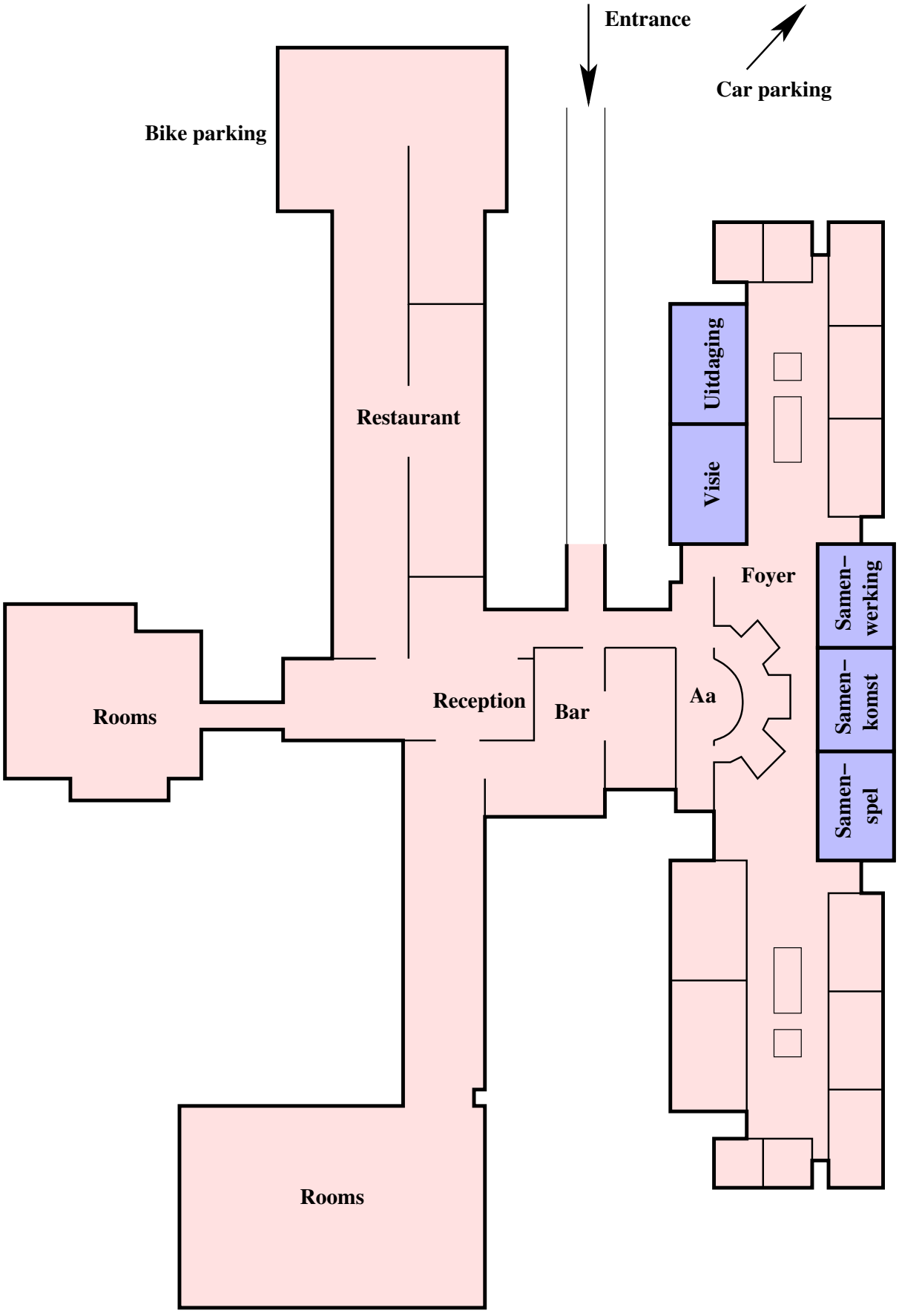
Entrance
Car parking
Bike parking
Restaurant
Uitdaging
Visie
Foyer
Samen–werking
Samen–komst
Samen–spel
Rooms
Reception
Bar
Aa
Rooms